
VEGETATION MODELLING

SYLLABUS

WRITTEN BY

HANS VERBEECK, FELICIEN MEUNIER, MARC PEAUCHELLE

GHENT UNIVERSITY



2021

Contents

1	Introduction	1
1.1	The central role of vegetation in the Earth system	1
1.2	Why do we need modelling?	6
1.3	Model types	7
1.4	The history of vegetation models	8
1.5	Components of a model	9
1.6	Modelling workflow and structure of the course	14
I	Biophysical and physiological models	16
2	Modelling plant basic processes	17
2.1	Photosynthesis models	17
2.2	Stomatal models	30
2.3	Upscaling from leaf to canopy	38
2.4	Case studies	40
3	Modelling radiation, vegetation canopies, and energy balance	44
3.1	Introduction	44
3.2	Radiative transfer modelling	49
3.3	Representing canopy structure in models	65
3.4	Ecosystem energy balance	72
3.5	Case studies	76
4	Modelling temporal and seasonal dynamics	80
4.1	Introduction on temporal dynamics	80
4.2	Phenology: the background	81
4.3	Leaf phenology models	83
4.4	Case studies	89

II Modelling vegetation dynamics **94**

5 Modelling C-allocation and biogeochemical cycles	95
5.1 Introduction	95
5.2 Carbon cycle models: stocks and fluxes	96
5.3 Carbon allocation models	103
5.4 Case Study 5.1	107
5.5 Soil biogeochemistry models	110
5.6 Case study 5.2	117
5.7 Water balance models	120
6 Modelling Vegetation Dynamics and Demography	121
6.1 Introduction	121
6.2 Gap models, area and cohort based models	123
6.3 Growth and allometric relations in demographic models	141
6.4 Competition for light in demographic models	150
6.5 Competition for water and nutrients in demographic models	154
6.6 Seed dispersal and recruitment	155
6.7 Mortality	156
6.8 Conclusion	157
6.9 Case study 6.1	159
6.10 Case study 6.2	161
7 Representing functional biodiversity in vegetation models	164
7.1 Introduction	164
7.2 Functional diversity	164
7.3 Representing 400.000 plant species in a single model: the PFT approach	174
7.4 Limitations of the PFT concept	175
7.5 Alternative approaches to account for trait variability	176
7.6 Case study 7.1	179
7.7 Case study 7.2	181

III Upscaling and applications 185

8 Spatial heterogeneity, landscape scale and disturbance	186
8.1 Introduction: landscape scale	186
8.2 Land use change	188
8.3 Disturbance	189
9 Upscaling from the leaf to the globe	205
9.1 The problem of upscaling	205
9.2 Vegetation models as part of earth system models	207
9.3 MOdelling work flow	209
9.4 Case study 9.1	210
9.5 Case study 9.2	211
10 Model simulations, projections and scenario analysis	215
10.1 Simulation setup	215
10.2 Model experiments	217
10.3 Paleo studies	218
10.4 Climate scenarios	219
10.5 Land use scenarios	224
10.6 Management scenarios	224

IV Appendix 226

Contributing to this document	227
First steps	227
New pull request	227
Supporting material	229

V Practicals 230

Practical A	231
Practical B	232

Practical C	233
Practical D	234
Practical E	235
Practical F	236

Chapter 1

Introduction

An ecosystem model is an abstract, usually mathematical, representation of an ecological system which is studied to better understand the real system. The scale varies from an individual population to an ecological community or an entire biome.

A dynamic global vegetation model (DGVM) is a computer program that simulates shifts in potential vegetation and its associated biogeochemical and hydrological cycles as a response to shifts in climate (see 1.5). Vegetation models can be used to conduct virtual experiments.

1.1 The central role of vegetation in the Earth system

Plants and vegetation play an essential role in the earth system. In Figure 1.1, we have represented the planetary boundaries and the significant environmental challenges we are facing. For some of them, we are reaching the system's boundary, such as genetic diversity, biogeochemical cycling, and climate change. It is crucial to understand how vegetation reacts to environmental problems (positive or negative feedback), as vegetation plays a central role in many of these boundaries. Environmental challenges we are facing include:

- Stratospheric ozone depletion: The stratospheric ozone layer in the atmosphere filters out ultraviolet (UV) radiation from the sun. If this layer decreases, increasing amounts of UV radiation will reach ground level. Because of the actions taken as a result of the Montreal Protocol, we appear to be on the path that will allow us to stay within this boundary.
- Atmospheric aerosol loading: Through their interaction with water vapour, aerosol play a critically important role in the hydrological cycle affecting cloud formation and global-scale and regional patterns of atmospheric circulation, such as the monsoon systems in tropical regions. They also have a direct effect on climate, by changing how much solar radiation is reflected or absorbed in the atmosphere. Humans change the aerosol loading by emitting atmospheric

pollution and through land-use change that increases the release of dust and smoke into the air. Shifts in climate regimes and monsoon systems have already been seen in highly polluted environments, giving a quantifiable regional measure for an aerosol boundary.

- Ocean acidification: Around a quarter of the CO₂ that humanity emits into the atmosphere is ultimately dissolved in the oceans. Here it forms carbonic acid, altering ocean chemistry and decreasing the pH of the surface water. This increased acidity reduces the amount of available carbonate ions, an essential ‘building block’ used by many marine species for shell and skeleton formation. Beyond a threshold concentration, this rising acidity makes it hard for organisms such as corals and some shellfish and plankton species to grow and survive. Losses of these species would change the structure and dynamics of ocean ecosystems and could potentially lead to drastic reductions in fish stocks. Compared to pre-industrial times, surface ocean acidity has already increased by 30 percent. The ocean acidification boundary has ramifications for the whole planet.
- Biochemical flows: Nitrogen and phosphorus are both essential elements for plant growth, so fertilizer production and application is the main concern. Human activities now convert more atmospheric nitrogen into reactive forms than all of the Earth’s terrestrial processes combined. Much of this new reactive nitrogen is emitted to the atmosphere in various forms rather than taken up by crops. When it is rained out, it pollutes waterways and coastal zones or accumulates in the terrestrial biosphere. Similarly, a relatively small proportion of phosphorus fertilizers applied to food production systems is taken up by plants; much of the phosphorus mobilized by humans also ends up in aquatic systems. These can become oxygen-starved as bacteria consume the blooms of algae that grow in response to the high nutrient supply. A significant fraction of the applied nitrogen and phosphorus makes its way to the sea, and can push marine and aquatic systems across ecological thresholds of their own. One regional-scale example of this effect is the decline in the shrimp catch in the Gulf of Mexico’s ‘dead zone’ caused by fertilizer transported in rivers from the US Midwest.
- Freshwater use: Human pressure is now the dominant driving force determining the functioning and distribution of global freshwater systems. The consequences of human modification of water bodies include both global-scale river flow changes and shifts in vapour flows arising from land use change. These shifts in the hydrological system can be abrupt and irreversible. Water is becoming increasingly scarce - by 2050 about half a billion people are likely to be subject to water-stress, increasing the pressure to intervene in water systems.
- Land-system change: Forests, grasslands, wetlands and other vegetation types have primarily been converted to agricultural land. This land-use change is one driving force behind the serious reductions in biodiversity, and it has impacts on water flows and on the biogeochemical cycling of carbon, nitrogen and phosphorus and other important elements. While each incident of land cover change occurs on a local scale, the aggregated impacts can have consequences for Earth system processes on a global scale. Forests play a particularly important role in

controlling the linked dynamics of land use and climate, and is the focus of the boundary for land system change.

- Biosphere integrity: The Millennium Ecosystem Assessment of 2005 concluded that changes to ecosystems due to human activities were more rapid in the past 50 years than at any time in human history, increasing the risks of abrupt and irreversible changes. The main drivers of change are the demand for food, water, and natural resources, causing severe biodiversity loss and leading to changes in ecosystem services. The current high rates of ecosystem damage and extinction can be slowed by efforts to protect the integrity of living systems (the biosphere), enhancing habitat, and improving connectivity between ecosystems while maintaining the high agricultural productivity that humanity needs.
- Climate change: Recent evidence suggests that the Earth, now passing 390 ppmv CO₂ in the atmosphere, has already transgressed the planetary boundary and is approaching several Earth system thresholds. The weakening or reversal of terrestrial carbon sinks, for example through the on-going destruction of the world's rainforests, is a potential tipping point, where climate-carbon cycle feedbacks accelerate Earth's warming and intensify the climate impacts.
- Novel entities: Emissions of toxic and long-lived substances such as synthetic organic pollutants, heavy metal compounds and radioactive materials represent some of the key human-driven changes to the planetary environment. Even when the uptake and bioaccumulation of chemical pollution is at sub-lethal levels for organisms, the effects of reduced fertility and the potential of permanent genetic damage can have severe effects on ecosystems far removed from the source of the pollution.

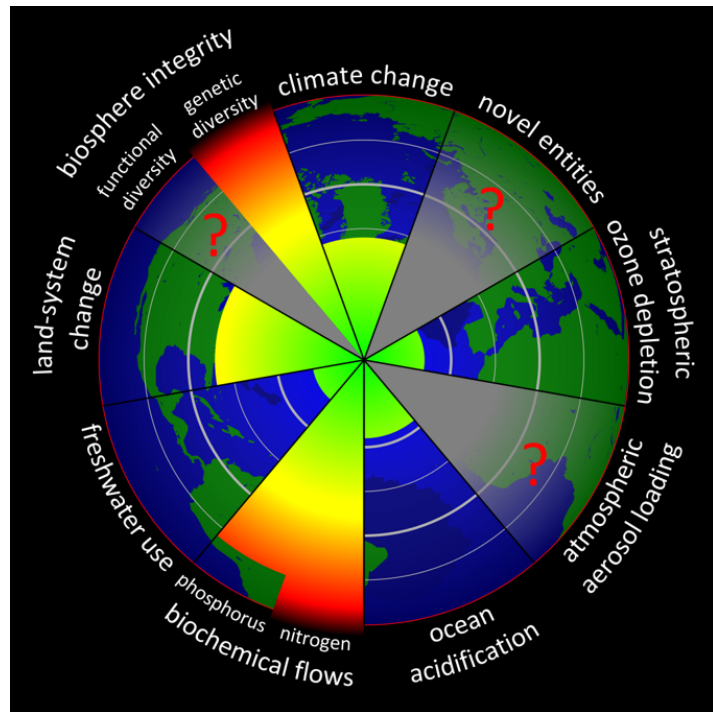


Figure 1.1: The planetary boundaries (www.stockholmresilience.org)

A more specific example of the plant-environment interactions is the global carbon budget. We are currently facing this significant change in biogeochemical cycling due to the rising fossil fuel emission over the last 150 years. Figure 1.2 represents the balance between carbon sources (fossil carbon and land-use changes) and sinks (oceans, land, and atmosphere). The more we emit, the more the Earth system is capturing. Naturally, the emitted CO₂ must go somewhere. Approximately half of it is taken up by the ocean and the land (soil + vegetation) sink. As stated earlier, roughly 25% of the emitted CO₂ is dissolved in the ocean sink. The land sink is highly variable: land and soils are very heterogeneous and difficult to model. Nevertheless, the land sink has taken up more emissions in the past 60 years than it did before. The atmosphere is responsible for most of the uptake. This takes us to a question, frequently addressed by global vegetation models, about how long these sinks will continue or not capture our increasing carbon emissions. Note that there is an imbalance: there was more CO₂ emitted than absorbed. So, where did the surplus go? This is an active area of research.

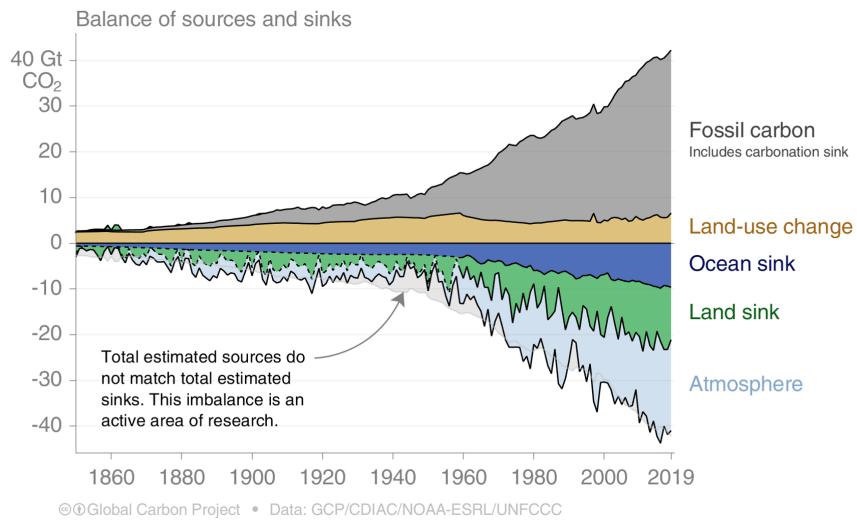


Figure 1.2: The global carbon budget (www.globalcarbonproject.org)

Climate Models predict how the long-term weather variation and average weather will evolve. These models include an atmosphere, land and ocean component (Figure 1.3 top). The original climate models focused on biophysics: energy and water balances, predicting precipitation, radiation and fluxes between the three components. More recently, climate models have evolved into **Earth System Models** (ESM). ESM have a more complex concept because they represent more processes (Figure 1.3 bottom). Why? If you want to predict the end of the century climate, we need to consider greenhouse gases and thus the full carbon cycle. ESM are more complex but also more realistic.

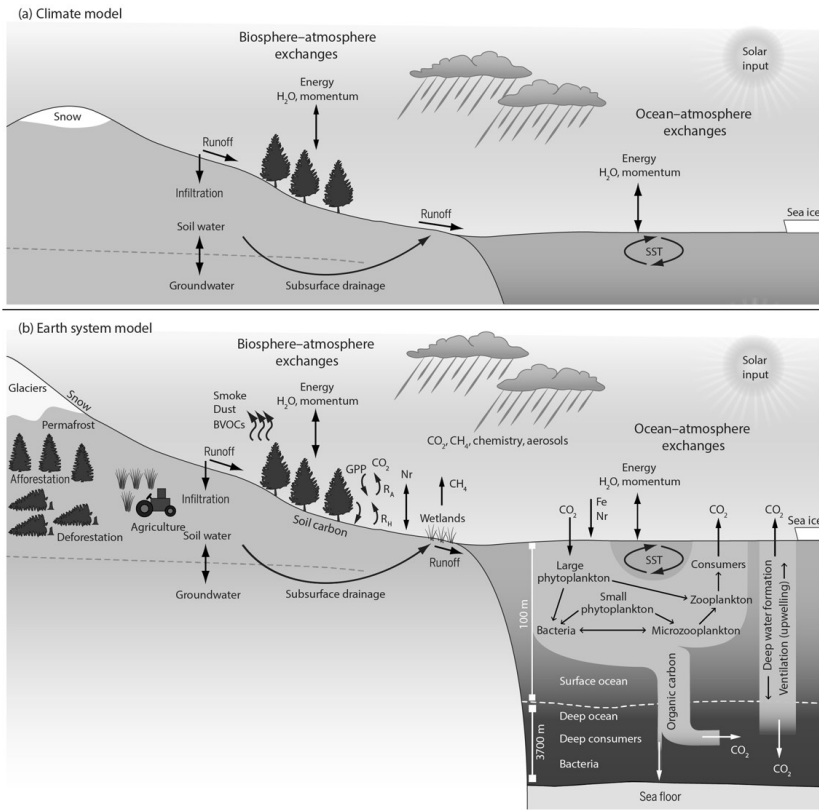


Figure 1.3: Scientific scope of (a) climate models and (b) earth system models. (Bonan 2019)

Vegetation models are often the land component of an earth system model. These ‘terrestrial biosphere models’ (TBM) or ‘land surface models’ (LSM)

- simulate **energy fluxes**: radiation, evapotranspiration and sensible heat fluxes between the land and the atmosphere. Depending on the vegetation type, the impacts are different.
- simulate the **hydrology** and the **carbon cycle**.
- simulate slower processes like **vegetation dynamics**: the succession of forest or **land use** and **urbanization**.

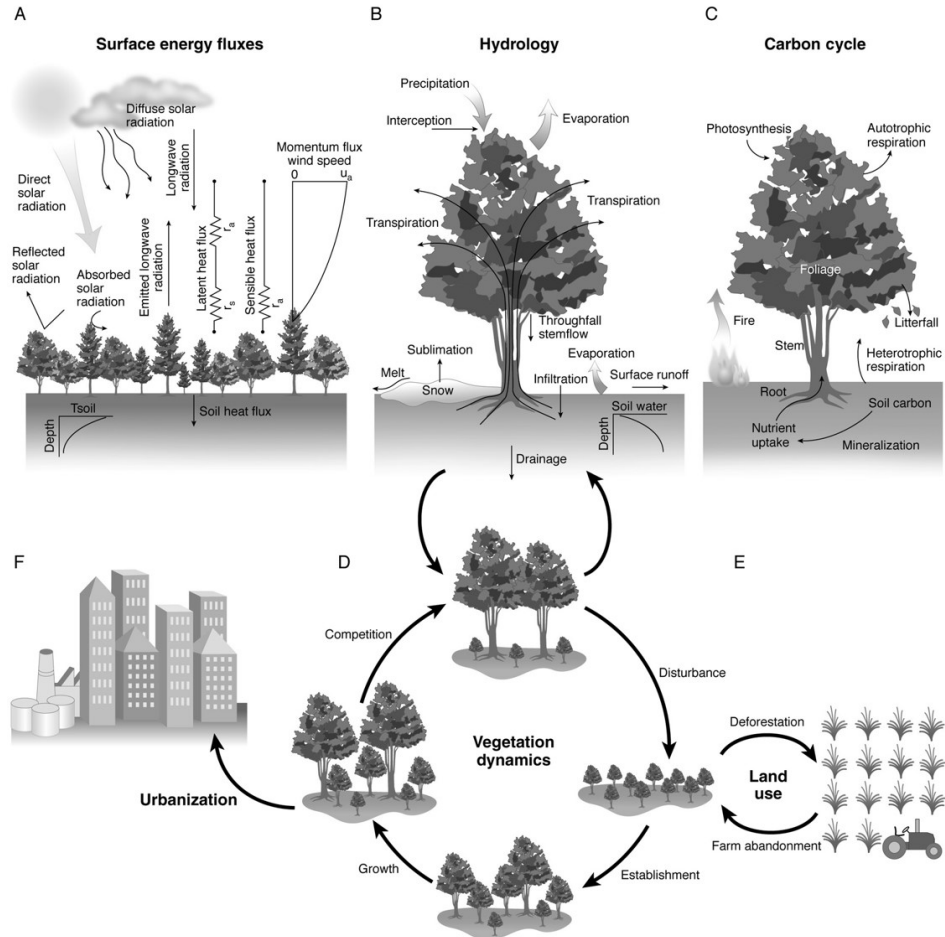


Figure 1.4: Scientific scope of terrestrial biosphere model. (Bonan 2019)

The coupler is a system that links different models. For example the terrestrial biosphere can be seen as the coupler between geochemistry and hydrology. A coupler can be the link between more than two other systems, so that a kind of satellite system is formed. The land model is mostly seen as the coupler. This results in the fact that both fast and slow processes depend on each other. The surface energy flux is an example of a fast process since it varies over the course of one day. Vegetation dynamics on the other hand, is a slow process. Succession does not happen overnight.

1.2 Why do we need modelling?

Modelling has proven to be a essential tool:

- For **understanding**: we need good theoretical foundations (understand processes) to generalize knowledge and observations in space and time (upscaling). Studying the inaccuracies in models leads to the formulation of new hypotheses.
- For **prediction**, how vegetation responds to expected changes (temperature or CO₂) to develop management strategies and policies.

- For **data integration**: a framework to bring together multiple data sources and to guide future data collection.

1.3 Model types

How can we look at the different model types that exist (Table 1.1)? Models are to be placed in a continuum ranging from empirical to process-based models. **Empirical models** are based on data and correlations, not describing precisely the biophysical processes — **process-based models** describing the biophysical processes and causal relations between the variables (Table 1.2). Most existing vegetation models are hybrid.

Table 1.1: Continuum of terrestrial biosphere/ecosystem models. (Bonan 2019)

Type of model	Description	Example
Biogeochemical	Ecosystem model with emphasis on biogeochemical pools and fluxes	CASA, BIOME-BGC, CENTURY
Forest gap models	Individual trees, population dynamics, demography, community composition	JABOWA, SORTIE
Ecosystem demography	As gap models but cohort based	ED
Dynamic Global Vegetation Models (DGVM)	Biogeochemistry, community composition, global biogeography	LPJ, LPJ-guess, ORCHIDEE, JULES, ED2
Land Surface Models (LSM)	Global models of the land surface, as part of climate models with focus on biophysical coupling with the atmosphere. They now include biogeochemistry, and vegetation dynamics → they became a DGVM	ORCHIDEE, JSBACH, CLM, FATES, ED2, ...
Plant canopy	Multilayer models with focus on coupling leaf physiology and canopy physics	CANOAK, FORUG
Canopy- chemistry	Plant canopy models that include chemical transport	CAFE
Ecohydrology	Similar to LSM, but spatially explicit with river routing, lateral flow	RHESSy

Table 1.2: Continuum of process-based versus empirical models. (Adams et al. 2013)

	Process-based	Empirical
Relationship type	Causal	Correlative
Relative comprehensiveness	More comprehensive	Less comprehensive
Incorporation of mechanism	Explicit	Implicit
Primary source of error	Unknown parameters and processes	Extrapolation
Model uncertainty	Higher	Lower
Data requirements	Higher	Lower
Spatial scale for calibration	Smaller	Smaller to larger
Spatial scaling of prediction	Smaller to Larger	Best at scale of calibration

The model type depends on:

- Purpose: will it be used for management support, policy support, research.
- Question: different people will be interested in different questions (foresters, ecologists, policy makers...)
- Scale: models that are to be applied for local use can be much more detailed than worldwide models because data gathering is much more straightforward on a small scale. Also the time-scale is of importance: will the model be used for research about the past, the present or the future?

1.4 The history of vegetation models

The history of vegetation models is one that parallels that of the computer. Computers made it possible to calculate much faster and much more, which made them suitable for modelling. The first vegetation models have emerged in the 1960s and 1970s.

One of the first models were the **box models** (1960); these models describe the flow of mass and energy through boxes. These models still exist in current biogeochemical models, where arrows represent the fluxes between the pools. In parallel, **gap models** had emerged. Gap models simulate the dynamics of the development of a gap in a forest and the growth of plants in this gap. Gaps can be created by fallen trees, by dead trees, This kind of models are individual-based and focused on population dynamics and the life cycle of species: growth, regeneration and mortality while taking environmental constraints in account. These models are the first models that were ever used for upscaling: from tree level, to plot-level, to landscape level. They were developed by forest scientists using forest inventories to derive growth, regeneration, and mortality in response to environmental variables. In 1973, the first model (MIAMI model by Lieth (1973)) was developed to derive global net primary productivity (NPP), relating NPP in an empirical way to climate variables (temperature) with vegetation productivity. This was the first attempt to make a global upscaling of a vegetation process. In the 1980s surged the first **land surface models**. Land surface models are the models where the other models start to integrate into, and evolved as such into – **Terrestrial biosphere models** (see Figure 1.5), which are now the state-of-the-art land components of ESMs. Vegetation modelling therefore is a very interdisciplinary field because it involves knowledge of different scientific fields, making it difficult to find a common terminology. Global EMS are currently still not good to simulate realistic vegetation dynamics.

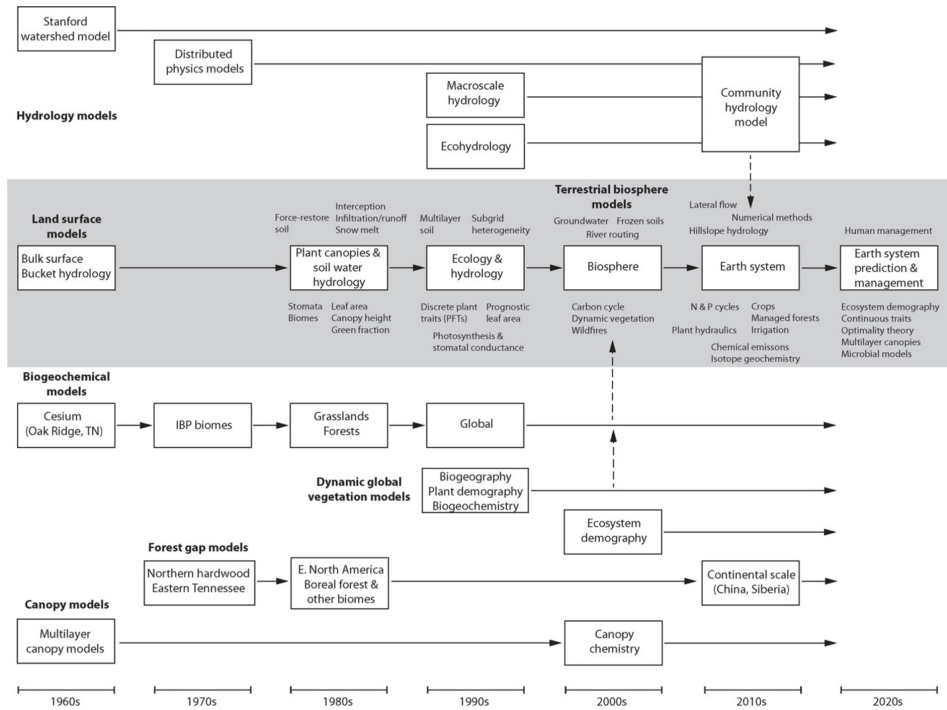


Figure 1.5: Timeline showing the parallel development of model types and the integration of model types into land surface models towards terrestrial biosphere models. (Bonan 2019)

1.5 Components of a model

What is a vegetation model? Two attempts for a definition:

- **Dynamic global vegetation models** (DGVMs) are powerful tools to project past, current and future vegetation patterns and associated biogeochemical cycles (Scheiter et al., 2013).
- A **Dynamic Global Vegetation Model** (DGVM) is a computer program that simulates shifts in potential vegetation and its associated biogeochemical and hydrological cycles as a response to shifts in climate. DGVMs use time series of climate data and, given constraints of latitude, topography, and soil characteristics, simulate monthly or daily dynamics of ecosystem processes. DGVMs are used most often to simulate the effects of future climate change on natural vegetation and its carbon and water cycles (Wikipedia 2021).

Table 1.3: Definition of key model components and examples for a typical TBM

Model component	Definition (syllabus)	Examples for a typical TBM
System boundary	What is in the system and what is out?	Lower atmosphere, deep soil
State variable	Time varying quantity	Carbon pools, soil water content
Model structure	The equations and connectivity	Photosynthesis equations
Parameters	Constants in process equations	Photosynthetic capacity, drought sensitivity parameter, ...
Forcing inputs ('forcings')	Quantities needed to evolve the model state	Air temperature, radiation, (meteo), atm. CO ₂ concentration
Initial conditions	State variables at model start-up	Carbon pools, soil water content
Model outputs	Quantities simulated by the model (state variables, fluxes,...)	Biogeochemical fluxes, dynamics of model states, ...

1.5.1 Processes

They are a key component because we are focusing on process-based models in this course. There is a long list of processes (energy, water, turbulent transport, canopy scaling, carbon, nitrogen, trace gasses, demography,...) that the models integrate, especially the more complex ones. These processes will be discussed in detail in the following theory chapters and we will mainly focus on how to translate them into equations.

1.5.2 Equations

These are the mathematical representations of the processes. However, there are important constraints to insert equations into a vegetation model, such as the specific time scale at which a process operates. For example, it makes little sense to resolve the equation for forest composition (succession) on a daily calculation time step. This is a prolonged process with an extremely low variance between consecutive days. The solution for the equation for photosynthesis, on the other hand, varies significantly throughout the day and between consecutive days (cloudy day vs sunny day).

There are three types of equations within vegetation models: - **prognostic equations**: time derivatives of differential equations – they calculate the state's change over time - **conservation equations**: equations describing the conservation of mass and energy - **diagnostic equations**: linking multiple variables independent from the time.

Often there is no analytical solution of the equations describing on-linear processes in biological systems; therefore, we must use numerical methods to solve the equations.

1.5.3 Parameters

These are the constants in the model. Some parameters are highly uncertain because we cannot measure them very well at the relevant scale. For example, we can make reliable measurements of the photosynthetic capacity of a single leaf. However, upscaling this parameter so that it is applicable for a forest or multiple PFTs (= plant functional types) induces uncertainty. The more parameters a model uses, the more uncertainties that are to be taken into account.

1.5.4 Time Steps

Vegetation models run at multiple timescales (combining processes that are resolved at multiple timescales). Models present fast processes, which are calculated every hour (e.g. photosynthesis and energy balance), intermediate processes calculated daily (e.g. carbon allocation and growth) and slow processes in order of years (e.g. mortality) (Fig.6).

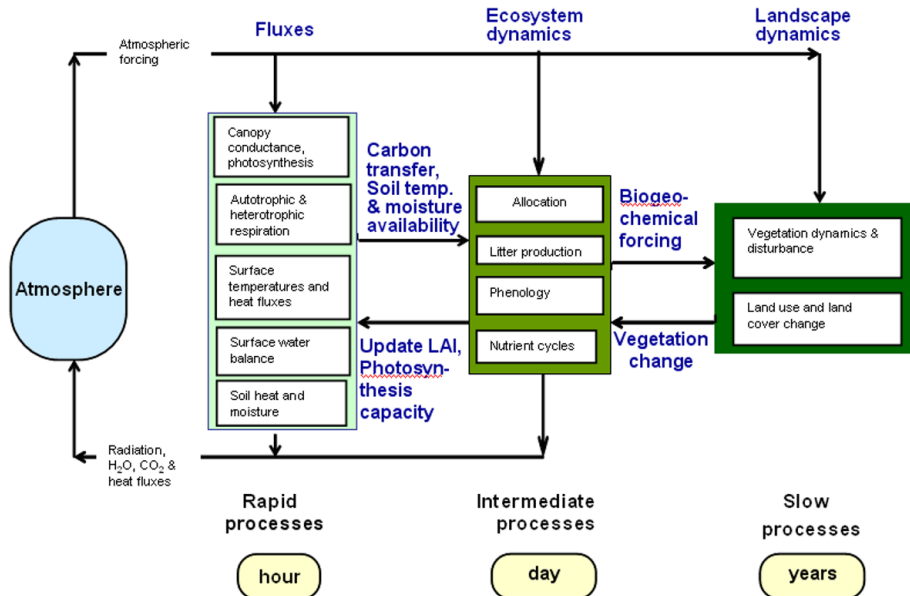


Figure 1.6: Structure of a vegetation model indicating the different time steps at which each process is simulated (Williams et al. 2009)

1.5.5 Spatial structure

The division of space in voxels, layers or grid cells and its resolution determines how many times we repeat our calculations in space. Global vegetation models have a typical spatial grid of 100km or even more and divide the landscape into patches. In each patch, they simulate the vegetation (forest, savannas, grassland...). Models also have a horizontal grid or horizontal layering: some models consider multiple soil layers. The same is true for above ground layers, where some models divide the canopy into multiple layers (Figure 1.7). For example, the Ecosystem Demography Model (ED2.2) divides the forest into multiple grid cells where the same meteorological conditions apply within each grid cell. Then within each cell, this model has different sites with different soils. Each site is divided into multiple patches (forests with a similar disturbance history). For each patch, the model simulates multiple cohorts of trees where size and plant functional types play a role (Figure 1.8).

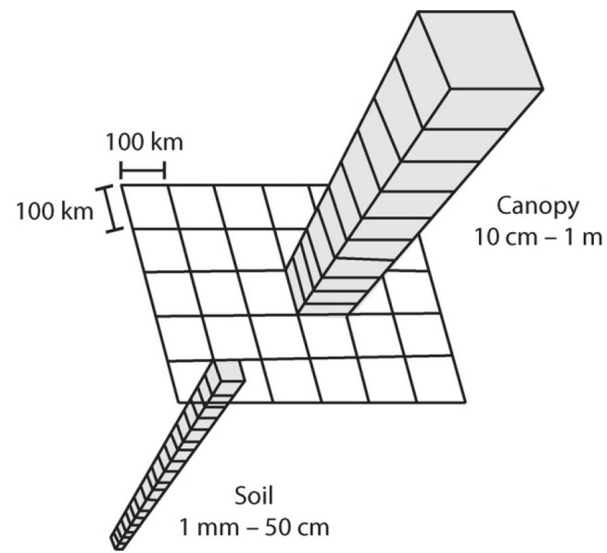


Figure 1.7: Three dimensional grid of a TBM structured in terms of longitude x latitude x level. The number of soil and canopy layers and the geographical resolution is model dependent, (Bonan 2019)

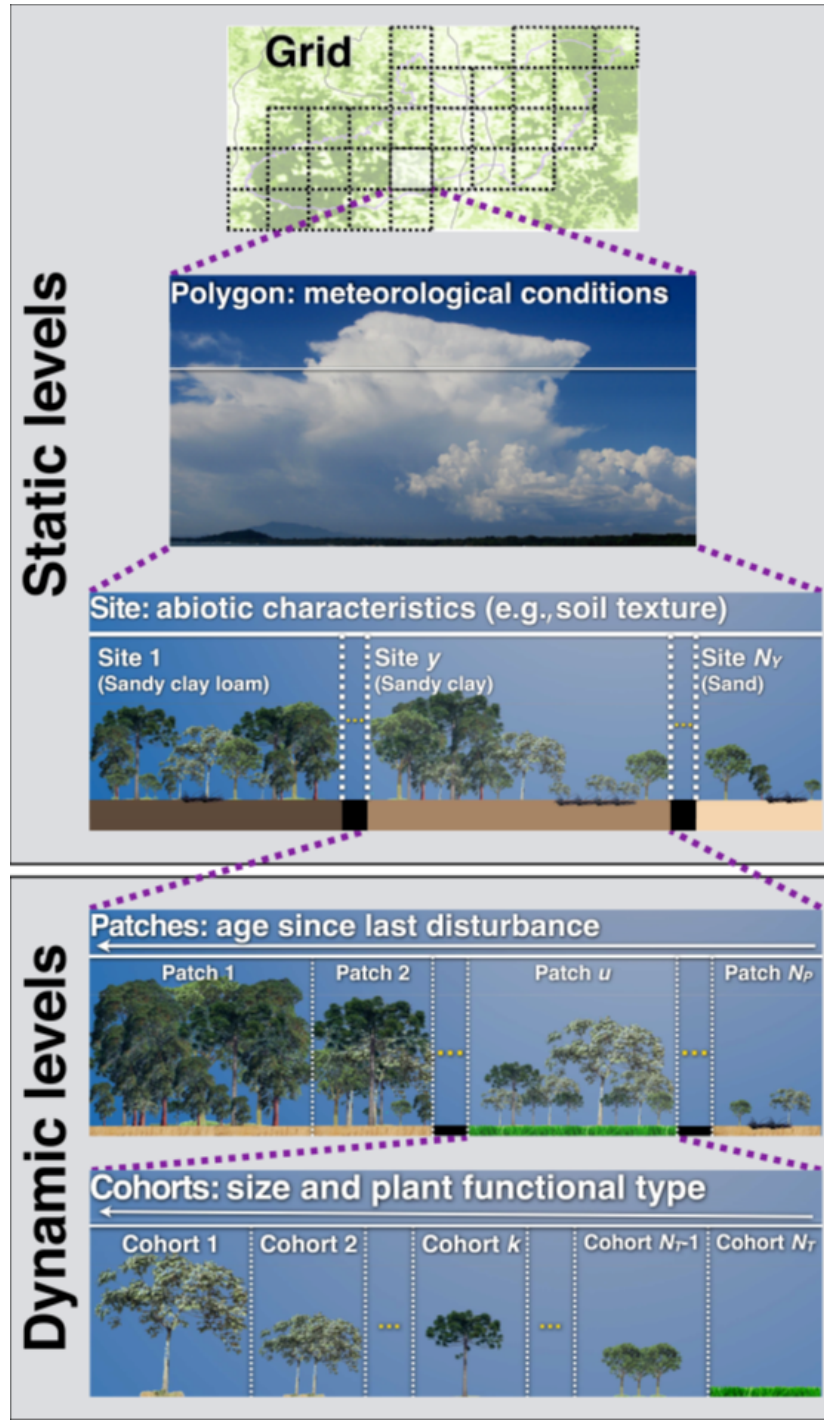


Figure 1.8: Example: the spatial multi-level grid structure of the ED2 vegetation model (Longo et al. 2019)

1.5.6 Model code, complexity and uncertainty

There is a gap between equations and how they are implemented in the actual model code. Also, a specific process can be implemented into an equation in various ways. Usually, large models also contain a “technical debt”, which means over the years,

multiple modelers have continued working on models and added code lines, but at some point, the code is so large that none of the developers still knows the entire code, resulting in persistent bugs or overlooked assumptions.

Models are always a simplification of the real world, but they tend to become overly complex.

More complex models (adding more processes) become more realistic, but we also add more sources of uncertainty. Therefore, we should choose our model carefully based on the research question we want to address.

1.5.7 Data

It is not possible to develop models without data. In general, the more data (multiple data sources), the better.

1.6 Modelling workflow and structure of the course

Vegetation modelling is a multidisciplinary field. This course will mainly focus on the mathematical formulation of processes and translating these equations into a working model.

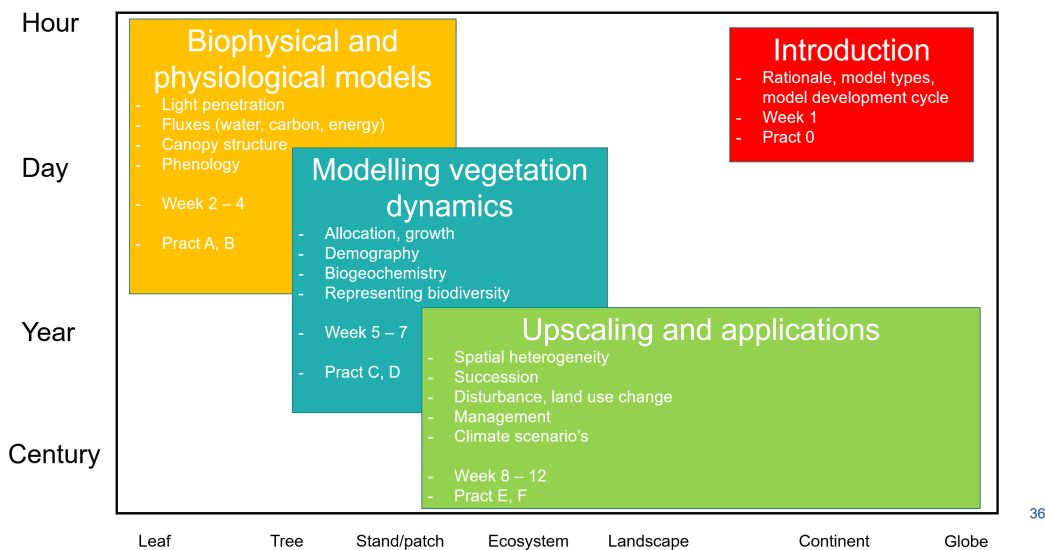


Figure 1.9: Progression through spatial and temporal scales throughout this course

The construction of a model is a continuous process – a model is never finished. As Figure 10 shows us, we start by describing our system in the form of equations, then running the computer program to characterize the model, perform parameter estimation and interpretation, and then apply it to other locations and validate against independent data.

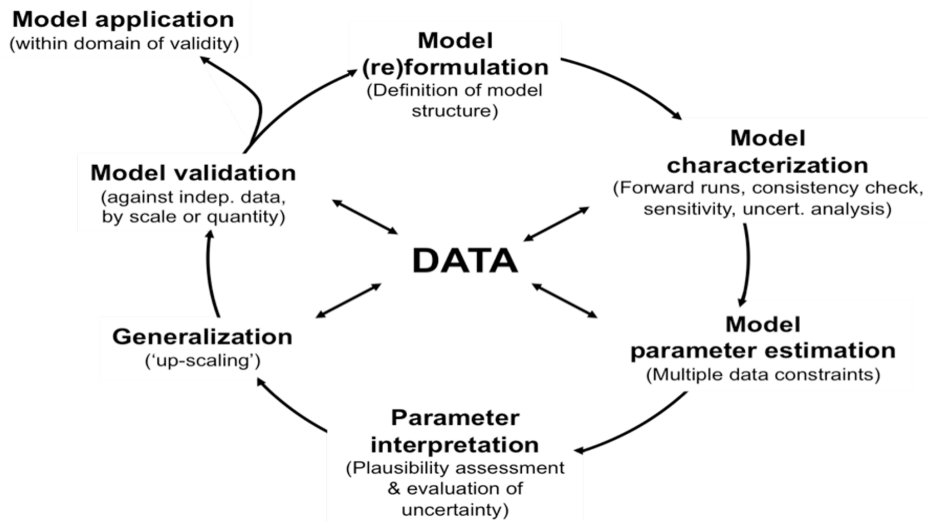


Figure 1.10: Model data fusion in every step of the model development cycle (Williams et al. 2009)

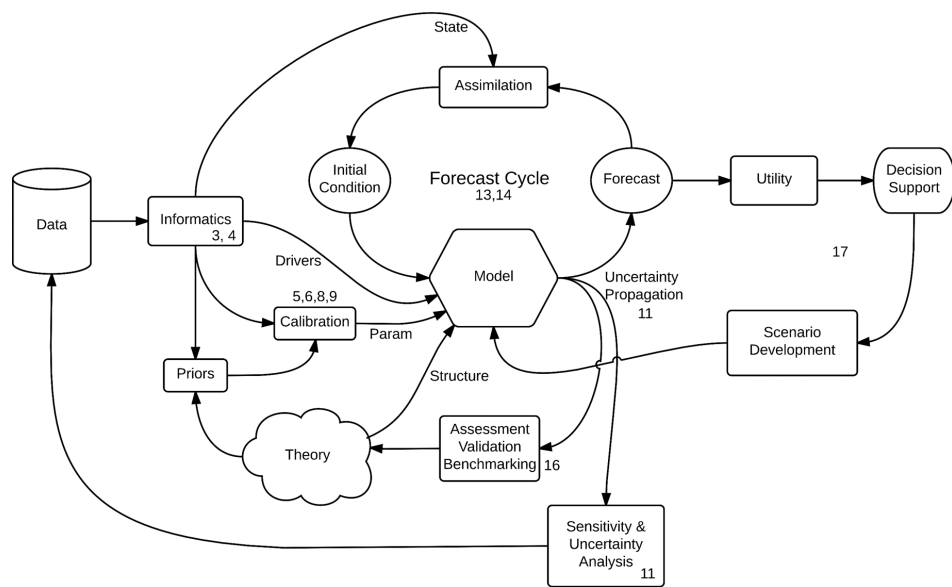


Figure 1.11: Methodological workflow of model data fusion (Dietze: Ecological Forecasting)

Part I

Biophysical and physiological models

Chapter 2

Modelling plant basic processes

2.1 Photosynthesis models

Photosynthesis is a process that takes place in all plants on earth. There is a huge variability in photosynthesis rates in space and time because of environmental variations (weather/climate) and properties of the vegetation (species composition, structure).

2.1.1 Refreshing the basic knowledge

Leaf processes that are discussed in this lecture occur at the small spatio-temporal timescale (Figure 1.9), but have an important impact on ecosystem functioning on the long term, for example: photosynthesis.

- Carbon assimilation (Photosynthesis) and water loss (Transpiration) are regulated by stomatal closure (Figure 2.1).
- Leaf temperature is the result of the energy balance at the leaf level which is tightly regulated by transpiration, and thus will impact photosynthesis.

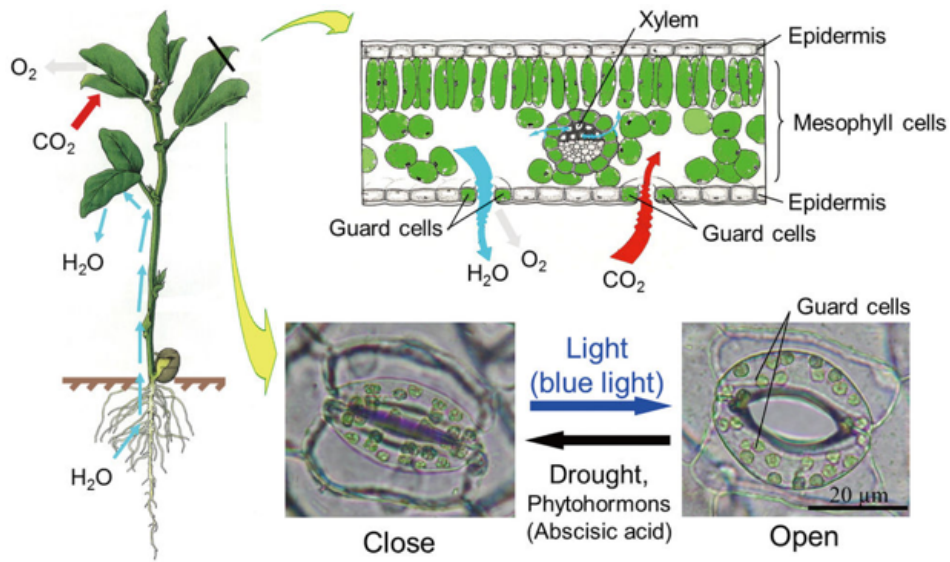


Figure 2.1: Leaf level processes transpiration and photosynthesis are strongly inter-linked and both regulated by stomatal conductance

Carbon assimilation follows two main reactions:

- Light harvesting (chlorophyll): the use of light to convert molecules into higher energy molecules through the photosystems
- Carbon fixation: converting CO_2 into sugars

The RuBisCO (ribulose-1,5-diphosphate carboxylase/oxygenase) enzyme plays an essential role for the carboxylation and oxidation reactions, while light harvesting is essential to regenerate the RuBP (ribulose 1,5-bisphosphate) -> see the Calvin cycle

Three different photosynthetic mechanisms:

- C3: PGA (phosphoglycerate) is the first product of CO_2 assimilation in the Calvin cycle, the entire process takes place in the mesophyll cell
- C4: PEP (phosphoenolpyruvate): make organic acids with a 4C skeleton, only 2% of all plants follow a C4 pathway. It represents only 5 % of the plant biomass on earth, but despite its scarcity, C4 plants account for around 23% of the terrestrial carbon fixation; they have the Kranz anatomy, with bundle sheath cells, process is separated between mesophyll and bundle sheet cells; The main advantage is that C4 plants have a higher CO_2 concentration in their bundle sheath cells, in which they also recycle CO_2 .
- CAM: will not be discussed in the models, here the CO_2 assimilation and CO_2 uptake are separated in time, plants adapted to very dry conditions. How to observe photosynthesis? Mainly done by leaf gas exchange measurements. This methodology measures the net CO_2 exchange of the leaf, which is the sum of the gross photosynthesis minus the respiration. The difference between these two fluxes is the net photosynthesis.

Photosynthesis reacts to different environmental factors (Figure 2.2).

- Light:** Assimilation increases with increasing light availability, but reaches saturation at higher light levels.
- Temperature:** Assimilation increases up to an optimum temperature. Beyond the optimal temperature there is a limitation of photosynthesis.
- VPD:** Assimilation is reduced with increasing VPD.
- Moisture:** Assimilation decreases with decreasing leaf water potential (drought stress), less turgor, stomates close.
- CO_2 :** Assimilation increases at elevated atmospheric CO_2 concentration, with saturation.
- Nutrients:** The more nitrogen a leaf contains (for example at the top of the canopy), the more CO_2 can be assimilated. Leaf N is a proxy of the amount of rubisco.

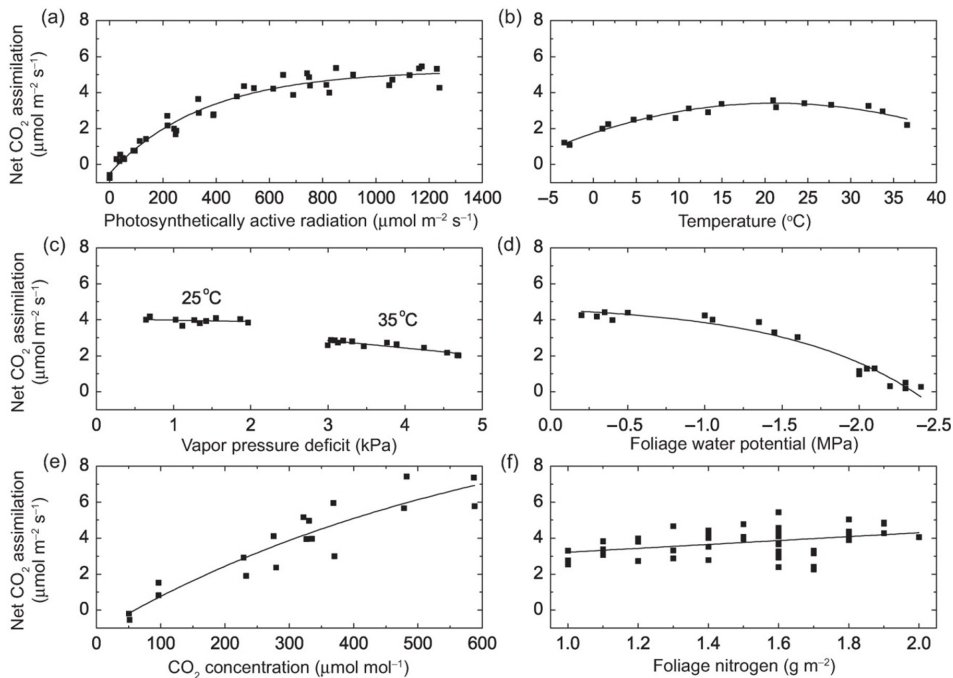


Figure 2.2: Net C assimilation in relation to (a) photosynthetically active radiation,(b) temperature, (c) vapor pressure deficit at 25°C and 35°C,(d) foliage water potential, (e) ambient CO_2 concentration, and (f) foliage water potential for jack pine trees (*Pinus banksiana*). Bonan (2019)

Different environmental parameters interact with each other (Figure 2.3).

Left: leaf respiration response is different than the photosynthesis response. Respiration keeps increasing with T, followed by a collapse (degrading enzymes), the respiration peak occurs at a higher temperature than the photosynthesis peak. The temperature response is also different for different CO_2 levels in the atmosphere.

Right: at lower light levels, the optimal temperature also drops. These interacting responses, need to be implemented in models!

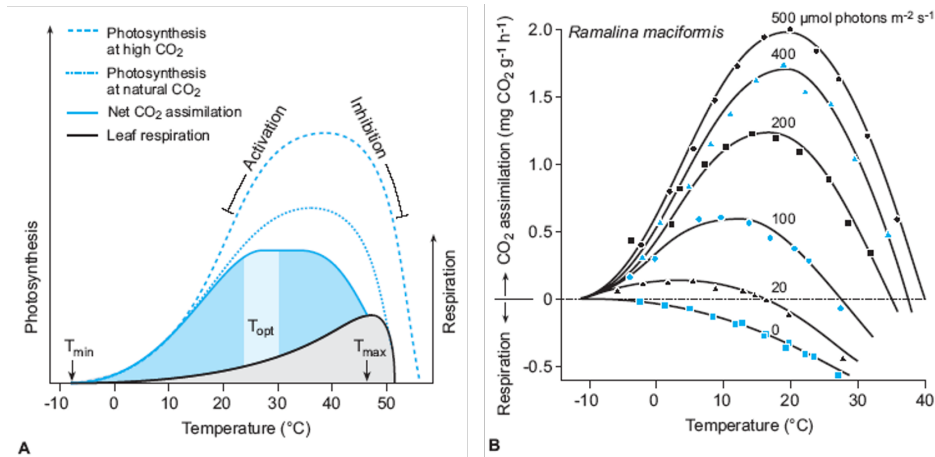


Figure 2.3: Temperature responses of photosynthesis, respiration and net CO_2 exchange, interaction with CO_2 concentration (A) and light (B) Schulze ()

2.1.2 C3 photosynthesis

2.1.2.1 Light response curve models

This model is based on light only. The slope of the curve (Figure 2.4) is the quantum yield, and describes the linear part of the curve.

Pmax: max photosynthesis rate, describes the level of the saturation plateau. Light compensation point, is that light level at which respiration equals the gross carbon uptake. Dark respiration: CO_2 released in the dark by respiration. This curve is described based on measurements on plants, and formulated as a mathematical equation.

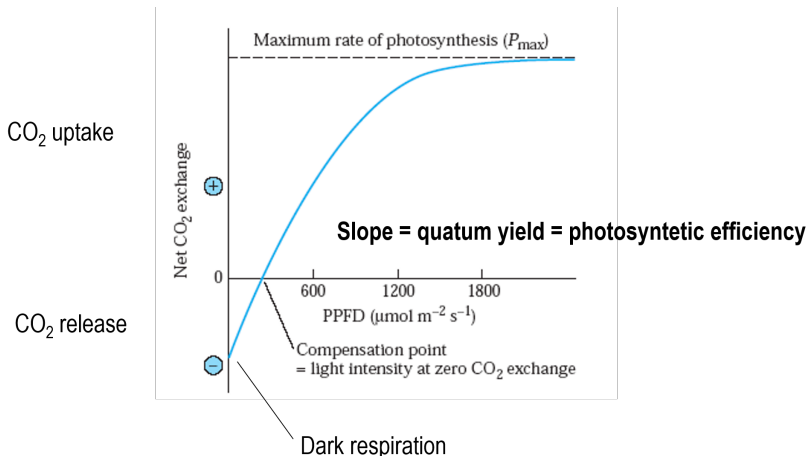


Figure 2.4: Conceptual figure of a leaf-level light response curve

In a second approach the light response is described as a co-limitation, a response with two phases: (1) light limitation and (2) light saturation (linear increase and plateau). Such a co-limitation is described by the non-rectangular hyperbola formula below

(Figure 2.5). The formula has two parameters: A_{max} (max photosynthesis rate) and E (quantum yield). The theta factor adapts the curve shape.

Disadvantages of these light response curve models: they are measured on a specific plant in specific conditions, and only applicable under the same conditions for the same plant, on the same location. They are only used in empirical studies, not really applicable for prognostic models.

$$\theta \cdot A^2 - (E \cdot I + A_{max})A + E \cdot I - A_{max} = 0$$

with θ the curvature of the light response curve, A the assimilation rate in $\text{micromol m}^{-2} \text{s}^{-1}$, and I the incident radiation in $\text{micromol m}^{-2} \text{s}^{-1}$.

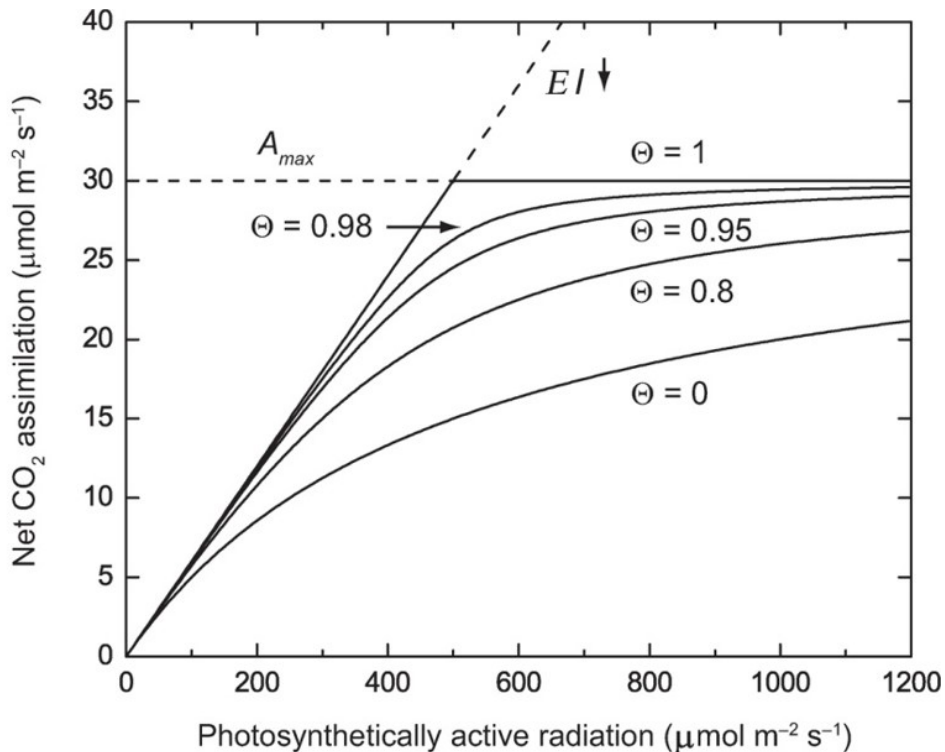


Figure 2.5: Co-limitation illustrated for photosynthetic response to light. The two dashed lines show the rates A_{max} and EI . The solid lines show the co-limited rate. (Bonan 2019)

2.1.2.2 Light use efficiency models

Light use efficiency (LUE) is the slope of the linear part of the light response curve. These LUE models calculate photosynthesis at a larger scale (GPP) by multiplying the available amount of light with a light use efficiency factor (Figure 2.6). Other factors are introduced to mimic saturation at stressful environmental conditions (e.g. temperature, soil water availability, atmospheric drought). These are empirical models, with its advantages and disadvantages (see above). Often used for large scale, remote sensing-based simulations of photosynthesis, as I can be measured by satellites.

$$GPP = LUE \cdot I \cdot f_1(T) \cdot f_2(\theta) \cdot f_3(D)$$

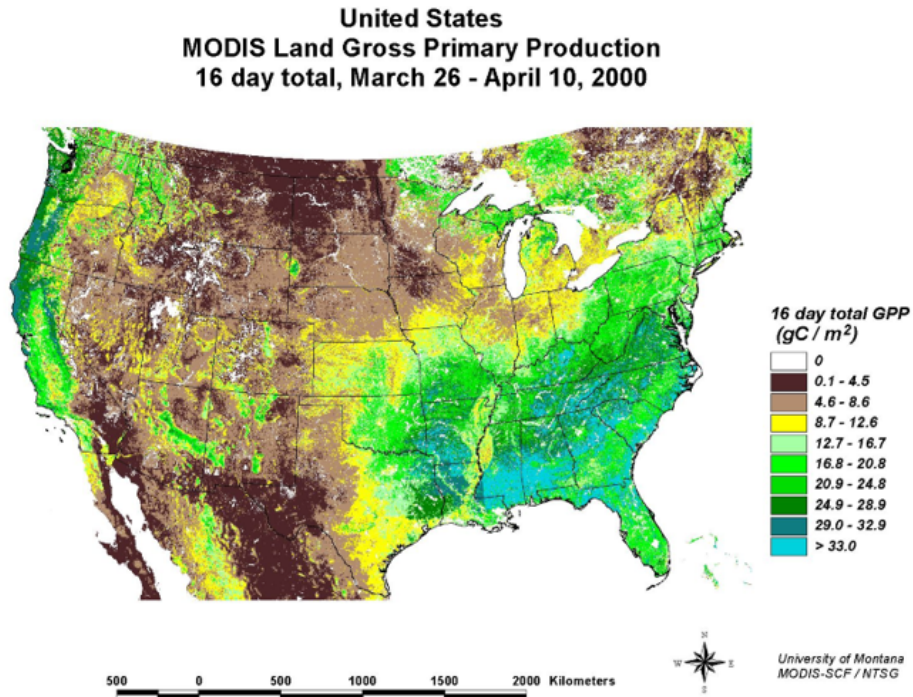


Figure 2.6: MODIS based GPP map of the US, based on a LUE model.

2.1.2.3 The Farquhar, Von Caemmerer and Berry model (FvCB)

Photosynthesis is not only limited by light response. Diffusion of CO_2 from atmosphere into the leaf plays an important role. This is driven by the CO_2 concentration gradient between the atmosphere and the substomatal space. Diffusion depends on the boundary layer of the leaf, the area of the stomatal cavity as well as the resistivity of the chloroplast membrane (Figure 2.7).

The FvCB model was developed in 1980, and is currently included in the large majority of (global) vegetation models. The FvCB model describes the rubisco kinetics, rubisco regeneration, the carboxylation rate when rubisco is saturated and the carboxylation rate when rubisco is limited.

See Bonan's book, Chapter 11.1

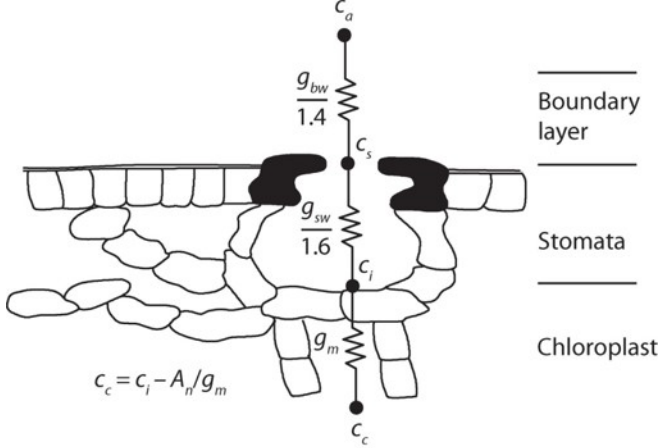


Figure 2.7: Diffusion of CO_2 from free air across the leaf boundary layer and through stomata to the intercellular space. Diffusion to the chloroplast is additionally regulated by mesophyl conductance. (Bonan 2019)

The net photosynthesis is described as the carboxylation rate V_c minus the photorespiration V_o and dark leaf respiration R_d .

$$A_n = V_c - 0.5V_o - R_d$$

with A_n , V_c , V_o and R_d in $\text{micromol m}^{-2} \text{s}^{-1}$.

V_c corresponds to the rate of carboxylation by RUBISCO, which follows a Michaelis-Menten response function:

$$V_c = \frac{V_{cmax} C_i}{C_i + K_c \left(1 + \frac{O_i}{K_o}\right)}$$

with V_{cmax} the maximum rate of carboxylation in $\text{micromol CO}_2 \text{m}^{-2} \text{s}^{-1}$, C_i and O_i the intercellular CO_2 and O_2 concentrations in micromol mol^{-1} , and K_c and K_o are the Michaelis-Menten constants for CO_2 and O_2 in micromol mol^{-1} , respectively.

Photorespiration releases 0.5 mole of CO_2

$$V_o = \frac{V_{omax} O_i}{O_i + K_o \left(1 + \frac{C_i}{K_c}\right)}$$

It exists a specific C_i concentration value at which oxygenation compensates carboxylation and no net CO_2 uptake occurs in the absence of mitochondrial respiration. We call this value the CO_2 compensation point Γ^* . Net assimilation can be reformulated as:

$$A_n = \left(1 - \frac{\Gamma^*}{C_i}\right) V_c - R_d$$

The term $1 - \Gamma^*/C_i$ accounts for CO_2 release during photorespiration.

In the simplest form of the model, carboxylation V_c is limited by either the activity of RUBISCO (CO_2 limitation), denoted by the rate W_c , or by the regeneration of RuBP (light limitation), denoted by the rate W_j , so that:

$$A_n = \left(1 - \frac{\Gamma^*}{C_i}\right) \min(W_c, W_j) - R_d$$

with W_c describing the Michealis-Menten kinetics of carboxylation.

$$W_c = V_{cmax} \frac{C_i}{C_i + K_c(1 + O_i/K_o)}$$

and W_j represents the rate of regeneration of the RuBP by light. It depends on electron transport rate, as such the photosynthesis light response is integrated in the Farquhar model.

$$W_j = J \frac{C_i}{4C_i + 8\Gamma^*}$$

J is the electron transport rate (in $\text{micromol m}^{-2} \text{s}^{-1}$) for a given irradiance.

The rate of electron transport is related to absorbed photosynthetically active radiation (PAR), the maximum electron transport rate and the amount of light utilized by photosystems. Different expressions can be found for J . We will use the most common form:

$$J = \frac{I_{abs} + J_{max} - \sqrt{(I_{abs} + J_{max})^2 - 4\theta_j I_{abs} J_{max}}}{2\theta_j}$$

with I_{abs} the absorbed PAR in $\text{micromol photon m}^{-2} \text{s}^{-1}$, θ_j is the curvature of the light response curve and J_{max} the maximal electron transport rate in $\text{micromol m}^{-2} \text{s}^{-1}$.

The absorbed incident radiation by the photosystem II (I_{abs}) depends on leaf absorptance α_l and the quantum yield of photosystem II ϕ_{PSII} :

$$I_{abs} = \frac{\phi_{PSII}}{2} \alpha_l I_r$$

where I_r is PAR in $\text{micromol m}^{-2} \text{s}^{-1}$, and only one half of absorbed light reaches the PSII.

In summary, a common form of the FvCB model represents photosynthetic CO₂ assimilation for plants utilizing the C3 photosynthetic pathway as limited by (i) A_c – the rate of Rubisco catalyzed carboxylation when RuBP is saturated (called Rubisco-limited photosynthesis because of its dependence on maximum Rubisco activity as set by V_{cmax}); and (ii) A_j – the rate of RuBP regeneration by light absorption and electron transport as determined by J_{max} (RuBP regeneration-limited, or light-limited, photosynthesis).

When accounting for the CO₂ compensation point, the general Farquhar model is thus written as follows:

$$A_n = \min(A_c, A_j) - R_d$$

with

$$A_c = V_{cmax} \frac{C_i - \Gamma^*}{C_i + K_c \left(1 + \frac{O_i}{K_c}\right)}$$

$$A_j = \frac{J}{4} \left(\frac{C_i - \Gamma^*}{C_i + 2\Gamma^*} \right)$$

Figure 2.8 illustrates the response of assimilation to intercellular CO_2 and light. We neglect TPU limitation (A_p) in the models we consider here. TPU limitation only occurs at elevated intercellular CO_2 .

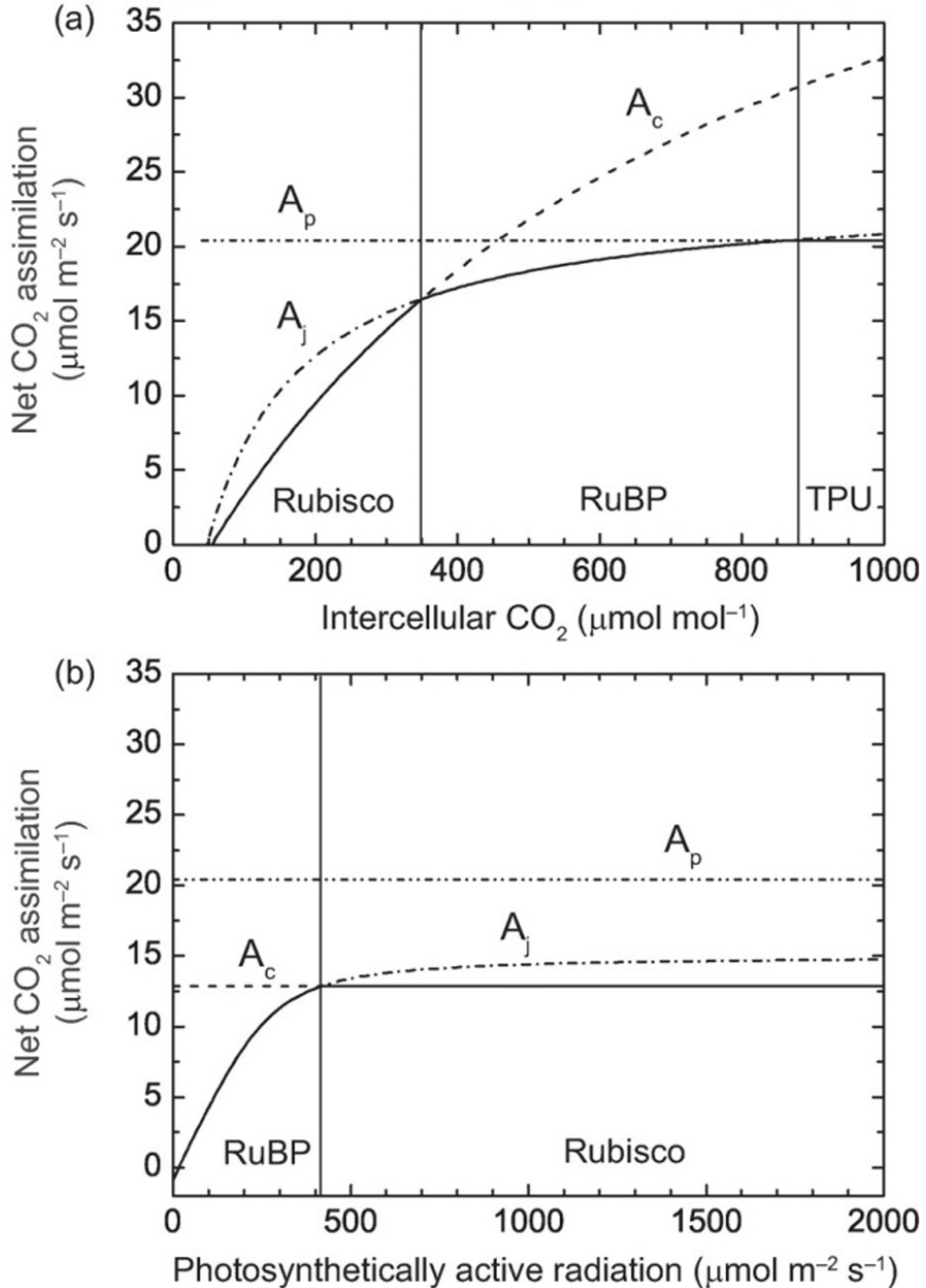


Figure 2.8: Simulated responses of C3 photosynthesis in relation to (a) intercellular CO_2 (at $I_{\downarrow} = 2000$ micromol $\text{m}^{-2} \text{s}^{-1}$) and (b) photosynthetically active radiation (at $c_i = 266$ micromol mol^{-1}). (Bonan 2019)

As an alternative formulation a co-limitation analytical model can be used. In this case we don't use the minimum equation of the original Farquhar model, but take both limitations into account simultaneously in the following equation.

$$\Theta_A A^2 - (A_c + A_j)A + A_c A_j$$

2.1.3 Parameter and temperature dependencies

See Bonan's book, Chapter 11.2

The FvCB model requires 6 physiological parameters: K_c , K_o , Γ^* , V_{cmax} , J_{max} and R_d . Additionally, the specification of electron transport requires θ_j and ϕ_j . Values for K_c , K_o and Γ^* are defined by the biochemistry of Rubisco and are similar among species. On the opposite, V_{cmax} is species-dependent.

V_{cmax} is a key parameter in the FvCB model. It directly determines the Rubisco-limited rate A_c and, for C3 plants, also influences the RuBP regeneration-limited rate A_j through its covariation with J_{max} . The maximum rate of carboxylation has a wide range among plant species and environments and is tightly linked to leaf nitrogen content; reported values for 109 species of C3 plants vary from less than 10 to more than 150 $\text{micromol m}^{-2} \text{s}^{-1}$.

Because J_{max} is well correlated to V_{cmax} , it can be approximated to:

$$J_{max} = 1.67V_{cmax}$$

R_d is also well correlated to V_{cmax} and can be approximated as:

$$R_d = 0.015V_{cmax}$$

The parameters K_c , K_o , Γ^* , V_{cmax} , J_{max} and R_d vary with temperature (Figure 2.9). The instantaneous responses of photosynthesis and respiration to temperature are driven by their underlying enzymatic responses. When warmed from low temperature, the enzymes involved in photosynthesis and respiration increase their activity as described by the Arrhenius function:

$$f(T_l) = \exp\left[\frac{\Delta H_a}{298.15R}(1 - \frac{298.15}{T_l})\right]$$

where T_l is leaf temperature (in K), R is the universal gas constant ($8.314 \text{ J K}^{-1} \text{ mol}^{-1}$), and ΔH_a is the activation energy (J mol^{-1}). This function is normalized to 25°C (298.15 K). Parameter values measured at 25°C are multiplied by $f(T_l)$ to adjust for leaf temperature.

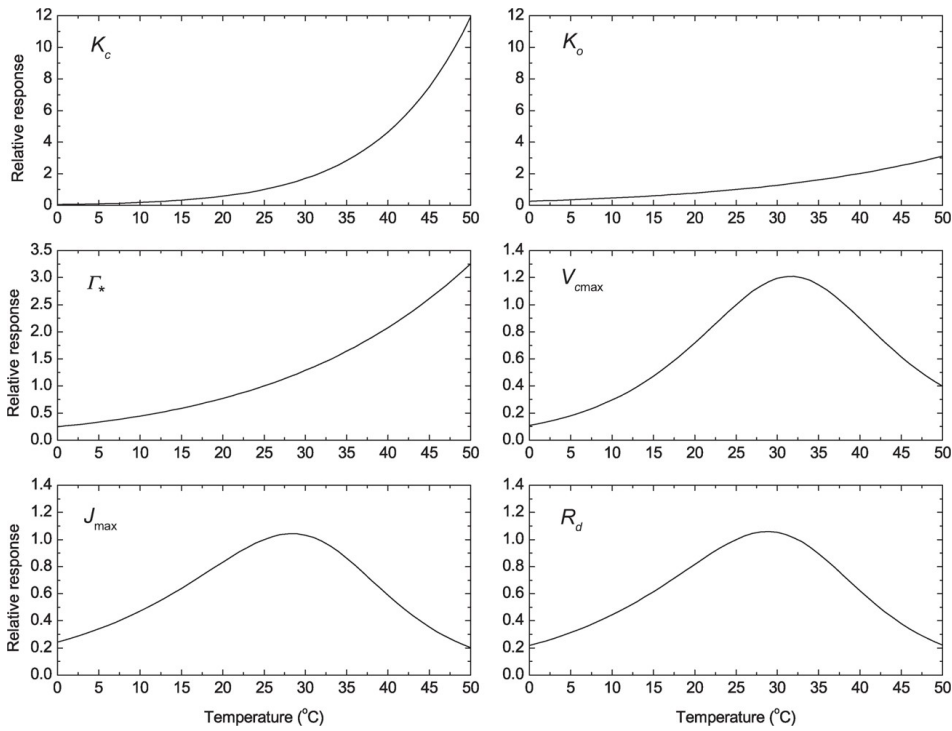


Figure 2.9: Relative temperature responses of the parameters of the Farquhar model (Bonan 2019)

The parameters V_{cmax} , J_{max} and R_d vary with temperature following the Arrhenius function but have a peaked response in which enzymatic activity increases up to a temperature optimum beyond which the reaction rate decreases when temperature is too high because of enzyme degradation. In this case, parameters such as V_{cmax} are written by:

$$V_{cmax} = V_{cmax25} f(T_l) f_H(T_l)$$

with V_{cmax25} the value of V_{cmax} at 25°C. The $f_H(T_l)$ function represents the thermal breakdown of biochemical processes:

$$f_H(T_l) = \frac{1 + \exp\left(\frac{298.15\Delta S - \Delta H_d}{298.15R}\right)}{1 + \exp\left(\frac{\Delta S T_l - \Delta H_d}{RT_l}\right)}$$

To correctly model photosynthesis over time, you should also take into account climate adaptation (acclimation): the temperature adaptation curve is different for the same species if they are grown under different climatic conditions.

Challenges with the Farquhar model: its parameter values are not well defined, or the values of the parameters are highly variable, depending on the type of plant or environmental conditions. V_{cmax} is highly variable over different leaves in the same tree, and on global scales. Which value should we use? -> V_{cmax} is scaling very well to photosynthesis, so V_{cmax} is often optimized with data available. However, by doing so you turn the model into an empirical model, so this should be avoided. The advantage we have, is that there are covariations between parameters (Figure 2.10) for

example the strong correlation between V_{cmax} and J_{max} -> you can describe J_{max} as a function of V_{cmax} , so you can remove one parameter from the model.

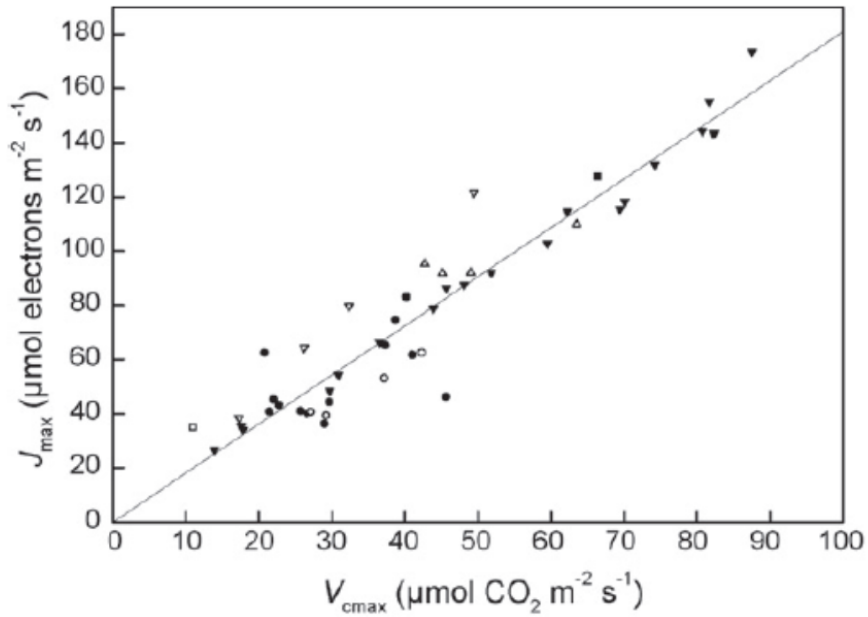


Figure 2.10: Linear relation between observed V_{cmax} and J_{max} values for Beech (Verbeeck et al. 2008)

V_{cmax} can also be calculated based on leaf nitrogen content. Some vegetation models model the N content of leaves, and simulated based on the V_{cmax} of the leaves. It's a linear relationship with two parameters. Some models also use more complex relations.

There are also attempts to propose average values per plant functional type.

$$V_{cmax25} = i_v + s_v \cdot N_a$$

The temperature functions also have dependence factors.

The Farquhar model has 4 input variables: O_i , C_i , PAR and T_{leaf} . Light depends on how the radiation is penetrating the canopy -> see lecture 3. O_i is assumed to be equal to the oxygen concentration in the atmosphere. Leaf temperature T_{leaf} is in most models assumed to be equal to air temperature or can be calculated based on an energy balance. C_i is calculated based on gas diffusion through the stomates -> you need an extra model to fully simulate the behavior of the stomates.

Definition	Equation
Rubisco-limited assimilation	$A_c = \frac{V_{cmax} (c_i - \Gamma_*)}{c_i + K_c (1 + o_i/K_o)}$
Light-limited assimilation	$A_j = \frac{J}{4} \left(\frac{c_i - \Gamma_*}{c_i + 2\Gamma_*} \right)$
Gross photosynthesis	$A = \min(A_c, A_j)$ (no colimitation) $\Theta_A A^2 - (A_c + A_j)A + A_c A_j$ (colimitation)
Net photosynthesis	$A_n = \min(A_c, A_j) - R_d$
Electron transport rate	$\Theta_j J^2 - (I_{PSII} + J_{max})J + I_{PSII} J_{max}$
PSII light utilization	$I_{PSII} = \frac{1}{2} \Phi_{PSII} \alpha_l I^l$
Maximum carboxylation rate	$V_{cmax} = V_{cmax25} \cdot f(T_l) \cdot f_H(T_l)$
Maximum electron transport rate	$J_{max} = J_{max25} \cdot f(T_l) \cdot f_H(T_l)$ $J_{max25} = 1.67 \cdot V_{cmax25}$
Leaf respiration	$R_d = R_{d25} \cdot f(T_l) \cdot f_H(T_l)$ $R_{d25} = 0.015 \cdot V_{cmax25}$
Michalis-Menten constant, CO_2	$K_c = K_{c25} \cdot f(T_l)$
Michalis-Menten constant, O_2	$K_o = K_{o25} \cdot f(T_l)$
CO_2 compensation point	$\Gamma_* = \Gamma_{*25} \cdot f(T_l)$
Arrhenius function	$f(T_l) = \exp \left[\frac{\Delta H_a}{298.15 - R} \left(1 - \frac{298.15}{T_l} \right) \right]$
High temperature inhibition	$f_H(T_l) = \frac{1 + \exp \left(\frac{298.15 \Delta S - \Delta H_a}{298.15 - R} \right)}{1 + \exp \left(\frac{T_l \Delta S - \Delta H_a}{T_l - R} \right)}$

Figure 2.11: Equations of the full Farquhar model

2.1.4 C4 photosynthesis

See Bonan's book, Chapter 11.7

The behaviour of the C4 and C3 models is really different

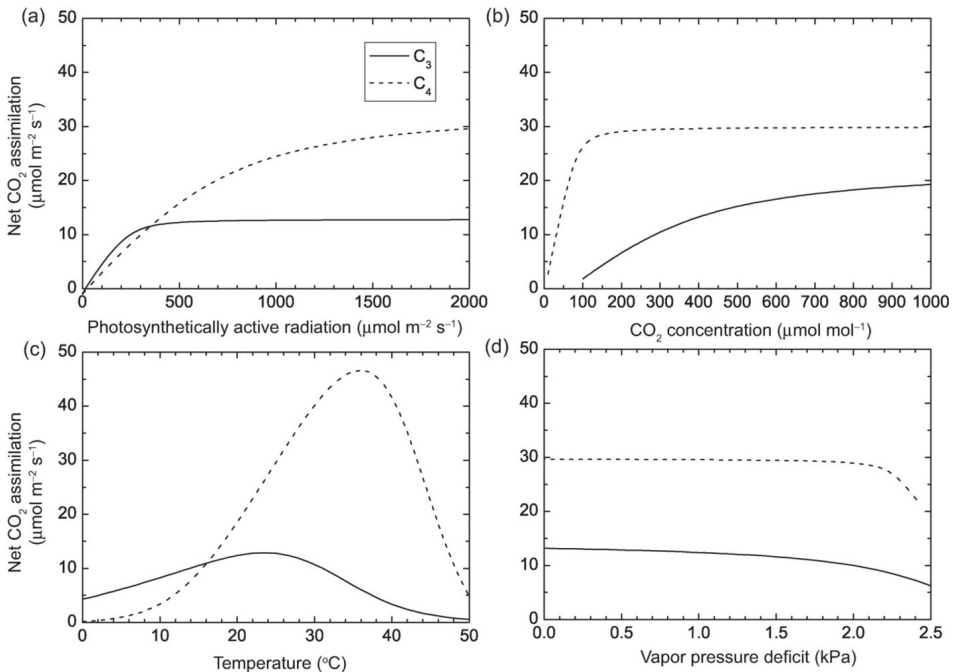


Figure 2.12: Comparison of C3 and C4 photosynthesis in response to (a) photosynthetically active radiation, (b) ambient CO_2 concentration, (c) leaf temperature, and (d) vapor pressure deficit. In this figure, stomatal conductance is calculated using the Ball-Berry model and c_i is obtained from the diffusion equation

2.2 Stomatal models

2.2.1 Refreshing the basic knowledge

Guard cells are transporting ions actively and passively into/out of the cells in order to open or close the stomates by adapting the turgor in the guard cells. The stomatal conductance represents how easy it is for a CO_2 molecule to diffuse in or out of the stomates. The higher the conductance, the easier the transfer. Stomatal models are needed for transpiration, leaf temperature and $CO_2 \rightarrow$ key process in the model. Stomatal conductance for CO_2 is lower than that of water as the molecule is a bit bigger. Sometimes expressed as a resistance in models that use the electric analog concept (Figure 2.13).

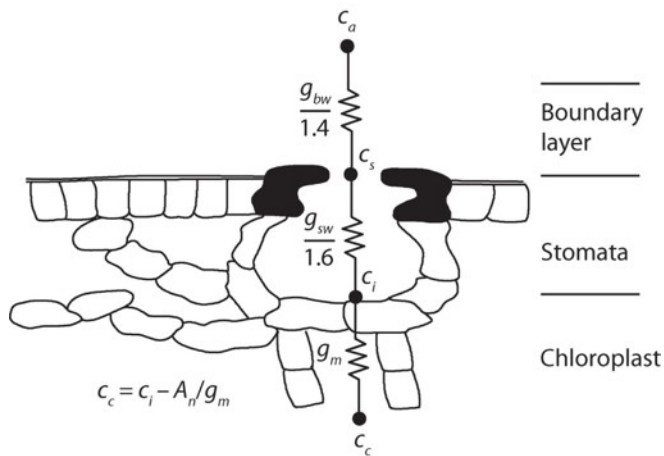


Figure 2.13: Diffusion of CO_2 from free air across the leaf boundary layer and through stomata to the intercellular space. Diffusion to the chloroplast is additionally regulated by mesophyl conductance. (Bonan 2019)

Plants constantly balance their physical and biochemical limitation, by adjusting their stomatal conductance.

Photosynthesis is expressed as a diffusion process. Photosynthesis flux is a range through the circuit of figure 2.13. A_n can be described as the flux going from the atmosphere to the internal part of the leaf, or as the flux going from the internal part of the leaf into the cell, or a combinations of the two methods.

$$A_n = \frac{g_{bw}}{1.4} (C_a - C_s) = \frac{g_{sw}}{1.6} (C_s - C_i) = \frac{1}{1.4g_{bw}^{-1} + 1.6g_{sw}^{-1}} (C_a - C_i)$$

with g_{sw} and g_{bw} the stomatal and boundary layer conductance for water, respectively, in $\text{mol m}^{-2} \text{ s}^{-1}$. the ratio 1.6 correspond to the molecular mass ration between H_2O and CO_2 to convert conductance to water to CO_2 . C_a , C_s and C_i are the CO_2 concentration from the atmosphere, at leaf surface and in the stomatal cavity, respectively.

Stomatal conductance is also dependent on environmental conditions (Figure 2.14). There is a saturated response to light, an optimum for temperature, strong response to

VPD, stomata close when VPD is too high, and there is a response to the leaf water potential. Again, there is interaction between the different environmental conditions.

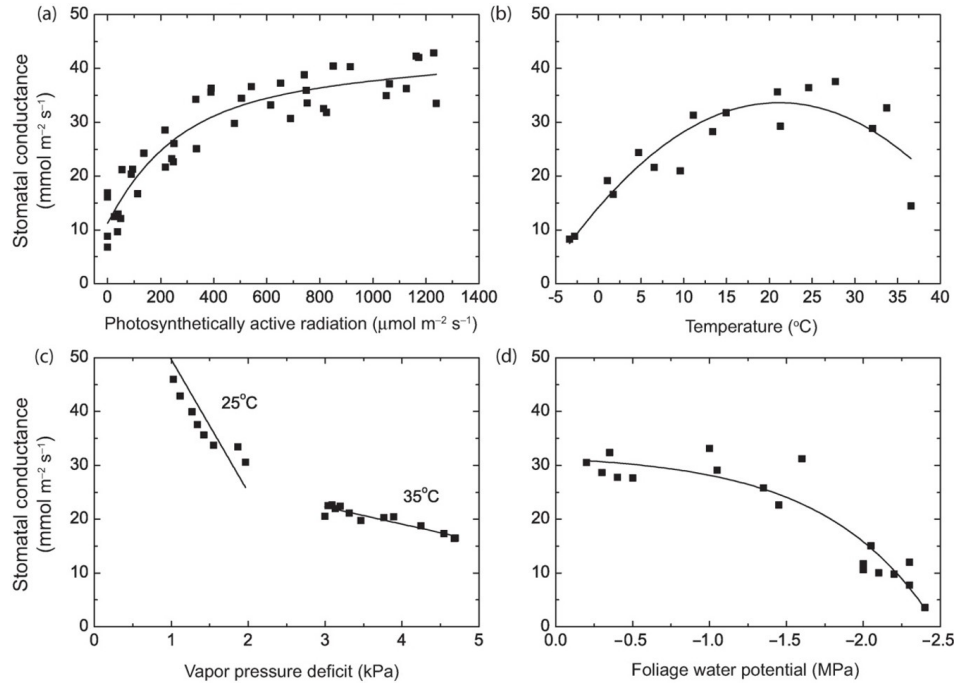


Figure 2.14: Observed responses of stomatal conductance for *Pinus banksiana*. (Bonan 2019)

If the air is dry stomates close to avoid losing too much water

accounting for all these effects makes it complex stomatal conductance is quite linear with photosynthesis

We have three unknowns in the combined photosynthesis-diffusion equations but only two equations: we need an extra equation to describe stomatal conductance to be able to solve for the unknowns. 4 Possibilities discussed: see below.

2.2.2 Empirical multiplicative models

This is an empirical approach. The actual stomatal conductance is calculated based on the max stomatal conductance (G_{smax}) multiplied by correction factors for light, temperature, etc. between 0 and 1. It is based on observations. G_{smax} is species dependent. There is no link with the carbon cycle/photosynthesis, this is why it is not used anymore in the global vegetation models as part of the earth system models of the IPCC

$$g_{sw} = g_{smax} f(I^\downarrow) f(T_l) f(D_l) f(\Phi_l) f(C_a)$$

2.2.3 Semi-empirical photosynthesis-based models

Semi-empirical models are still commonly used in vegetation models and are based on the linear relation between stomatal conductance and photosynthesis (Figure 2.15).

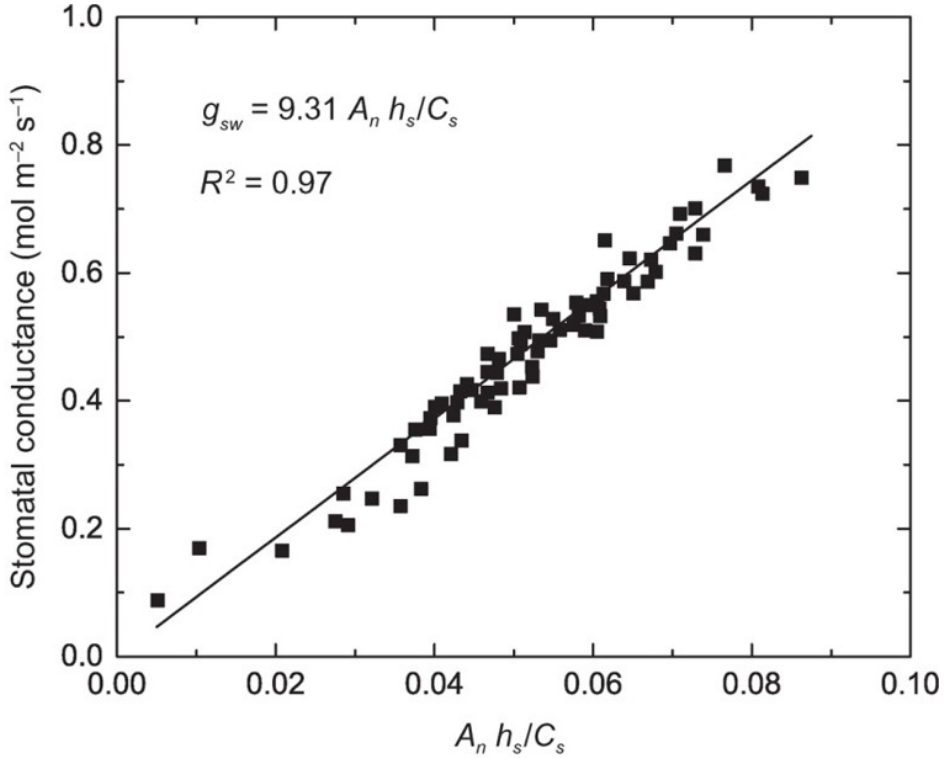


Figure 2.15: Relationship between stomatal conductance and $A_n h_s/C_s$ for soybean.(Bonan 2019). On the x axis, the photosynthesis is depicted, but multiplied by relation humidity and CO_2 concentration at the leaf surface.

Ball-Berry model: Stomatal conductance is calculated based on photosynthesis, relative humidity and CO_2 concentration at the leaf level. This is the third equation needed to solve the problem. The model needs observations to determine the parameters (i.e. semi-empirical). Plants adapt their stomatal opening to maintain a constant C_i/C_a ratio, or the CO_2 concentration in the leaf and the concentration outside the leaf (atmosphere). As the model uses the CO_2 concentration at the surface of the leaf, we also need the boundary layer conductance.

$$g_{sw} = g_0 + g_1 \frac{A_n}{C_s} h_s$$

with g_0 and g_1 empirical model parameters, A_n the net assimilation, C_s the CO_2 concentration at the leaf surface and h_s the relative air humidity.

The model becomes a combination of multiple non-linear equations, which cannot be solved analytically. Some model try to find an analytical solution by simplifying the equations, this gains calculation speed. Other models use numerical techniques based on the scheme below (Figure 2.16): we start with an initial guess of C_i and do enough

iterations until the guess converges with the outcome value of the model. This approach is slower as multiple iterations have to be calculated, which is time-consuming. This model still needs empirical input to determine the Ball-Berry parameters. SO it is a theoretical model that needs empirical constraints.

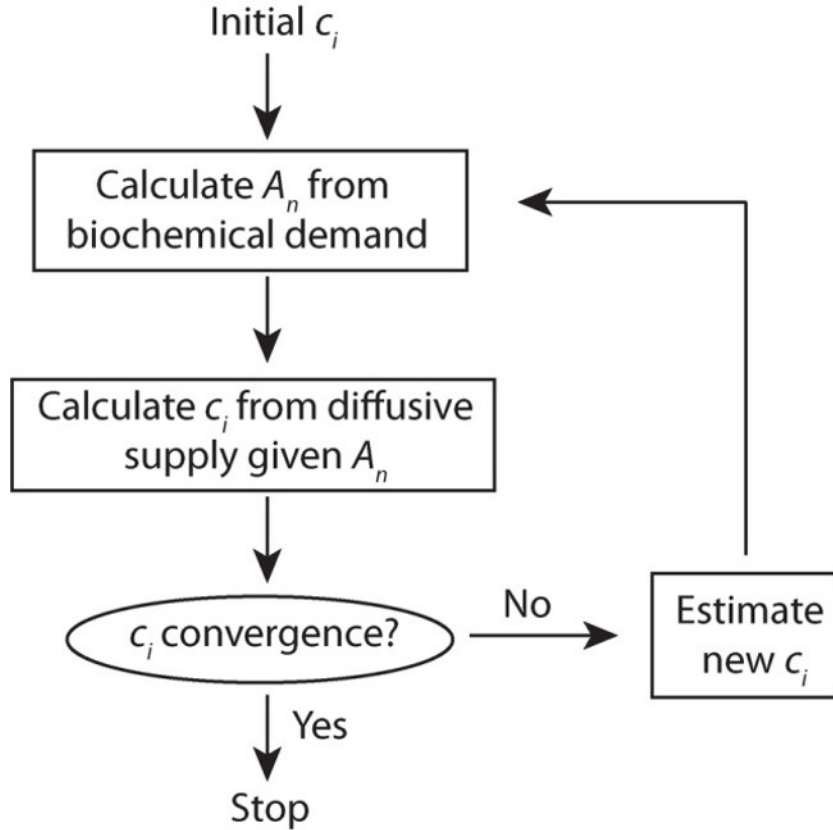


Figure 2.16: Flow diagram of the iterative procedure to numerically calculate c_i . (Bonan 2019)

2.2.4 WUE models and optimality theory

Not discussed in detail, but this approach is increasingly implemented in models as it overcomes the use of empirical parameters. They are based on ecological theories. Here, the stomatal conductance is optimized by maximizing the water use efficiency. We assume that plants try to optimize the benefit of photosynthesis with the cost of water loss. Stomatal conductance is not described explicitly by an equation, but it emerges from the model. The concept of calculations is shown in figure 2.17: we start with an assumed stomatal conductance value, we go through all calculations and in the end calculate WUE and do the same for an increased/decreased stomatal conductance, and check what the gain of WUE is.

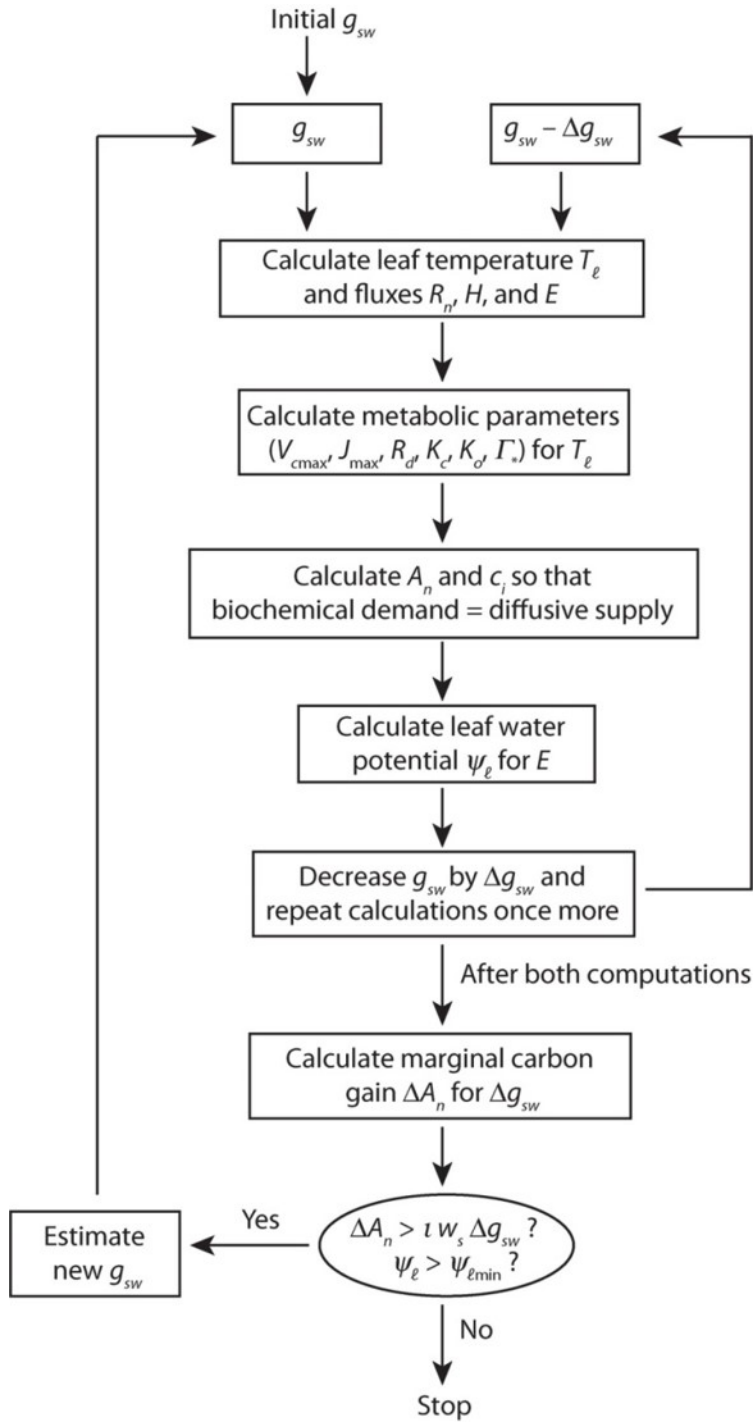


Figure 2.17: Flow diagram of leaf flux calculations to numerically solve for stomatal conductance that optimizes water-use efficiency.(Bonan 2019)

2.2.5 Soil drought stress

Basic models do not account for soil drying. Many models add an additional factor that describes the soil wetness. The beta factor varies between 0 (wilting point) and 1 (field capacity), with different courses between the two extremes (see figure 2.18). Various

vegetation models differ in the way they account for this factor. Some models apply this factor on Vcmax other model integrated the factor in the stomatal equation. Some models simulate leaf figure (Figure 2.18) or soil (Figure 2.19) water potentials. Species have a different response to the leaf water potential. First there is no impact, species have a tolerance, but after threshold, a decrease in photosynthesis occurs.

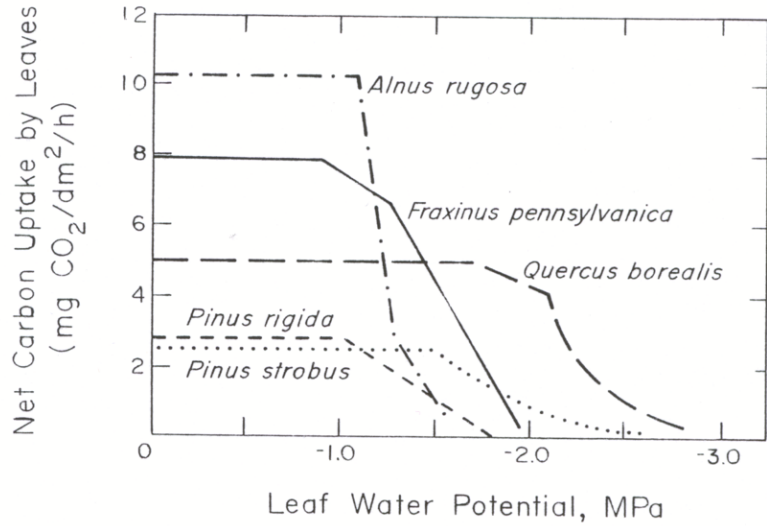


Figure 2.18: Leaf carbon uptake in response to leaf water potential for multiple tree species.

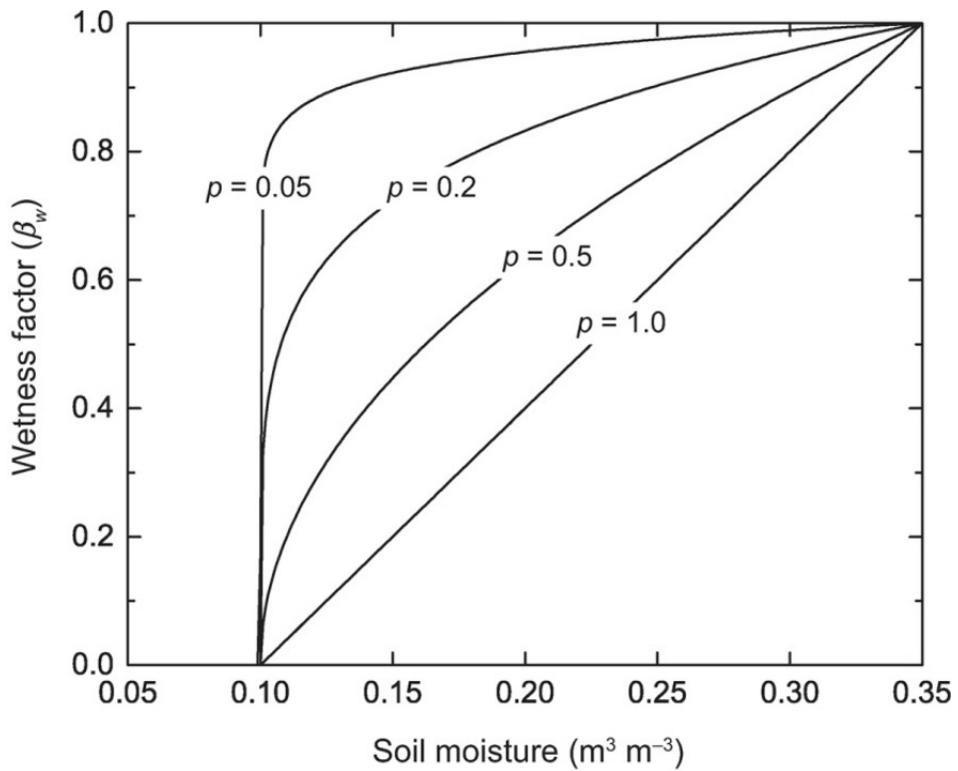


Figure 2.19: Soil moisture wetness factor in relation to volumetric water content. (Bonan 2019)

2.2.6 Hydraulic models

These models are originally developed to simulated plant water relations of individual plants/trees (Figure 2.20). The model simulates the water transport through the trees. Challenging to apply at the large scale. Isohydric species: maintain their leaf water potential, independently from the soil water potentials.

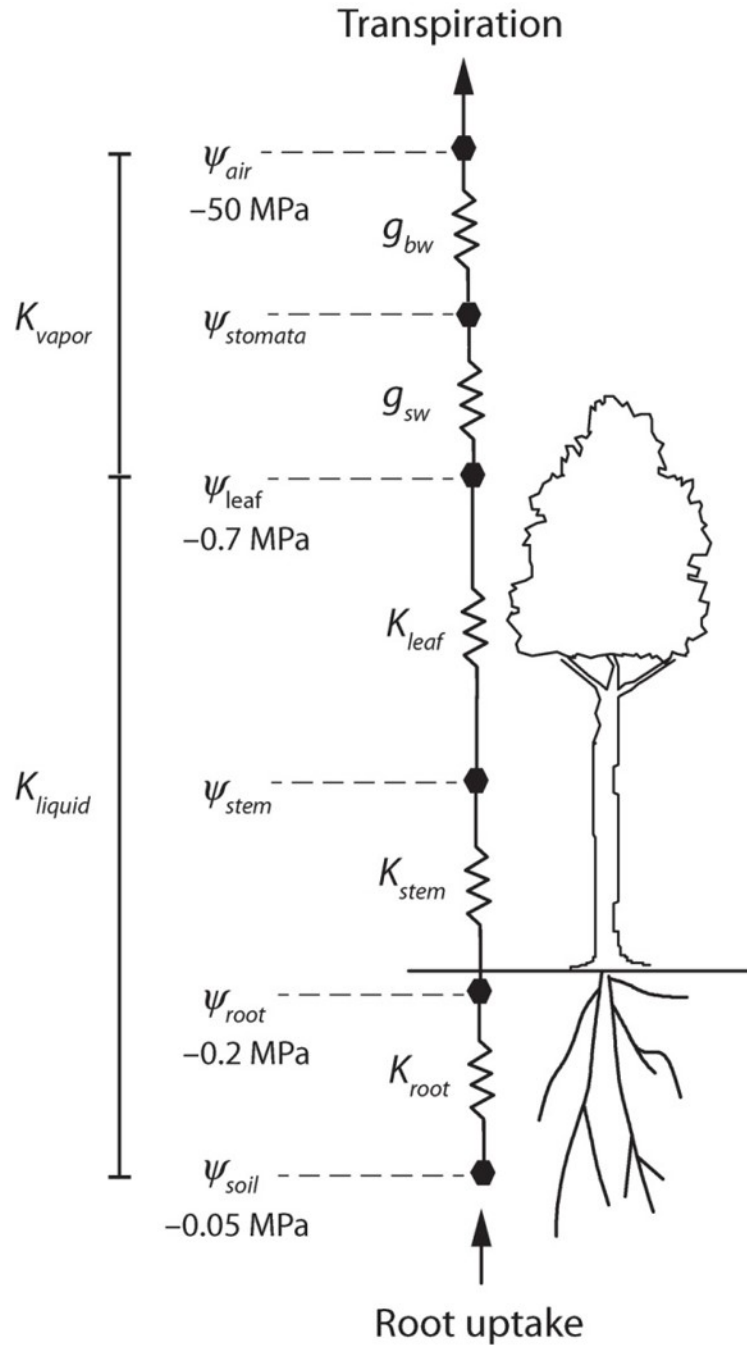


Figure 2.20: Flow of water and representative water potentials along the soil–plant–atmosphere continuum. Also shown are conductances along the hydraulic pathway.(Bonan 2019)

Soil-Plant-Atmosphere (SPA) model: combines a plant hydraulic model with photosynthesis model, and they interact with each other. Such models have a high level of complexity (Figure 2.21).

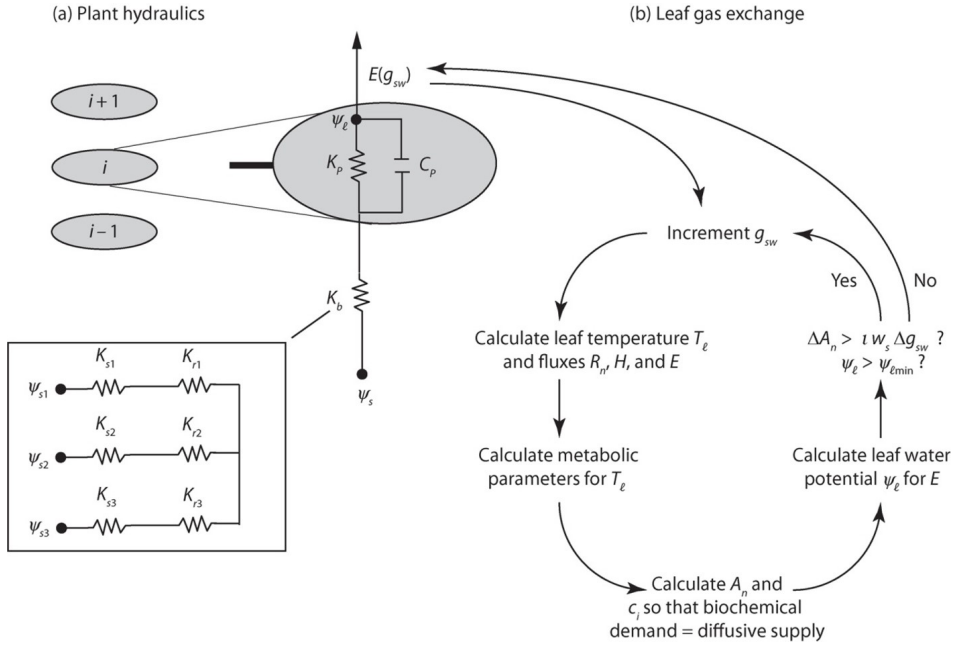


Figure 2.21: Depiction of (a) plant hydraulics and (b) leaf gas exchange in the Soil–Plant–Atmosphere (SPA) model. SPA is a multilayer canopy model.(Bonan 2019)

Different models give different results (Figure 2.22): full line: Ball-Berry, dashed line: other models. The shapes of the curves are similar, but there is a difference between them.

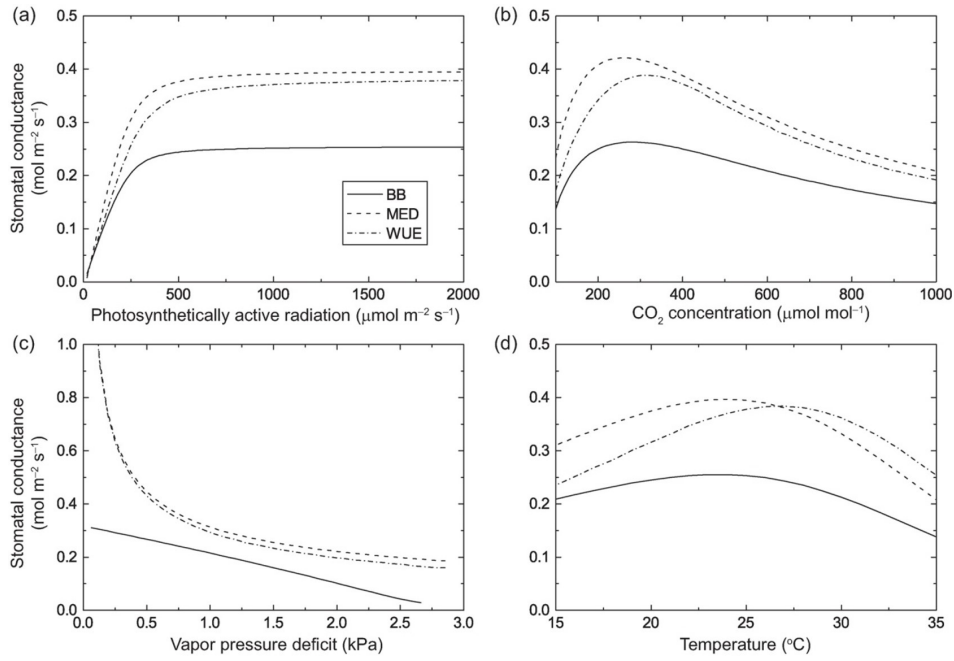


Figure 2.22: Simulated stomatal responses for various modelling approaches. (Bonan 2019)

2.3 Upscaling from leaf to canopy

In this chapter we discussed all processes at the leaf level, but in a forest or other vegetation type, every leaf is different. E.g. the difference between sun and shade leaves.

Figure 2.23: different responses for shade and sun leaves: big differences! on the long term there is also genetic adaptation to the environmental conditions they are living in.

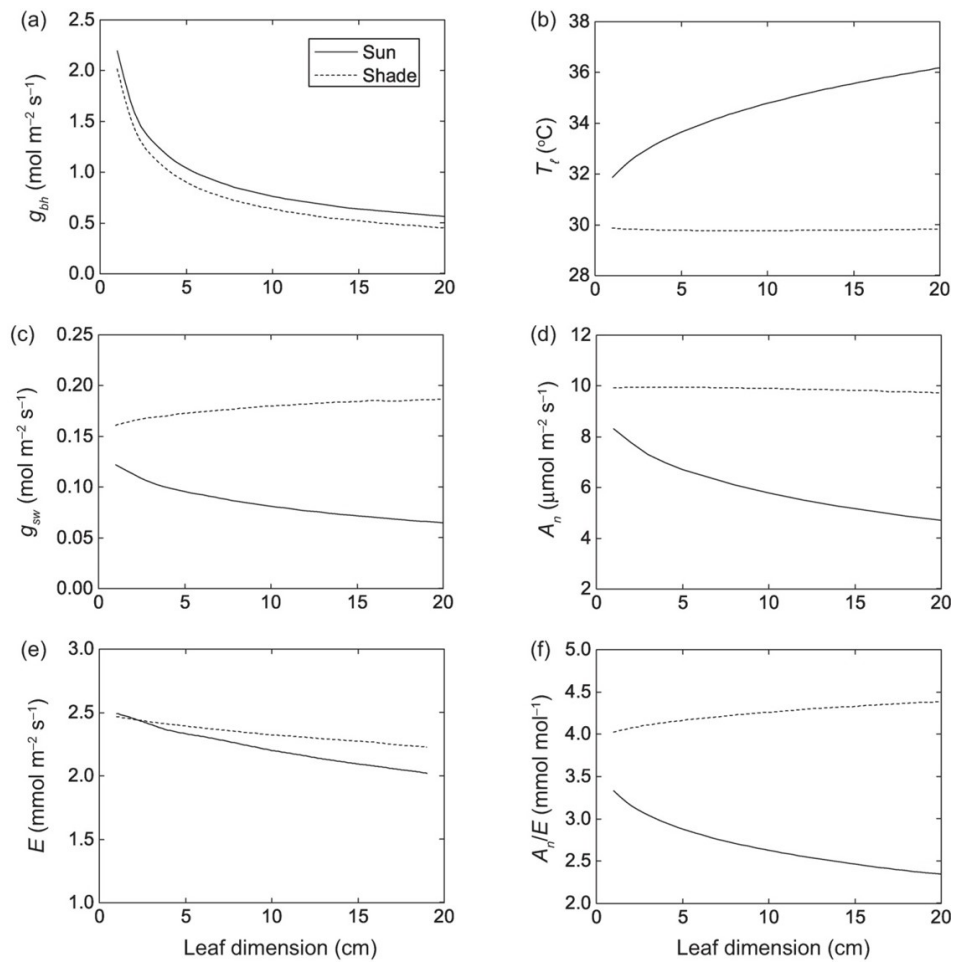


Figure 2.23: Leaf microclimate and boundary layer processes in relation to leaf dimension for sun and shade conditions.(Bonan 2019)

If you calculated GPP (Figure 2.24), you need to take into account that leaves are not the same all over the world -> see coming lectures.

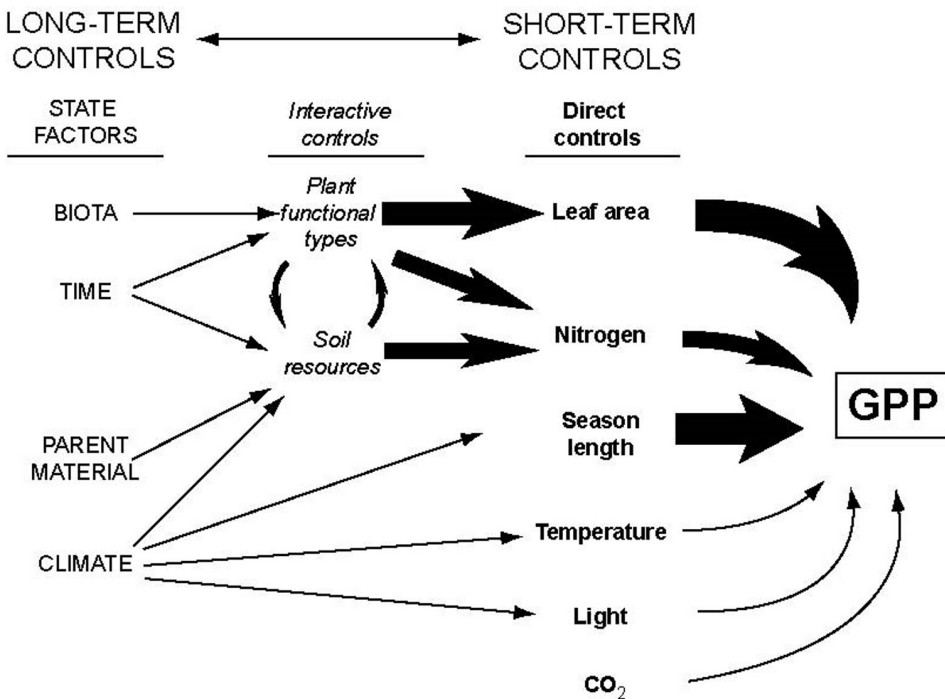


Figure 2.24: Controlling factors on ecosystem GPP. (Chapin)

Thicker arrow means a stronger influence on ecosystem long term GPP.

2.4 Case studies

2.4.1 Case study 2.1 Ozone impact on global GPP

Sitch et al. 2003: Indirect radiative forcing of climate change through ozone effects on the land-carbon sink

The evolution of the Earth's climate during the 21th century depends on the rate at which CO_2 emissions are removed by the ocean and land carbon cycles . To asses/simulate this removal, climate-carbon cycle models are used, but these typically neglect the impacts of changing atmospheric chemistry (e.g. CO_2 and ozone concentration). Ozone causes cellular damage inside leaves that adversely affects plant production and reduces photosynthesis. In this case study, a global land carbon cycle model - modified to include the effect of ozone and to account for interactions between ozone and CO_2 - is used to estimate the impact of projected changes in ozone levels on the land-carbon sink.

Large scale model. It used a similar leaf gas exchange model as discussed above, but they added an extra equation that reduces stomatal conductance depending on the ozone concentrations (higher ozone levels reduce photosynthesis). The impact of the ozone is highest in tropical zones, with reductions up to 30%, which will impact the CO_2 storage of tropical forests.

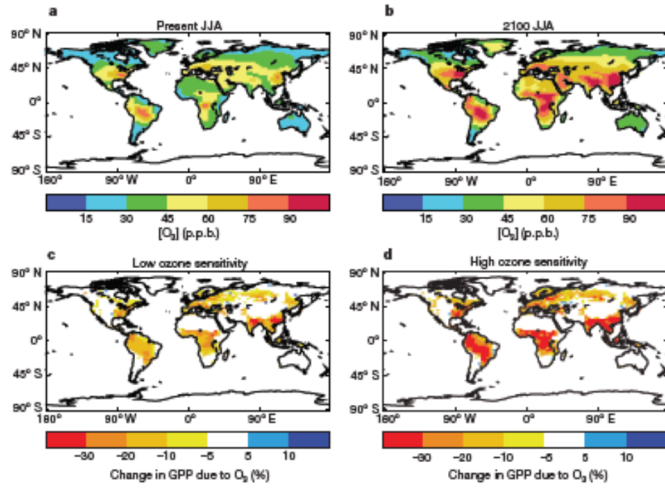


Figure 2.25: Simulated global GPP reduction in response to current and future atmospheric ozone concentrations

2.4.2 Case study 2.2 Drought impact on rainforest GPP

Fisher et al. 2007: The response of an Eastern Amazonian rain forest to drought stress: results and modelling analyses from a throughfall exclusion experiment

Climate change projections predict harsher droughts in the Amazon rain forest which could change the amount of CO_2 the forest can absorb, creating a positive feedback system. A lack in appropriate data and process-level understanding creates uncertainty in predicting the forest gas exchange as a response to drought. In this paper these two problems are addressed: new and better data is collected with a TFE experiment and a model (SPA) that predicts sap-flow with soil moisture data is created and fitted to the TFE data. This model is then validated with other independent data.

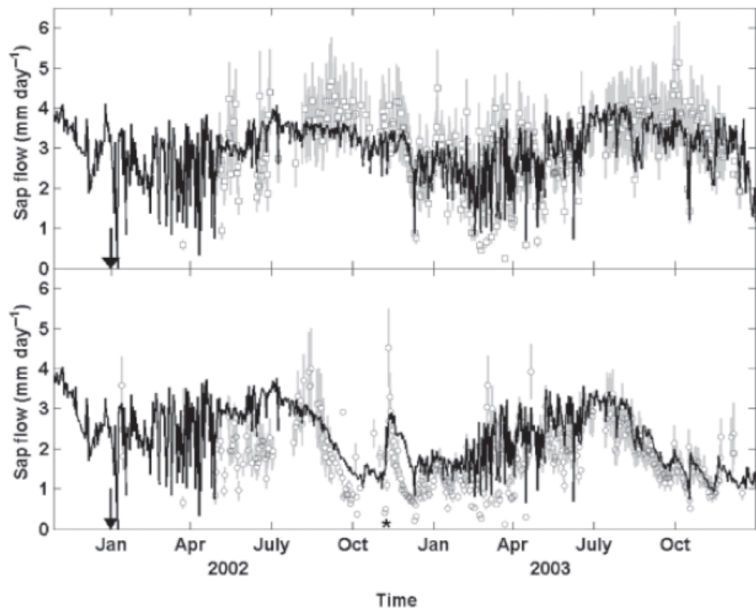


Figure 2.26: Simulated (SPA model) and observed sapflow for a drought experiment in the Amazon; Fisher et al. 2007

Figure 2.27 shows the simulations of g_s and GPP, black: control plot, grey: dry plot.

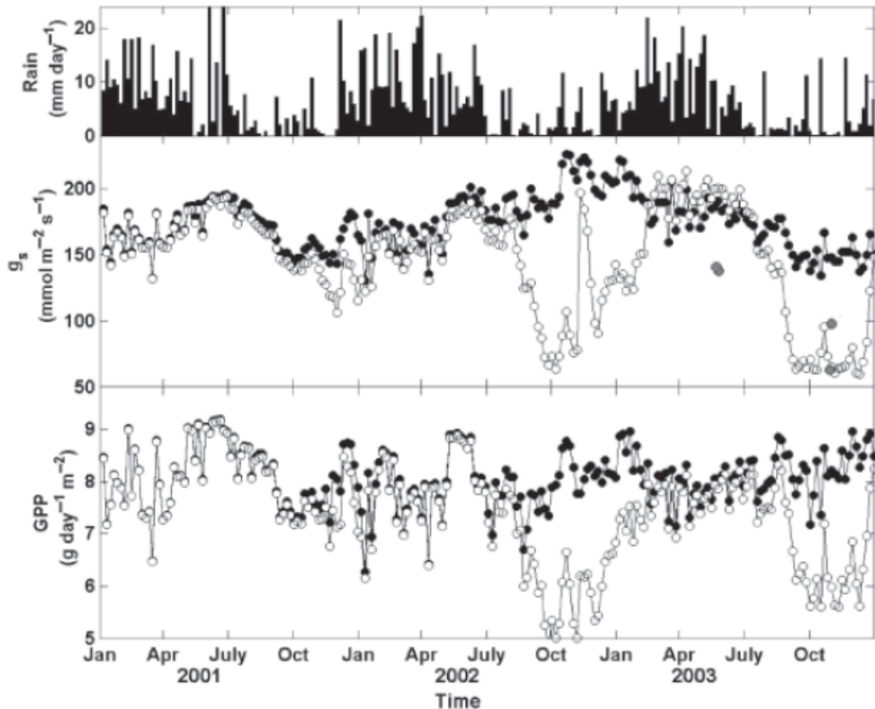


Figure 2.27: Simulated (SPA model) g_s and GPP for a drought experiment in the Amazon. Fisher et al. 2007

Conclusions: this model worked better than empirical models, which really predict

a collapse of the system. This model is doing better because it simulates the water transport through the tree. Models need to take into account deep rooting, trees do have access to water in the deep soil, even in the dry period.

Chapter 3

Modelling radiation, vegetation canopies, and energy balance

3.1 Introduction

This chapter deals with upscaling processes from leaf level to canopy level, but still on a (very) short timescale (~hours, sub-daily).

We want a model that is consistent over different scales. If we measure parameters at the leaf level and put those parameter values in our model, we want the results to be as consistent as possible with the data at the canopy scale, for example data from eddy covariance flux towers. Also the other way around, if we optimize model parameters based on flux tower measurements, we want the resulting leaf parameters to be as close as possible to the parameters observed in the field at leaf level.

We first refresh some basics on radiation. The sun emits shortwave radiation, the earth emits longwave radiation (invisible). Longwave radiation has its maximum intensity at a much longer wavelength and contains a much lower amount of energy (surface under the spectral intensity curve). The spectrum of wavelengths the sun emits is different when we measure it on the earth surface (compared to the spectrum at the top of the atmosphere, as the atmosphere absorbs some of the radiation, e.g. in the ultraviolet light and infrared light absorption takes place. Diffuse radiation (which indirectly reaches the surface) is more shifted towards the blue light, which is one of the wavelengths used by plants. On a sunny day, both diffuse and direct radiation reach the plants. Under full cloud cover, plants only receive diffuse radiation. 50% of the shortwave radiation is PAR (Photosynthetic Active radiation). PAR is typically expressed as a photon flux density (micromols of photons per m² per s). The lower the zenith angle (higher sun), the higher the PAR fraction in the diffuse and direct radiation that reaches the earth surface. The relative PAR fraction is higher in diffuse radiation.

Secondly, we need to refresh some basics on canopy structure parameters. The leaf area index (LAI) is the total leaf area per unit of ground area. Sometimes it is also defined as the total double-sided surface of the leaves (so the two sides of the leaf), but this is not commonly used. The projected leaf area depends on the orientation of the leaf. Vertically oriented leaves have a smaller projected leaf area than if they would be

horizontally oriented. Figure 3.1 shows a generalized example of the leaf area density distribution for different vegetation types. The peak of leaf area density is different depending on the vegetation type, with a peak higher in the vegetation for forests and more in the middle for grass. The total LAI is calculated by integrating the function $a(z)$ showed in figure 3.1 over the height. If you keep in mind that trees are higher than grass, it is clear that the total LAI will be bigger for trees than for grass.

$$\text{total LAI} = \int_0^{h_c} a(z) \cdot dz$$

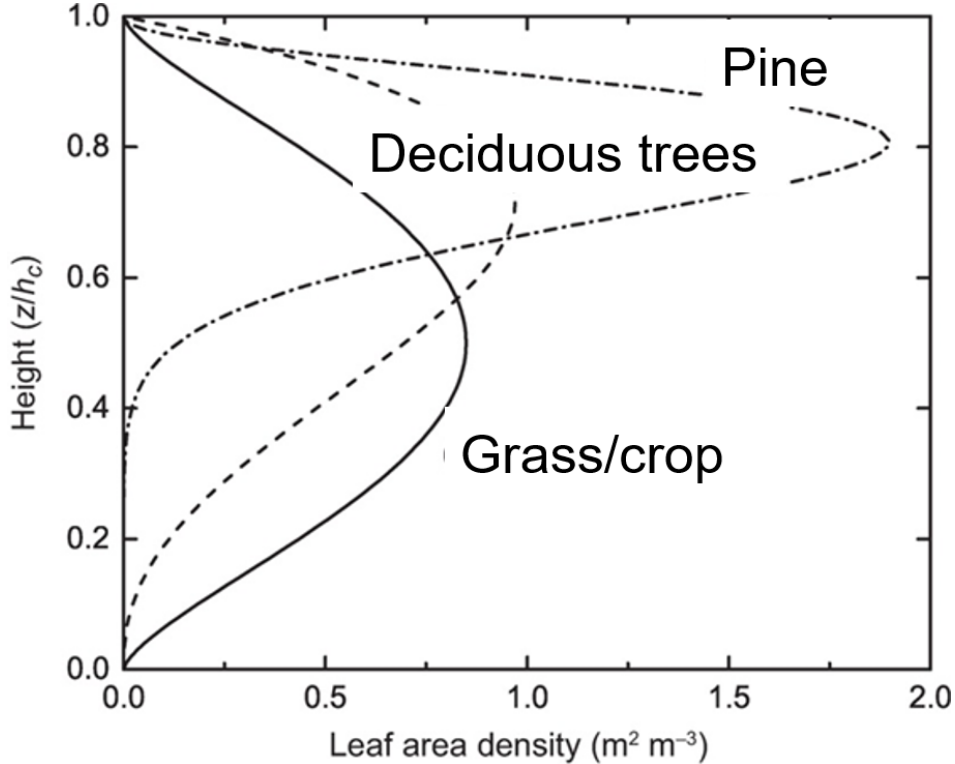


Figure 3.1: Generalized profiles of leaf area density in plant canopies. (Bonan)

The cumulative LAI represented in Figure 3.2 shows the LAI above a certain point in the canopy. It is calculated as the integral of the function between that point and the canopy height. This figure also shows the cumulative wood area index. If we make the sum of the LAI and the wood area index (WAI) we get the plant area index PAI, which is the total area of plant material per unit of ground area.

$$\text{cumulative LAI} = \int_z^{h_c} a(z) \cdot dz$$

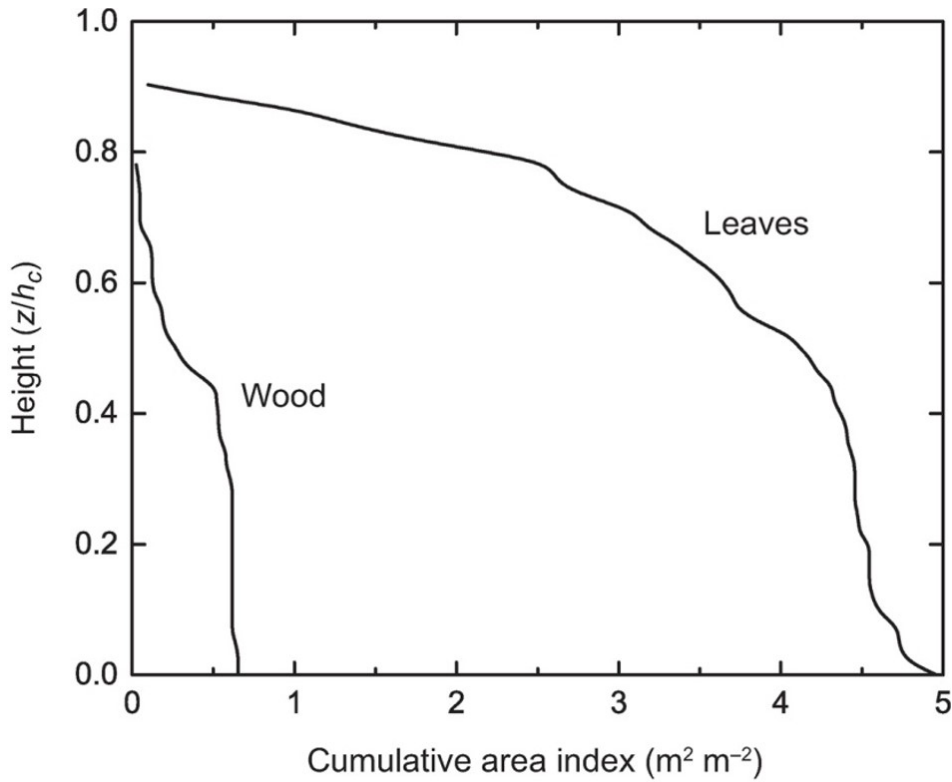


Figure 3.2: Cumulative LAI and WAI in a deciduous oak-hickory forest. (Bonan)

The leaf angle (distribution) is a key structural property of a vegetation canopy. It will largely determine how light will penetrate in the canopy, and is important for other processes, like precipitation interception. Figure 3.3 illustrates that the leaf angle can be expressed as the angle between the leaf and the horizontal plane, or as the angle between the zenith line and the line perpendicular to the leaf surface.

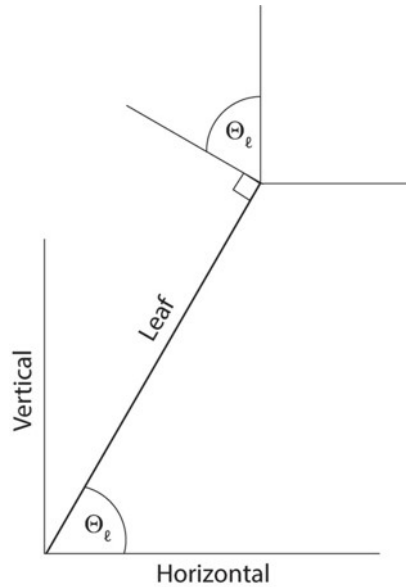


Figure 3.3: Illustration of a leaf (thick line) oriented at an angle Θ to horizontal. (Bonan)

Leaf angle distributions describe a probability density function of leaf angles of a plant or vegetation. Based on these distributions we can distinguish differences between plants and vegetation types. Planophile leaf angle distributions: most leaves are horizontally oriented; erectophile: most leaves are vertically oriented; plagiophile: average leaf inclination angle is 45° ; spherical: mostly used in modelling, corresponds somehow to erectophile, it is a kind of idealized form. These distributions are illustrated in Fig. 3.4. Subplot b indicates the cumulative distribution of the leaves.

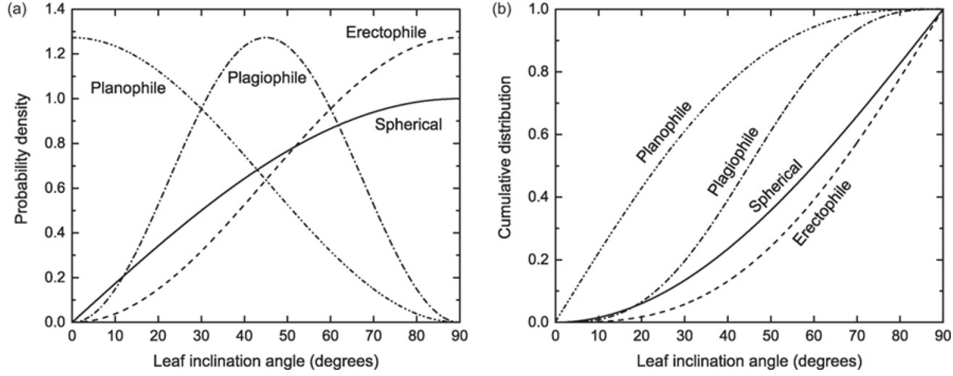


Figure 3.4: Planophile, erectophile, plagiophile, and spherical leaf angle distributions showing (a) the probability density function $f(\theta)$ and (b) the cumulative distribution $F(\theta)$. (Bonan)

Figure 3.5 illustrates the impact of leaf orientation in two crops on light penetration in the canopy of two crops (lower panel). The complexity of the vegetation plays an important role in where the light is intercepted and how much is intercepted (upper panel). In an erectophile leaf orientation, the light interception is more evenly spread through the vegetation than for a planophile profile, where most of the interception takes place at the center of the vegetation.

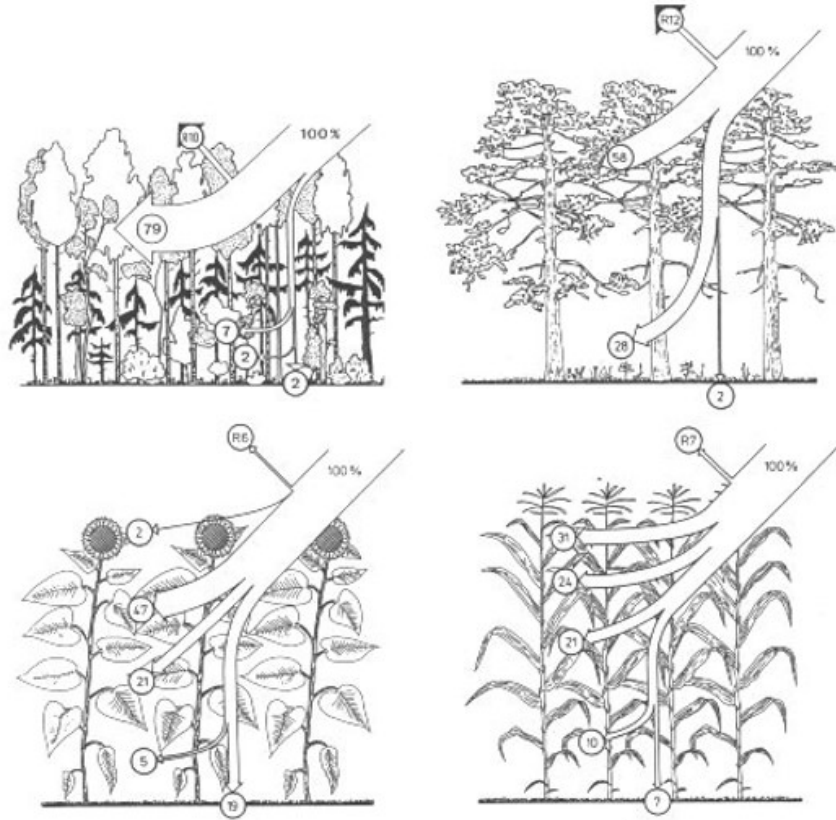


Figure 3.5: Illustration of leaf angle distributions and canopy architecture in general influences radiation attenuation in vegetation canopies.

Light extinction follows a typical exponential course when it is observed at multiple heights in vegetation, it decreases very fast at the top of the canopy, with almost no light reaching the soil in this example (Fig. 3.6). We can conclude that radiative transfer in the canopy depends on:

- the LAI (amount of leaves),
- the optical properties (which depend on the morphology and chemical composition) of the leaves
- the organization of the leaves (architecture, angles,..)

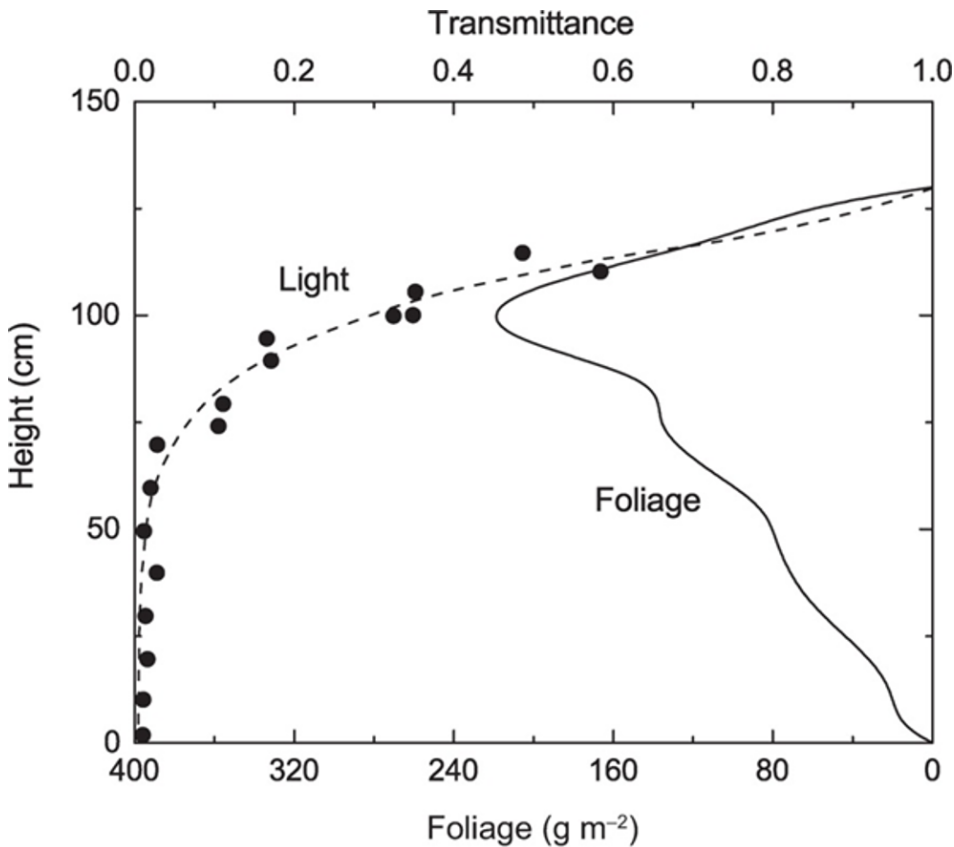


Figure 3.6: Profile of light and foliage in a stand of herbaceous plants approximately 130 cm tall. The horizontal axis shows transmittance as a fraction of incident radiation (top axis) and foliage mass (bottom axis) at various heights in the canopy. (Bonan)

Radiative transfer theory aims to integrate the light environment of individual vegetation elements (leaves, branches, ...) over the entire canopy. It must distinguish between the specific behavior of direct beam radiation and omnidirectional diffuse radiation and it should account for wavelength.

3.2 Radiative transfer modelling

Radiative transfer modelling in full 3D is very complex and is a separate branch of science. The radiative transfer schemes in vegetation models are usually relatively simple approximations of full 3D radiative transfer. Such schemes have a lot of assumptions: all leaves are plane-parallel oriented, leaf layers are horizontally homogeneous. We mostly use a one dimensional representation of the canopy (Fig.3.7), which is often used in vegetation models. Such an approach neglects the horizontal heterogeneity of vegetation and only assume a simplified vertical heterogeneity. A more complex model, subplot b, represents a three dimensional representation of the canopy, with vertical and horizontal variation.

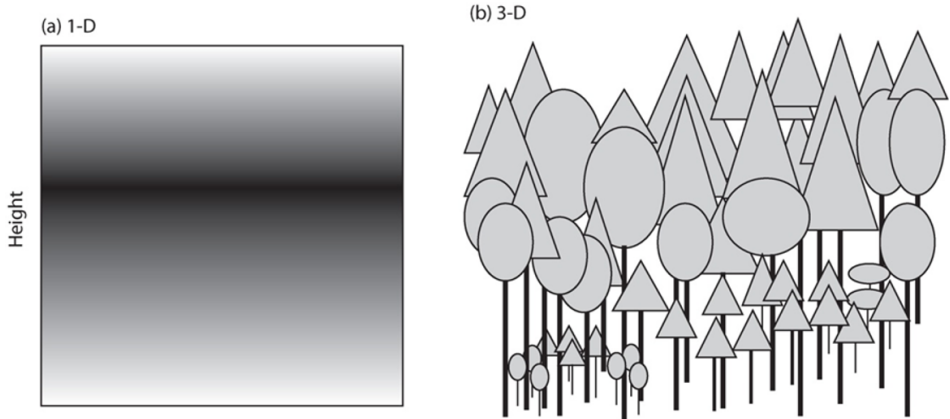


Figure 3.7: Representation of a canopy as (a) one-dimensional with a vertical profile of leaf area (shown by grayscale gradation in which darker shading denotes more leaves) that is horizontally homogenous and (b) three-dimensional with vertical and spatial structure determined by crown geometry and spacing. (Bonan)

3.2.1 Leaf optical properties

What happens to light when it reaches a leaf? It can be absorbed, reflected or transmitted. We express these in relative fractions as ρ = reflectance (albedo), τ = transmittance, α = absorbance. Leaves absorb PAR, with a small negative peak at the green light, which they reflect more compared to blue and red light. Also in the infrared wavelength band, radiation is absorbed (mostly longwave radiation). UV light is absorbed by the cuticula to protect the leaves. The reflectance and transmittance curves are inverse curves from the absorptance curve. Here, infrared radiation and green light are reflected/transmitted. The clear difference between VIS and NIR is used in remote sensing for vegetation indices (e.g. NDVI). Transmittance depends on the thickness of the leave.

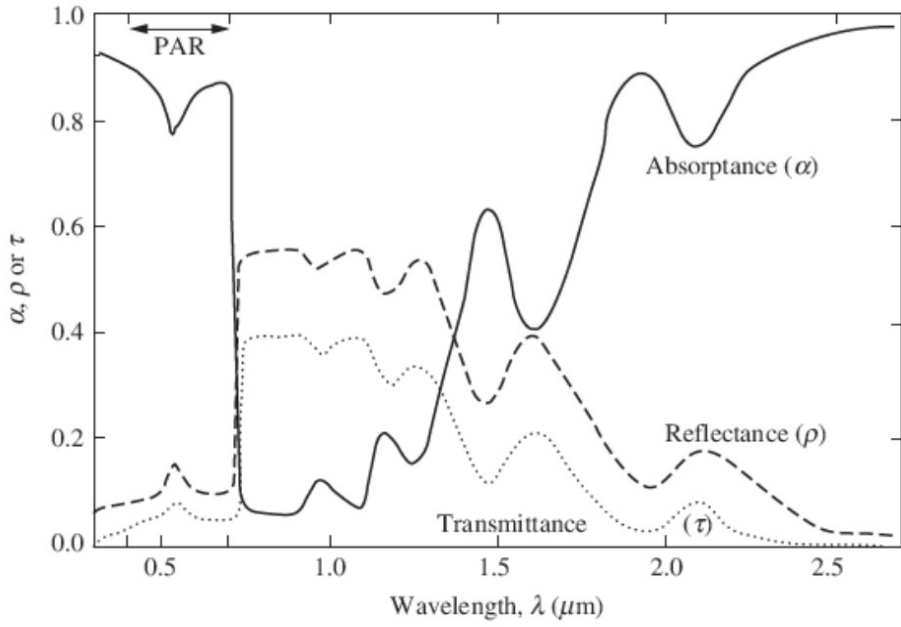


Figure 3.8: Spectrum of absorptance, reflectance and transmittance of a typical plant leaf (Jones, 2014)

The albedo of the total canopy is typically lower than that of its individual leaves, as light that is transmitted or reflected by one leave can be absorbed by another leaf (multiple scattering) (see Table below). Reflectance of needles is lower than the reflectance of broadleaves.

Table 3.1: Table showing typical reflectance and absorptance values for leaves and vegetation canopies of different Plant Functional Types (PFT).(Jones, 2014)

	ρ_s (%)	α_s (%)
Single leaves		
Crop species	29–33	40–60
Deciduous broad leaves (low sun)	26–32	34–44
Deciduous broad leaves (high sun)	20–26	48–56
<i>Artemisia</i> sp. (white pubescent, high sun)	39	55
<i>Verbascum</i> sp. (white pubescent, high sun)	36	52
Conifers	12	88
Typical mean values for total shortwave (ρ_s, α_s)	~30	~50
Typical mean values for PAR ($\rho_{\text{PAR}}, \alpha_{\text{PAR}}$)	~9	~85
Vegetation		
Grass	24	
Crops	15–26	
Forests	12–18	
Typical mean values for total shortwave (ρ_s)	~20	
Typical mean values for PAR (ρ_{PAR})	~5	
Other surfaces		
Snow	75–95	
Wet soil	9 ± 4	
Dry soil	19 ± 6	
Water	5–>20	

3.2.2 Light transmission without scattering

The most basic radiative transfer models, do not consider scattering (no reflection on the leaf). The Beer-Bouguer-Lambert law describes the attenuation of light through a homogeneous medium with thickness dz in absence of scattering. The absorbed radiation is proportional to the thickness of the medium, the amount of light that comes in and a constant K .

$$dI^\downarrow = -KI^\downarrow dz$$

with dz : thickness; I^\downarrow : incoming radiation; K : constant; dI^\downarrow : absorbed radiation in the medium.

After integration we can calculate the radiation I leaving the medium from I_0 , the radiation intensity entering the medium.

$$I^\downarrow = I_0^\downarrow \cdot e^{-Kz}$$

For leaves in a canopy, and based on probability theory, Monsi and Saeki (1953) applied the Beer law for a volume with crown thickness dz , with randomly distributed horizontal elements (leaves) with density N (number of elements per volume, see Fig. 3.9.

$$dI^\downarrow = -I^\downarrow a N dz$$

where the total leaf area in the volume can be calculated as:

$$L = a N z$$

with N : density of leaf elements; L : total leaf area; a : surface of individual leaf perpendicular to the path of light; z the total thickness of the canopy.

After integration we get an exponential function that describes the radiation extinction in the canopy:

$$I^\downarrow = I_0^\downarrow \cdot e^{-L}$$

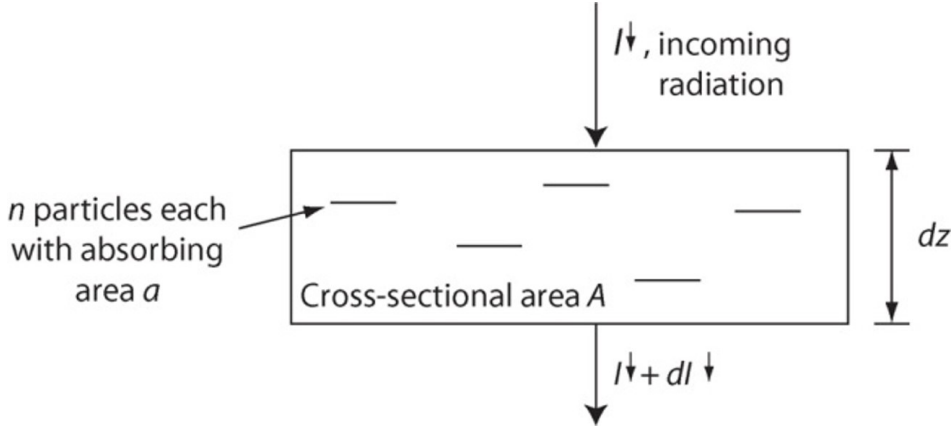


Figure 3.9: Transmission of solar radiation through a homogeneous medium in the absence of scattering. In this example, n non-overlapping opaque particles each with cross-sectional area a oriented perpendicular to the path of light are placed in a medium with cross-sectional area A and thickness dz . The radiation absorbed in the medium is dI . (Bonan)

However, in real canopies not all leaves are horizontal, and the light is not coming in perpendicular as assumed in the original equation of Monsi and Saeki. In the exponential function, L should therefore be adapted to the projected leaf area perpendicular to the light beams, as the model assumes that light comes in perpendicularly.

$$I^\downarrow = I_{sky,b}^\downarrow \cdot e^{-K_b L}$$

Where K_b : direct beam extinction coefficient, and LH (horizontal leaf area) = $K_b L$. And $I_{sky,b}^\downarrow$ is the incident radiation at the top of the canopy. K_b describes how severely light is attenuated in the canopy depending on the LAI. A higher K_b indicates a faster extinction, so a more dark forest. Fig. 3.10 describes the light transmittance with increasing LAI for different K_b values.

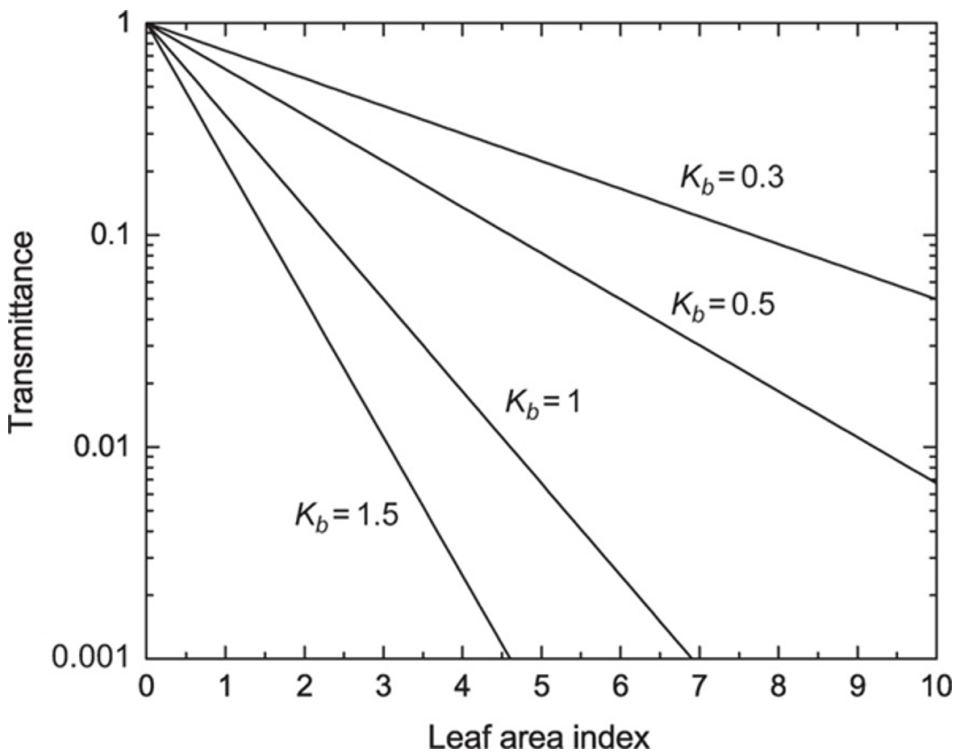


Figure 3.10: Transmission of direct beam radiation b in relation to leaf area index for typical values of the extinction coefficient K_b . (Bonan)

The extinction coefficient depends on solar zenith angle and leaf orientation (as illustrated in Fig.3.11).

$$K_b = \frac{L_H}{L} = \frac{G(Z)}{\cos Z}$$

With Z : solar angle; Θ_l : leaf angle; $G(Z)$: function depending on the zenith angle (shown in figure 3.11). Divided by $\cos Z$ because we project to the horizontal plane. L_h : leaf area projected on the horizontal plane.

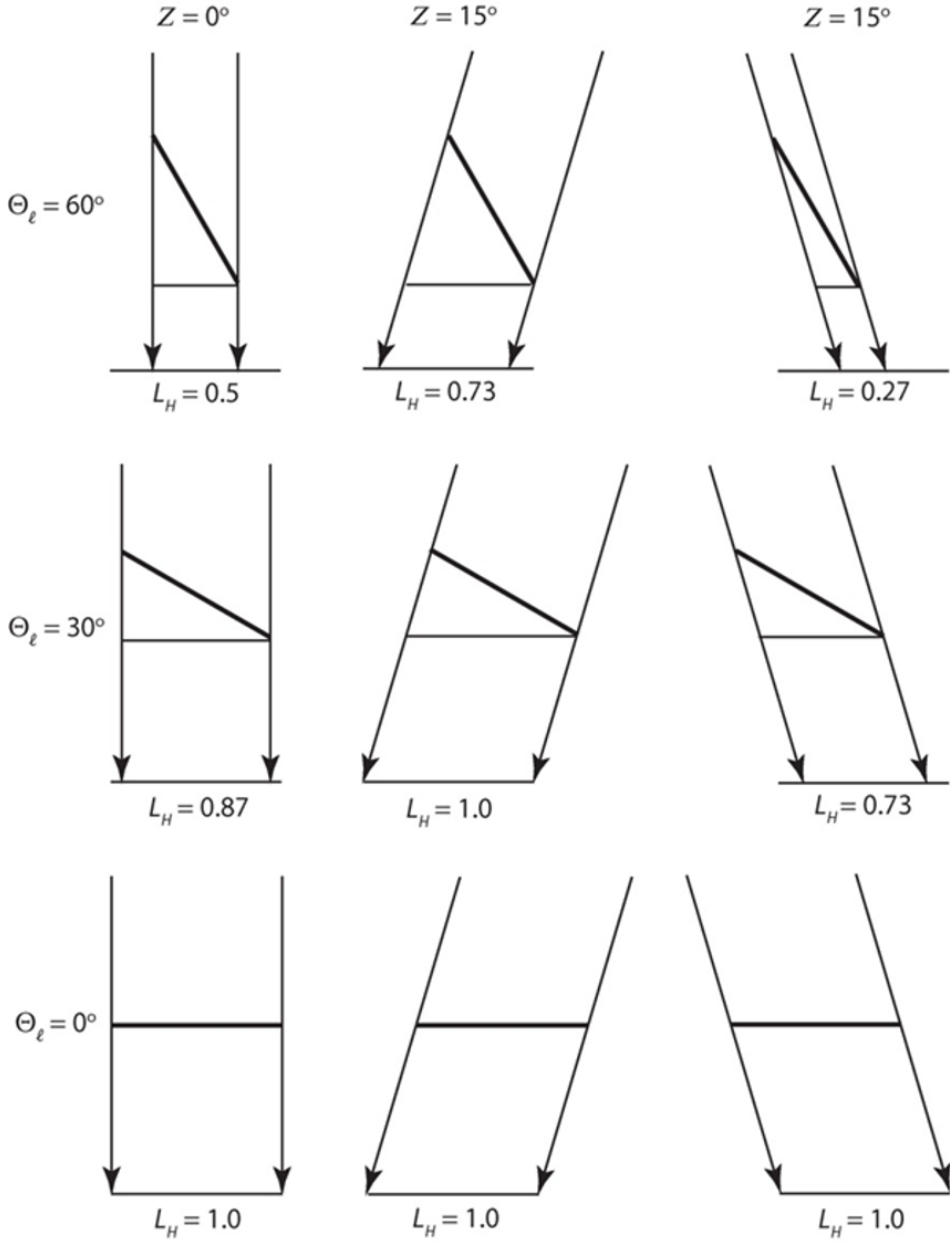


Figure 3.11: Extinction coefficient in relation to solar zenith angle Z and leaf inclination angle. In each panel, a unit leaf area ($L = 1$), shown with a thick line, is projected onto a horizontal surface L_H so that $K_b = L_H$. The leaf inclination angle is 0° (bottom panels), 30° (middle panels), and 60° (top panels). In the left and middle columns, the leaf is oriented towards the Sun and the solar zenith angle is 0° (left column) and 15° (middle column). In the right column, $Z = 15^\circ$, but the leaf is oriented away from the Sun. In each panel, the arrows indicate the solar beam (Bonan)

The lower the sun is to the horizon (the higher the zenith angle), the higher the extinction coefficient is, except for horizontal leaves, which have a constant K_b of 1.

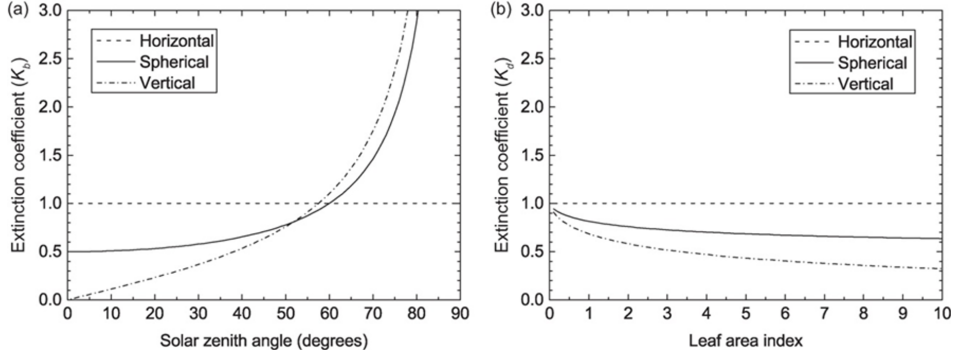


Figure 3.12: Extinction coefficients for horizontal, spherical, and vertical leaf angle distributions. (a) Direct beam radiation K_b in relation to solar zenith angle. (b) Diffuse radiation K_d in relation to leaf area index(Bonan)

The above described formulas do not only allow us to describe the light extinction in the canopy, but also to calculate the sun and shaded fraction of leaf are in the canopy. If we divide the canopy into multiple layers, we can calculate for each layer which part is in the sun and which part is in the shade. For every canopy layer, the fraction of sunlit leaves is equal to the $f_{sun}(x)$ function. It represents the amount of light that comes through the layers above it.

$$f_{sun}(x) = e^{-K_b x}$$

Where x is the cumulative LAI above the layer of interest. Similarly we can calculate the actual sunlit leaf area within a certain layer:

$$\Delta L_{sun} = \frac{e^{-K_b x} (1 - e^{-K_b \Delta L})}{K_b}$$

Where ΔL is the actual amount of leaves in that layer, this formula calculates the difference between the sunlit fraction at the top of the layer minus the “reduction of sunlit fraction” within the layer. If we apply that formula on a full canopy we can calculate the sunlit leaf area of the full canopy L_{sun} :

$$L_{sun} = \frac{(1 - e^{-K_b L})}{K_b}$$

L_{sun} : integrated over the whole canopy. Based on this equation you can calculated the amount of leaves that is sunlit in the canopy. And also the shade fraction based on the difference with the total LAI.

In the example below (Fig. 3.13) the sunlit and total LAI are compared between a vegetation with horizontal and with vertical foliage. The latter has more sunlit leaves, as top leaves don't shade the underlaying leaves. In the horizontal foliage, more light is absorbed, so less light is transmitted than in the vertical foliage.

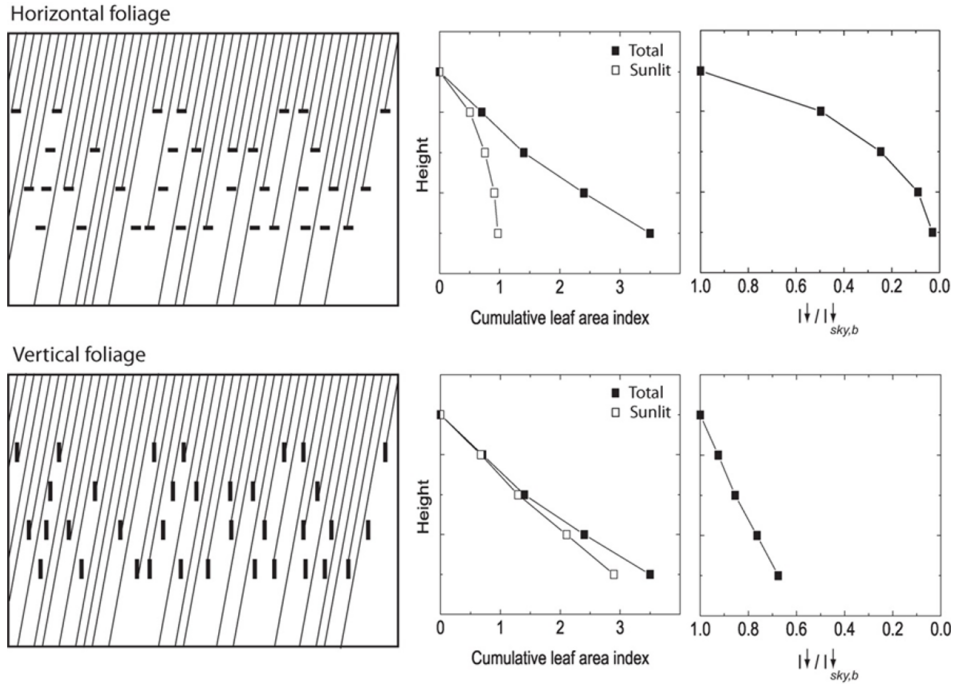


Figure 3.13: Radiative transfer and sunlit leaf area index for a canopy of horizontal leaves (top panels) with $K_b = 1$ and vertical leaves (bottom panels) with $K_b = 0.112$. The left-hand panels show a canopy consisting of four layers of leaves. Each thick black line represents a leaf area index of $0.1 \text{ m}^2 \text{ m}^{-2}$. The thin lines depict interception or transmission of beam radiation with a zenith angle of 10° . The middle panels show cumulative leaf area index and sunlit leaf area index with depth in the canopy. The right-hand panels show direct beam transmittance with depth in the canopy. (Bonan)

When we study the sunlit LAI with increasing cumulative LAI (Fig.3.14) for different leaf orientations, the same course of the curve applies: first, there is a linear increase of the amount sunlit leave are index with increasing LAI, after which a saturation occurs when the vegetation becomes more dense (higher LAI). The level of saturation depends on the leaf angle distribution.

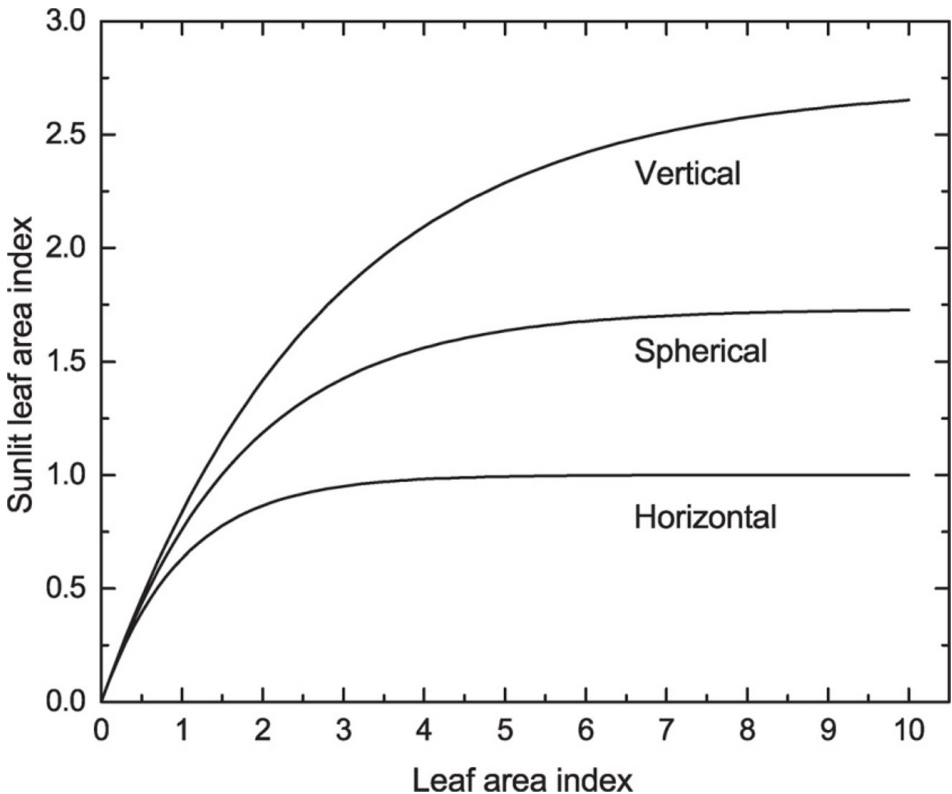


Figure 3.14: Sunlit leaf area index in relation to total leaf area index for horizontal, spherical, and vertical foliage orientations with solar zenith angle $Z = 30^\circ$. $K_b = 1$, 0.577, and 0.368 for horizontal, spherical, and vertical foliage. (Bonan)

A final complicating factor that we want to highlight here is that leaves and canopies are not distributed randomly in space, but occur clumped. Leaf clumping means that leaves appear in groups and that there are larger gaps in between. Clumping can occur at different scales: at leaf level, canopy level or landscape level (Fig.3.15). The clumping factor (Ω) adjusts the amount of light that goes through the vegetation (more light passes through). The factor is added in the radiation extinction equations to adjust the extinction coefficient. Where a clumping factor of 1 represents randomly distributed leaves, while values lower than 1 represent clumped leaves (e.g. 0.74 for needleleaf evergreen forest).

$$I^\downarrow = I_{sky,b}^\downarrow \cdot e^{-K_b \Omega L}$$

$$f_{sun}(x) = e^{-K_b \Omega x}$$



Figure 3.15: Images illustrating leaf/canopy clumping at various scales: leaf, crown, stand.

3.2.3 Diffuse transmittance

Diffuse radiation is omnidirectional, and therefore it penetrates better into the canopy. The formula below represents the diffuse transmittance. The last part of the equation represents the contribution of a certain sky angle to the total sky irradiation (e.g. contribution of zenith angle between Z_1 and Z_2 in Fig.3.16). The exponential curve with the leaf area L is the light extinction curve, but here it is also integrated over the zenith angle.

$$\tau_d = \frac{I^\downarrow}{I_{sky,d}^\downarrow} \int_0^{\pi/2} \exp \left[-\frac{G(Z)}{\cos Z} L \right] \sin Z \cos Z dz$$

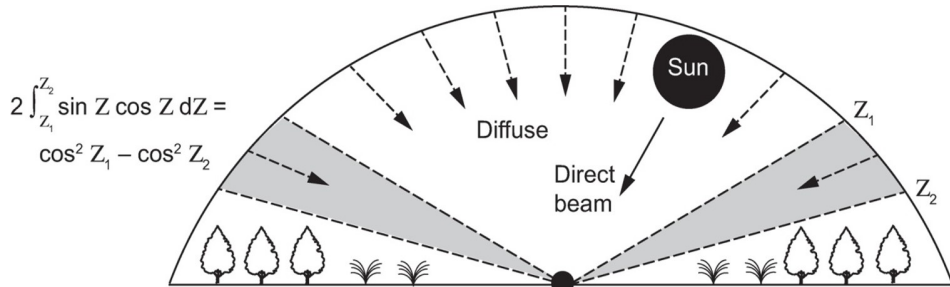


Figure 3.16: Illustration of direct beam and diffuse radiation. The sky forms a bowl, or inverted hemisphere, over a horizontal surface. Shown is a cross section of the sky hemisphere. Direct beam (solid line) originates from the direction of the Sun with zenith angle Z . Diffuse radiation (dashed lines) can be treated as independent beams of radiation each with an angle Z . The shaded region is the relative contribution between sky angles Z_1 and Z_2 to total sky irradiance.(Bonan)

The more leaves, the less diffuse light is transmitted through the canopy. The contribution of the zenith angles is shown on Fig.3.17. There is more light transmitted in the 30° - 60° zenith angle range than in the other two groups. Thus perpendicular diffuse sunlight penetrates less easily in the canopy than sunlight under a 30° - 60° angle.

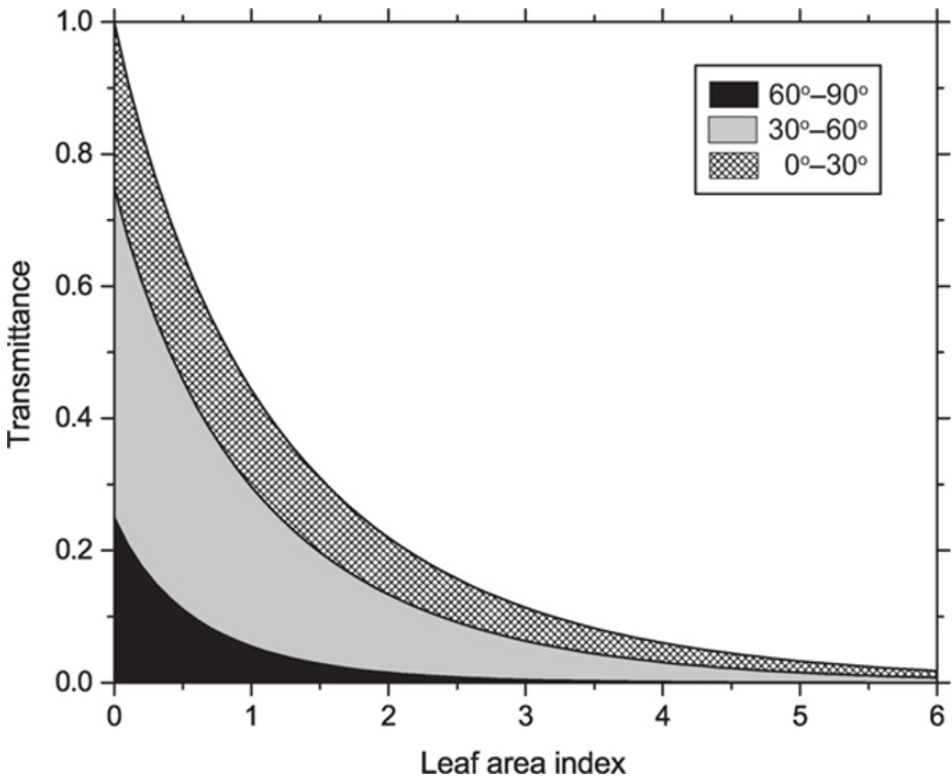


Figure 3.17: Transmittance of diffuse radiation d in relation to leaf area index for a spherical leaf distribution. Show are the transmittances for sky zones of 0° – 30° , 30° – 60° , and 60° – 90° and also the total transmittance. Fill patterns show the contribution of each sky zone to total transmittance.(Bonan)

It is also interesting to compare the diffuse transmission to the direct transmission. The dashed line (Fig.3.18) indicates the transmittance for diffuse light (omnidirectional), the solid lines indicate the transmittance for direct light at different solar zenith angles. The transmittance of diffuse light is higher than that of direct light for solar zenith angles greater than 40 – 50° , direct light penetrates less easily through the canopy compared to diffuse light.

It is important to include diffuse radiation into models as it penetrates deeper into the canopy, it is shifted towards the blue light, which is used by plants for photosynthesis, and because plants depend on it in cloudy conditions.

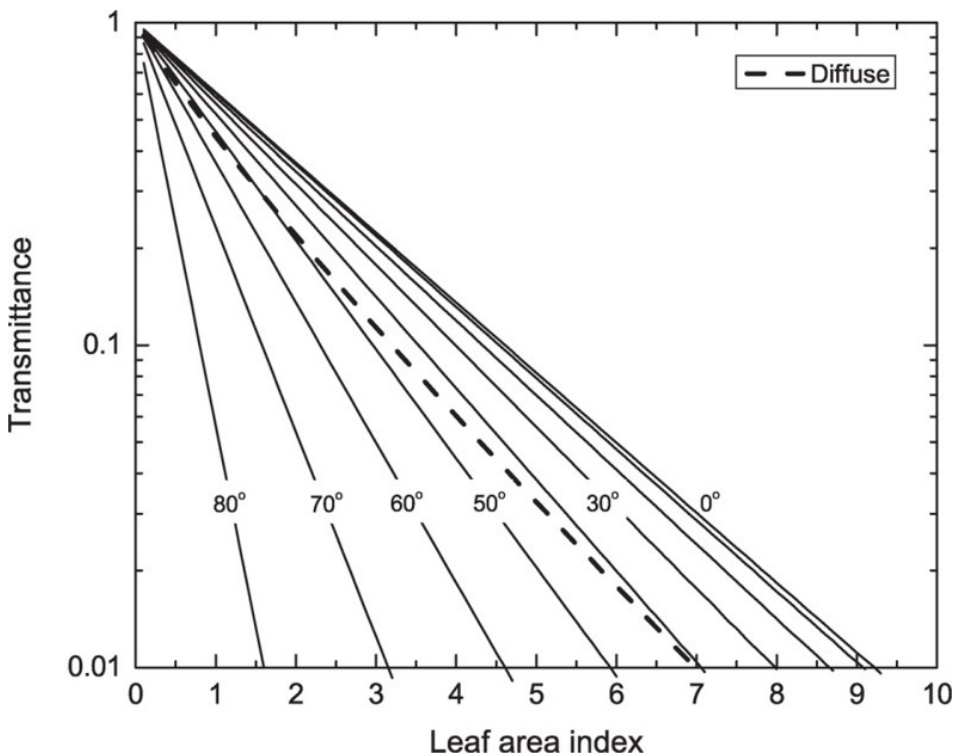


Figure 3.18: Transmission of solar radiation through a canopy with spherical leaf distribution in relation to leaf area index. The solid lines show direct beam transmittance b for solar zenith angles of 0° – 80° (in 10° increments). The dashed line shows the diffuse transmittance d . (Bonan)

3.2.4 The Norman Model(1979)

In the Norman model, the canopy is divided into multiple layers of typically 0.5 LAI per layer. For each layer the diffuse, direct and longwave radiation balance is calculated: reflection, absorption and transmission. The model thus accounts for scattering. We do not discuss the equations in detail, but the large number of equations have to be solved numerically, which is very computational expensive, especially in model versions where a sunlit and shade fraction per leaf layer are considered.

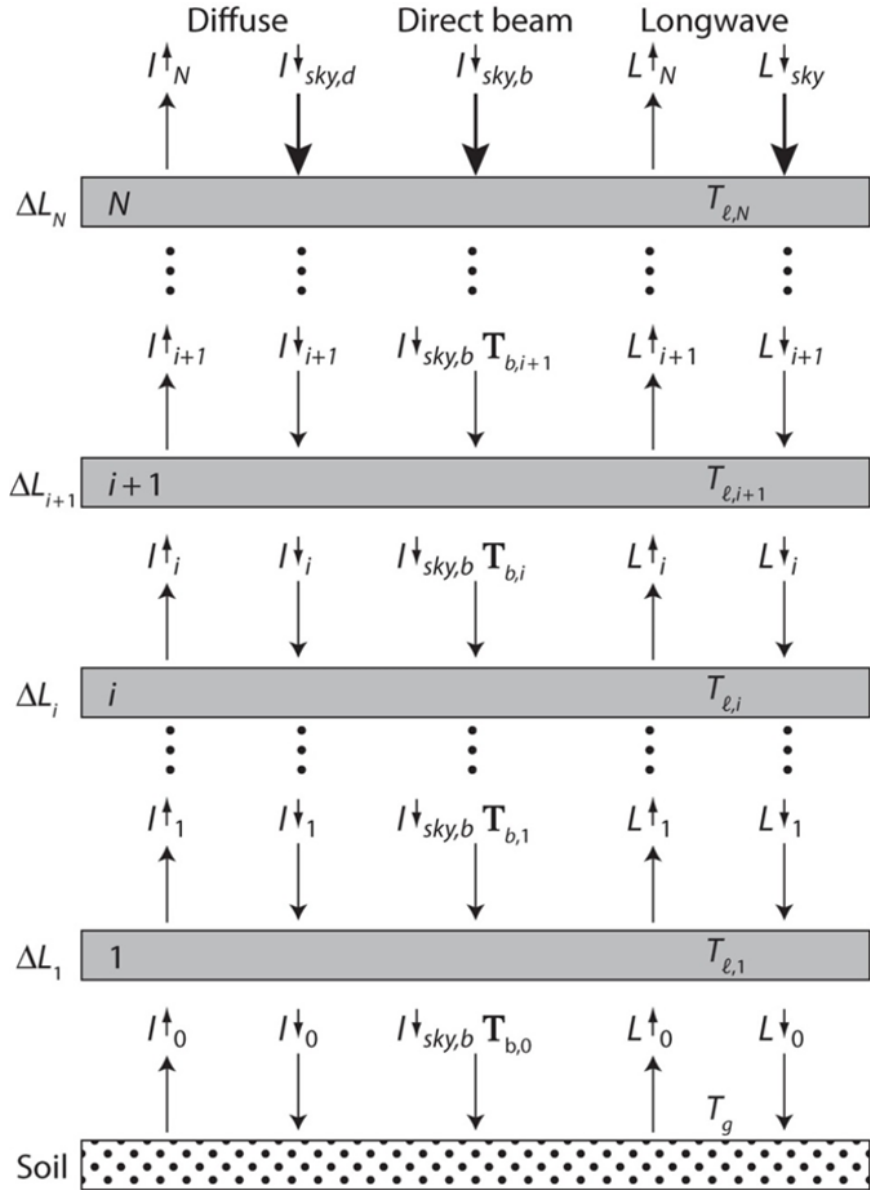


Figure 3.19: Radiative fluxes in a canopy of N leaf layers. The vertical profile is oriented with $i = 1$ the leaf layer at the bottom of the canopy, leaf layer $i + 1$ above layer i , and $i = N$ the leaf layer at the top of the canopy. Each layer has a leaf area index ΔL_i . $I_{\downarrow i}$ is the downward diffuse shortwave flux onto layer i , $I_{\uparrow i}$ is the upward diffuse shortwave flux above layer i , and $I_{\downarrow sky,b}$ is the unscattered direct beam flux onto layer i . $L_{\uparrow i}$ and $L_{\downarrow i}$ are the corresponding downward and upward fluxes of longwave radiation. These depend on leaf T and ground T_g temperatures. Thick arrows denote boundary conditions of diffuse solar radiation, direct beam solar radiation, and atmospheric longwave radiation at the top of the canopy. (Bonan)

3.2.5 The Goudriaan and van Laar Model (1994)

This is an analytical solution of the model, which integrates over a single calculation step. To be able to do so, one integrated extinction coefficient for all layers is assumed

($K'b$, adapted extinction coefficient). One light extinction coefficient is thus used for diffuse and direct radiation together, which is the major simplification in the model. This coefficient also includes a clumping factor. This model is widely used due to its simplicity and low computational demand. It can be applied to a single layer or multi-layer canopy. Due to its assumptions, this model produces more errors, especially for diffuse light (under cloudy conditions).

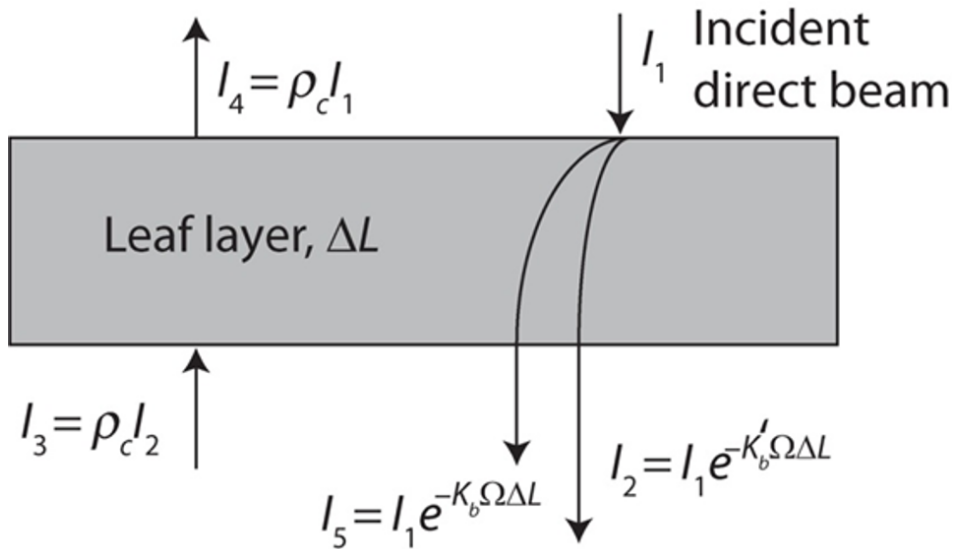


Figure 3.20: Derivation of absorbed direct beam solar radiation for a leaf layer with leaf area index ΔL (Goudriaan 1982). ρ_c is the reflectance of the leaf layer.(Bonan)

3.2.6 The Two-Stream approximation

This model takes “the best of both worlds”. It is called “two stream” because it calculates light penetration separately for direct and diffuse radiation, but it has an analytical solution. It can be used for multilayer models.

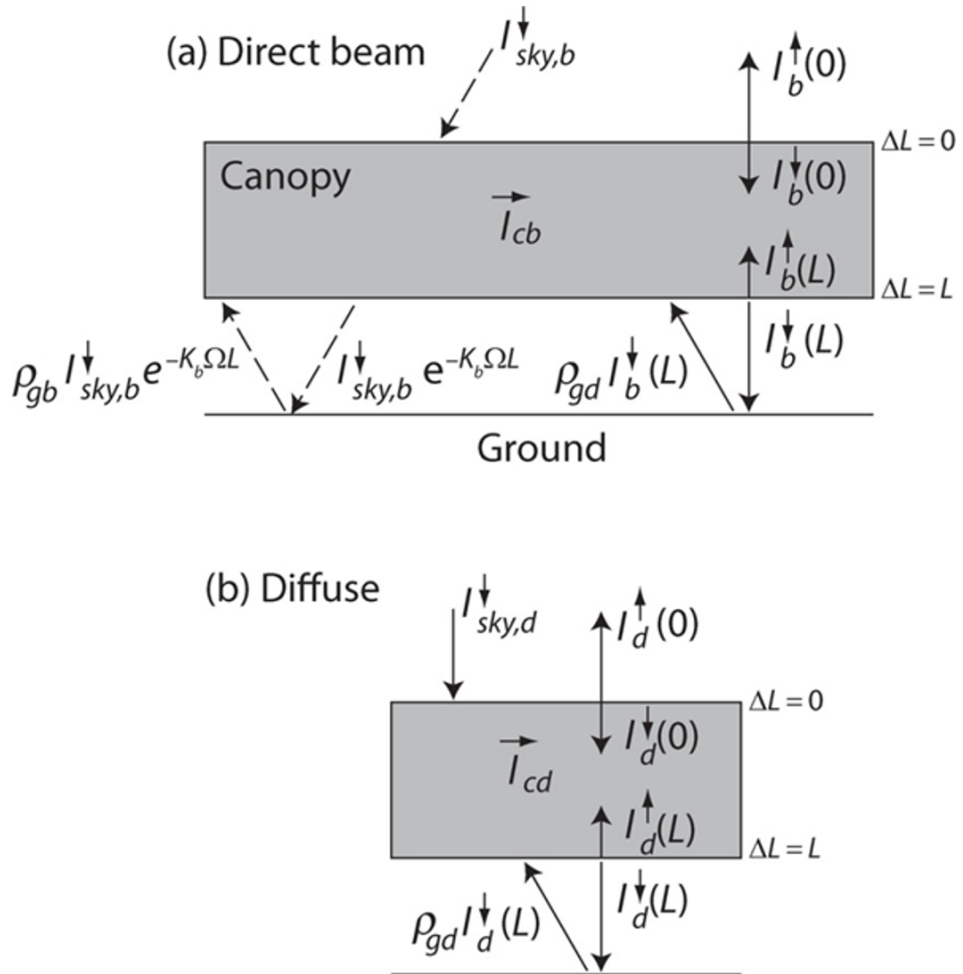


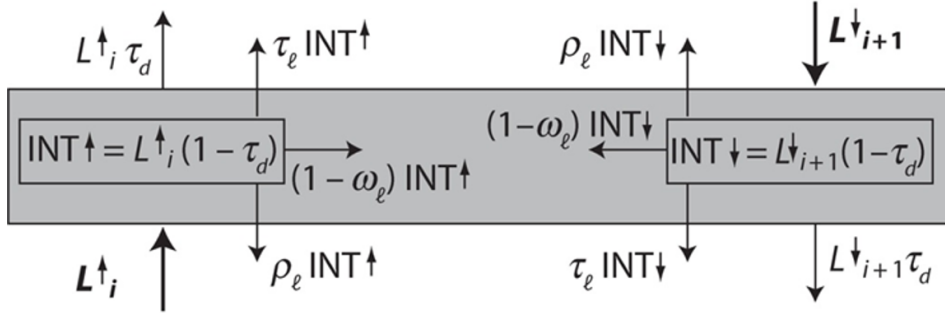
Figure 3.21: Fluxes for (a) direct beam and (b) diffuse radiation in the twostream approximation for a canopy with leaf area index L . (Bonan)

The three approaches (Norman/Goudriaan/two stream) are all based on the same theory. They are implemented in a different way, but the results are very similar for direct light. However they show substantial deviations for diffuse light, shaded leaves and denser canopies.

3.2.7 Longwave radiation

Longwave radiation is important for closing the energy balance. To simulate longwave radiation transfer in canopies, similar approaches as above are used, but the emission of longwave radiation by the ground, and leaf surfaces need to be accounted for.

(a) Numerical



(b) Analytical

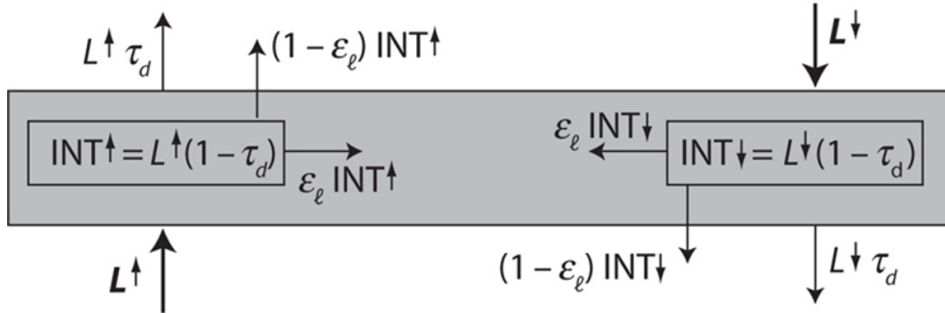


Figure 3.22: Longwave radiation fluxes represented for a single leaf layer.(a) Norman's (1979) numerical model. Shown is the radiative balance for leaf layer $i + 1$ located above leaf layer i . (b) A simplified model to allow only forward scattering and to permit an analytical solution integrated over a canopy. In both panels, emitted radiation is excluded. Thick lines denote fluxes incident onto the layer. (Bonan)

3.3 Representing canopy structure in models

3.3.1 Big-leaf models

Big leaf models can have a shaded and a sunlit fraction in the canopy, or can consider sunlit leaves only. The forest/vegetation is represented as one big leaf, with a leaf area equal to the total leaf area of the forest/vegetation. Such models do not account for the vertical structure of the canopy. These models calculate properties of the big leaf, by upscaling. For example by calculating an average stomatal or canopy conductance. Evapotranspiration can then be calculated by applying the Penman-Monteith equation and a canopy level conductance. The leaf boundary layer is replaced by the atmosphere surface layer and gsw is the average stomatal conductance of the whole forest.

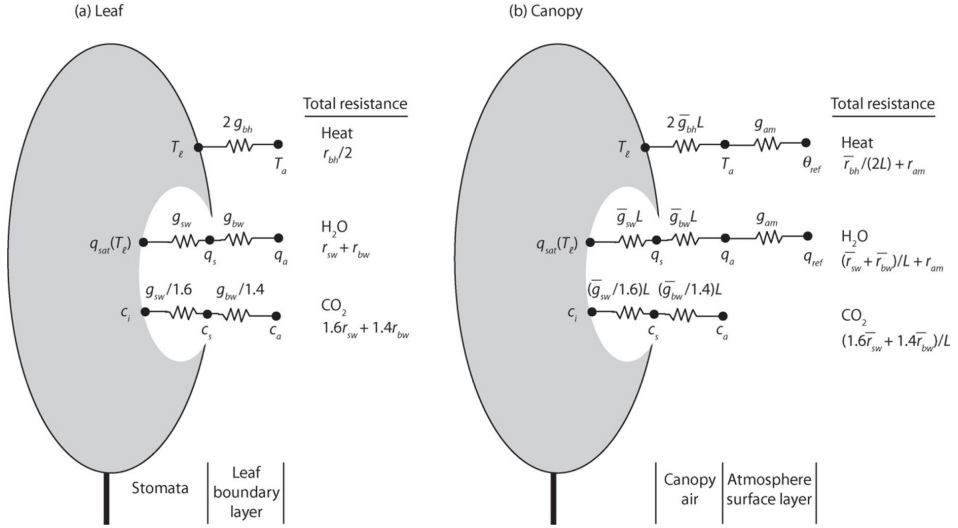


Figure 3.23: Scaling of leaf fluxes to the canopy using a big-leaf model. (a) Shown are leaf sensible heat, transpiration, and CO₂ fluxes in relation to various conductances. Fluxes are exchanged between the leaf and air around the leaf. Also shown is the total resistance. (b) Shown are big-leaf canopy fluxes in which leaf fluxes are scaled by the average conductance and leaf area index and are further modified by turbulent transport in the atmospheric surface layer. Surface layer processes are commonly omitted for CO₂ exchange. Only a single big leaf is shown, but separate sunlit and shaded big leaves can be similarly depicted. (Bonan)

It is not an easy task to integrate GPP (e.g. calculated by the Farquhar model of Chapter 2) over a canopy represented by a big leaf. We cannot just give the total light absorbed by the canopy to a photosynthesis model, as we need to account for the non-linearity in the process. The task is easier if Amax is assumed to decrease exponentially together with light availability I the canopy, which is a reasonable assumption, as we know that leaf nitrogen content is decreasing from the top to the bottom of the canopy. As such we are assuming a “photosynthesis extinction” instead of a light extinction in the canopy.

$$GPP = \int_0^L A(x) dx$$

$$A_{max}(x) = A_{max0} e^{-K_b x}$$

$$GPP = \int_0^L A(x) dx = A(0) \left[\frac{1 - e^{-K_b L}}{K_b} \right]$$

However, this is a rough approach, and it does not account for the nonlinear canopy responses. A better approach is to include a sunlit and shade fraction of the leaves. Where the GPP is calculated as the sum for sunlit and shaded leaves separately. Each fraction has a separate value for g_s , A_m etc...

$$GPP = [A_{sun}f_{sun} + A_{shade}(1 - f_{sun})] L$$

Big leaf models that use the Fraquhar approach often assume an integrated V_{cmax} value for the canopy, calculated based on an exponential profile of V_{cmax} .

$$V_{cmax}(x) = V_{cmax0}e^{-K_n x}$$

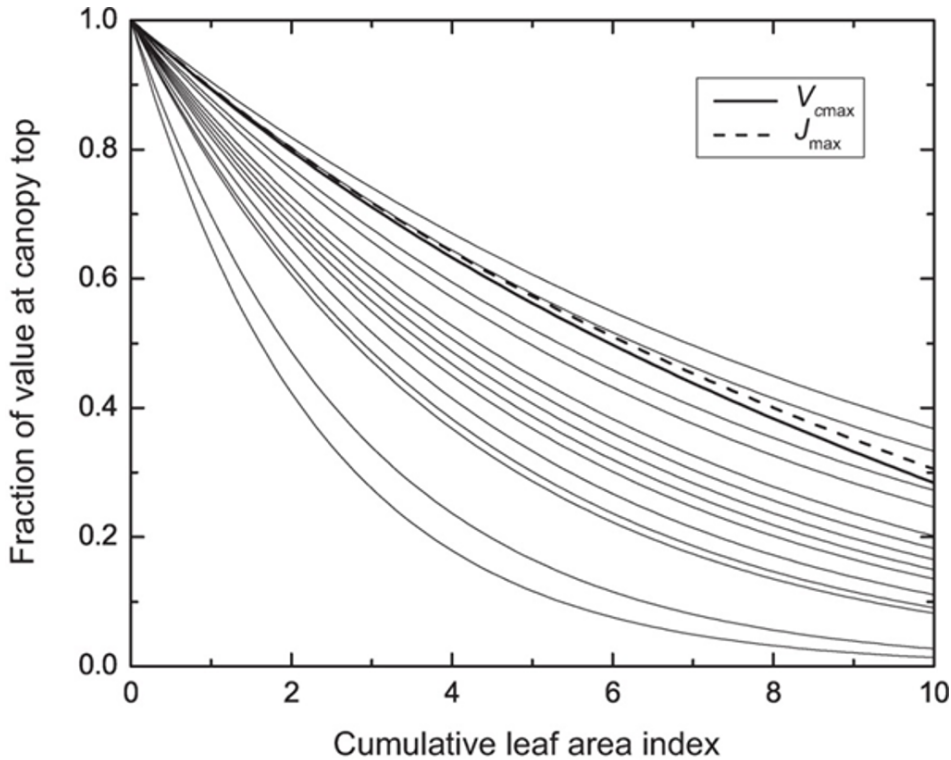


Figure 3.24: Canopy profiles of relative photosynthetic capacity in relation to cumulative leaf area index. Thin lines show exponential profiles using values of K_n for 16 temperate broadleaf forests and two tropical forests ranging from 0.10 to 0.43 (Lloyd et al. 2010). The two thick lines show observed profiles of V_{cmax} and J_{max} from Niinemets and Tenhunen (1997) obtained for sugar maple (*Acer saccharum*). (Bonan)

3.3.2 Multilayer models

Account for all vertical heterogeneity, such as light, leaf physiology, leaf traits and even micrometeorology, e.g. RH is different at different leaf layers in the model. All equations (fluxes, energy balance) are calculated for each layer, and GPP is the sum of the photosynthesis of all layers. Figure 3.25: each layer is a big leaf to calculate all leaf level processes. Radiative transfer and leaf fluxes are thus simulated for each layer. Sometimes, even leaf hydraulics are simulated, to simulate leaf water potential and its influence on stomatal conductance. Such models are computationally expensive, especially because they are solved for each layer a set of equations in an iterative way (Fig. 3.26). Nevertheless, such multilayer models are very common in large scale land surface

models. Be aware that horizontal heterogeneity is not considered in these models, see later chapters for that.

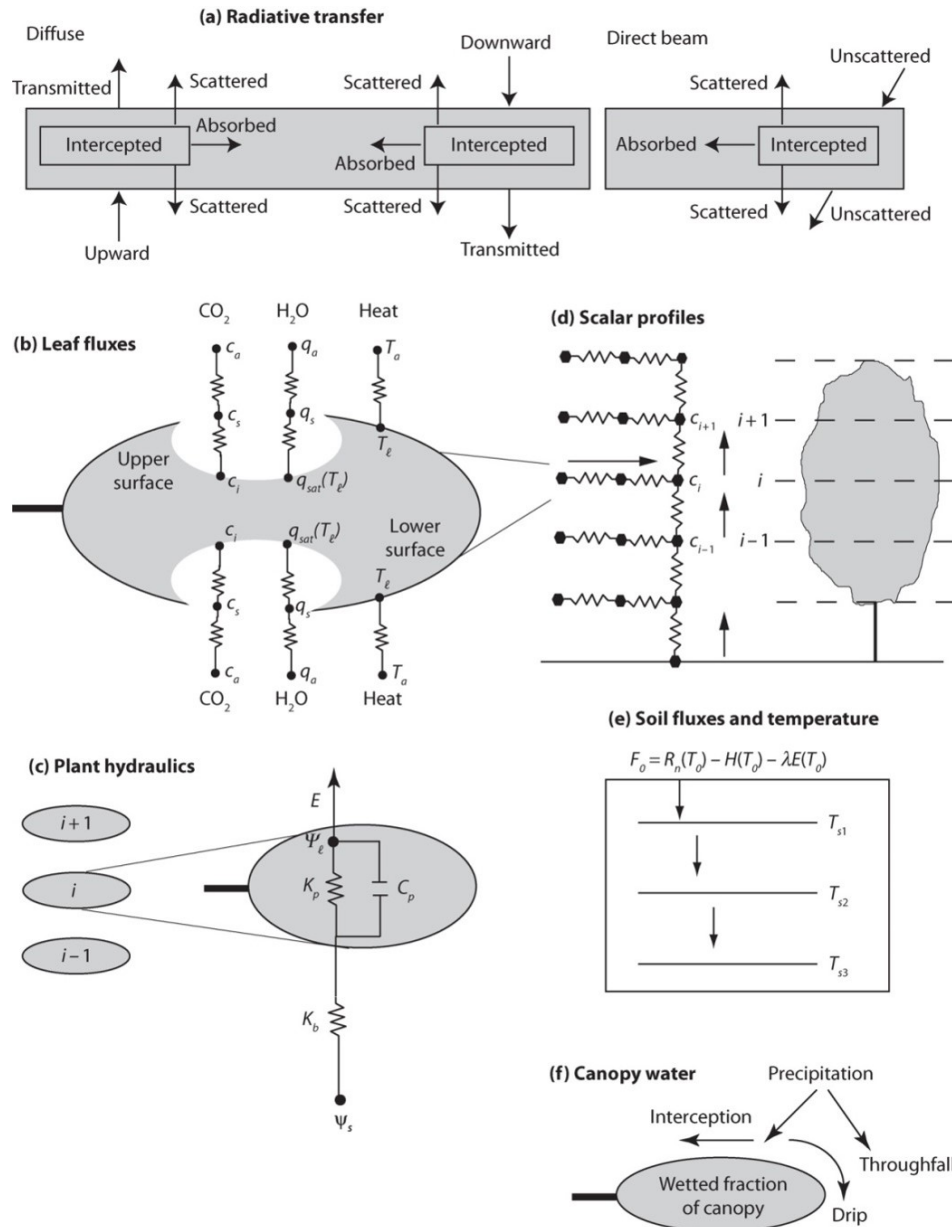


Figure 3.25: Overview of the main processes in a multilayer canopy model. The canopy is represented by N leaf layers with layer $i + 1$ above layer i . (a) Diffuse and direct beam solar radiation is transmitted or intercepted. The intercepted portion is absorbed or scattered in the forward and backward direction. Longwave radiation is similar to diffuse radiation. (b) Leaf sensible heat, transpiration, and CO₂ fluxes depend on absorbed radiation and leaf boundary layer and stomatal conductances. Sensible heat is exchanged from both sides of the leaf. Water vapor and CO₂ can be exchanged from one or both sides of the leaf depending on stomata. Leaf temperature is the temperature that balances the energy budget. (c) Stomatal conductance depends on leaf water potential. Plant water uptake for a canopy layer is in relation to belowground soil and root conductance and aboveground stem conductance acting in series and also a capacitance term. (d) Scalar profiles are calculated from a conductance network. Leaf fluxes provide the source or sink of heat, water vapor, and CO₂, along with soil fluxes. (e) Sensible heat, latent heat, and heat storage in soil depend on the ground temperature that balances the soil energy budget. (f) The wetted fraction of the canopy layer depends on the portion of precipitation that is intercepted. (Bonan)

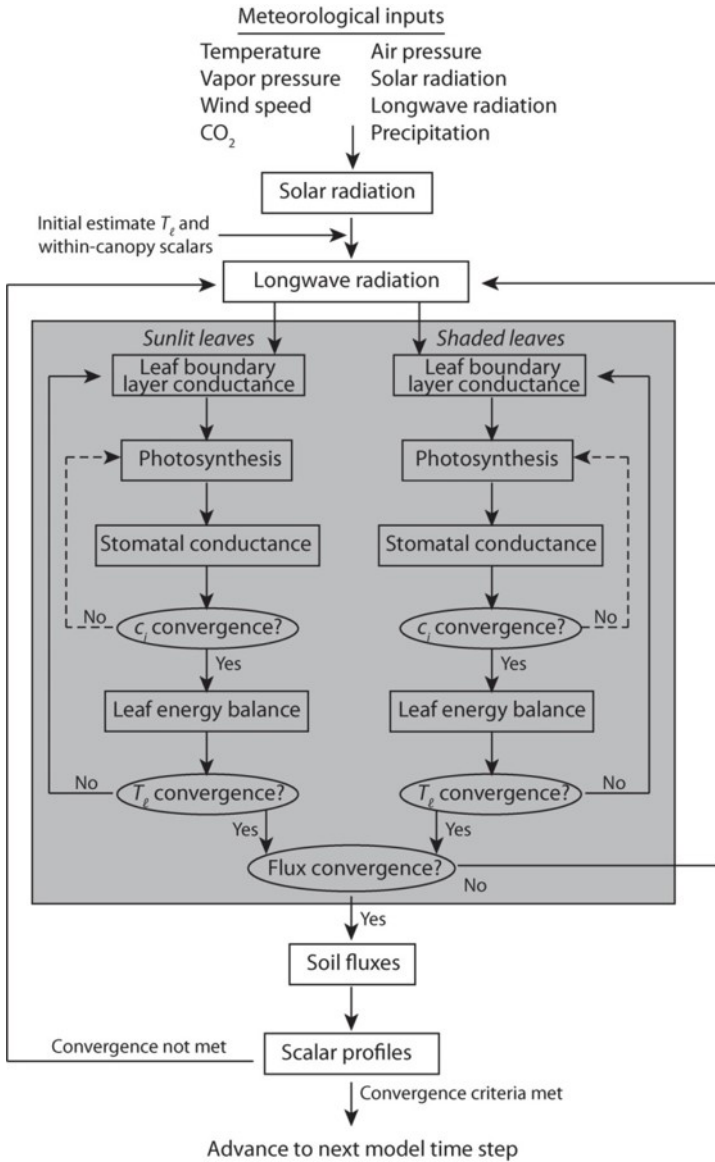


Figure 3.26: Flow diagram of processes in a multilayer canopy model. The shaded area denotes leaf processes resolved at each layer in the canopy. This is a generalized diagram of the required calculations for a dry leaf. Specific models differ in how the equation set is solved and the iterative calculations. Evaporation of intercepted water requires additional complexity.(Bonan)

3.3.3 3D ray tracing models

3D ray tracing models are not (yet) use as part of operational vegetation models. They rather for a separate group of models, focus on radiative transfer only (they do not simulate other processes such as photosynthesis). These models are typically used to simulate what a satellite (or other remote sensing sensor) would observe in specific wavelength bands. As such these models are very useful for interpretation of remote sensing observations. They really simulate how light, or individual sun rays penetrate the canopy and do that for the different wavelengths. Based on such models we can

also get better insight in radiative transfer and derive better radiative transfer schemes for operational vegetation models.

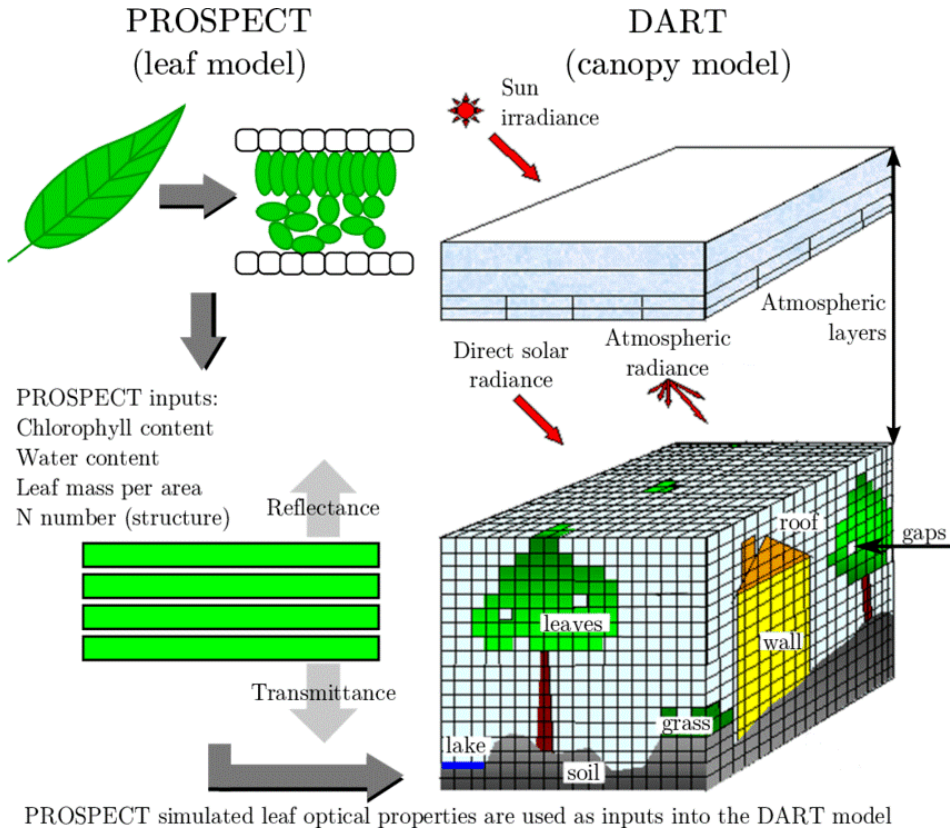


Figure 3.27: Example of the PROSPECT leaf optical model and the DART 3D ray tracing model.

These models typically consider simple 3D objects with specific optical properties. However, the newest addition to this research is using detailed 3D reconstructions of trees from lidar scans as model input and run the model with the lidar data as scattering objects in the 3D scene.

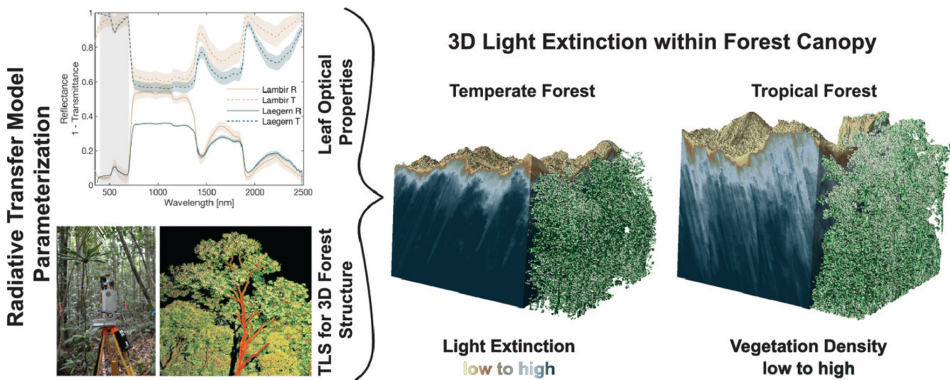


Figure 3.28: Example of a study that uses terrestrial laser scanning (TLS) to construct a full 3D model of a forest as input for a 3D ray tracing model (Kükenbrink et al. 2020)

3.4 Ecosystem energy balance

3.4.1 Basic principles

The energy balance is a fundamental part of vegetation models. The goal is to calculate how much energy comes in, how much is lost and in what the resulting temperature is for the leaf or the surface. The energy balance is governed by non-linear equations. However linearizations exist (e.g. Penman Monteith equations to calculate ET).

3.4.2 Surface radiation balance

The formula below (Fig. 3.29) calculates the radiation balance

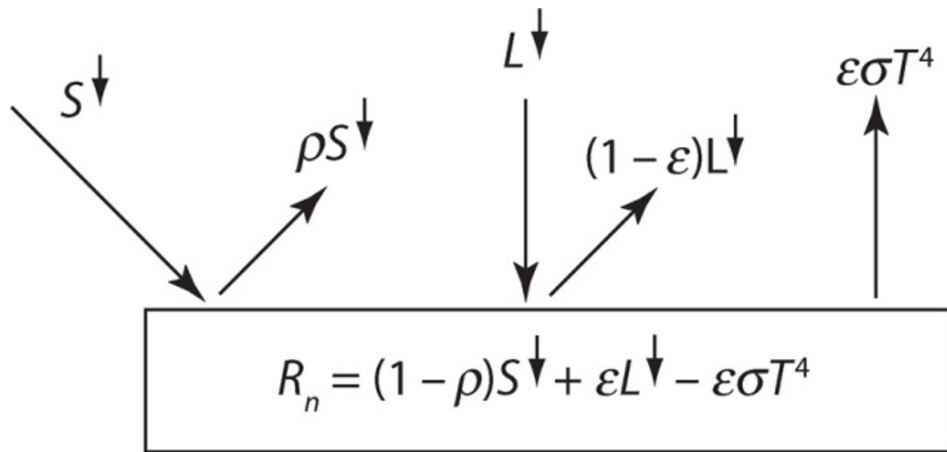


Figure 3.29: Radiative balance of an opaque gray body receiving downwelling solar S and longwave L radiation.(Bonan)

where R_n : net radiation (how much energy is available for system), $\rho S \downarrow$: reflected shortwave radiation, $\varepsilon\sigma T^4$ the Stefan-Boltzmann law. The equation essentially makes the balance between how much shortwave net comes in, and how much longwave is net reflected. The net radiation forms the major input term of the energy balance.

3.4.3 Bulk surface energy balance

This is the central equation of the surface energy balance:

$$R_n = \lambda E + H + G + S$$

The net radiation is the input of energy to the ecosystem which is dissipated via multiple loss terms: latent heat (evapotranspiration), sensible heat flux, ground heat flux and energy storage (in the biomass of the ecosystem). Most of the energy goes to the latent heat to well-watered active vegetation (e.g. a beach forest in summer).

It is really important to close the energy balance in models. All factors in the equation can be formulated in terms of input factors of the model, such as incoming radiation, and in function of the surface temperature. The equation below is rewriting the above equation in terms of surface temperature.

$$\sum_{\Lambda} (1 - \rho_{\Lambda}) S_{\Lambda}^{\downarrow} + \epsilon L^{\downarrow} = Q_a = \epsilon \sigma \theta_s^4 + c_p (\theta_s - \theta_{ref}) g_{ac} + \frac{\lambda [q_{sat}(\theta_s) - q_{ref}]}{g_c^{-1} + g_{ac}^{-1}} + \frac{k}{\Delta z} (\theta_s - T_1)$$

Where S input energy (shortwave) in a certain wave length band (Λ), Q is the total gross incoming energy. At the right side of the equation we see: the longwave loss term, sensible heat loss, latent heat (in response to vapor pressure) , and the ground heat flux. The surface temperature (Θ_s) is the big leaf surface temperature.

The big leaf latent heat (evapotranspiration), is often accounted by the Penman-Monteith equations (as function of net radiation and vapor pressure deficit).

$$\lambda E = \frac{s(R_n - G) + c_p (q_{sat}(T_a) - q_a) g_{ac}}{s + (1 + \frac{g_{ac}}{g_c}) \frac{c_p}{\lambda}}$$

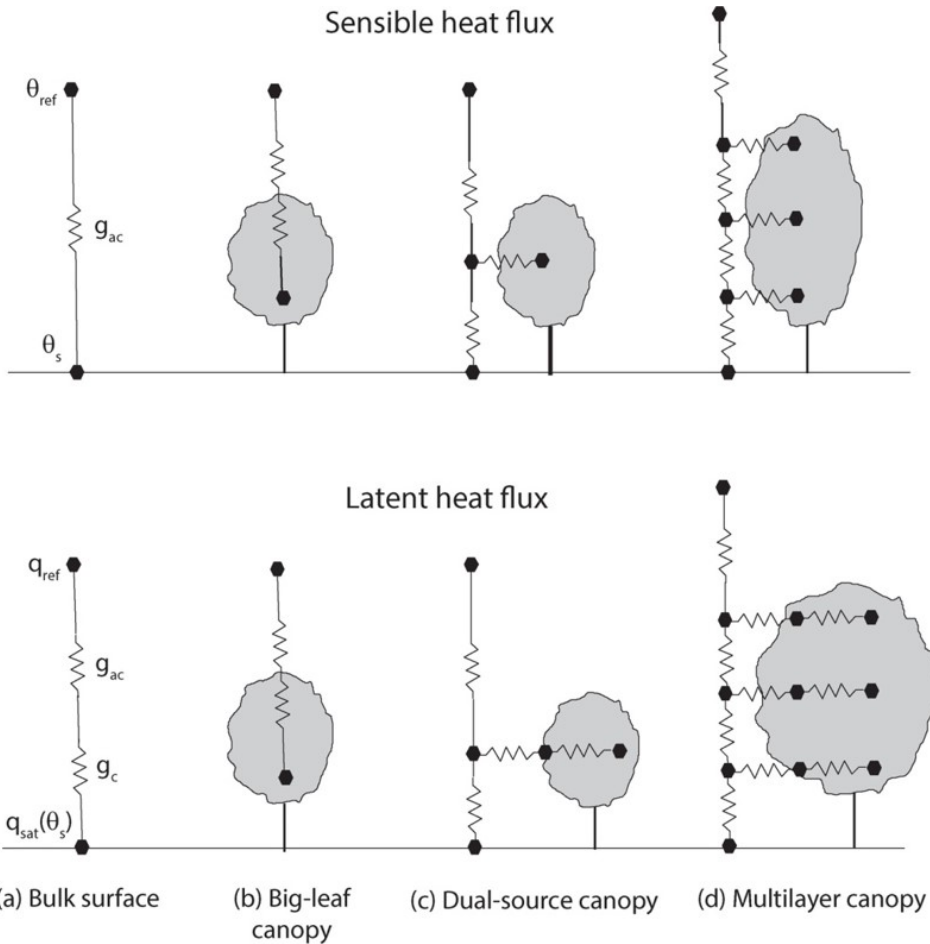


Figure 3.30: Conductance networks for sensible heat flux (top) and latent heat flux (bottom) for various depictions of the land surface. This chapter describes the bulk surface and big-leaf canopies. (Bonan)

3.4.4 Leaf energy balance

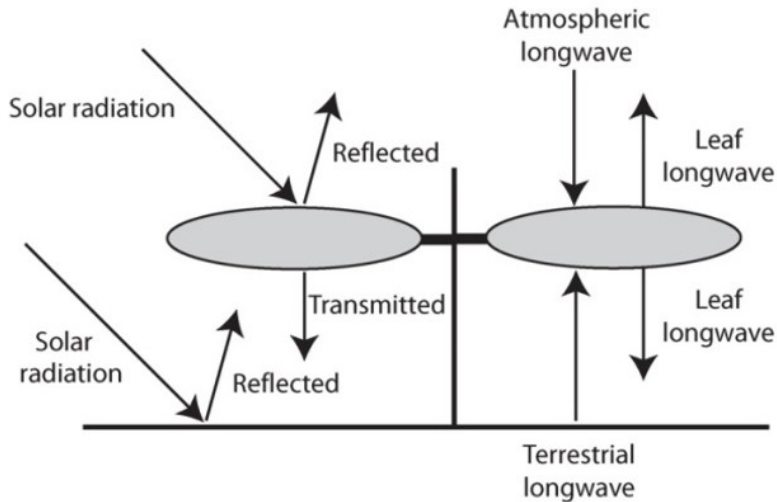
Some models make the leaf energy balance, which is essentially using the same equations as the bulk energy balance, but applying them at the leaf (layer) level and solving team for leaf temperature. The leaf energy balance depends on radiative forcing, boundary layer processes and stomatal physiology. The stomatal conductance is balance photosynthesis, transpiration and energy fluxes.

$$c_L \frac{\delta T_l}{\delta t} = Q_a - 2\epsilon_l T_l^4 - H(T_l) + \lambda E(T_l)$$

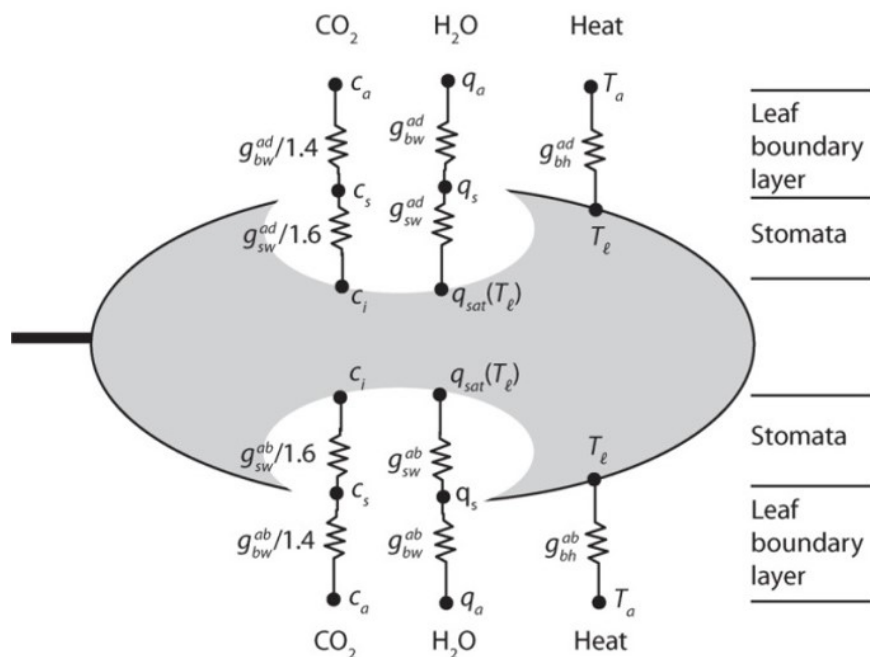
$$Q_a = \sum_{\Lambda} S_{\Lambda}^{\downarrow} (1 + \rho_{g\Lambda}) (1 - \rho_{g\Lambda} - \tau_{l\Lambda}) + \epsilon_l (L_{sky}^{\downarrow} + L_g^{\uparrow})$$

The dimension of the leaf plays an important role in the solving of the leaf energy balance, for example, the boundary layer conductance depends on the leaf dimensions and the wind speed.

(a) Radiative environment



(b) Boundary layer processes



(c) Stomatal physiology

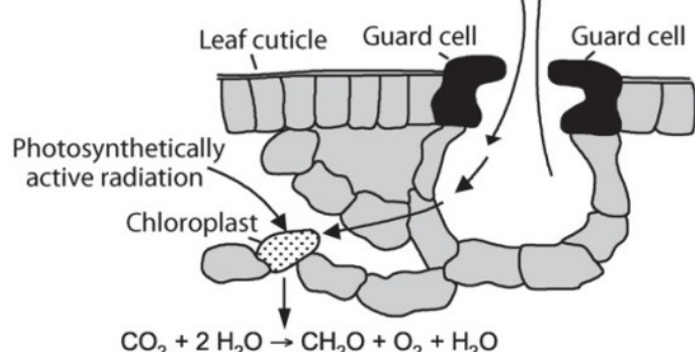


Figure 3.31: Biophysics and biochemistry of leaves. (a) The radiative environment consists of solar radiation (left) and longwave radiation (right). (b) Leaf fluxes include CO₂, H₂O, and heat through the boundary layer. These fluxes are shown as a network of resistors for the adiabatic (a) and barometric (b) boundary layers. (c) Leaf structure and photosynthesis. ⁷⁵

3.5 Case studies

3.5.1 Case study 3.1

How is the amount of diffuse light impacting photosynthesis? (diffuse radiation fertilization) In normal circumstances, the sun leaves are in the saturated zone of photosynthesis, while shaded leaves are somewhere on the linear increase part. If you would change the radiation composition (e.g. more clouds), this would result in less light for the sunlit leaves, which has only limited impact on their photosynthesis. For the shaded leaves on the other hand, more diffuse radiation has a big impact on the photosynthesis. So, the hypothesis in this study is that if you have more diffuse radiation, more photosynthesis takes place at the canopy level. This hypothesis is tested by using data of two fluxtower stations and a multilayer vegetation model.

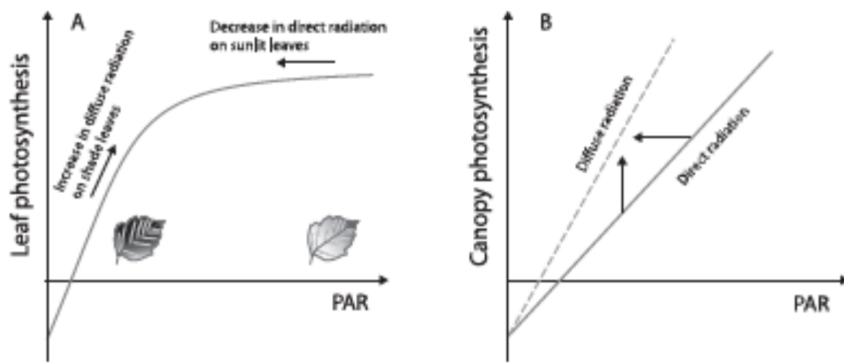


Figure 3.32: Principle of the effect of increased diffuse radiation on leaf/canopy photosynthesis. (Knohl et al. 2008)

The x axis (Fig. 3.33) represents the diffuse radiation over the total radiation. Photosynthesis increases with increasing diffuse radiation and reaches a maximum at 45% diffuse light. Transpiration increases also but at a slower pace, and the water use efficiency increases faster. So, forests have a higher water use efficiency when the amount of diffuse radiation is higher (again with max but now around 0.65). On cloudy days the R_d/R_s is higher than the optimum. The net carbon balance increased if you have more diffuse light (in relative terms), the transpiration remains stable but the WUE is increasing (more photosynthesis for the same amount of transpiration). However, for the studied sites, the situation is in 61% of the time beyond the optimum (on cloudy days), resulting in a net decreasing impact on the net carbon uptake.

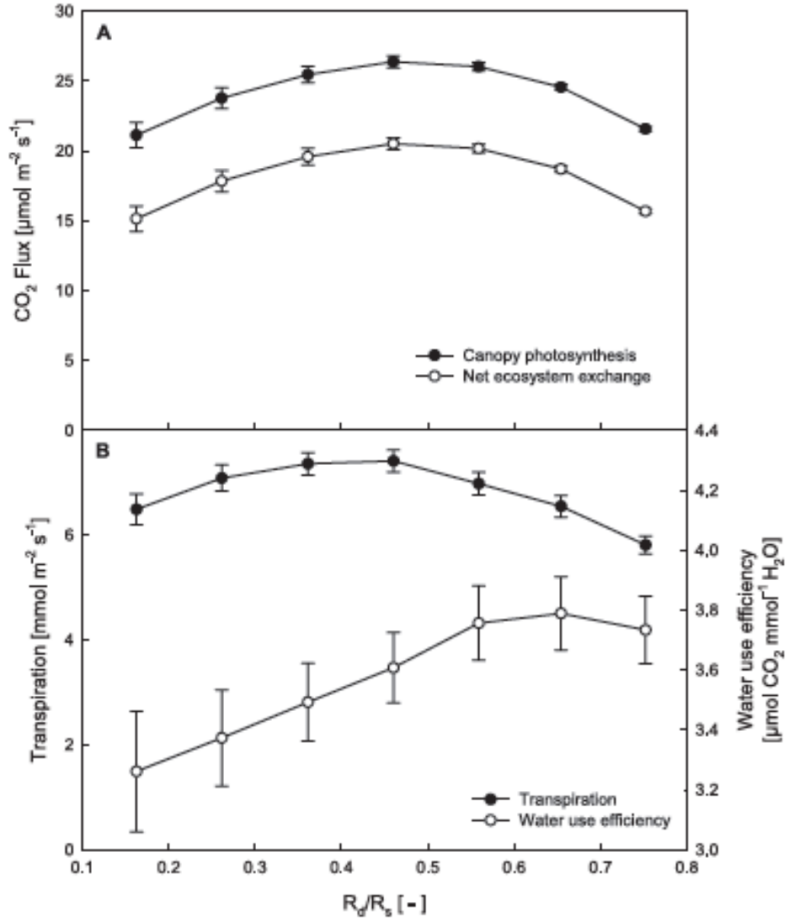


Figure 3.33: Resulting impact of changing diffuse fraction on carbon and water fluxes and WUE (Knohl et al. 2008)

3.5.2 Case study 3.2

Studies have shown that the increase of atmospheric CO₂ since the 1850's caused an enhancement in plant growth, but the magnitude varies. This enhancement also manifests itself in the enhancement of LAI (leaf area index), the area of leafs on a specific ground area. In the paper, Boreal Ecosystem Productivity Simulator (BEPS) was used as process-based diagnostic model. It initially was used, as the name states, for boreal ecosystems, but has been adapted for all ecosystems on Earth. It simulates the impact of drivers (climate, CO₂ concentration, and nitrogen deposition) on the GPP (Gross Primary Production) and as well carbon pools below GPP and respiration activities, generally, the whole carbon cycle, this on a daily time interval for each pixel. It makes use of various satellite data (assimilate LAI) and LUE (light-use efficiency) models.

Running these simulations on three LAI series, it stated that the enhancement of LAI contributed 12,4% to the accumulated carbon sink. In satellite observations it was observed that the global leaf area index has increased over the past 40 years, and they wanted to investigate whether this has had an effect on global carbon sink. The model used in this study is driven by remote sensing data, it is a diagnostic and not really

a process-based model. The model calculates the GPP based on the equation (seen today) which used LAI_{shade} and LAI_{sun} based on similar equation with exponential function, clumping factor and so on. The study aims to quantify how much the LAI increase is contributing to the simulated carbon uptake globally. Map shows the trends of the LAI in the world.

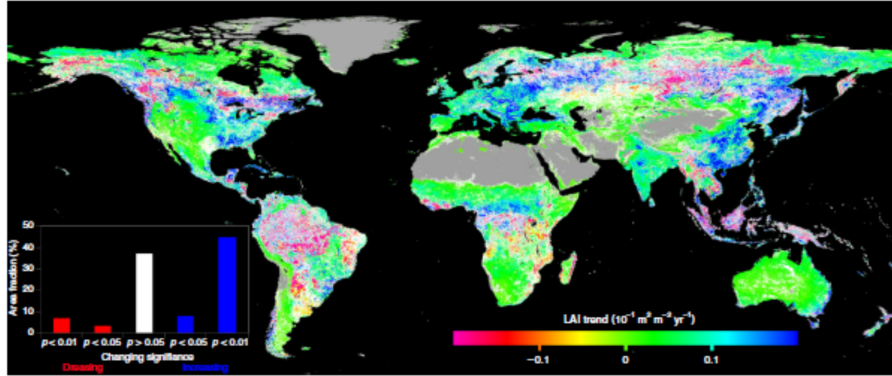


Fig. 1 Global map indicating the trend of LAI from 1981 to 2016. The gray color indicates non-vegetated areas and the white color denotes that the trend is statistically insignificant ($p > 0.05$). Positive values indicate increasing trends of growing season mean LAI and vice versa

Figure 3.34: Global map of LAI trend between 1981 and 2016 based on remote sensing (Chen et al. 2021).

They calculated the different factors which are accounted for in their model and tested how sensitive their model result was to that different driving factors. According to the model, global ecosystem productivity has increased (light blue line in Fig. 3.35). N deposition did not a net effect. Climate change (T increase, drought stress) has reduced the sink strength. The LAI increase had a positive impact, contributes to the increased sink. They observed that the relative increase of the maximum LAI per year was larger than the relative increase of the average LAI per year. This indicates that the average LAI increase is mainly caused by the higher maximum LAI, and not by the lengthening of the growing season.

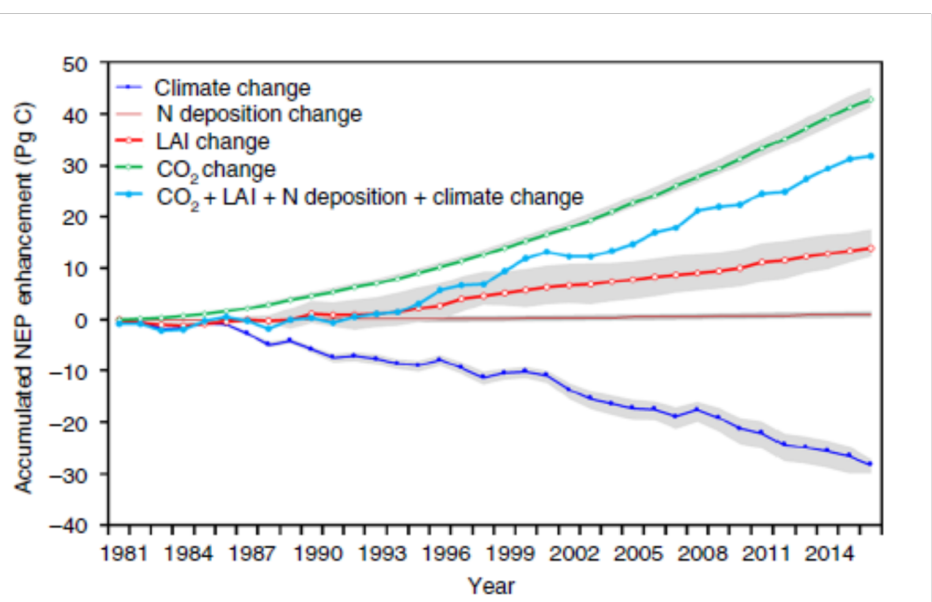


Figure 3.35: Simulated impact of different factors contributing to the increased global land C sink since 1981 (Chen et al. 2021)

Chapter 4

Modelling temporal and seasonal dynamics

The main topic of this chapter is temporal variations in fluxes and leaf seasonality. We will study the upscaling in time, going from instantaneous processes to daily and seasonal dynamics (temporal dynamics), focusing on phenology.

4.1 Introduction on temporal dynamics

An example shows how we use flux data to evaluate the diurnal and seasonal cycles of models (Figure 4.1). The modeled data is shown in black, the measured data in different colors, for different variables. The model can predict diurnal (instantaneous) fluxes good, seasonal cycles are more difficult to predict because the leaf area changes over time.

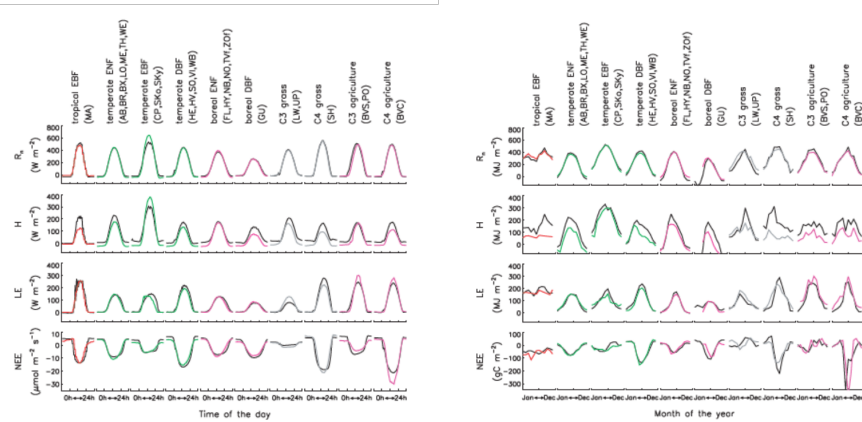


Figure 4.1: Evaluation of the temporal dynamics of fluxes (R_n : Net Radiation, H : sensible heat, LE : latent heat, NEE : net ecosystem exchanges of CO_2) simulated by the global model ORCHIDEE. LEFT: measured (color) and modelled "summer" diurnal cycle for each flux and each PFT. RIGHT: measured (color) and modelled seasonal cycle for each flux and each PFT. (Krinner et al. 2005)

The temporal dynamics of fluxes respond to multiple factors and depending on the scales we are looking at, we need to take other processes into account. If we are interested in **instantaneous** responses, we need to modulate the physiological processes (stomata of leaves). On the other hand, if we look at **seasonal** responses, we need to consider both physiology and phenology (the amount of leaves the vegetation has). It is also important to mention **long-term** responses; for example, if you want to simulate carbon fluxes for the coming decades, more (slower) processes need to be considered (e.g. forest succession). The focus of this chapter will be on seasonal responses and phenology. These are processes that are typically calculated on an intermediate time step (e.g. daily or monthly) in vegetation models.

4.2 Phenology: the background

Phenology is the study of periodic events in biological life cycles and how these are influenced by seasonal and interannual variations in climate, as well as habitat factors (such as elevation). There is a link with carbon allocation, which means how much carbon will be distributed over different plant compartments. The phenological processes respond to climate variability, the so-called environmental cue, an environmental trigger. For example, from observational data, the ecodormancy responds both to high temperatures and longer day length. It is a complex mechanism with many factors, and we still don't know the underlying physiological processes.

4.2.1 Trends in phenology

There are important trends in phenology with climate change because it's not only global average temperatures that are changing, but also spring temperatures are advancing. Autumn temperatures are coming later in the year. Figure 4.2 shows an example of needle appearance dates (for larch), where it is possible to identify a trend of needles appearing earlier. New needles of larch trees appear more early over time and this shift is accelerating. Shifts are occurring in the range of weeks. Such phenological trends have an impact on ecosystem functioning, and those impacts of shifting leaf phenology can manifest in multiple ways (Fig. 4.3).

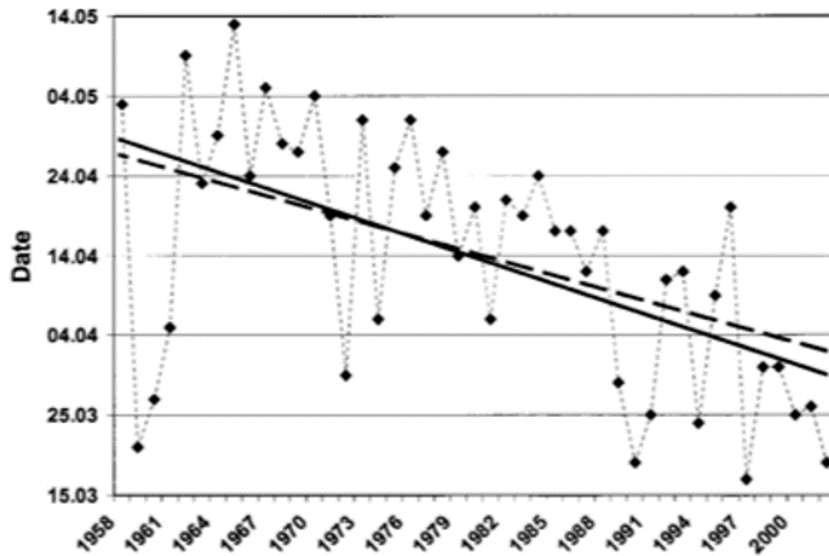


Figure 4.2: Larch needle appearance in Sargans 1958-2002. Dashed line is trend 1958-1999, solid line is trend 1958-2002. (Defilia and Clot 2005)

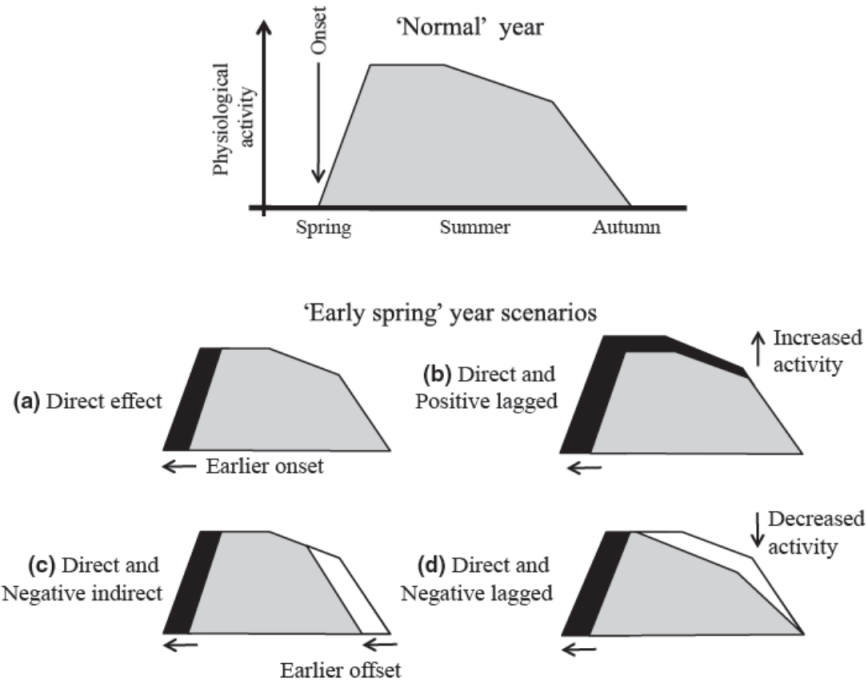


Figure 4.3: Concept of various effect that changing phenology can have on ecosystem processes (e.g. productivity or transpiration). (Polgar and Primack 2011)

A shift in phenology has an impact on the functioning of ecosystems. In a normal year the physiological activity (e.g. photosynthesis) increases after leaves are formed, reaches a maximum, and after the summer a decrease occurs because of less efficient

leaves and less light input. Due to changes in phenology, this is influenced (direct or lagged, positive or negative):

- A) Full positive effect, faster maximum
- B) A total increase in amount of leaves, also benefits in summer
- C) Earlier onset of leaves cause earlier senescence of leaves, causing less assimilation in autumn
- D) Faster ageing leaves: decrease activity after spring

4.3 Leaf phenology models

Leaf phenology models are essentially models used to update the leaf area state variable for PFTs in vegetation models.

Phenology is typically a PFT dependent process in vegetation models:

- Evergreen PFTs typically have a constant background leaf turnover rate.
- Summer green and rain green PFTs have a leaf phenology driven by environmental factors (temperature, water, light, ...).

How to model phenology? We don't have (bio)physical models, only empirical models:

- Option 1: prescribed phenology
 - Prescribed dates of leaf onset and offset (4 dates to determine carbon allocation phases to leaves).
 - Or data assimilation of remote sensing data (LAI).
- Option 2: prognostic phenology
 - A complete leaf phenology model includes carbon allocation, leaf onset and growth, and litterfall as influenced by environmental conditions (still empirical).

4.3.1 Prescribed phenology

An option to model phenology is using the dates of leaf onset and offset (typical 4 dates; start leaf formation, maximal activity, start senescence, all leaves 'are gone') .

An alternative is to fit a function to remote sensing data. What is typically done is fitting a logistic function of time to remote sensing observations of leaf phenology:

$$y(t) = \frac{c}{1 + e^{a+bt}} + d$$

If we observed phenology with satellites, it could be done using vegetation indices (NDVI, EVI, ...). Based on observation indices throughout the year, we could define dates to phenological events (Figure 4.4)

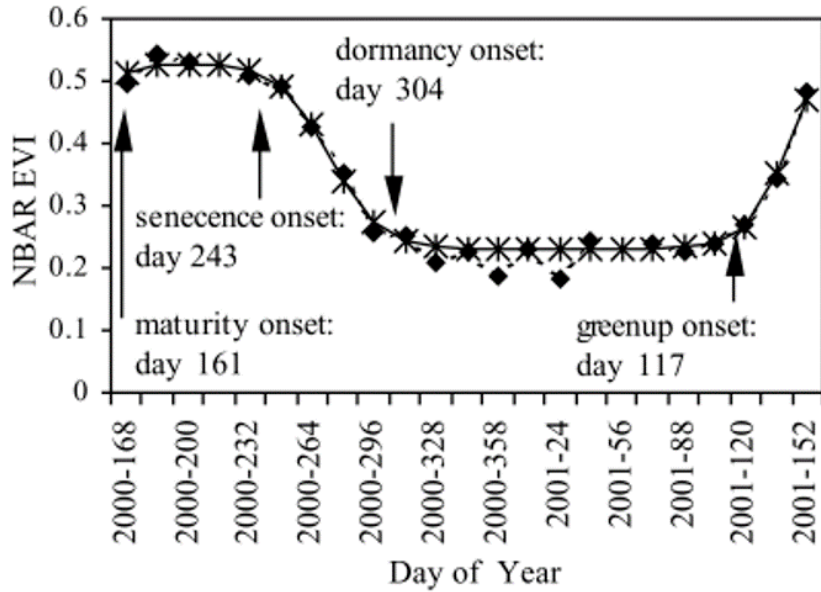


Figure 4.4: Sample time series of MODIS EVI data and estimate phenological transition dates for a mixed forest pixel in New England. Diamonds: EVI data, solid line with stars: fitted logistic model. (Zhang et al. 2003)

This approach allows plotting maps with the key days for phenology (Figure 4.5) and seeing the spacial variance in shifts in phenology. Such datasets can be used to train prognostic models.

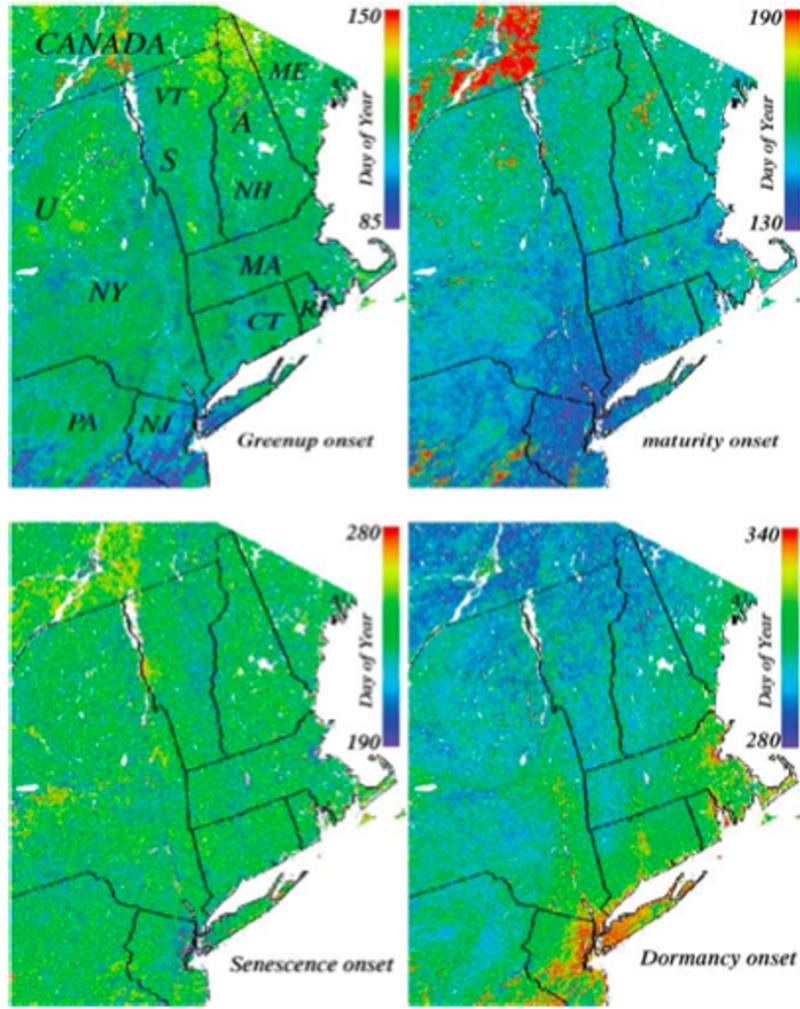


Figure 4.5: Maps of phenological transition dates for New England. (Zhang et al. 2003)

4.3.2 Budburst models

Budburst models are prognostic models and are the most developed ones (compared to senescence models for example). They simulate when a bud is becoming a leaf. These models are based on environmental signals (cues), and the most common approaches are:

- Degree day sums (summation of daily temperature above 5° , for example).
- Chilling requirement (to pass the danger of spring frost) (accumulation of cold T).
- Photoperiod (daylength).
- Soil moisture (for rain green plants).

Some models combine approaches of the above, and others use just one approach. Most of the time, air temperature is used in these models (and not bud temperature).

Growing degree-day model

It's the simplest version of the budburst models but also the most widely used. However, this approach only works well in systems where temperature is the only limiting factor:

$$GDD = \sum_{T > T_{base}} (T - T_{base}) \text{budburst} : GDD > F^*$$

Identify some threshold value of GDD F^* that corresponds to the metric of interest, which is budburst in this case. Similar models can be made for fruiting or harvest.

Photoperiod

Used only for some species where there is empirical evidence that photoperiod plays a dominant role. Typically not used in global models.

Models including chilling

More complicated phenology models use a combination of growing degree days and a chilling requirement (amount of cold days). There are different ways to implement such a combination:

- *Sequential models*: forcing (GDD) only starts when the chilling requirement is met.
- *Parallel models*: chilling and forcing accumulated in parallel and critical values then applied to both.
- *Alternating models*: the temperature F^* is a decreasing function of chilling.

4.3.3 Senescence models

Process of leaf ageing. Many models are based on daylength (photoperiod), but many others use temperature or drought. Some models are also driven by the negative carbon balance of the leaf.

4.3.4 Leaf age

Leaf age is quite important because if you want to simulate fluxes throughout the season, it will depend not only on the number of leaves but also on the physiological activity of leaves related to their physiological age (e.g. young leaves perform typically photosynthesis at a higher). For example, the leaf's functional traits (nutrient content and water content) will change over time. This effect is especially important for evergreen species. If we want to have a good simulation for boreal forests, we should account for leaf age.

Some models track (big) leaf age and link the values of leaf parameters to leaf age. Figure 4.6 shows an example based on data where V_{cmax} is linked to leaf age. The photosynthetic capacity is typically reduced significantly from a certain leaf age threshold.

Some models also use leaf age classes, where it is assumed that a certain fraction of the leaf area of the system is young and a different fraction is constituted of middle-aged leaves. Of course, with the beginning of the growing season, more young leaves are added, but the leaves aged and change fraction. However, the majority of vegetation models do not account for leaf age classes.

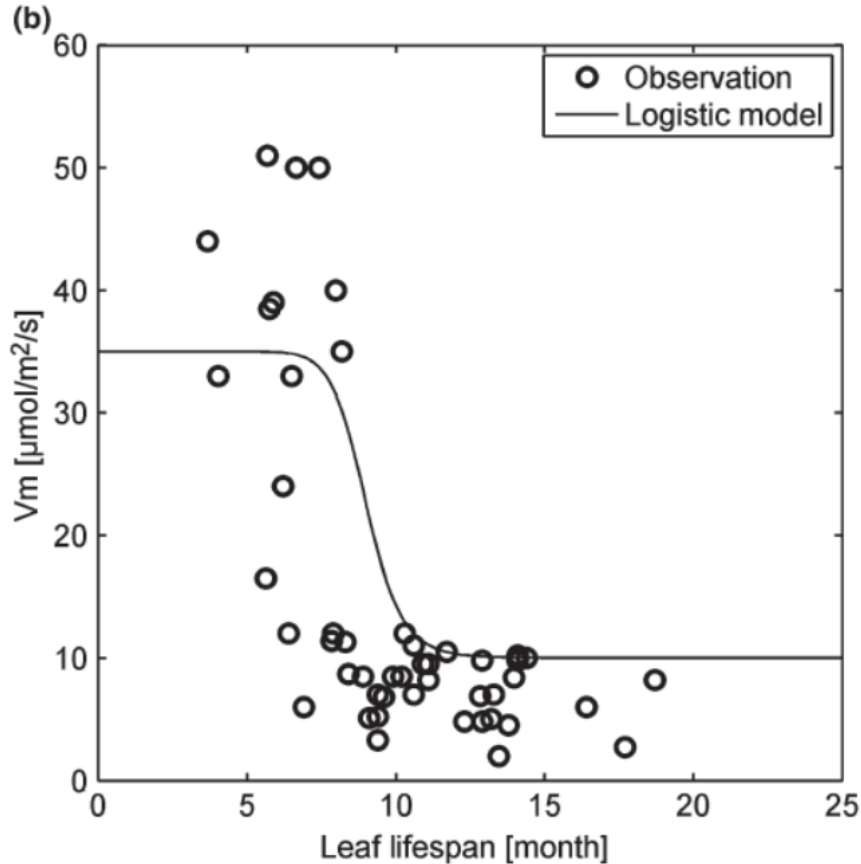


Figure 4.6: Relation between V_{cmax} and leaf age in the ED2 vegetation model. (Kim et al. 2011)

4.3.5 Phenology in DGVMs

A few general facts are important to know concerning phenology in global vegetation models:

- The precise way to model phenology is highly uncertain
- Vegetation models differ significantly in detail for modelling phenology
- The phenology models are mainly based on empirical equations and parameters
- Phenology is an important process in monitoring, modelling and understanding vegetation dynamics and their response to climate variations.

- The growing amount of observational data on phenology at various scales will allow us to make better phenology models in the future.
- Likely that for some areas at least, species-specific (or slightly broader groupings of species) parameterizations of phenology need to be considered rather than just broad PFT definitions.

4.3.6 Phenology in the tropics

Phenology is very complex if we focus on evergreen tropical forests. Figure 4.7 shows an example of the Yangambi reserve (centre of the Congo basin) classified as a semideciduous tropical forest. Based on digitized historical data, we can make an overall summary (Figure 4.8) showing the phenology complexity of the tropical rainforests. It is very hard to see an overall pattern. In the semi-deciduous forest, many trees lose their leaves at (ir)regular moments. Evergreen species are continuously dropping leaves, whereas deciduous trees have more specific periods (more clear seasonality). Most models in evergreen forests assume that the leaf area is (more or less) constant over time, but this figure shows that in reality the leaf area can also change over time in evergreen forests. An attempt of improving phenology modelling in evergreen forests is discussed in case study 4.2.

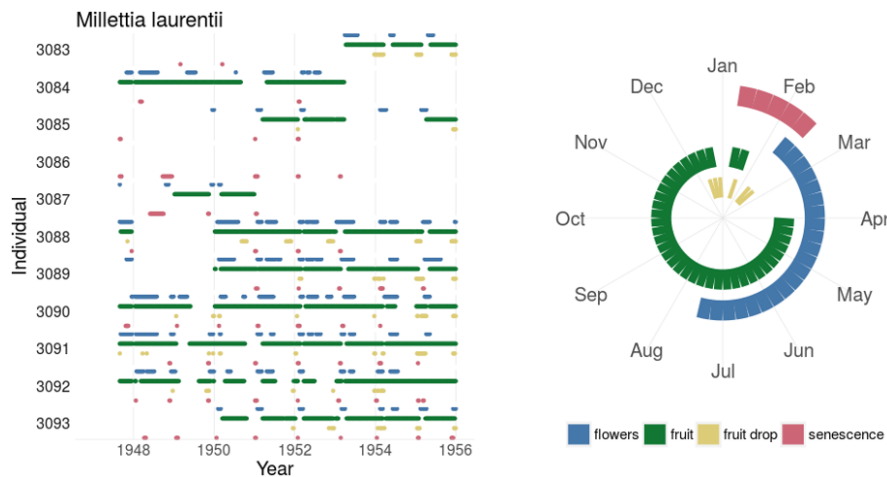


Figure 4.7: Example of how manual historical phenology observations in Yangambi (DR Congo) are translated in a visual phenology pattern for a single tree species. (junglerythms.org))

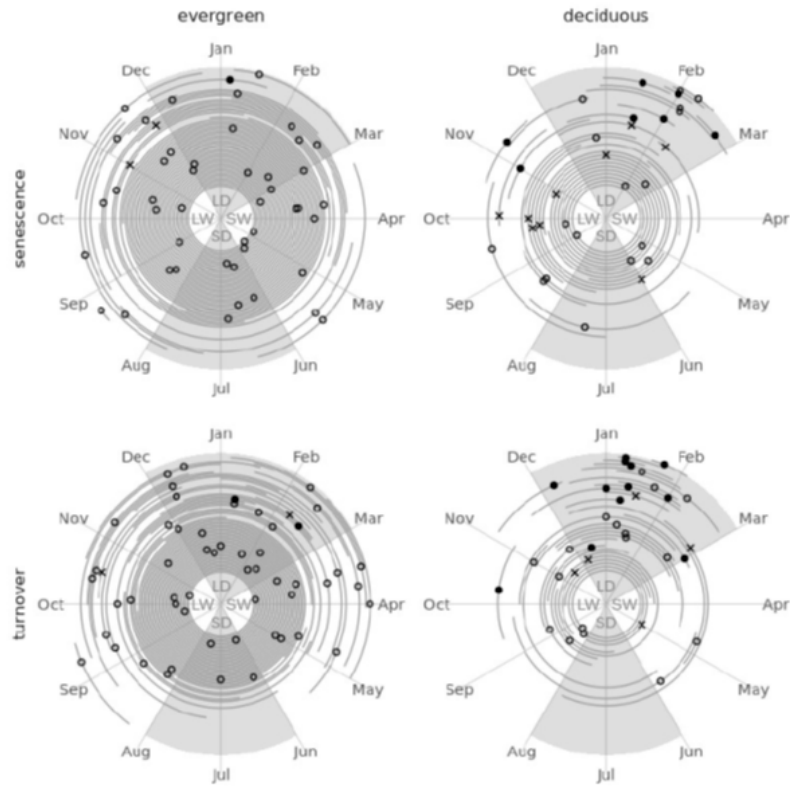


Figure 4.8: Overview of species-specific timing of onset of leaf phenophases for evergreen and deciduous species in tropical forest in Yangambi (DR Congo). The median timing of the onset of leaf senescence and turnover is indicated for each species. Species-specific bootstrapped 95%-confidence intervals are indicated with a line segment. Species are arranged according to the variability in the timing of the phenophase, with species with the lowest uncertainty at the outer edge and continuing towards the center. Species with an annual (full circles) or sub-annual (crosses) fourier-based seasonality are indicated. Grey shaded areas represent the average timing of the long and short dry seasons (LD and SD; monthly precipitation < 150 mm), separated by the long and short wet seasons (LW and SW). (Kearsley et al. 2021))

4.4 Case studies

4.4.1 Case study 4.1

Richardson, A. D., Anderson, R. S., Arain, M. A., Barr, A. G., Bohrer, G., Chen, G., ... & Xue, Y. (2012). Terrestrial biosphere models need better representation of vegetation phenology: results from the North American Carbon Program Site Synthesis. *Global Change Biology*, 18(2), 566-584.

The study of Richardson et al.(2012) is part of the North American Carbon Program, an initiative that is studying the North American land carbon cycle using various data platforms, including multiple flux tower stations. In this specific project, 14 vegetation

models are compared and ran for the same flux towers with a very detailed protocol to make results comparable. The study is focused on how good models are predicting seasonal cycles. Figure 4.9 represents the simulated leaf area index (LAI) for five sites on deciduous forests. The overall growing season was predicted too long by models (too early spring and too late autumn), leading to an overestimation of GPP.

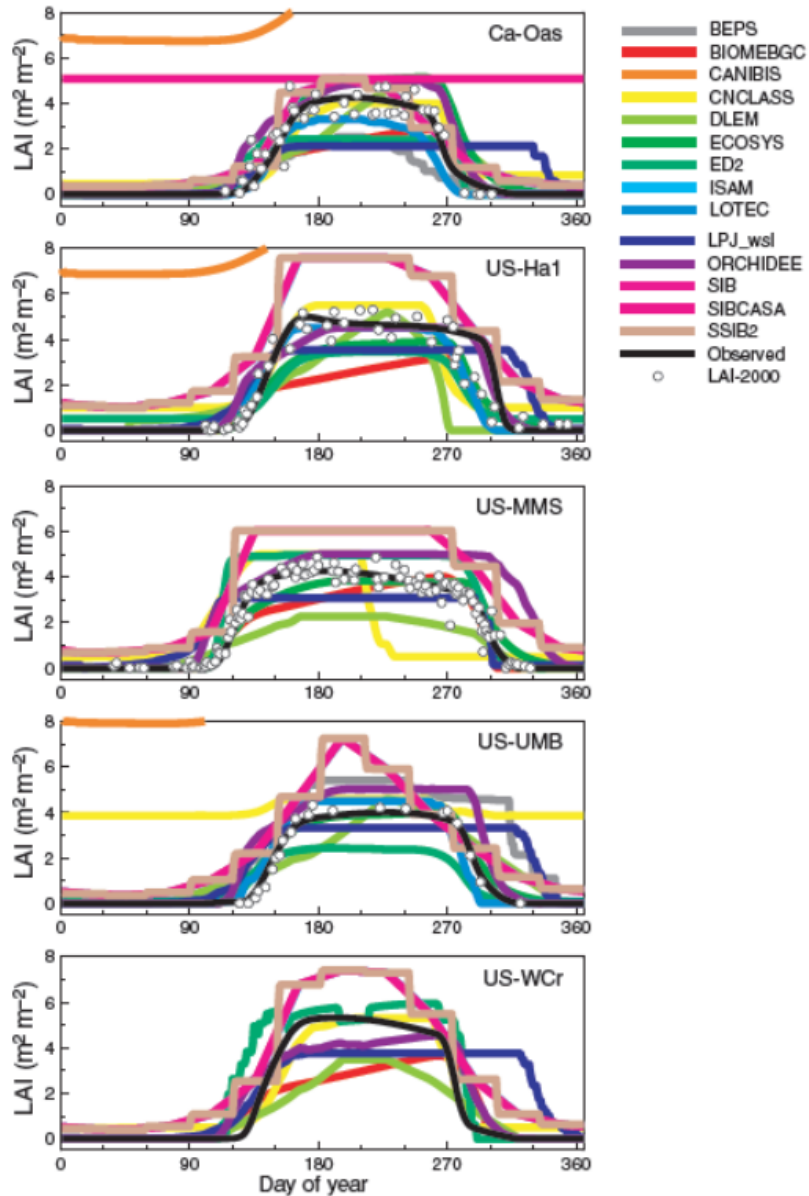


Figure 4.9: Simulated and observed LAI for 5 deciduous forest sites and 14 vegetation models participating to the NACP model intercomparison project. (Richardson et al. 2012)

Large biases are present for deciduous forests, evergreen forests are better predicted. If we want to be able to perform better C-fluxes simulations in the future, better understanding of phenology is necessary.

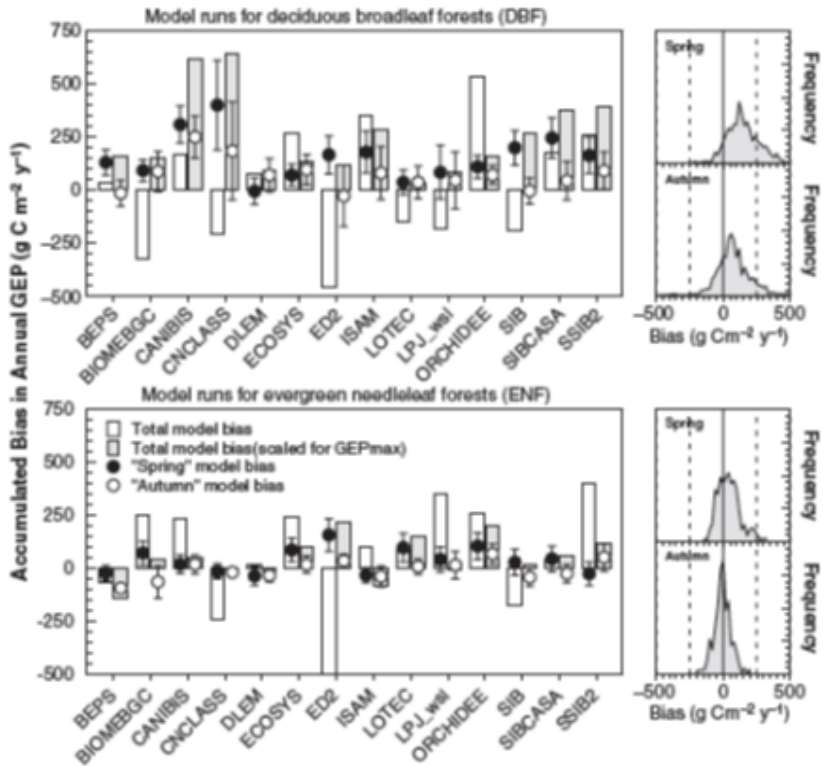


Figure 4.10: Bias in modeled gross ecosystem photosynthesis (GEP=GPP) for deciduous broadleaf (top) and evergreen needleleaf (bottom) forests. Left panels show bias, by model. Right panels show the frequency distribution of these spring and autumn biases in re-scaled model GEP, across all models, sites, and years of data, for each forest type. The sign convention is that positive bias means that modeled GEP > tower GEP. (Richardson et al. 2012)

The conclusion of this study is the models are not very good at predicting the timing of seasonality.

4.4.2 Case study 4.2

Chen, X., Maignan, F., Viovy, N., Bastos, A., Goll, D., Wu, J., ... & Ciais, P. (2020). Novel representation of leaf phenology improves simulation of Amazonian evergreen forest photosynthesis in a land surface model. *Journal of Advances in Modeling Earth Systems*, 12(1), e2018MS001565.

The study of Chen et al. (2018) is an attempt to improve phenology modelling in evergreen forests. This study uses a leaf age – leaf functioning relation and shows clearly the **links between phenology and photosynthetic activity**.

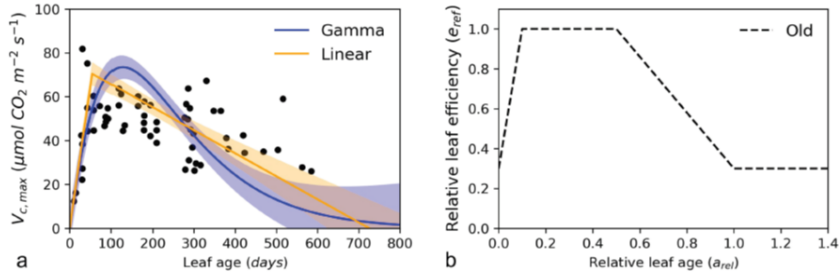


Figure 4.11: Observed and assumed relation between $V_{c,\text{max}}$ and leaf age in the ORCHIDEE global model, for the tropical evergreen PFT. (Chen et al. 2018)

Improved GPP simulation if phenology and leaf age is better represented.

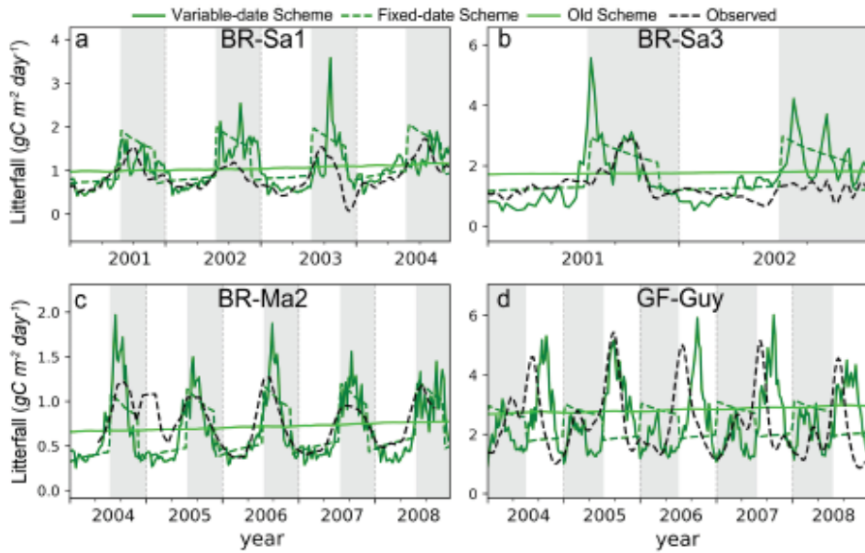


Figure 4.12: Comparison of litterfall data with two new and the old leaf turnover schemes in the ORCHIDEE model for 4 sites in the Amazon. (Chen et al. 2018)

Improved GPP simulation if phenology and leaf age is explicitly discussed.

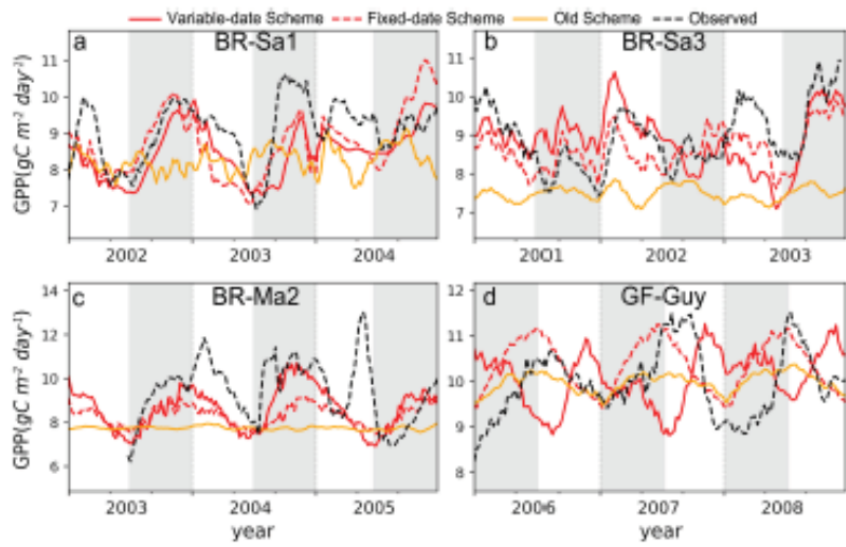


Figure 4.13: Comparison of GPP fluxtower data with two new and the old leaf turnover schemes in the ORCHIDEE model for 4 sites in the Amazon. (Chen et al. 2018)

Part II

Modelling vegetation dynamics

Chapter 5

Modelling C-allocation and biogeochemical cycles

5.1 Introduction

In Part I of the course we focused on modelling fluxes, but ecosystem dynamics involve other aspects (biogeochemistry, demography, biodiversity) that determine its functioning. The aspects, discussed in Part II, are typically important at larger temporal and spatial scales than the processes that determine fluxes. In this chapter we will focus on the biogeochemical perspective, studying the full cycle of carbon or nutrients, accounting for pools and fluxes. The biogeochemical perspective is illustrated by the Figure 5.1. Bauters et al. (2019) studied a landscape with forests of different age on the same soil and with the same climate (a chronosequence). Figure 5.1b shows the classical description of these forests in terms of stem density, basal area and tree height. While Figure 5.1a shows the situation from a biogeochemical perspective, focusing on aboveground and below ground carbon pools (not accounting for the number of trees etc.).

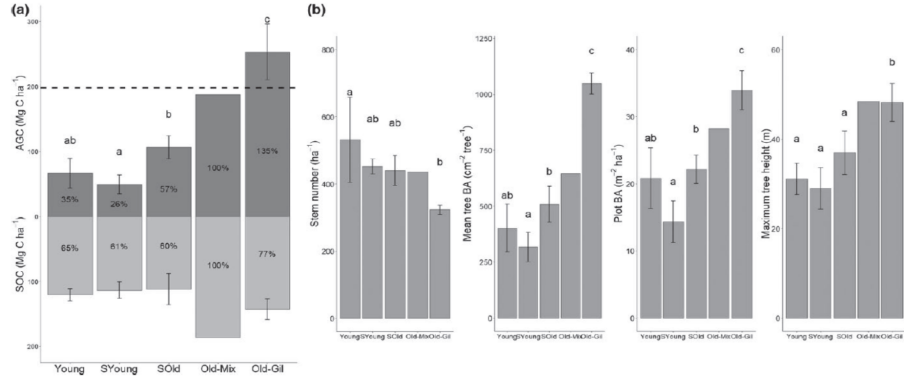


Figure 5.1: Forest succession. (a) the biogeochemical perspective: variation of above-ground carbon (AGC) and soil organic carbon (SOC) along the forest succession in the Maringa-Lopori-Wamba landscape (DR Congo). Young: recently abandoned farmland, 5–25 years; SYoung: second growth young forest, 25–30 years; SOld: second growth old forest, approx. 150–300 years; Old-Mix: old growth mixed forest, 1700 years; Old-Gil: old growth Gilbertiodendron forest.BA stands for basal area. Error bars represent standard deviations. Percentages are stock values relative to the value of Old-Mix forest. The dashed horizontal line indicates the regional mean AGC of old growth forests across Central Africa (Lewis et al., 2013). (b) the forest structure perspective: Variation of four forest structure plot variables along the successional stages at our study site. Bars represent mean plot values per successional stage. Error bars represent standard deviations. BA stands for basal area. Error bars represent standard deviations. No standard deviations were calculated for Old-Mix because of its single plot replicate. Significant differences across forest types are indicated by different letters per type ($p < 0.05$)(Bauters et al. 2019)

5.2 Carbon cycle models: stocks and fluxes

In this section we refresh your knowledge on the carbon cycle and translate that into a basic carbon cycle model. We typically study carbon pools and fluxes (Figure 5.2). The fluxes are the flow of carbon between pools, e.g litter fall, respiration,... The gross primary productivity (GPP) is the photosynthesis at the ecosystem level and is the largest gross flux. The carbon taken up by photosynthesis is allocated to different plant parts (roots, stems, leaves). This is a key process, as the pool where the carbon is ending up will determine the residence time and the potential long-term carbon storage in the system. In addition to GPP and allocation, the carbon balance is controlled by autotrophic and heterotrophic respiration and carbon turnover (litter fall, mortality and disturbances). As we will discuss later in this chapter, in parallel with carbon fluxes we can also study nutrient fluxes between the different plant and soil pools.

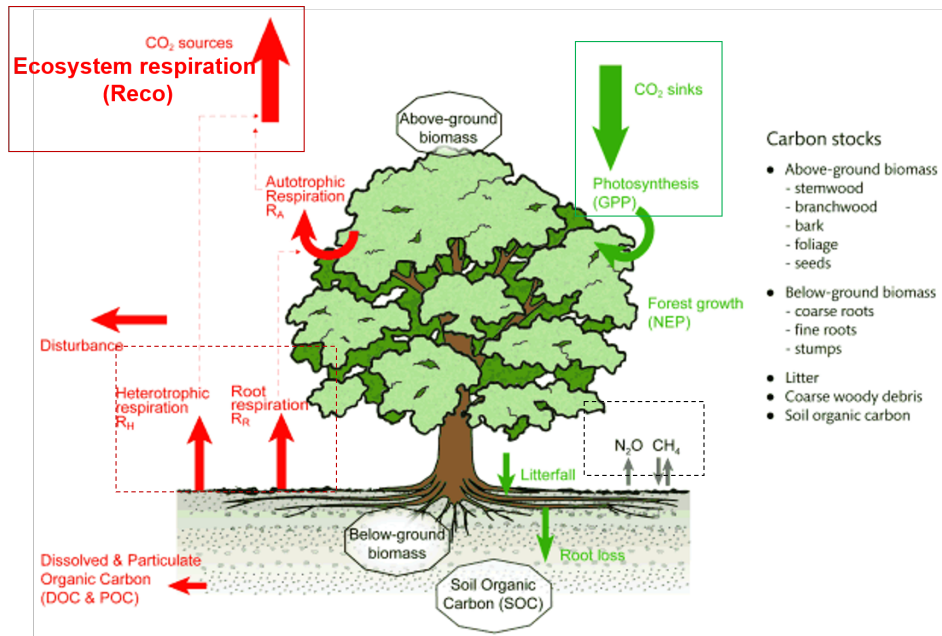


Figure 5.2: Forest carbon cycle: stocks and fluxes.

The carbon cycle of ecosystems is typically studied in terms of productivity (Figure 5.3). The net primary productivity (NPP) is the net production of the vegetation calculated as the difference between the GPP and the autotrophic respiration. A positive NPP corresponds to a net carbon uptake (growth) of the vegetation. If we subtract from the NPP the heterotrophic respiration we get the net ecosystem productivity (NEP), which is the full carbon balance of the ecosystem (vegetation + soil). A positive value of NEP means carbon uptake by the ecosystem from the atmosphere. Atmospheric scientists are estimating the NEP by using fluxtowers. In that case the measure the net ecosystem exchange (NEE) as estimate of NEP. Remark: for fluxtower measurements an opposite sign convention is used, where a negative NEE means a net carbon uptake, corresponding to a positive NEP.

When “non-respiratory” components are taken into account you get the net biome productivity (NBP):

$$NEP = GPP - R_a - R_h = NPP - R_h$$

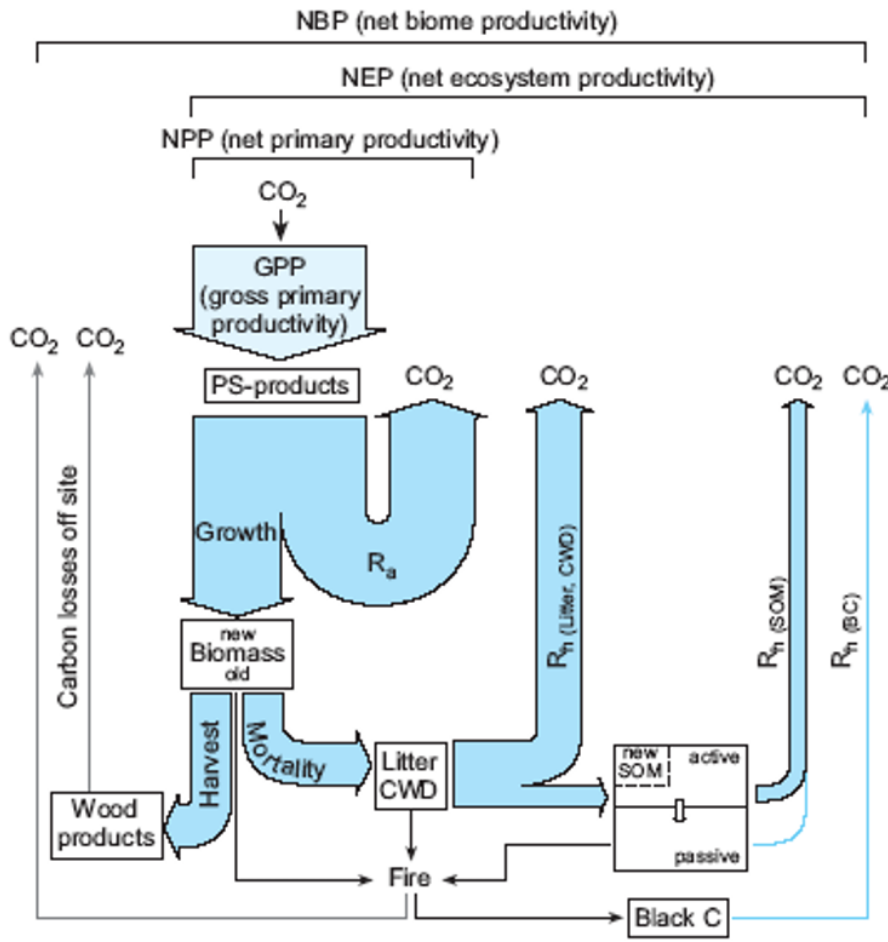


Figure 5.3: Definitions of productivity terms in the carbon cycle (Schulze et al. 2000)

When considering all carbon stocks and fluxes in an ecosystem (Figure 5.2), it is striking that usually only a few components are (or can be) measured. In most monitoring plots only carbon stocks in wood (inventories) and soil (soil sampling) are observed. In terms of fluxes, woody productivity and litterfall are the most commonly observed. In some cases NEE is observed by eddy covariance fluxtowers and sometimes soil respiration is observed via chamber measurements. All other stocks and fluxes are hard to measure (e.g. root growth, ...). In that respect vegetation models are very useful to estimate those stocks and fluxes that cannot be measured and to close the full carbon cycle of the ecosystem.

Biogeochemical models for the carbon cycle are relatively simple models, essentially doing the bookkeeping of the carbon stocks. These models follow a few key principles:

- the net carbon input of the ecosystem is calculated by subtracting the autotrophic respiration (R_a) from the GPP: $NPP = GPP - R_a$
- Within the ecosystem, carbon flows (fluxes) between donor to receiver pools are depending on: Donor pool size, Chemical quality, and the Environment

- Mass balance must be maintained (no carbon can be lost, except via respiration to the atmosphere)
- Decay of litter and soil organic matter releases CO₂ heterotrophic respiration (R_h).

These principles result in a system of first order linear differential equations (see CASA CNP model below). The above-mentioned principles are common to any type of ecosystem, which has facilitated the wide use of biogeochemical models in global vegetation models.

The GPP is calculated based on the various photosynthesis models that were presented in chapter 2. Some models calculate R_a as a constant fraction of GPP (example: $R_a = 0.5 \cdot GPP$), but most biogeochemical models consider the autotrophic respiration as the sum of maintenance and growth respiration.

$$R_a = R_m + R_g$$

The maintenance respiration (R_m) is the cost to support living biomass (including the repair of membranes and proteins). R_m is temperature dependent and therefore typically Q10 or Arrhenius functions are used. In addition, R_m is proportional to the amount of biomass of specific organs and the type of tissue. Leaves and fine roots are for example more costly, depending on their protein content.

The growth respiration (R_g) is the cost of synthesis of new biomass, and is independent of temperature. Some models assume a fixed fraction of NPP ($R_g = 0.25 \cdot NPP$). Growth has a double carbon cost: the cost to incorporate C into the biomass and the energy (respiration) needed to drive the biosynthetic reactions. If you know the biochemical constitution of the plant tissue (leaf, wood, etc.), we can calculate the cost of transforming basic sugars into the complex molecules (e.g. lignin) out of which the plant/tree is built. To illustrate the functioning of biogeochemical model, we will study in detail the CASA CNP model (Figure 5.4). This model has 9 pools: 3 plants pools, 3 litter pools and 3 soil organic matter pools. The three litter pools are: structural litter (not yet decomposed), metabolic litter (easy decomposable), CWD (coarse woody debris, dead branches lying on the forest floor). The model essentially consists of 9 equations that calculate the change of each carbon pool over time, which is calculated by summing up the incoming carbon and subtracting the outgoing carbon of each pool. The change of carbon content of each plant pool is calculated according to the equations below, where the input is determined by the NPP which is the carbon available for growth:

$$\frac{dc_1}{dt} = b_1 NPP - \xi_1 k_1 c_1$$

$$\frac{dc_2}{dt} = b_2 NPP - k_2 c_2$$

$$\frac{dc_3}{dt} = b_3 NPP - k_3 c_3$$

Where b_i are allocations factors to leaves, roots and wood respectively. These allocation factors may vary over time with phenology and are specific for their pool, the CASA-CNP model uses constant fractions.

k_i are turnover rates for plant and organic matter pools in litter and soil. The example values in the figures are given for broadleaved forest. These turnover rates can be modified for environmental conditions, for examples for leaf turnover by the factor ξ_1 . If a turnover rate (e.g. for leaves) is higher than 1, it means that leaves are replaced more than one time per year. The change of carbon content of each litter and soil pool is calculated by the following equations:

$$\frac{dc_4}{dt} = a_{41}\xi_1 k_1 c_1 + a_{42}k_2 c_2 - \xi_4 k_4 c_4$$

$$\frac{dc_7}{dt} = a_{74}\xi_4 k_4 c_4 + a_{75}\xi_5 k_5 c_5 + a_{76}\xi_6 k_6 c_6 - \xi_7 k_7 c_7$$

Where the turnover rates k_i are modified for soil temperature and moisture using the ξ_i factors and where the a factors depend on lignin content and C/N ratio of the respective pools. The a factors can be calculated as:

$$a_{ij} = (1 - r_{ij})f_{ij}$$

with:

f_{ij} = fraction that is allocated from j to i, and r_{ij} = fraction lost as heterotrophic respiration R_h (represented by the small arrows in Figure 5.4).

Biogeochemical models like CASA-CNP can work on various timesteps. Some models simulate the allocation and biogeochemistry on a daily calculation step, others use a monthly or annual time step.

The equations of the CASA-CNP model, and any similar biogeochemical model can also be written in generalized matrix form, with PFT specific parameters, to calculate the biogeochemical pools and fluxes in a rather efficient way.

Other biogeochemical models work in a very similar way, but the implementation can differ strongly (e.g. the number of pools considered, the environmental factors accounted for, etc.).

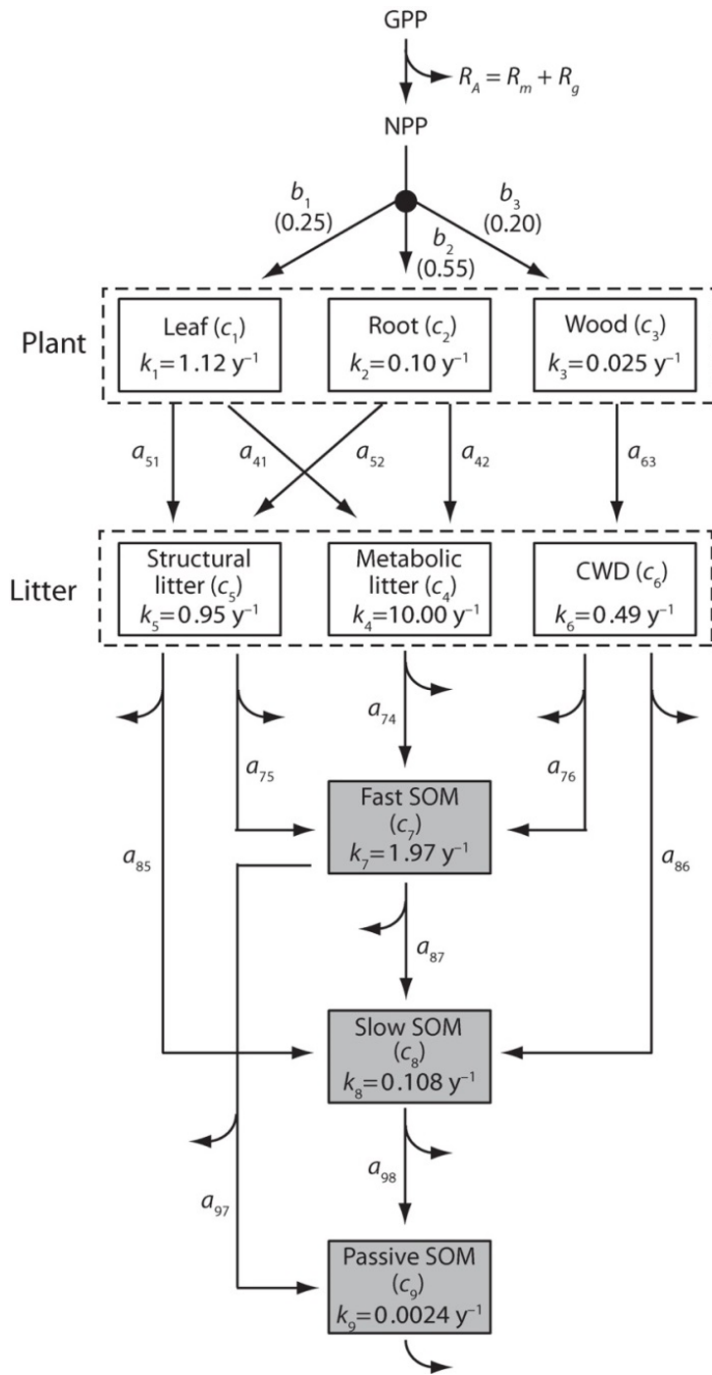


Figure 5.4: Structure of the nine-pool CASA-CNP biogeochemical model (Wang et al. 2010). Plant carbon mass consists of leaf c_1 , fine root c_2 , and wood c_3 . Net primary production is allocated to plant material in proportion to b_i . Plant residue becomes metabolic litter c_4 , structural litter c_5 , or coarse woody debris c_6 . These pools decompose to fast c_7 , slow c_8 , and passive c_9 soil organic matter. Pools differ in base turnover rate k_i . Lines indicate carbon pathways, with a_{ij} the fraction of carbon turnover from pool j that enters pool i after heterotrophic respiration loss. Curved arrows denote heterotrophic respiration fluxes for each pathway. Shown are representative allocation and turnover rates for evergreen broadleaf forest. (Bonan)

Figure 5.5 illustrates the result of a simulation over 1000 years by the CASA-CNP model. It illustrated that long time scales are needed to bring carbon pools at equilibrium. Plant pools reach there maximum carbon stocks relatively quickly, while SOM pools needs more time, illustrating that old forest keep on sequestering CO₂ for centuries in this simulation. The broadleaved evergreen forest simulated here, needs more than 3000 years to reach equilibrium. The residence time of carbon in the respective carbon pools is also very different.

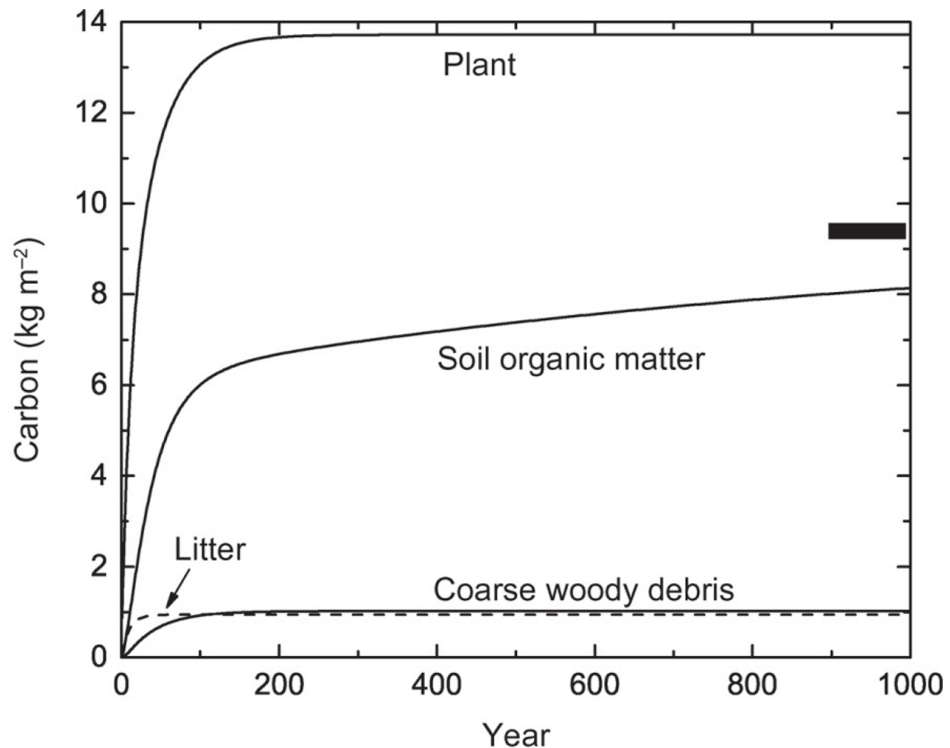


Figure 5.5: Carbon dynamics of evergreen broadleaf forest using parameters described in (Bonan Table 17.3 and Table 17.4) with net primary production equal to 1000 g C m⁻² y⁻¹. The thick black line denotes soil organic matter at equilibrium. Definitions of productivity terms in the carbon cycle. (Bonan)

The carbon turnover rate is the inverse of the residence time. Figure 5.6 illustrates that long term carbon storage depends a lot on allocation towards pools with various turnover times (in the boxes in Figure 5.6). Leaf level respiration fluxes result in very short turnover times, while carbon allocated to wood has a much longer turnover in the system.

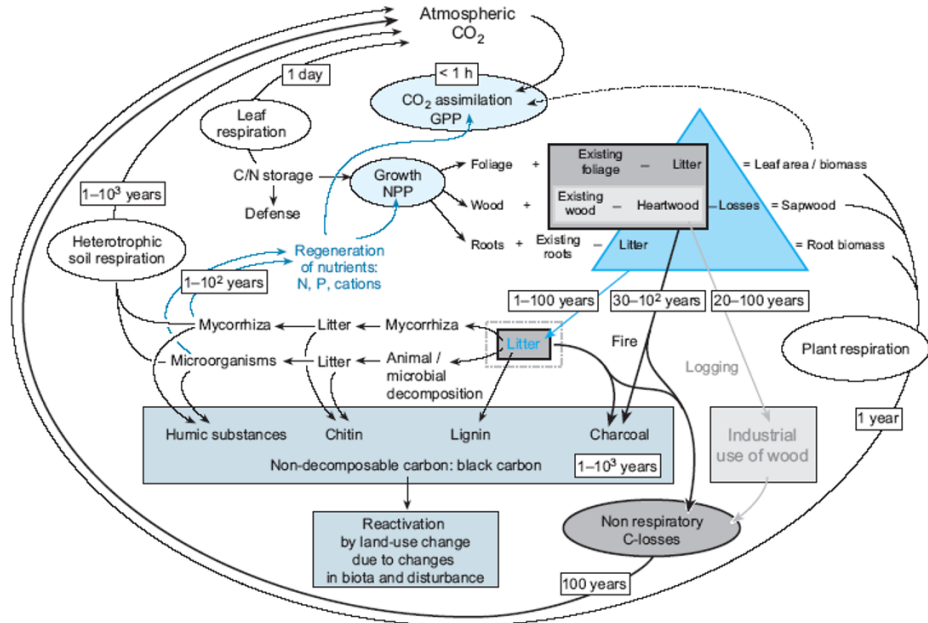


Figure 5.6: Turnover of carbon in terrestrial ecosystems (Schulze 2000).

5.3 Carbon allocation models

As indicated at the end of the previous section, carbon allocation is a key process for the ecosystem carbon cycle. It is the process which determines the carbon accumulation in various plant components (leaves, wood, roots), and it affects the structural characteristics of the plant (leaf area, rooting profile, plant height) which determine resource acquisition (e.g. higher leaf area results in higher photosynthesis of the plant or ecosystem). However, the process-based knowledge on carbon allocation is limited. It is uncertain how carbon allocation varies with environmental factors. We know that plants allocate more to roots when soils are dry or nutrient poor and we know that plants allocate more to leaves when light is limiting, but the exact process are unknown or unquantified. It is clear that plants are constantly adjusting their allocation to prevent an overwhelming limitation by one resource, which tends to make plants limited by multiple resources. Allocation is usually studied/observed very roughly, by studying aboveground/belowground biomass ratios or sapwood/leaf area ratio.

Due to our limited knowledge of the underlying processes, growth of plants and the allocation processes can only be showed by means of a schematic model (e.g. Figure 5.7) because there exists no fully physiological model that describes the distribution of assimilates over the different organs. In the example of Figure 5.7 also the interaction with the nutrient cycle is accounted for.

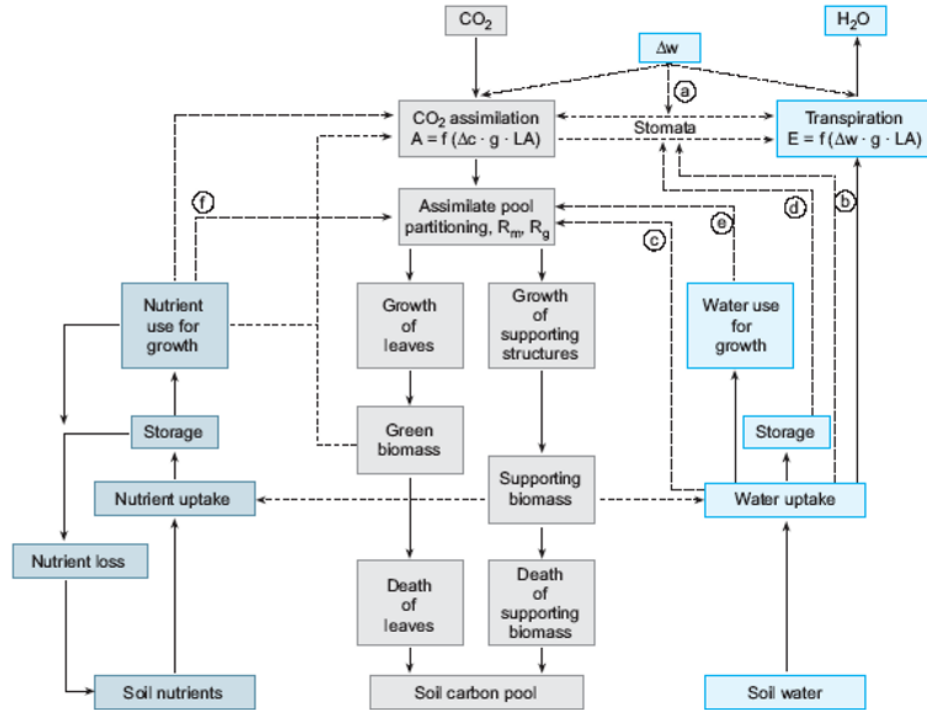


Figure 5.7: Schematic model of internal carbon, water and nutrient pools and fluxes within the plant (full lines) as well as important feedbacks and regulation (dashed lines). regulating factors are climate (a), stomata and impact of water balance on carbon allocation (b, c, d, e) and nutrient impacts (f) (Schulze and Chapin 1987).

Current carbon allocation models make use of one of the following approaches:

1. Time-invariant partitioning coefficients (per PFT or climate type)
2. Empirical algorithms with variable allocation in response to environment
3. Functional relations affected by resource limitations (e.g. balance in sapwood and leaf area) (scaling relationships)
4. Optimality approaches that balance multiple resource limitations (e.g. optimize allocation to maximize NPP, or to balance water (root) and light (leaves) acquisition and water transport (stem))
5. More mechanistic approaches (for single plants) (e.g. explicitly simulating phloem transport, etc...)

The example of Figure 5.8 illustrates the dependency of allocation factors of the CTEM model to environmental factors (light availability) for dry and wet soils.

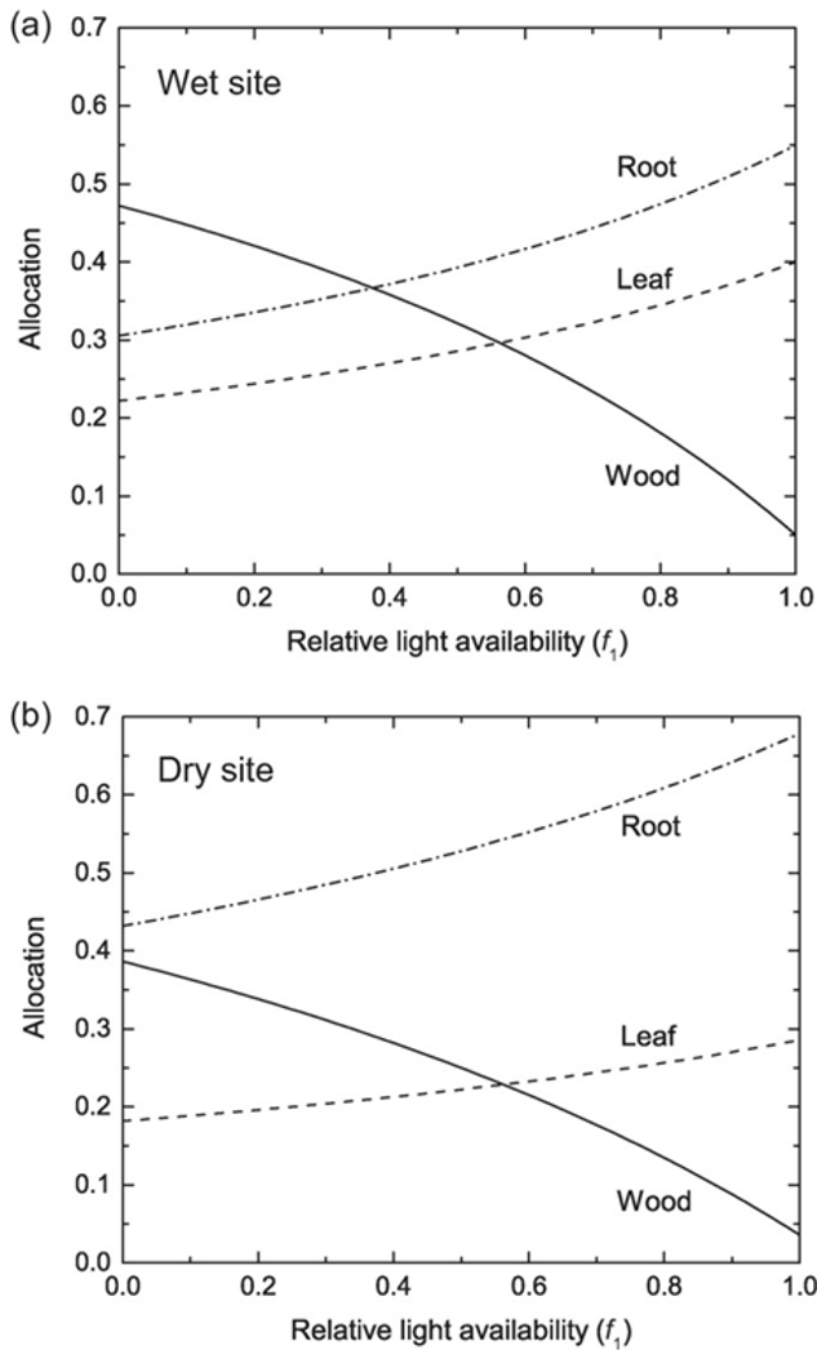


Figure 5.8: Biomass allocation to leaf, root, and wood in relation to relative light availability f_1 for (a) wet ($f_2 = 1$) and (b) dry ($f_2 = 0.5$) soil as in Arora and Boer (2005).

We know that plants (trees) have a storage pool of (labile) carbon (NSC: non-structural carbohydrates), which they can use to buffer variation in resource supply. Many models account for such a storage pool, example to allow for initial leaf growth in spring for deciduous vegetation. Such a buffer allows plants to acquire most resources when they are abundant and use accumulated carbon when needed for growth. Plants as such follow ‘economic rules’ similar to those of business firms. The actual implementation of a storage pool differs from model to model (as illustrated in Figure 5.9).

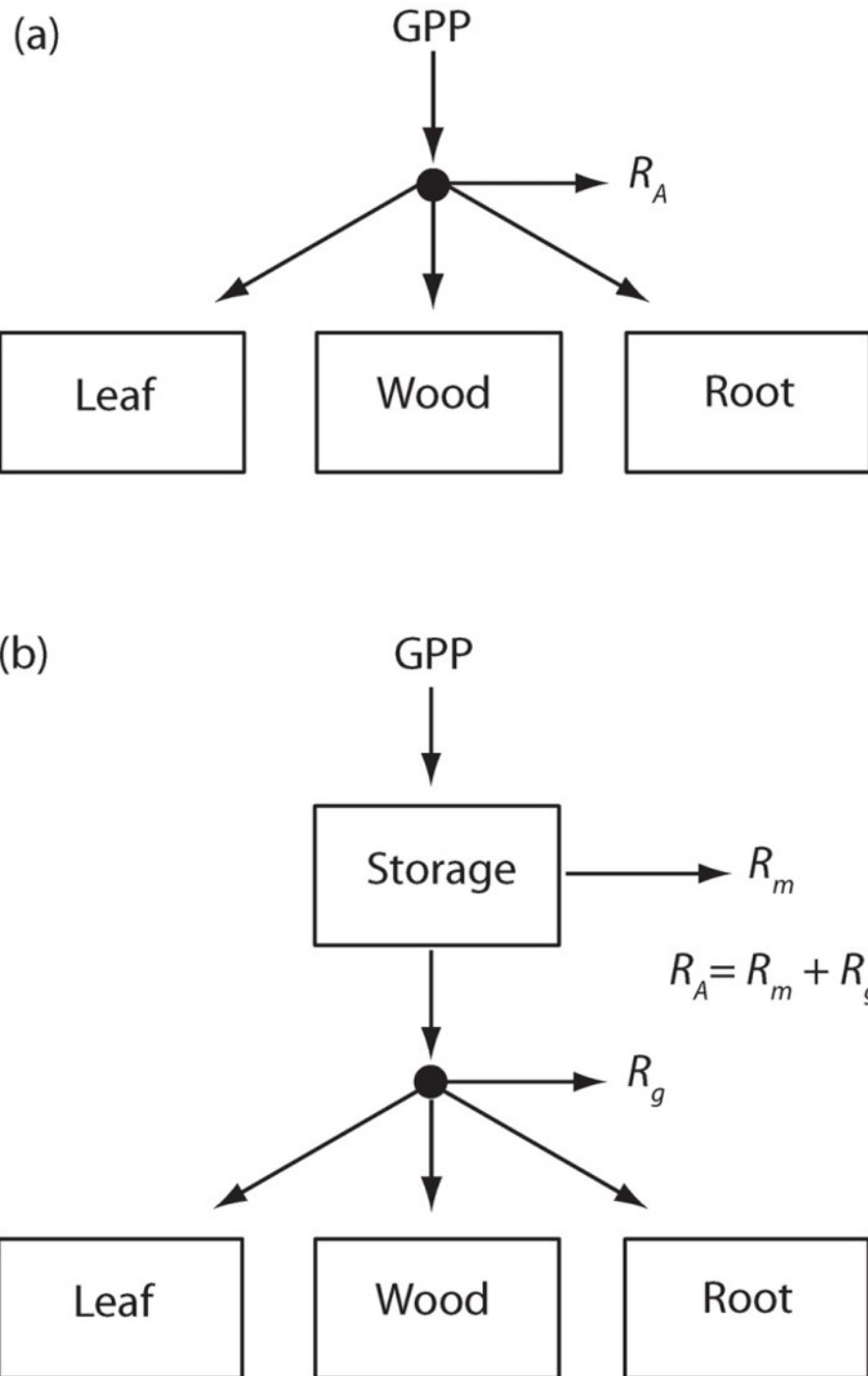


Figure 5.9: Two different representations of plant growth. (a) Autotrophic respiration R_A is subtracted from gross primary production (GPP) and the remaining carbon is allocated to the growth of leaves, wood, and roots. (b) GPP first enters a storage pool from which maintenance respiration R_m is subtracted. The remaining carbon is allocated to growth after accounting for growth respiration R_g . (Bonan)

It is important to mention here that the allocation process is tightly linked with phenology (as discussed in chapter 4). Phenology will determine how some allocation factors will vary over time, for example determined by the timing of budburst and senescence.

5.4 Case Study 5.1

In this case study the Thetys-Chloris model, with detailed carbon allocation, was tested for a FACE experiment in Switzerland. A FACE (free air CO₂ enrichment) is an experimental setup on open air where an ecosystem is exposed to elevated CO₂ as global change experiment (Figure 5.10). In the Swiss setup a tubing system in the tree crowns is used to continuously spray CO₂ in the experimental plot. The site also has a ‘canopy-crane’ used for direct in-situ measurement on the leaves of the trees. Multiple supporting measurements are executed (sap flow, stomatal conductance, litterfall, stem growth) for model-data comparison.

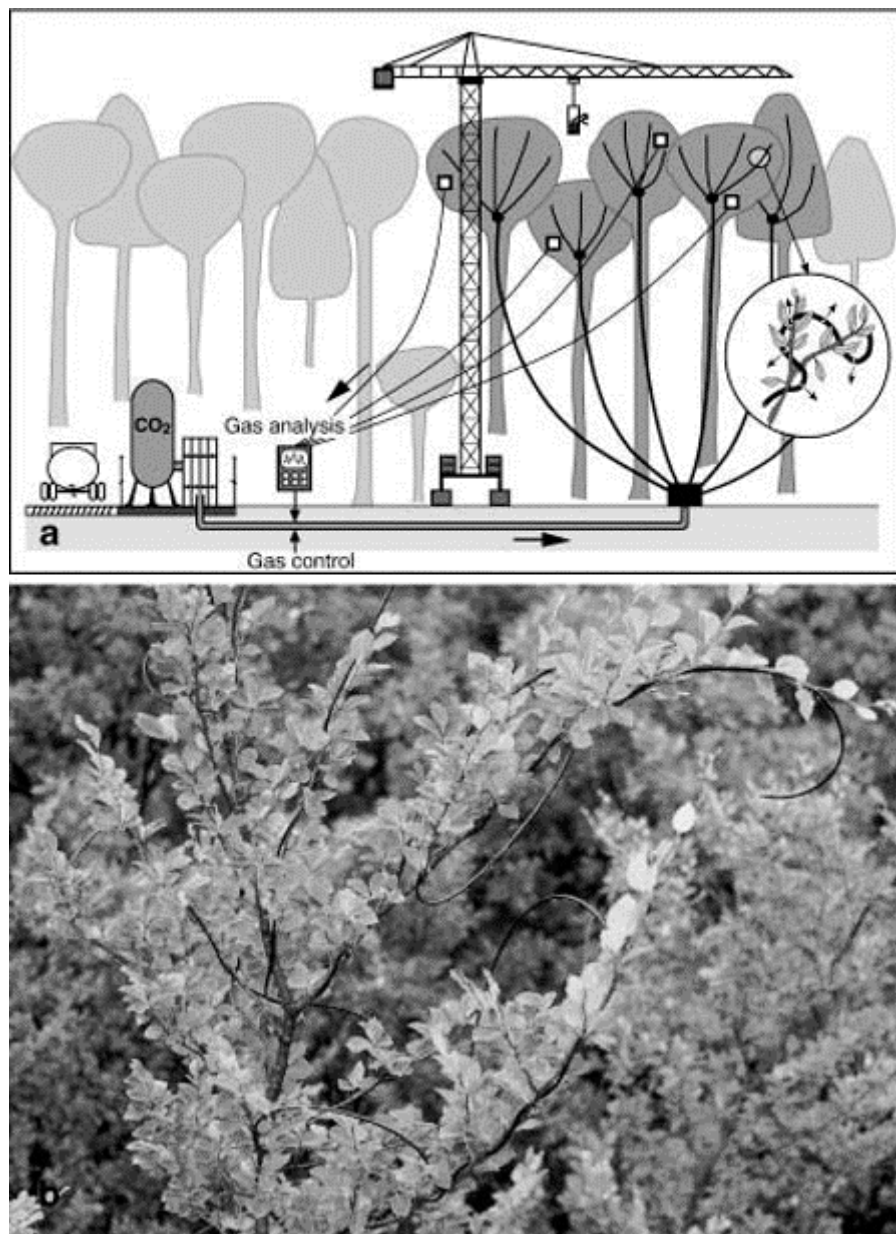


Figure 5.10: The Swiss Canopy Crane (SCC) free air CO₂ enrichment (FACE) experiment conducted in a mature mixed deciduous forest near Hofstetten, 15 km south of Basel, Switzerland. Fatichi et al.2013.

The study illustrate that the model works well to simulated carbon, water and energy fluxes (Figure 5.11), however testing of the model remains difficult for carbon allocation (Figure 5.12).

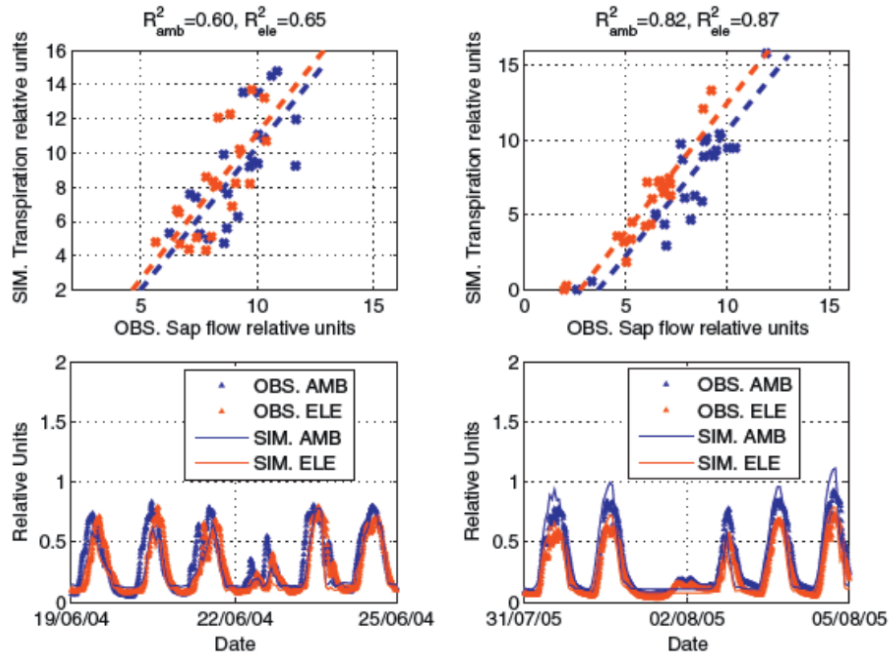


Figure 5.11: A comparison between observed sapflow and simulated transpiration in relative units for the Swiss Crane forest stand in ambient (AMB) and elevated (ELE) CO₂ conditions during the growing season of 2004 (subplots a and c) and 2005 (subplots b and d). Scatter plots of daily sums (subplots a and b) and time series for two representative five day periods (subplots c and d) are shown. Faticchi et al. 2013.

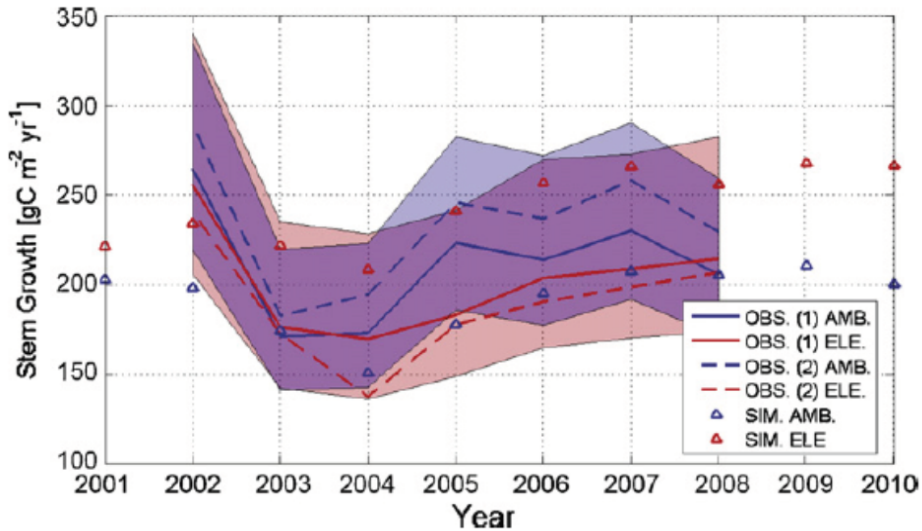


Figure 5.12: A comparison between observations [OBS. (1)] (solid lines) with uncertainty bounds (colored area) and model simulations (SIM., triangles) of stem growth (species averaged) per unit surface area for the period of 2000 through 2010 in ambient (AMB.) and elevated (ELE.) CO₂ conditions. The stand carbon increments using only the Acrown derived for trees equipped with dendrometers in ambient and elevated conditions [OBS. (2)] in the upscaling are also reported (dashed lines). Fatichi et al. 2013.

Figure 5.13 illustrates the strength of this models that allows to simulated the dynamics of all carbon pools at the species level. It shows that beech is more drought-sensitive than oak at this site, with a clear impact of the 2003 drought on the reserves and sapwood pools for beech.

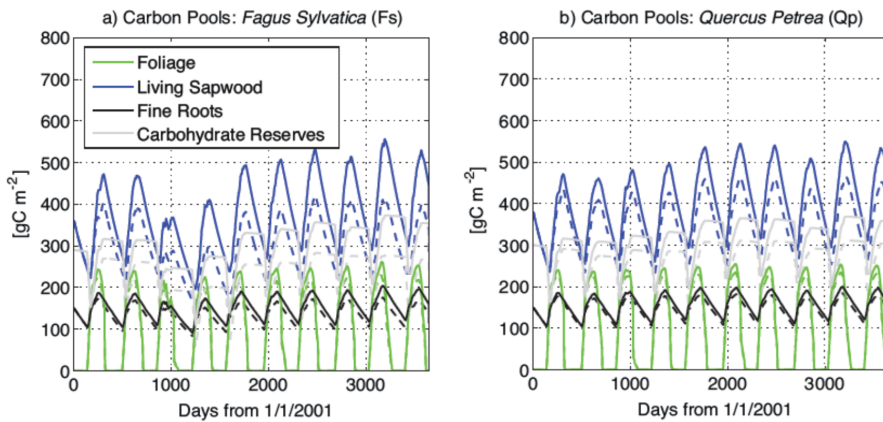


Figure 5.13: The simulated dynamics of green aboveground, living sapwood, fine roots and carbohydrate reserves carbon pools of (a) *Fagus sylvatica* (Fs) and (b) *Quercus petraea* (Qp) under ambient (dashed lines) and elevated (solid lines) CO₂ conditions for the period of 2001 through 2010. Fatichi et al. 2013

It is important that in many detailed site level studies, such as the one illustrated here,

parameter optimisation is applied to get an as good as possible match between simulated results and measured data. Such model tuning can be achieved in an automated way, for example by algorithms that minimize the mismatch between model output and data, or by manual tuning of specific parameters to achieve a better fit.

5.5 Soil biogeochemistry models

In this section we take a closer look to the soil component of biogeochemical models. We are not only considering the carbon cycle here, but also nutrients cycling (for which plants also play a key role of course). It is important to be aware that carbon cycling (decomposition) is a standard process in most vegetation models, while the nitrogen cycle has only been included in vegetation models during the last decade. The P cycle is currently only included in a handful of models, will other nutrients (Mg, K, ..) are usually not accounted for at all.

5.5.1 Decomposition models

Decomposition is the physical and chemical breakdown of dead organic matter. It is an important process as it (1) provides energy for microbial growth, (2) releases nutrients for plant uptake and (3) influences ecosystem carbon storage (and therefore the global climate). Decomposition basically consists of 3 processes: (1) leaching of soluble materials by water, (2) fragmentation of organic matter by soil fauna (which increases the surface for microbial attack), (3) chemical alteration of the organic material. As such the decomposition process changes the chemical composition of the detritus, breaks down the organic matter to CO₂ and nutrients and forms recalcitrant compounds.

Decomposition models assume that the decay rate of organic matter over time is proportional to the amount of material in the litter pool and a decay rate k.

$$\frac{dm}{dt} = -km$$

When integrating this relation over time we can calculate the litter mass in function of time following an exponential decline:

$$m(t) = m_0 e^{-kt}$$

where the decay rate k depends on substrate quantity and quality (Figure 5.14), the properties of the microbial community and the physical environment. To account for the physical environment, many models correct the decay rate for soil temperature, pH and/or soil water content. Figure 5.15 gives an overview of the various factors controlling decomposition.

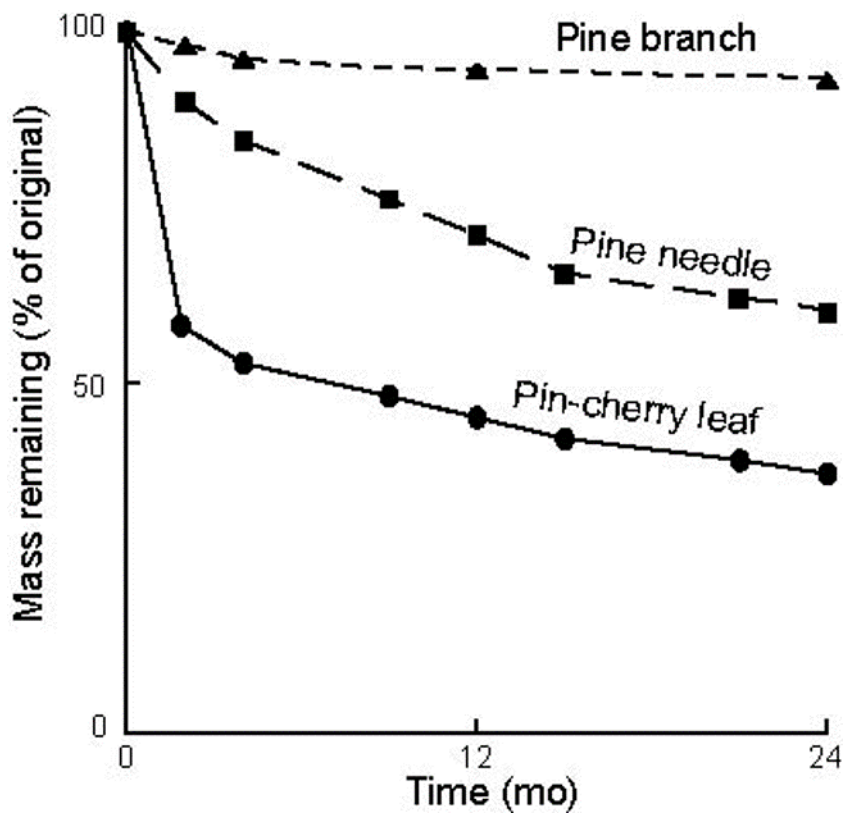


Figure 5.14: Mass decline over time during decomposition of different plant materials.

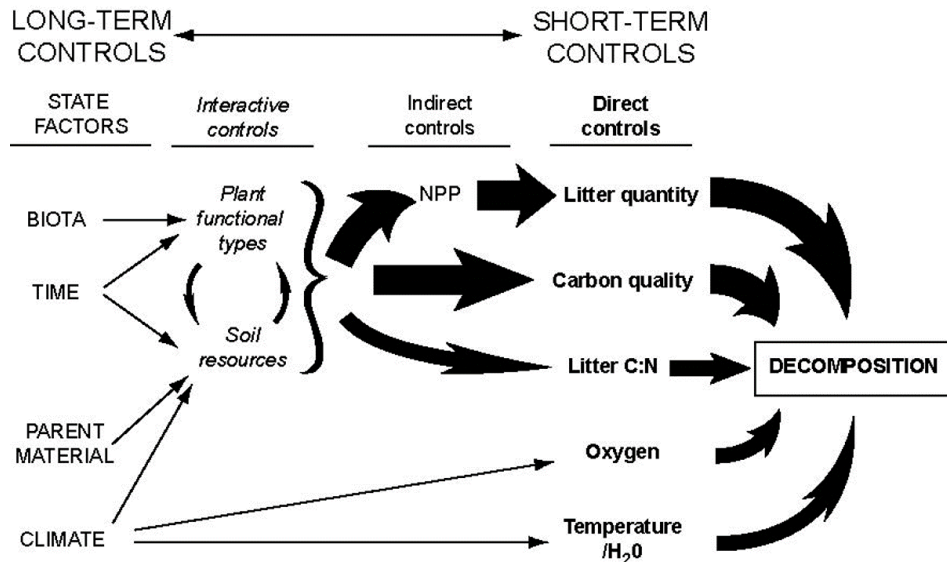


Figure 5.15: Controlling factors on the decomposition process. The thickness of the arrows are proportional to the level of control. (Chapin).

Some models use specific decay rates for each type of SOC depending on its composition (C/N ratio, lignin content (Figure 5.17),...). This results in models with multiple SOC and litter pools with specific decay rates (as illustrated earlier with the CASA-CNP model). A decomposition model with three pools will then have the following form:

$$m(t) = m_1 e^{-k_1 t} + m_2 e^{-k_2 t} + m_3 e^{-k_3 t}$$

Based on such a model, one can simulate the different phases of decomposition depending on the composition of the remaining litter (Figure 5.16). In phase 1 the leaching dominates. In phase two we still have a relatively high value of k , because the labile substrates are broken down. In phase 3 a low value of k , reflects the recalcitrant substrates that predominate. Figure 5.16 also illustrates the fact that the time scale of decomposition heavily depends on the environment, with a much longer time scale in the arctic compared to the tropics where conditions are much more favorable (warm and humid) for decomposition.

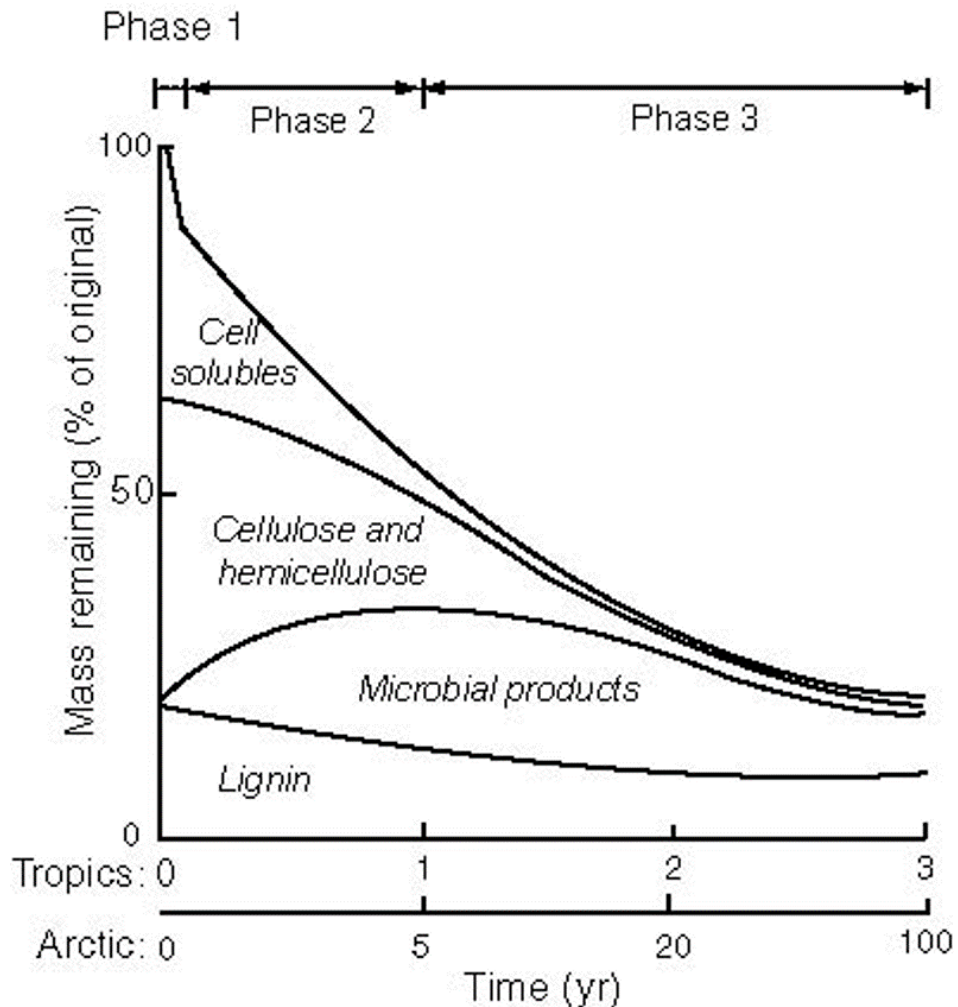


Figure 5.16: Phases of decomposition over time depending on the constitution of the remaining litter.

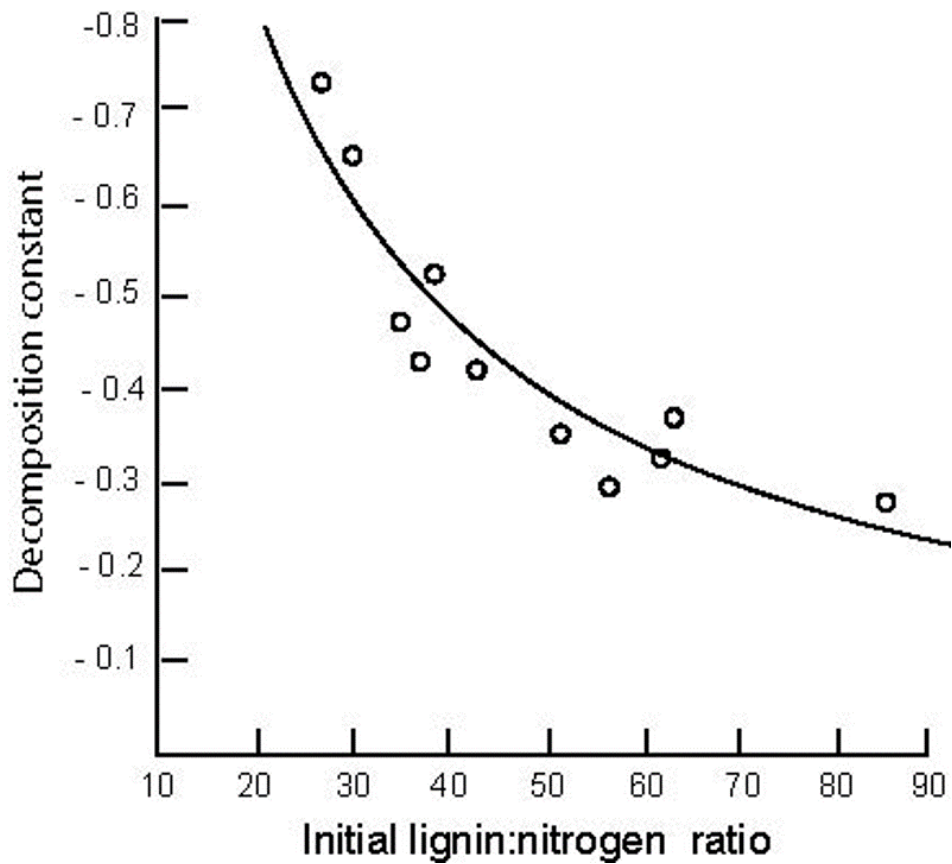


Figure 5.17: Relation between the decomposition constant and the lignin:nitrogen ratio.

Some recent vegetation models use a ‘litter cohort model’ in their soil biogeochemical component (Figure 5.18). These models track each litter type at different stages of decomposition (litter cohorts). Such models can assign a specific decay rate to each litter cohort and can simulate transfer of organic material between cohorts. Within a cohort the C/N ration can change over time, impact the decay rate.

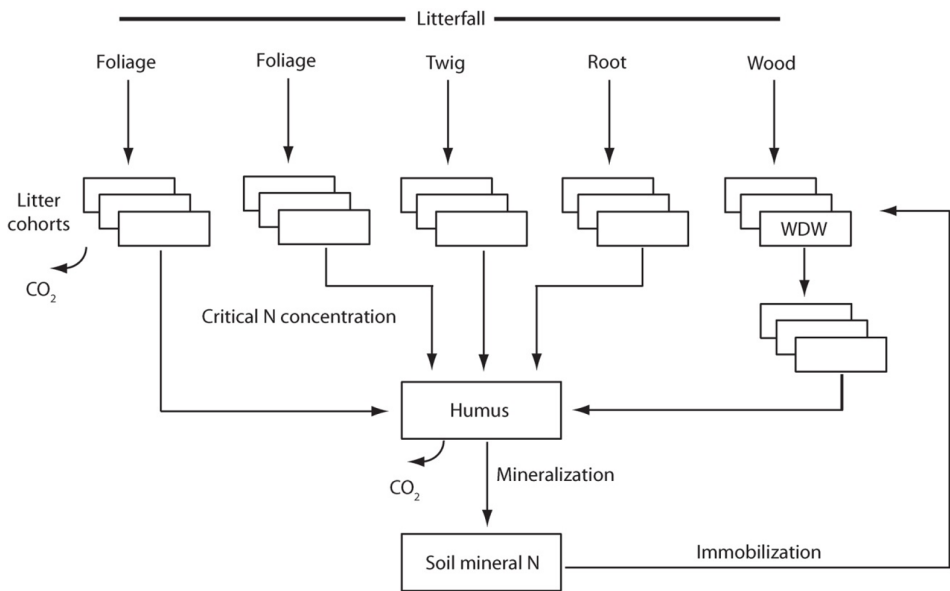


Figure 5.18: Decomposition as represented by a litter cohort model. Foliage, twig, root, and wood litter form individual cohorts with an initial carbon, nitrogen, and lignin mass. Each box represents an individual cohort for a particular year. Foliage litter can vary in initial quality, represented by multiple litter cohorts. The cohorts decompose over time, immobilize nitrogen, and transfer to humus upon reaching a critical nitrogen concentration. Fresh wood first passes through a well-decayed wood pool (WDW) before becoming humus. Humus decomposes and mineralizes nitrogen.(Bonan)

Figure 5.19 illustrates the structure of the DAYCENT model, which is a recent full biogeochemical soil model (based on the original CENTURY model, which is reference in the field). It shows the complex structure of this very detailed model, which considers cohorts in different stages of decay with different k values, tracking lignin contents, accounting for the impact of temperature, soil water pH, aerobic conditions, texture, et cetera. It is important to mention here that most of the global vegetation models do not have such a detailed biogeochemical soil component. Current developments in soil biogeochemical models are focusing on implementing multiple soil layers, the specific conditions of permafrost soils and impact of the composition of the soil microbial community.

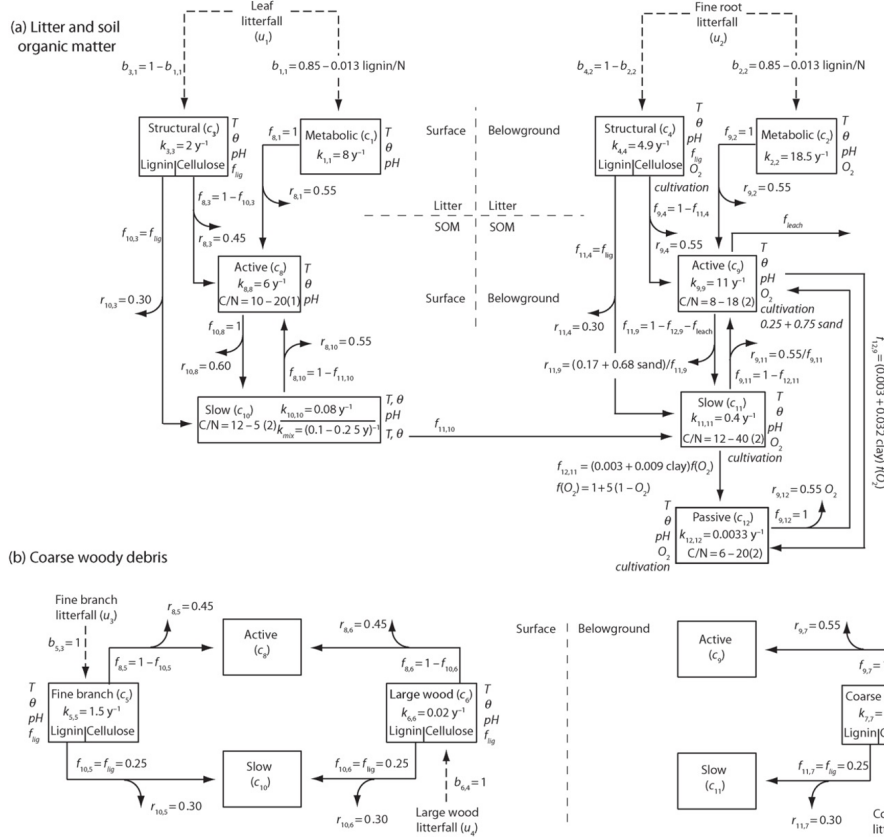


Figure 5.19: Example of a full soil biogeochemical model DAYCENT. Litter, soil organic matter, and coarse woody debris pools and fluxes represented. The model has leaf, fine root, and three coarse woody debris litter flux inputs (u_1-u_5) and twelve carbon pools (c_1-c_{12}). Shown are litter flux partitioning parameters b_{ij} , base decomposition rates k_{ii} (per year), fractional carbon transfer f_{ij} , and respiration fraction r_{ij} . Solid lines indicate decomposition pathways, with curved arrows denoting heterotrophic respiration fluxes for each pathway. DAYCENT allows for photodegradation from solar radiation, but that was not included in Bonan et al. (2013). Nor was leaching loss included. (a) Leaves decompose as surface material represented by two litter pools and two organic matter pools (shown on the left). Fine roots decompose as belowground material represented by two litter pools and three organic matter pools (shown on the right). The actual decomposition rate varies with soil temperature T , soil moisture θ , and pH. Belowground decomposition additionally varies with anaerobic conditions (O_2), cultivation, and soil texture. Structural litter decomposition also depends on lignin fraction $f_{1,g}$. The total turnover of the surface slow pool depends on decomposition and mixing, with a fraction to the belowground slow pool and the remainder to the surface active pool. The C/N of organic matter differs among pools and varies with soil mineral nitrogen. Shown is the minimum and maximum value for each pool and (in parentheses) the soil mineral nitrogen (g N m⁻²) for the minimum C/N. (b) Coarse woody debris decomposes to the active and slow pools. Fine-branch and large-wood debris flows to surface pools, and coarse root flows to belowground pools. (Bonan)

5.5.2 Nutrient cycle models

We will only discuss nutrient cycles (and the associated models) superficially here. Many other (soil) courses in the program focus on nutrient cycles. Implementation of nutrient cycles in vegetation/soil models is pretty similar as the carbon biogeochemistry models discussed above. When there is a carbon model in place, a nitrogen model can be implemented by tracking for each carbon pool or flux an associated N pool or flux. However, the soil nitrogen cycle is more complex than the soil carbon cycle (Figure 5.20) because we need to account for:

- Reabsorption of N from litter fall and reallocation of N from leaves during senescence
- N has gas forms: N_2 , NH_3 , N_2O , NO (losses)
- Plants use inorganic ions nitrate (NO_3^-) and ammonium (NH_4^+)
- Multiple input processes: biological fixation, atmospheric deposition, fertilizer
- Specific role of micro-organisms

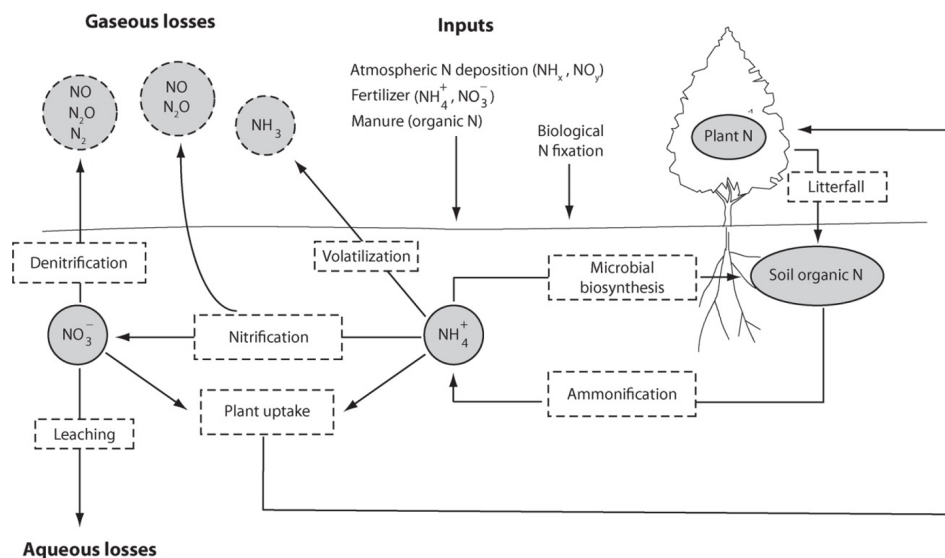


Figure 5.20: Depiction of the nitrogen cycle. Circles indicate various pools (solid lines) or gaseous losses (dashed lines). Boxes denote processes. Also shown are natural inputs from biological nitrogen fixation and anthropogenic inputs from nitrogen deposition, fertilizer, and manure.(Bonan).

Research in the past decade has shown the important impact of the nitrogen cycle on carbon cycle simulations (e.g. a decrease of NPP when soil N is limiting). Figure 5.21 illustrates that recent earth system models (with and without accounting for N) simulated a global carbon sink which is smaller when accounting for nitrogen limitation. This shows that up until last IPCC report (where models did not account for the N cycle) future potential carbon stocks have been over estimated. So, the importance of implementing the N cycle in global models is widely accepted. However, a variety of approaches exists, where models differ largely in the way they represent:

- N impact

on photosynthesis - N uptake processes - Constant or variant C:N ratios - Competition for soil mineral N by plants and microbial community

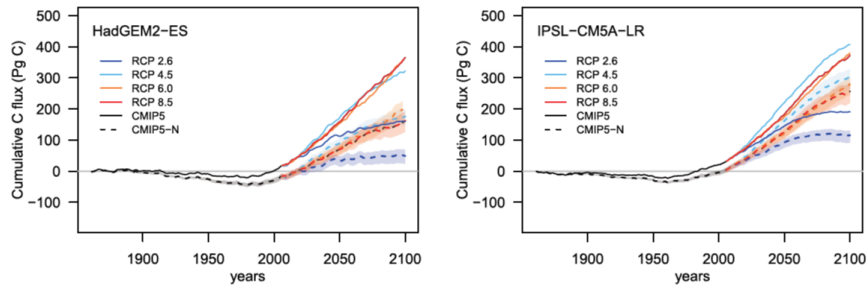


Figure 5.21: Cumulative C sequestration from the CMIP5 models and plausible range of C sequestration considering N constraints (CMIP5-N) for the HadGEM2-ES and IPSL-CM5A-LR models. Zhaele et al. 2015

5.6 Case study 5.2

In the second case study of this chapter, we take a closer look to one of the first global models (JSBACH) that accounted for the P cycle. The study presents how the P cycle was implemented and tested the impact on the global land carbon cycle. Figure 5.22 illustrates how the N and P cycle are implemented in JSBACH and how these nutrient cycles are interacting with the C cycle. The model allowed for global simulated maps of phosphorus in vegetation and soil, which illustrate the low P content in tropical areas.

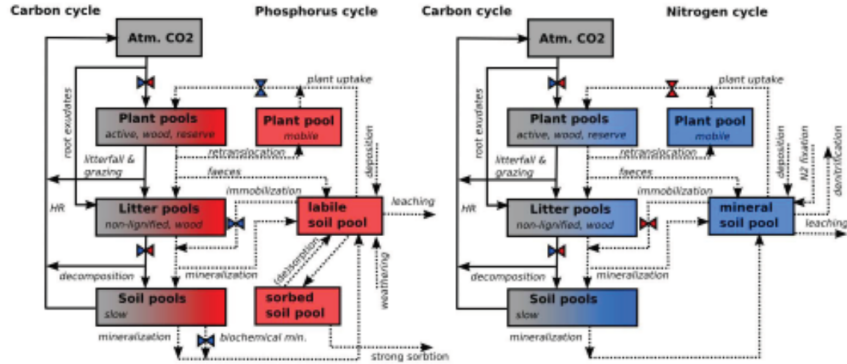


Figure 5.22: Schematic representation of pools and fluxes in JSBACH. Solid arrows indicate carbon fluxes and dashed arrows nutrient fluxes. The plant compartment consists of the three C pools: active (leaves and non-lignified tissue), wood (stem and branches) and reserve (sugar and starches). The litter compartment consists of non-lignified litter, and woody litter (lignified litter and fast-decomposing soil organic matter). The soil compartment consists of one pool (slow) representing slow-decomposing organic matter. All carbon pools except the reserve pool have a corresponding nutrient pool with variable C :N: P ratio (slow, non-lignified litter) or fixed C :N: P ratio (rest). There is one mobile plant pool representing mobile nutrients stored internally in plants. Soil mineral nitrogen is represented by a single pool (soil mineral pool), while mineral P is represented by labile (available) pool and sorbed pool. The opposing triangles indicated that the flux is controlled by phosphorus (red triangles), nitrogen (blue triangles) or both (mixed triangles). Goll et al. 2012

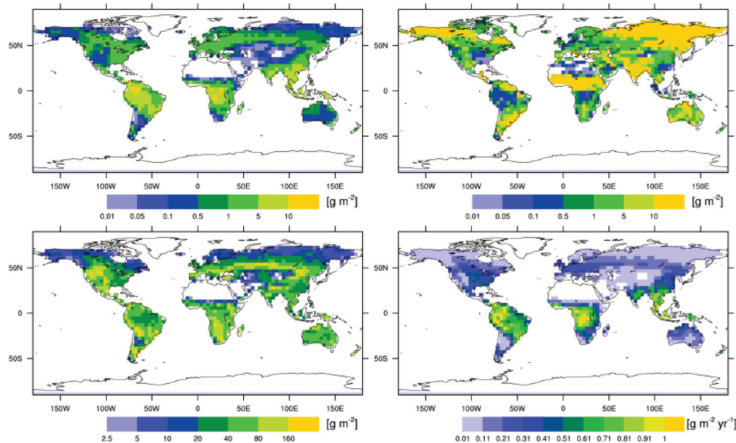


Figure 5.23: The simulated P in vegetation (top left), sorbed P (top right), P in soil organic matter and litter (bottom left), and the annual P uptake by vegetation (bottom right) for present day as simulated by JSBACH. Goll et al. 2012.

The study compared simulation of the accumulated land carbon uptake between 1860 and 2100 with and without the nutrient cycles activated in the model. The results show a simulated global land carbon sink which was 13% lower when the N cycle was accounted for (mainly contributed by effects in the high latitudes). When the P

cycle was accounted for the sink was even 16% lower (mainly contributed by tropical ecosystems). The combined N and P cycle resulted in a 25% lower land sink (Figures 5.24 and 5.25).

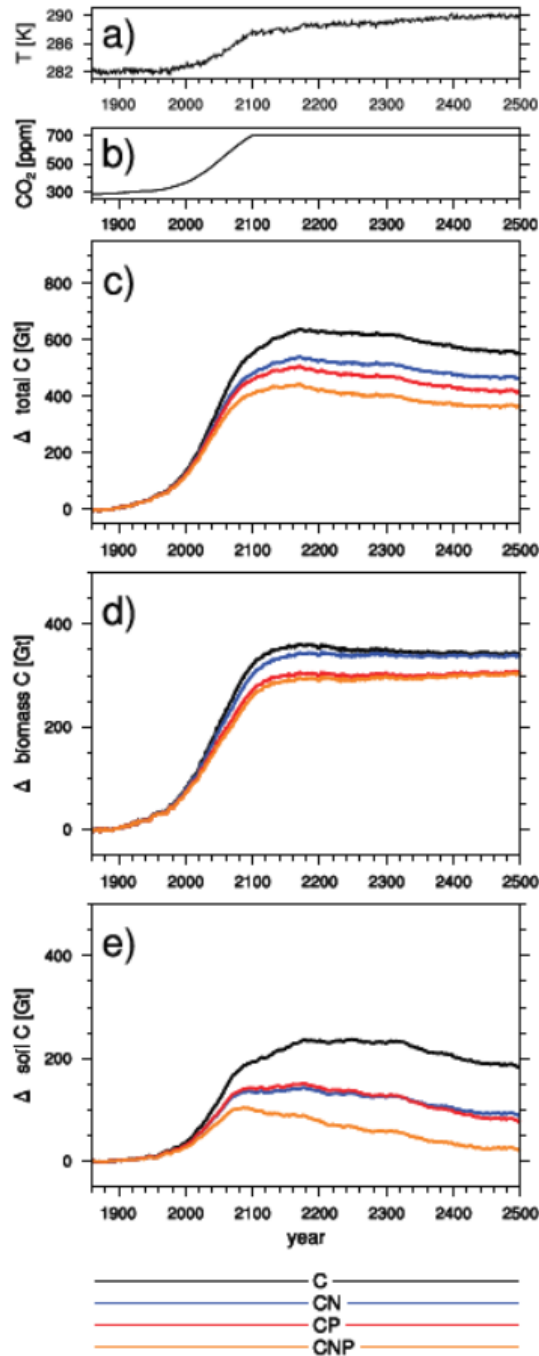


Figure 5.24: The simulated change in land carbon storage under the SRES A1B scenario. Shown are the 10-yr mean of soil temperature (a), the CO₂ concentration as used in the forcing simulation (b), the resulting change in total land C storage (c), and the changes in the two main land compartments vegetation (d) and soil (e). Goll et al. 2012.

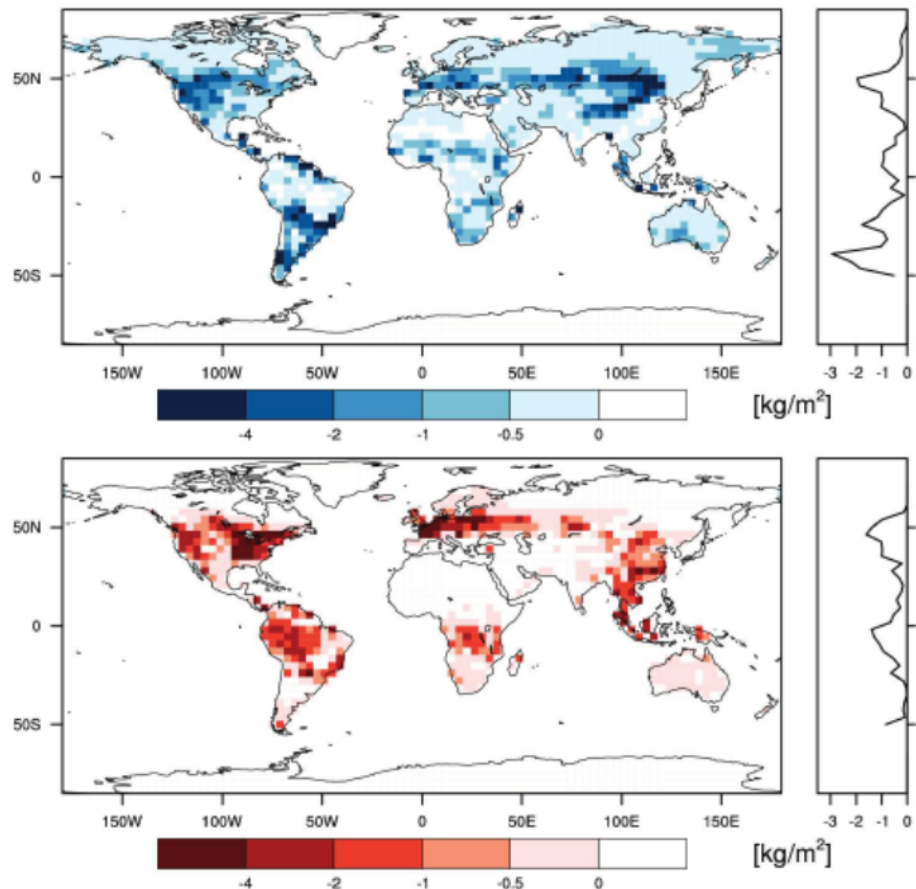


Figure 5.25: The reduction in C storage (kgm^{-2}) by nutrient limitation at the end of the 21st century. Shown is the difference in the mean C storage (2070–2099) between the CN simulation and the C-only simulation (upper panel), and between the CP simulation and the C-only simulation (lower panel). The latitudinal means over land points are shown on the right side. Goll et al. 2012.

5.7 Water balance models

We will not focus on water balance models in this course. As these are discussed in detail in hydrology courses. However, it is important to mention the key role of water balance models here, which are usually an integral part of vegetation models. The water balance is essential to simulate the energy balance of the system via evapotranspiration (latent heat flux). Moreover, reliable soil water balance models (see soil physics course) are essential to simulate water availability. It is also important to mention that the C allocation model will influence the water cycle. More allocation to leaves will result in high transpiration and a higher rainfall interception.

Chapter 6

Modelling Vegetation Dynamics and Demography

6.1 Introduction

Biogeography is the study of the distribution of species and ecosystems in geographic space and through geological time. A group of models that studies the distribution of species geographically is called “**species distribution models**” (SDM) (e.g. Fig. 6.1). These models are typically empirical models, as they link species distribution to other parameters, e.g. climate and soil parameters, by using statistical approaches. We just mention these models briefly here (as they are not the focus of this course, but they are still important as biogeographical model outputs are used as an input to the vegetation models, to inform the vegetation model where a species occurs or can occur. SDMs link the current distribution of a species, to a range of environmental properties, typically climate and soil properties, by using statistical approaches. The models typically use climate envelopes for this, where a specific species occurs within a range of a certain parameter. These data can then be used to predict where a species will occur in the future, or where it occurred in the past, neglecting the possible barriers of species migration. A second group is a more mechanistic type of model that uses plant physiology and plant traits to predict the distribution of a species. These models should be able to account for climate adaptation and acclimation.

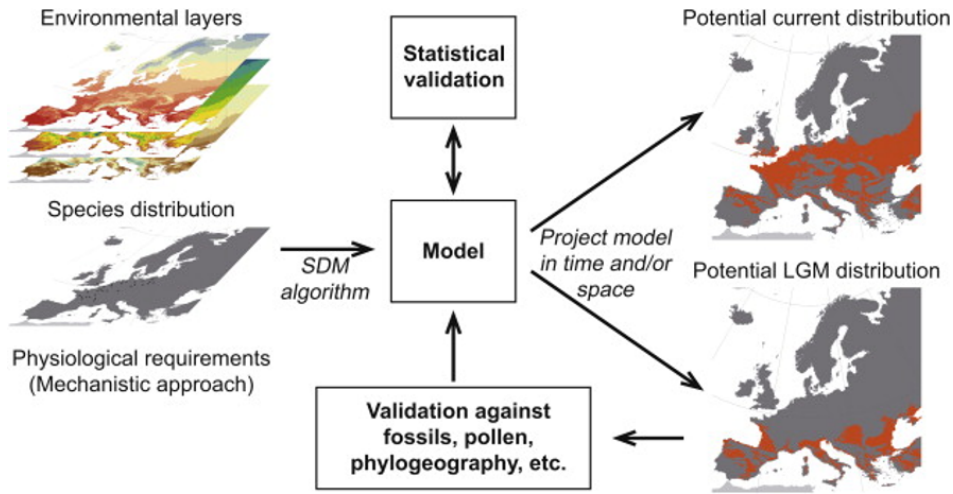


Figure 6.1: Example of a species distribution model (SDM), used to simulate current and past species distribution (Svenning et al. 2011). LGM: Last Glacial Maximum. Such models can also be used to predict future species distributions.

The study of **ecosystem demography** tries to understand and quantify vegetation dynamics. Temporal dynamics in vegetation, community composition and ecosystem structure are typically driven by demographic processes: recruitment and establishment, growth, and mortality (Fig. 6.2).

Vegetation dynamics

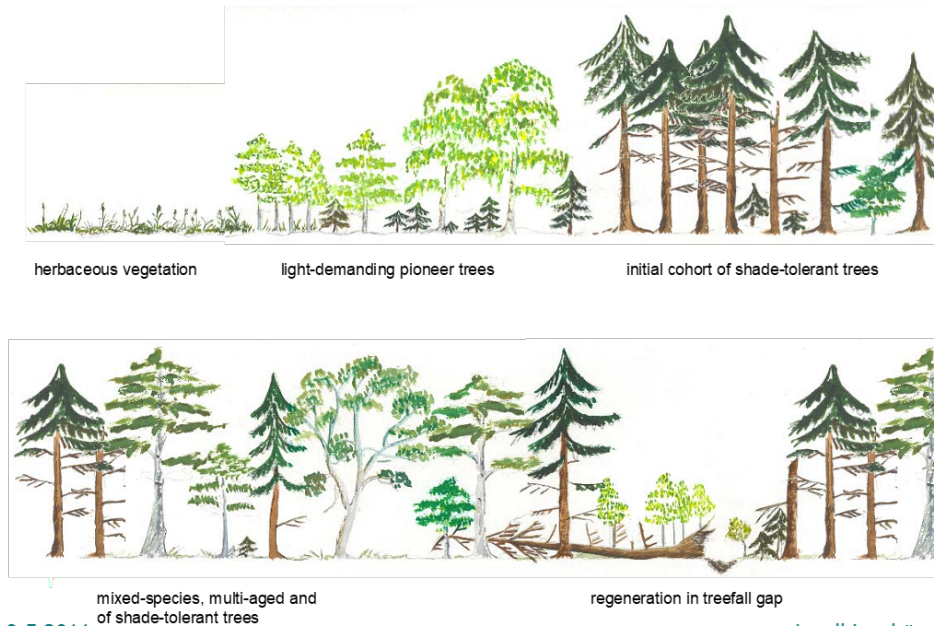


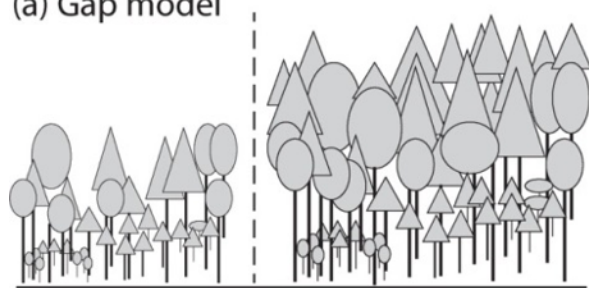
Figure 6.2: Illustration of successional forest dynamics.

6.2 Gap models, area and cohort based models

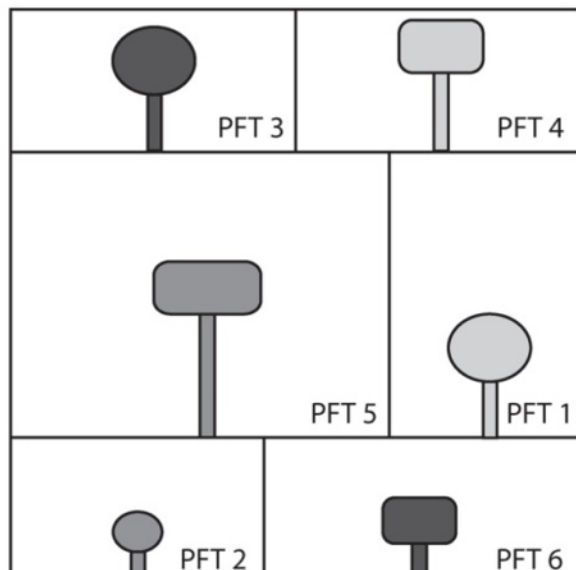
From the perspective of vegetation dynamics we can consider three types of vegetation models (Fig. 6.3). **Gap models** were developed in parallel with biogeochemical models. They simulate demographic processes for each individual tree. The landscape consists of different patches, which can be in different stages of succession. The model output is typically an output per tree. The second group of models are the **area-based models**, most dynamic global vegetation models (DVGM) belong to this model type. This group is on the other side of the spectrum, as this model does not calculate values for individual plants, or the number of individuals, but it simulates allocation at ecosystem scales. In these models, the landscape is divided in different patches, but every patch is only occupied by one PFT. Every patch is then represented by an average tree, after which the output is calculated at landscape model. The third type of model falls in the middle of the spectrum between two previous model types. **Cohort based models** do not track each individual tree in the landscape, but group trees from similar size and function in cohorts. Each cohort is represented by an average tree, for which the calculations are made. Contrary to the area models, the number of individuals is tracked. Gap models/individual based models and cohort-based models are both called **demographic models**, as they are both able to model demography and the account for demographic processes.

What are plant functional types (PFT)? They represent broad groupings of plant species that share similar characteristics (e.g. growth form) and roles (e.g. photosynthetic pathway) in ecosystem function. However, PFTs have a different meaning in demographic models and area-based models. In the latter, they represent an ecosystem functional type, whereas in cohort/individual based models they represent a specific plant type.

(a) Gap model



(b) Area-based DGVM



(c) Ecosystem demography

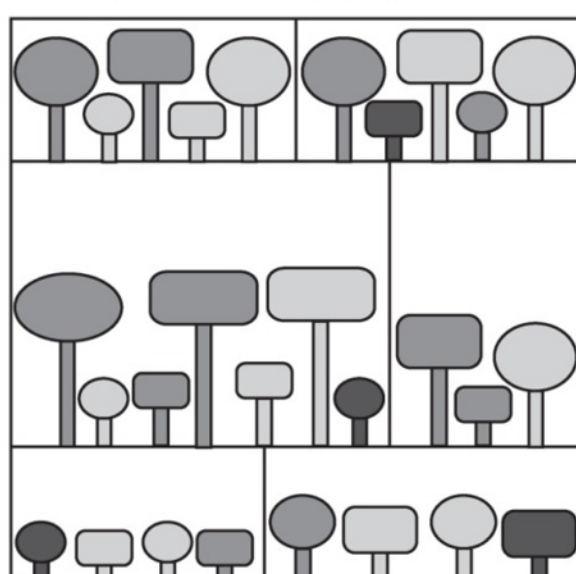


Figure 6.3: Representation of vegetation patches in models. (a) Forest gap models are individual-based models and represent a landscape as patches that differ in stage of post-disturbance development. Shown are two patches, each comprised of multiple trees that differ in size and species. (b) Area-based dynamic global vegetation models (DGVMs) represent vegetation as discrete patches of plant functional types (PFTs) that differ in area. In this example, the model grid cell has six plant functional types (distinguished by canopy shape and shading) that differ in biomass (size of plant) and

6.2.1 Area based models

Area based models typically focus on biogeochemical processes. In area-based models, a region is subdivided in pixels, and every pixel is occupied by one or multiple plant functional types (PFT). If more than one PFT is present, the pixels are subdivided in different patches, where the area of the patch relates to the abundance of the PFT. Plant functional types are not mixed, e.g. a savanna pixel is represented by two patches, a grass patch and a forest patch. The size of the patches can change over time if the conditions are more in favor of a specific PFT. The calculation of the surface of the patches is based on simplistic rules, based on productivity, mortality, establishment, fire, bioclimate tolerance,... Example: if the upper soil dries, grasses die, but trees have access to deeper water so they survive and the size of the tree-patch will increase. In this perspective, area-based models are also dynamic models.

Within each pixel (or grid-cell), the same homogeneous climatic conditions apply. PFTs are determined based on growth form, leaf longevity, leaf type, photosynthetic pathway and bioclimate in area-based models. This typically results in 12 up to 14 functional types to cover the entire world. As only one average plant is simulated, the light availability within the PFT (patch) is homogenous, and no canopy dynamics are included. As the model is deterministic, depending on the climatic parameters you set, a certain area will be occupied by a certain PFT. Co-existence (e.g. two competing trees in a mixed forest living together) is very difficult to simulate with such models, because if the parameter of one PFT is a bit more advantageous, this PFT will eventually expel the other and dominate the model.

Despite the above described strong assumptions, these models are nowadays mostly used in the current earth system models, because they are computational efficient, and they are good in simulating broad scale landscape patterns. Examples of vegetation models that are using an area-based approach are ORCHIDEE (French model), JS-BACH (German model), JULES (UK model). Sometimes the models are used with prescribed vegetation, e.g. a vegetation map, and are then executed without the dynamic vegetation. This is mostly done when simulations are run over a shorter time period, e.g. 20 years.

The LPJ-model is a very widely used model and the model occurs in many of the examples in this syllabus. LPJ-GUESS is the demographic variant of the LPJ-model. It is a particular type area-based model because it simulates the average plant, but it also simulates the number of plants in each patch. The overall scheme of the LPJ model is shown below (Fig. 6.4). The model contains the biogeophysics (see first lectures), biogeochemistry (e.g. Carbon pools), and had vegetation dynamics, which is calculated at a yearly basis. It has a background mortality of 1% and mortality caused by negative NPP, heat stress, fire, ...

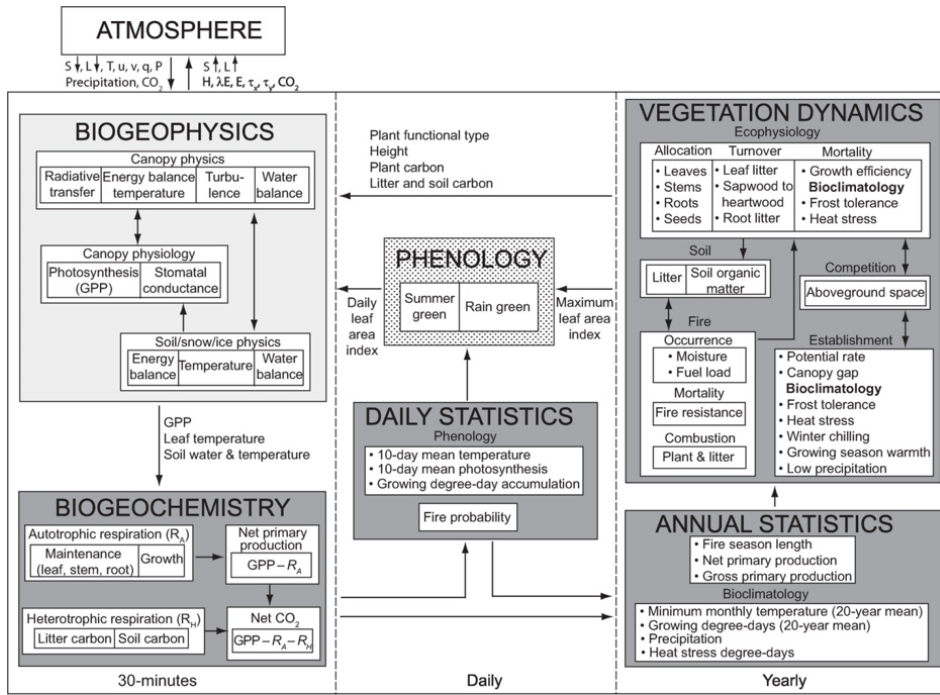


Figure 6.4: Coupling of a dynamic global vegetation model with a land surface model. Shown are linkages among the biogeophysics, biogeochemistry, and vegetation dynamics components of the model. The lightly shaded biogeophysical processes represent the traditional hydrometeorological scope of land surface models. The darker boxes represent the greening of land surface models with the introduction of dynamic vegetation and the carbon cycle. (Bonan)

The figure below (Fig. 6.5) shows some dynamic simulation results of the original LPJ-model. The color of the grid cells shows the most dominant vegetation type simulated in that cell. The resulting world map of potential vegetation is very realistic.

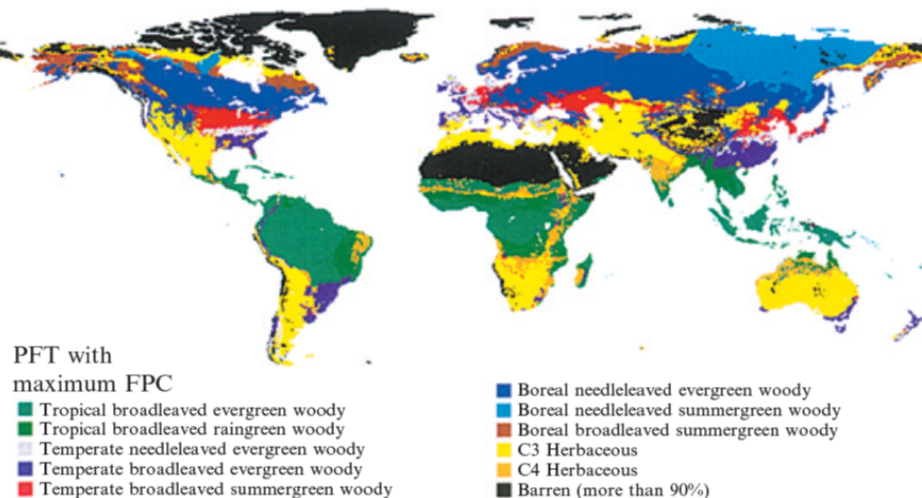


Figure 6.5: Map of LPJ simulated dominant PFTs (Sitch et al. 2003)

In Figure 6.6 LPJ simulations are compared with satellite data. The comparison shows

that the model does a reasonable job, but for some regions, the model simulations are not good, e.g. Spain: there are no dominating evergreen species, while the model predicts this. Also, tundra vegetation is not simulated well.

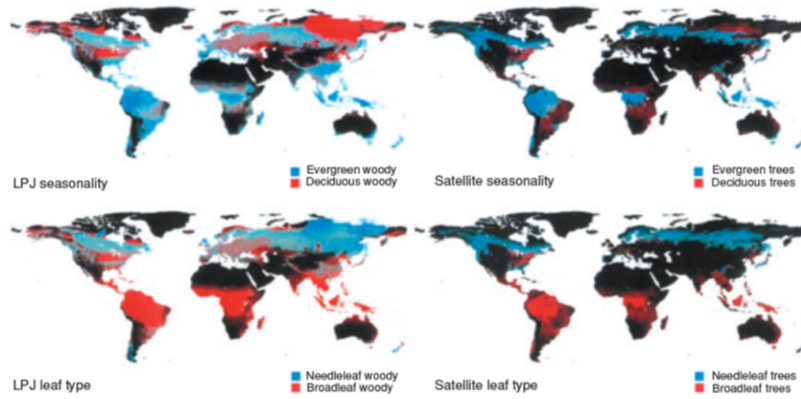


Figure 6.6: Comparison of LPJ-simulated distributions of woody vegetation with satellite-based maps, for percentages of tree cover, partitioned according to phenology (evergreen vs. deciduous), and leaf morphology (broadleaf vs. needleleaf). (Sitch et al. 2003)

These models are also able to simulate successional vegetation dynamics: see figure 6.7. Within one grid cell, the relative cover of different pft is calculated, and in this way, the forest succession is simulated. The start is from bare ground, and the model then dynamically simulates that it is first covered by grasses, which are gradually replaced by trees, with first a peak in broadleaved trees, which are eventually replaced by needleleaf trees in this example. The simulated competition is a kind of ‘prescribed’ as each PFT covers a separate landscape patch. Problems with area-based models: They cannot be linked to real inventory observations because the model does not simulate a number of individuals or a size of individuals. They also neglect important aspects of the successional dynamics: for example, height, size distribution and species diversity are not simulated, but they are very important as they affect the dynamics and habitats of forests. The model is also not capable of simulating disturbances. For example, if you want to take thinning into account, you can only remove a certain amount of biomass, not a specific number of trees. Therefore, we need other models to simulate demographic processes.

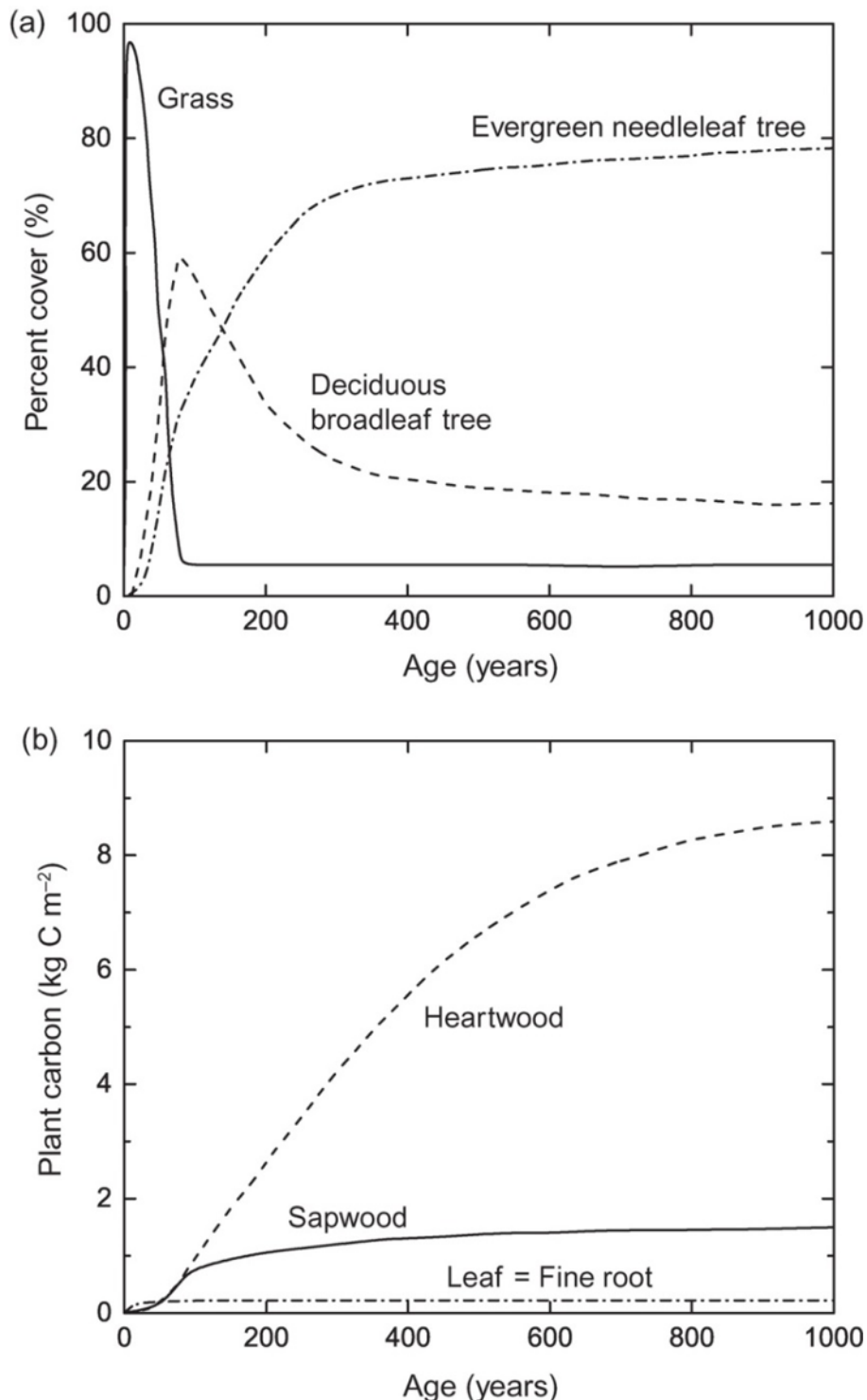


Figure 6.7: Boreal forest dynamics in terms of (a) percentage cover and (b) plant carbon pools as simulated by a dynamic global vegetation model. The simulation is from initially bare ground for a single model grid cell in the boreal forest over 1000 years in the absence of fire. Percentage cover is the annual extent of plant functional types in the grid cell.(Bonan)

The Triffid model: is the predecessor of JULES mode, competition is based on lotka-

volterra competition model, a general equation originally developed to predict predator-prey interactions. A well-known study (Cox et al. 2004) predicted the Amazon dieback by using this area-based model, coupled to a climate model. It predicted a drying of the Amazon forest, and following the drying pattern, the forest would be replaced by grasses, creating a savanna (Fig 6.8). However in follow-up studies, it turned out that the Amazon forest is more resilient than in the original model simulations by Triffid, if you consider that patches are interacting with each other, which was not simulated in this model (see examples later in this syllabus).

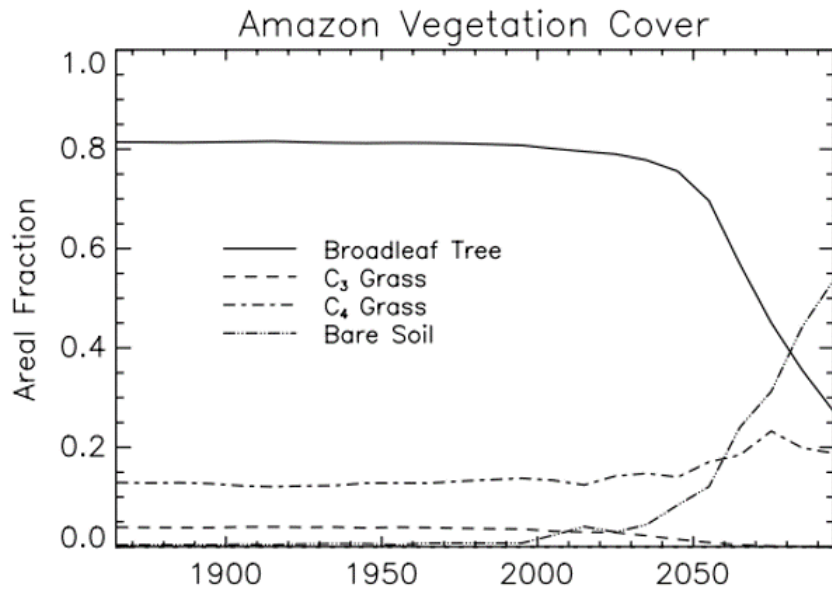


Figure 6.8: Evolution of the vegetation cover in the Amazon from a coupled climate-carbon cycle simulation with the TRIFFID DGVM and the HadCM3LC climate models. (Cox et al. 2004)

6.2.2 Gap models

Gap models (or IBMs individual based models) were developed in parallel with area-based models in the 1970s. However, both model types were developed from a different perspective. Area based models are driven by an interest to simulate global carbon cycle, and global energy balance and water cycles, and vegetation dynamics were only a secondary element of these models. Gap models are originally developed by foresters. They were interested in the dynamics of forests as such, in individual trees, but not in the energy balance or the carbon cycle. The models are based on studies of gap dynamics, and therefore, they have patches of circa 100-800 m², which is the size of the gap created by one big tree that dies.

Within a gap, trees are competing for resources, and growth, mortality and regeneration are simulated (Fig 6.9 and Fig 6.10). The main mechanism that drives the dynamics in gap models is the competition for light between individuals. Growth, diameter, age and height are simulated in response to environmental variables. Mortality is simulated in response to environmental constraints such as stress (climate), fire and insects.

Regeneration is calculated based on seed availability, sprouting, which in turn depend on environmental constraints. All these variables are calculated for every individual, typically at annual timesteps.

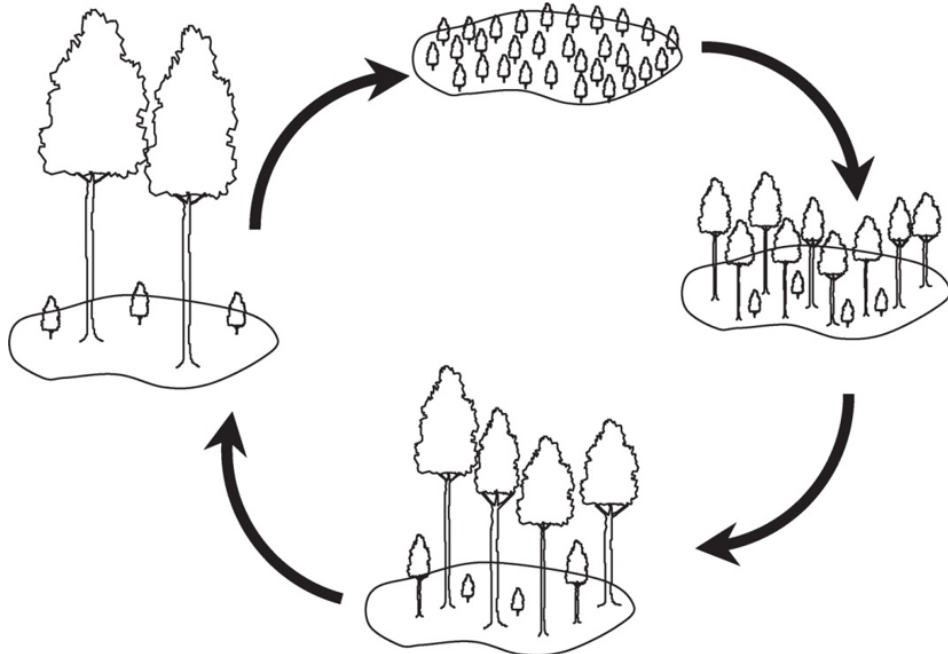


Figure 6.9: Cyclic growth and thinning of trees in a forest patch during gap dynamics.(Bonan)

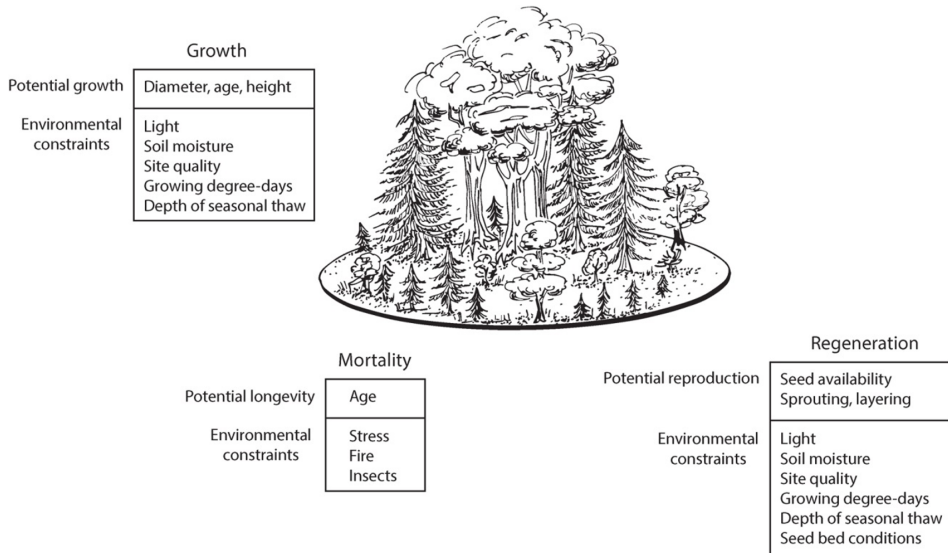


Figure 6.10: Depiction of a boreal forest gap model. The growth of an individual tree depends on its diameter, age, and height as modified by environmental constraints. Mortality depends on the age of the tree as modified by stress, wildfire, and insects. Regeneration depends on seed availability, the ability to sprout or layer, and site conditions. (Bonan)

By simulating demographic processes for each tree, the model can track stem density over time, also the size distribution and the species composition. Gap models are stochastic: as each simulated patch is different and can evolve in a different way, depending on stochastic elements. However, all patches combined results in a landscape with stable properties.

In these models, biomass is not in the center, but can be calculated as the model simulates the growth of all individual trees. This also applies to the community composition and the biogeochemical cycles. These are all emergent outcomes, as they are not described explicitly in the model, but emerge from its output.

In gap models, landscapes are simulated by different patches, in which each individual is modelled by the model. There are different possibilities to put the patches together in the landscape (Fig 6.11): first, a monte Carlo simulation is run to select random places, and for these places, the growth is simulated, after which it is upscaled (averaged out) to the landscape. A second possibility is to use a grid of patches and average out, while a third method simulates all processes for adjacent plots. Finally, you can start a simulation from existing inventories. If you have inventories over different parts of the landscape, you can average simulations of these inventories to come to a landscape average.

Gap models are computationally very intensive, as they simulate each individual tree, which makes it problematic to implement them in earth system models. They also don't simulate short time scale leaf physiology, but simulate growth based on specific growth equations, that describe growth directly as a response to the available light or other factors.

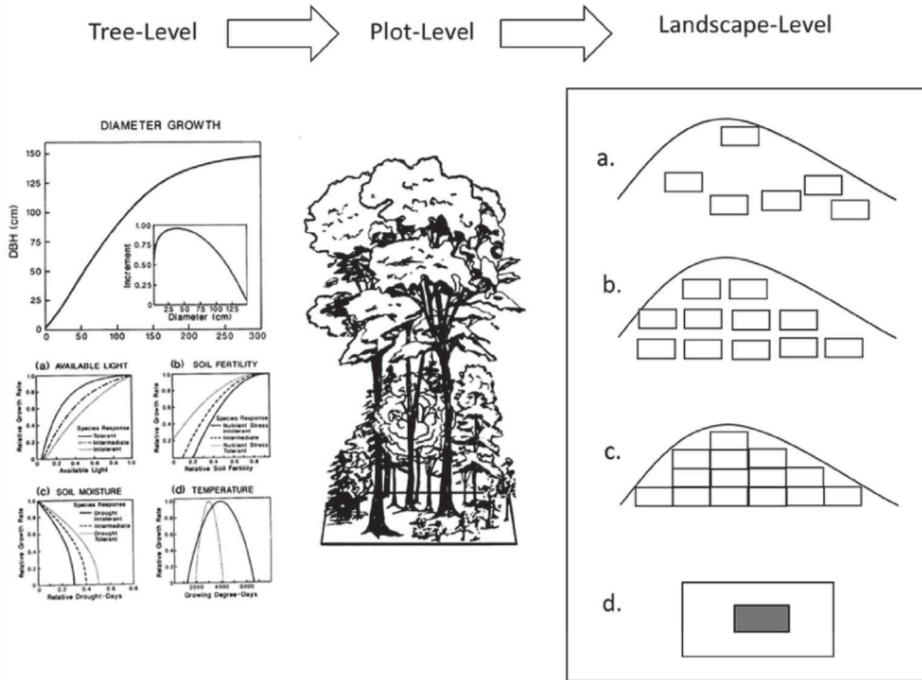


Figure 6.11: General functioning of a gapmodel. As one moves to the right to left, spatial scale increases from an individual tree to a small plot to a landscape. The tree-level response shown here is the elementary growth equation from the FORET (Shugart and West 1977) model. The magnitude of the tree-mortality probability of each tree is also determined at the tree-level depending on tree growth as an index of vigor, species longevities and other conditions. The form of the growth equation with no constraints is shown at the top and the decrement to this optimal growth equation is found below according to the particular controlling environmental factors (available light, soil moisture, etc). At the plot level, the vertical profile of light, available soil moisture, and other environmental and biogeochemical factors are calculated and tree to tree interactions are computed. Conditions for potential new seedlings for each year are determined factors such as the environmental conditions and seed sources. At the landscape model, a basic gap model can be used to represent the landscape as: (a) the summation of a Monte Carlo collection of independent random points; (b) gridded points at some spacing, (c) a tessellation of adjacent plots; (d) a spatially explicit landscape simulation with a spatial map of trees that is ‘windowed’ or updated for tree birth, growth and death by dropping a gap-model computational window onto the tree-stem map to solve for a subset of a new map. This is repeated to produce the new map. The size of this subset determines the resolution of the spatial map. (Shugart et al. 2018)

Examples: ForClim model Fig 6.12 shows simulations for forests in the alps, where different species are competing. The model is initiated from bared ground, and also includes some disturbances with a stochastic character: e.g. wind or management impact. The figure shown is a typical figure for this kind of models, where calculations are made on an annual basis, and simulations are run for centuries or even millennia. In this graph, the abundance of a species is expressed as its total biomass.

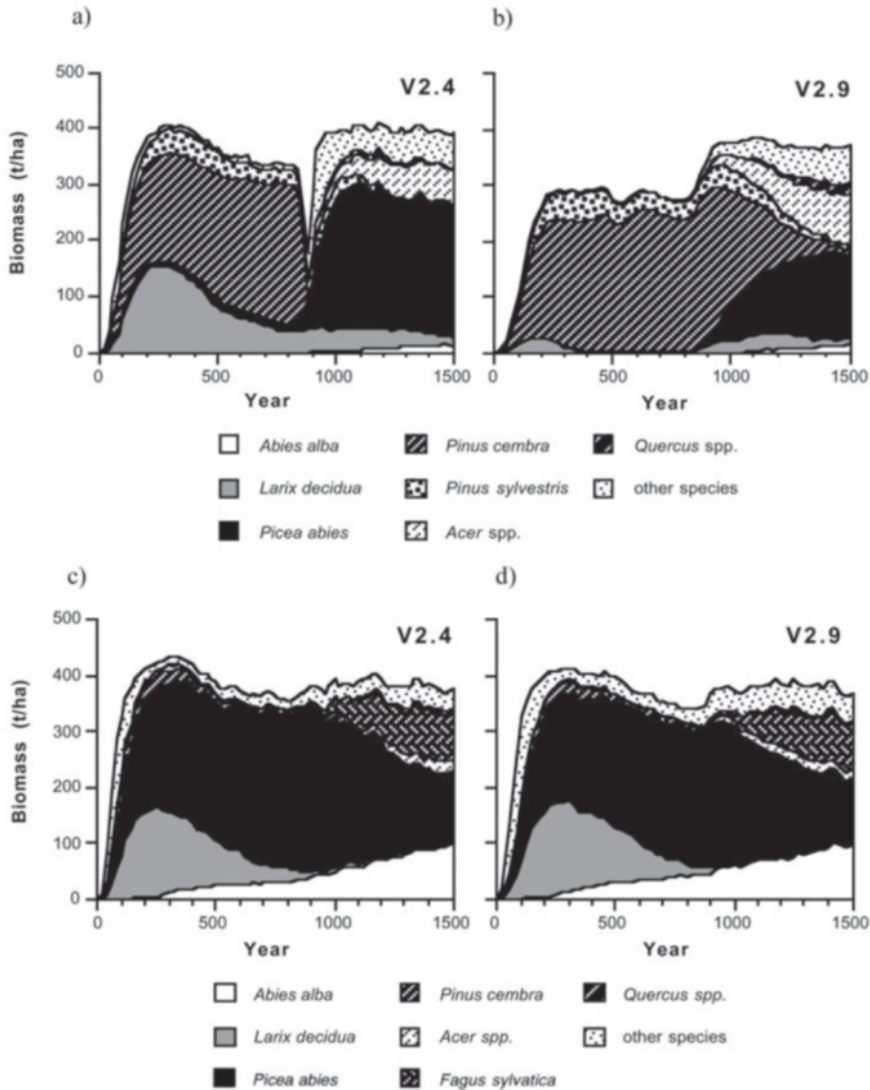


Figure 6.12: Comparison of the behavior of two versions of the gap model ForClim under current climate (years 0–800) and under conditions of climatic change (years 800–900) and under a hypothetical future constant climate (years 900–1500) at two sites in the European Alps, Bever (a, b) and Davos (c,d). Model version 2.4 (a, c) has a parabolic temperature response function (like JABOWA model), whereas model version 2.9 (b, d) features an asymptotic response function. (Bugmann 2001)

Gap models are mostly applied locally but can sometimes be upscaled to larger areas (Fig 6.13 and Fig 6.14). However, for such large scale applications they don't simulate every single tree over the large area but simulate representative areas and extrapolate that data over the entire study area. Sometimes a model data fusion approach is followed, and the data is matched with satellite data, to have a more realistic representation of reality (as in example Fig 6.13). In this example for the Amazon they used satellite data to parameterize the FORMIND model. The model gives a very

detailed biomass map at a very high resolution. This is only possible with this kind of model, with an area-based model for example, you would have very homogenous biomass patterns over the amazon.

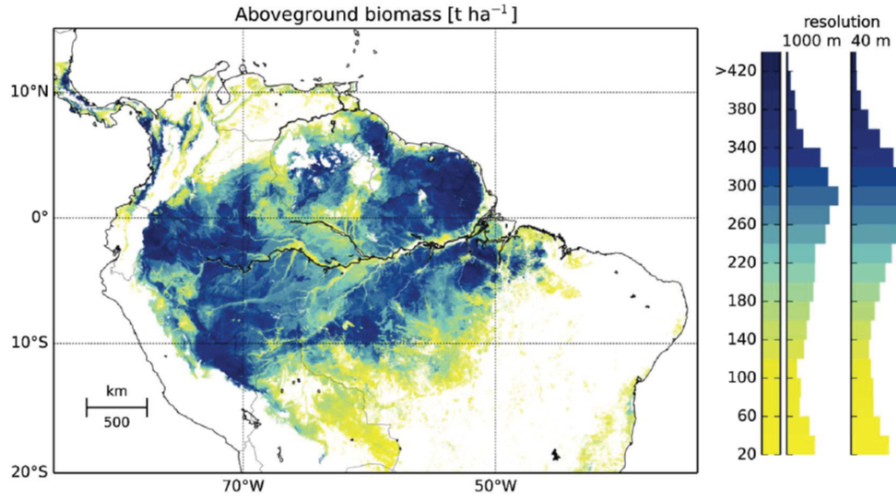


Figure 6.13: High-resolution biomass map for the Amazon rainforest at 1000 m resolution (left) and relative frequency distributions at 40 m resolution (right) derived by linking FORMIND (IBM) simulation results with remote sensing data. (Rödig et al. 2017)

In the example of Fig 6.14 projections for the change in carbon biomass in Russia are shown over the period from now to the end of the century, by using two different climate scenarios. Red areas indicate a large decrease in carbon biomass, green areas indicate a growing carbon biomass. For example, northern Russia is now too cold for tree growth, but could be warmer towards the end of the century, allowing tree growth and leading to a higher carbon biomass.

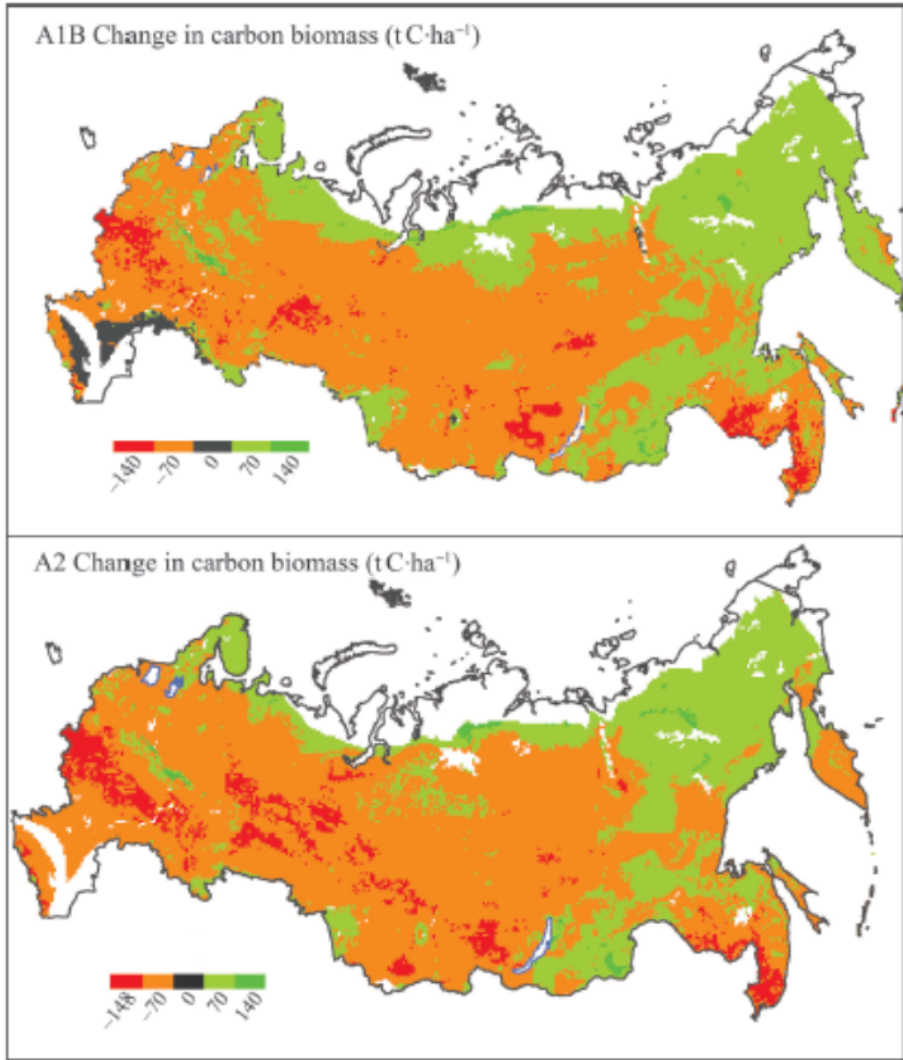


Figure 6.14: Difference in UVAFME simulated total carbon biomass (tonnes of carbon per hectare ($t\text{ C} \cdot \text{ha}^{-1}$) for a mature forest between year 2000 and year 2095 following 95 years of temperature and precipitation as represented by NCAR CCSM A1B and A2 scenarios.(Shuman et al 2015)

6.2.3 Cohort based models

Cohort based models (also called ‘ecosystem demography models’) are an approximation of IBM’s. They group all similar plants into cohorts and simulated one average plant for each cohort, enormously reducing the computational demand. They bridge the gap between IBM and area-based models. They do simulate very short time-scale processes such as photosynthesis and simulate demographic processes. They are not stochastic, i.e. they don’t simulate the mortality of each individual tree but have a more deterministic description of mortality. For example, every year, a fraction of x% of the trees is removed. The cohort approach retains the dynamics of IBMs, with reduced computational cost, but removes stochastic processes that can enhance the representation of functional diversity. Just like in IBMs, the model has emergent outcomes for

community composition, stand biomass and productivity and biogeochemical cycles, as these are not explicitly simulated by the model.

We will focus on one example: the ED model (ecosystem demography model). In ED the landscape is divided into multiple grid cells (Fig 6.15). In each grid cell, the same climatological conditions apply. Within each grid cell, multiple sites exist, based on abiotic conditions, such as soil texture. The sites and grid cells belong to the static part of the model, these characteristics don't change over time. Each site has two dynamic levels, i.e. patches and cohorts. A patch represents a fraction of the landscape grouping all pieces of land that have the same disturbance history. The size of the patches and the number of patches is dynamic, and changes during the simulation. E.g. if there is a lot of mortality, a large patch of young, new forest will be created. Or if there is almost no mortality, the size of the patch of old growth forest will increase. Each patch is covered by a vegetation community, built by different cohorts. A cohort represents a number of individual trees belonging to the same size class and the same plant functional type. Cohorts are also dynamic and change over time (number of plants can increase or decrease), and cohorts can merge (e.g. a cohort of young beech trees that grew enough can become part of the cohort of old large beech trees).

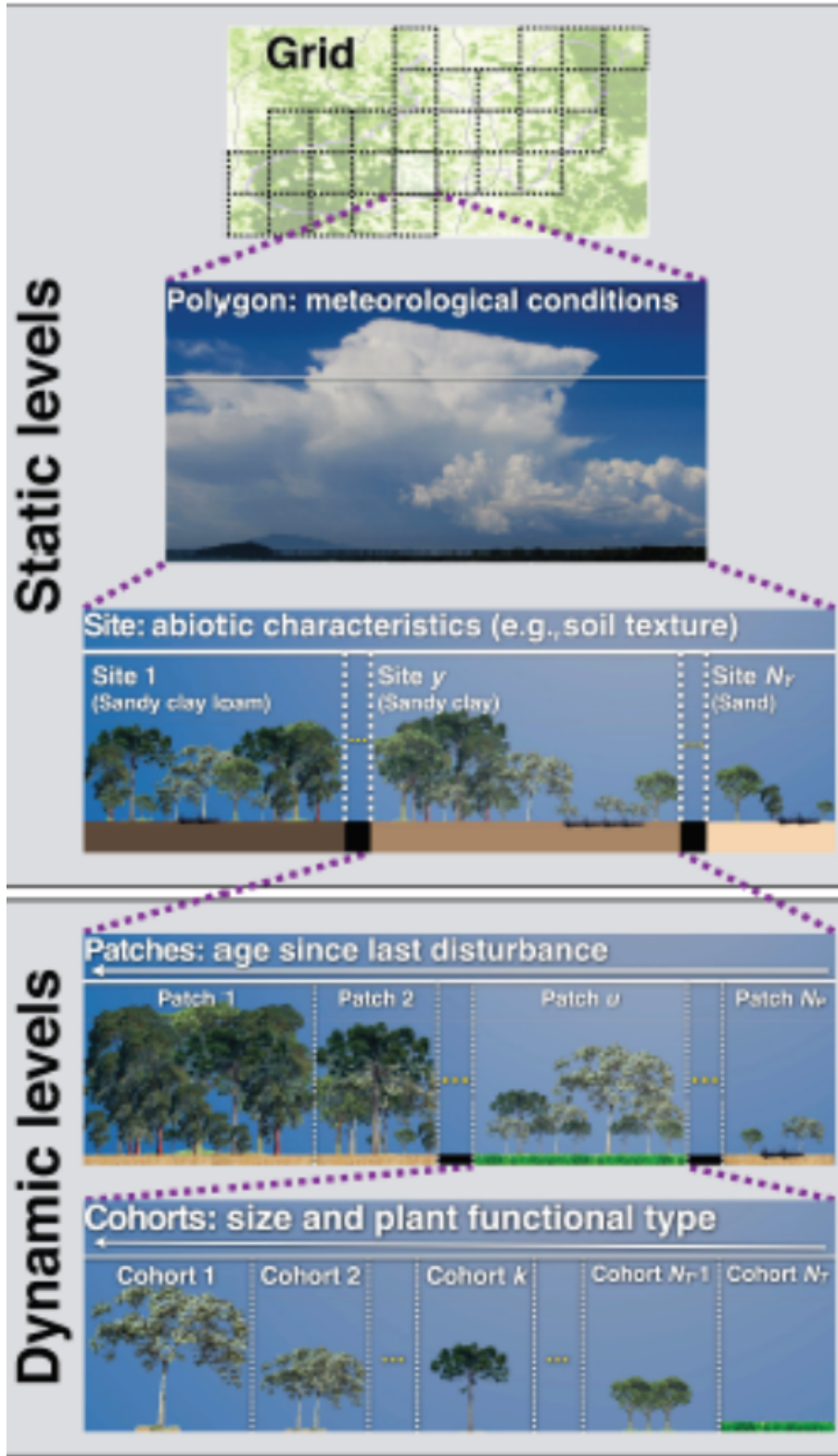


Figure 6.15: Schematic representation of the multiple hierarchical levels in the ED-2.2 model, organized by increasing level of detail from top to bottom. Static levels (grid, polygons, and sites) are assigned during the model initialization and remain constant throughout the simulation. Dynamic levels (patches and cohorts) may change during the simulation according to the dynamics of the ecosystem.(Longo et al 2019)

The ED2.2 model is an advance version of ED that has the full biophysics and biogeochemistry cycle and energy balance included (Fig 6.16, Fig 6.17). For each cohort, all these variables and processes are calculated, and the different cohorts are competing within the patch. This implies that it will be more difficult for a young tree to develop in this model, a struggle for life which is not represented in an area-based model, as here, the tree stands underneath another cohort, which reduces the light and nutrients available for the young tree. The advantage of this model compared to gap models and area-based models is that we can simulate fast time processes and vegetation dynamics with one model.

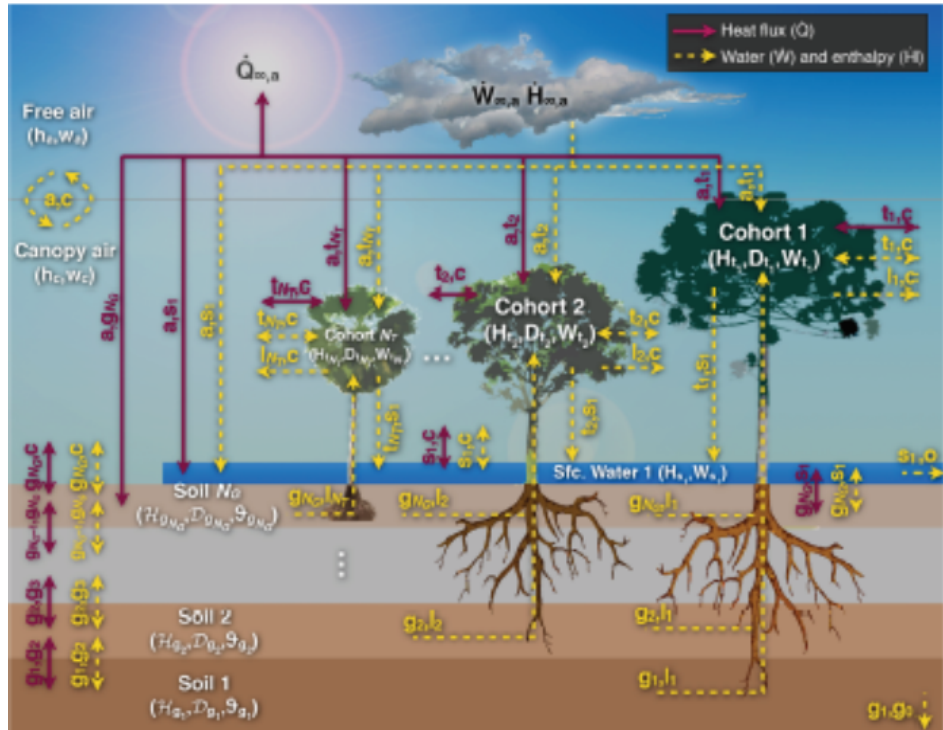


Figure 6.16: ED2.2 biophysics. Schematic of the fluxes that are solved in ED-2.2 for a single patch (thermodynamic envelope). In this example, the patch has NT cohorts, NG soil layers, and NS=1 temporary surface water. Both NG and the maximum NS are specified by the user; NT is dynamically defined by ED-2.2. Letters near the arrows are the subscripts associated with fluxes, although the flux variables have been omitted here for clarity. Solid red arrows represent heat flux with no exchange of mass, and dashed yellow arrows represent exchange of mass and associated enthalpy. Arrows that point to a single direction represent fluxes that can only go in one (non-negative) direction, and arrows pointing to both directions represent fluxes that can be positive, negative, or zero. (Longo et al 2019)

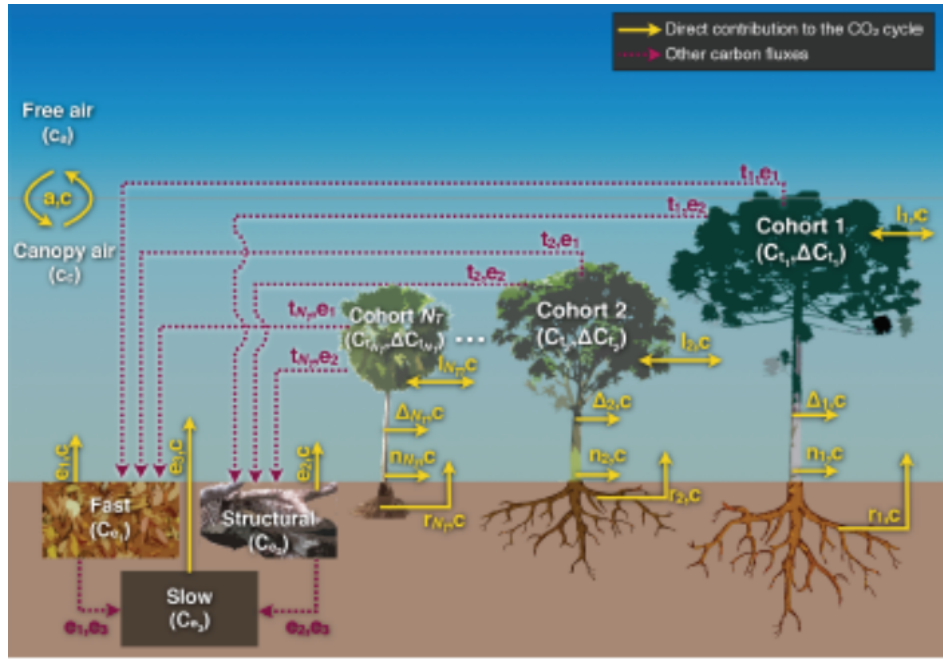


Figure 6.17: ED2.2 biogeochemistry. Schematic of the patch-level carbon cycle solved in ED-2.2 for a patch containing NT cohorts. Like Fig. 6.15, letters near the arrows are the subscripts associated with fluxes. Fluxes shown in solid yellow lines are part of the CO₂ cycle, and dashed red lines are part of the carbon cycle but do not directly affect the CO₂ flux. (Longo et al 2019)

Fig 6.18 illustrates some outputs of the ED2 model for a temperate forest. Fig 6.19 shows the output of the model for tropical ecosystems. The visualization in these figures (6.18a, 6.19a and b) are produced based on the outputs of ED2.2, they are not simulated directly by the model, as the model is not spatially explicit (it is not tracking the location of cohorts). The model simulates carbon fluxes, but also size distribution, which gives a lot of opportunities, as it can be compared with many different datasets: fluxtowerdata, inventory data,

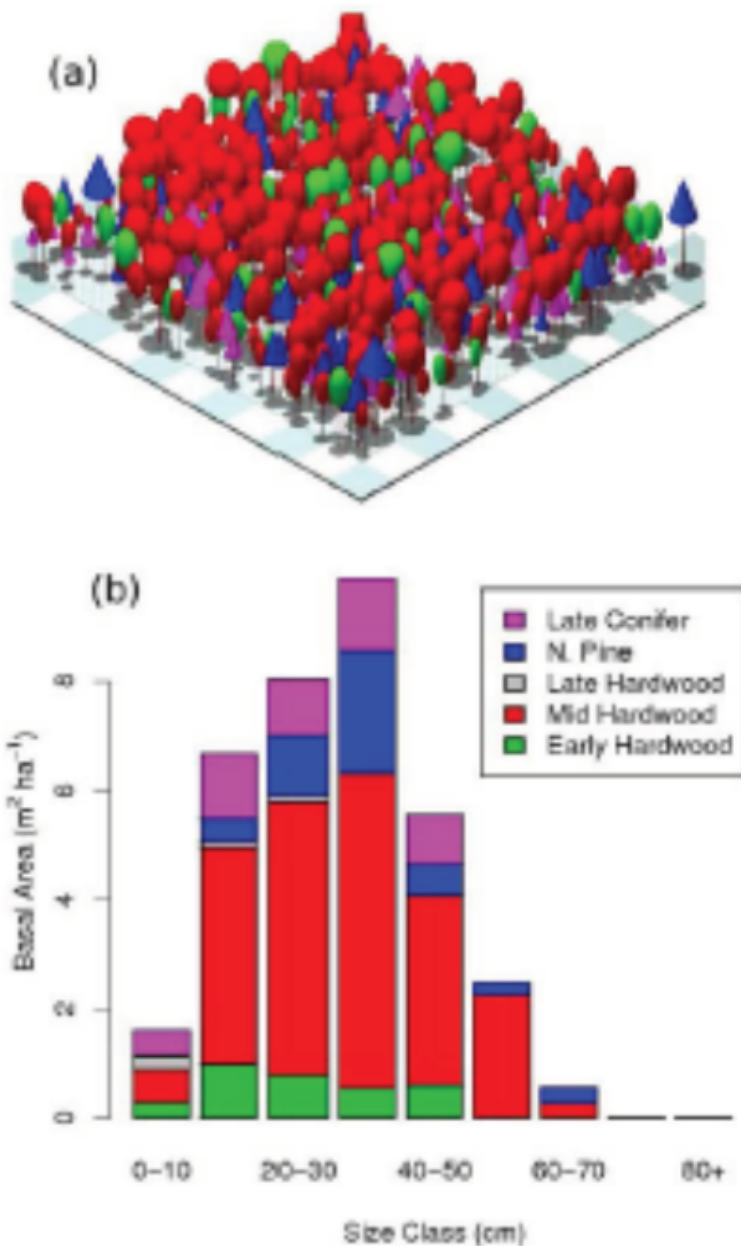


Figure 6.18: Visualization of the ecosystem composition in the Harvard Forest flux tower footprint as simulated by ED2. Midsuccessional hardwoods (red) dominate, but the footprint also contains early successional hardwoods (green), pines (blue), late successional conifers (magenta) and late successional hardwoods (gray). (b) Distribution of basal area of the different plant functional types across tree diameter classes.(Medvigy et al. 2009)

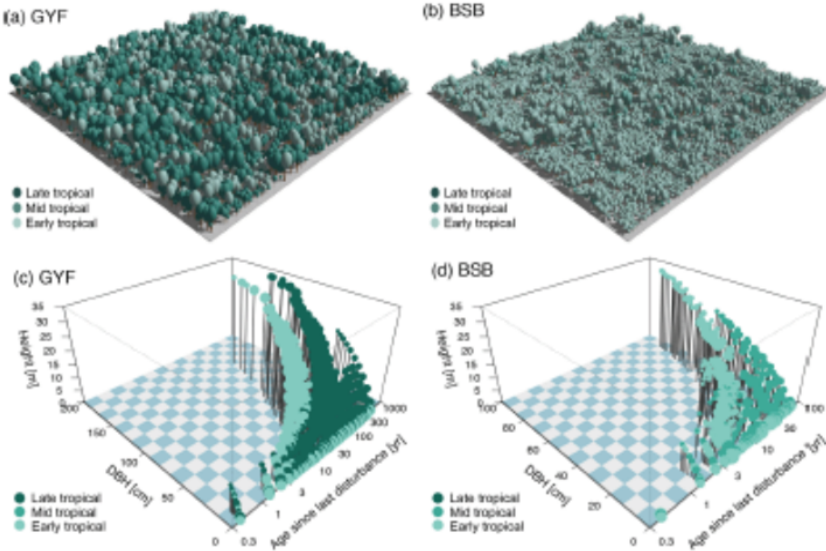


Figure 6.19: Examples of size, age, and functional structure simulated by ED-2.2, after 500 years of simulation using local meteorological forcing and active fires. (a, b) Individual realization of simulated stands for sites (a) Paracou (GYF, tropical forest); (b) Brasília (BSB, woody savanna). The number of individuals shown is proportional to the simulated stem density, the distribution in local communities is proportional to the patch area, the crown size and stem height are proportional to the cohort size, and the crown color indicates the functional group. (c, d) Distribution of cohorts as a function of size (DBH and height) and age since last disturbance (patch age) for sites (c) GYF and (d) BSB. Crown sizes are proportional to the logarithm of the stem density within each patch.(Longo et al 2019)

6.3 Growth and allometric relations in demographic models

Allometric relations are a critical driver for growth in demographic models. Most variables are scaled to the diameter at breast height. The allometries are like the allometries for biogeochemical models but are applied to individual (in IBM) and cohorts (in cohort-based models). Further, these models also use growth specific equations, as can be seen below where we will typical examples of growth and allometric equations.

The **diameter height allometry** of the JOBOWA IBM has three parameters, b_1 is breast height (1.5m) and the other parameters are species specific and can be derived from the maximum height and diameter that specific species can reach, using empirical equations (Fig. 6.20).

$$h = b_1 + b_2 D - b_3 D^2$$

with h the tree height in m, D the tree diameter in m and b_1 is breast height (1.5m),

b_2 and b_3 empirical parameter following:

$$b_2 = 2 \left(\frac{h_{max} - 1.37}{D_{max}} \right)$$

and

$$b_3 = \frac{h_{max} - 1.37}{D_{max}^2}$$

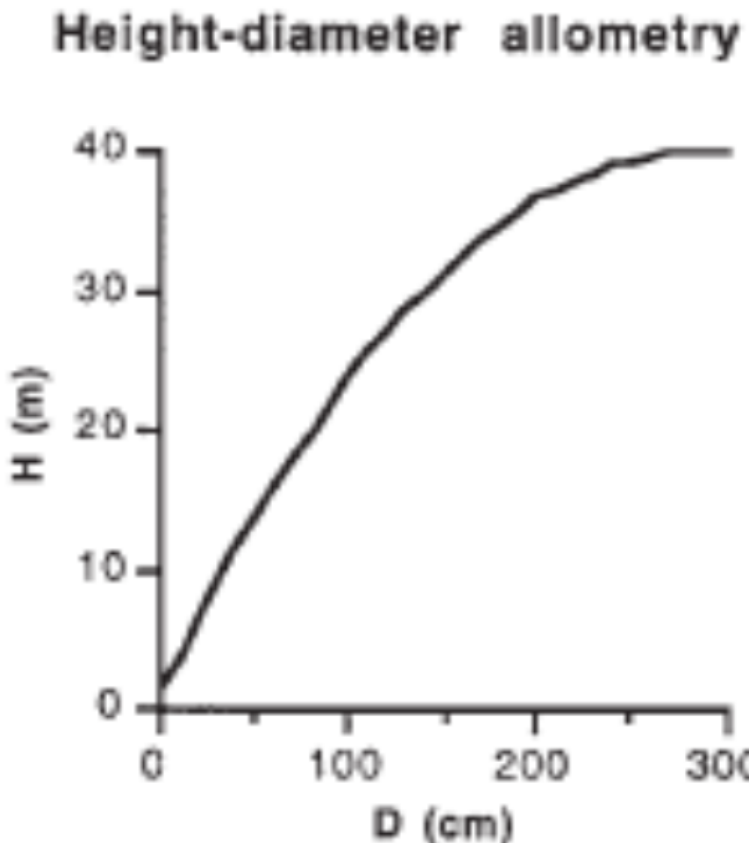


Figure 6.20: Height-diameter allometry in the JABOWA individual based model.(Buggman 2001)

Allometric equations have also been developed for **biomass**, where an exponential relationship is used. a_i and b_i are species specific parameters. This leads to different curves for different species (see Fig 6.21). For the tropics, no such equations are available, and the use of pan-tropical equations or average equations based on destructive measurements are used.

$$M_i = a_i D^{b_i}$$

with M_i the mass of individual i , D_i its diameter and a_i and b_i empirical coefficients.

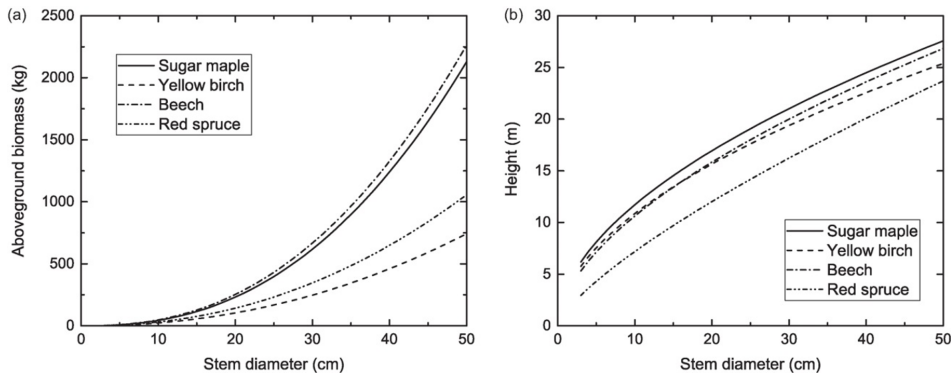


Figure 6.21: Relationships between stem diameter and (a) aboveground biomass and (b) height for sugar maple, yellow birch, beech, and red spruce trees at the Hubbard Brook Experimental Forest, New Hampshire using allometric relationships. (Bonan)

The **leaf biomass allometry** is also an exponential relation between the diameter and leaf biomass, which can then be recalculated to LAI using the specific leaf area (SLA). This allometry is not often used in forestry, but is interesting from a modelling point of view, as the size and area of the crown determines the competition for light with other trees.

$$M_{leaf} = cD^2$$

with M_{leaf} the mass of leaves, D the diameter and c an empirical coefficient.

Leaf area allometry

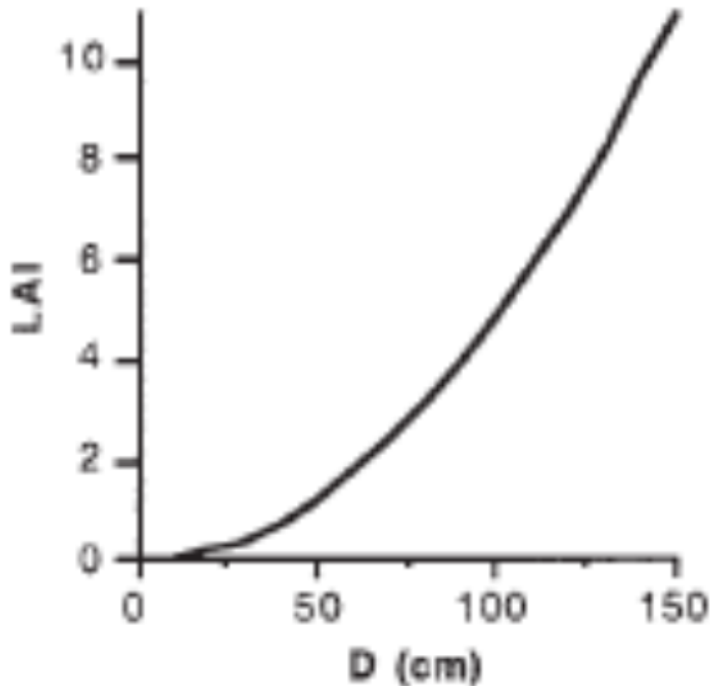


Figure 6.22: Leaf area - diameter allometry in the JABOWA individual based model.
(Buggman 2001)

The **growth equation** used in the JABOWA model is shown in Fig 6.23. This is a key equation in the model to calculate the diameter increment, as the other variables are calculated based on the diameter. IBM's apply growth functions every year, whereas cohort-based models typically apply them at a shorter calculation step, mostly every month. The equation of JABOWA is an empirical equation, based on inventories, and the diameter is the only state variable. The equation calculates the maximum obtainable growth (first 4 terms) and multiplies this with a correction factor (values between 0 and 1), which is based on environmental conditions. This results in the fact that the obtained growth in the model is different for every individual, based on the competition it has with neighboring trees for light and other resources.

$$\frac{\Delta D}{\Delta t} = GD \left(1 - \frac{DH}{D_{max}H_{max}}\right) \frac{1}{b(D)} f(e)$$

with D the tree diameter, H its height, t the time and b and $f(e)$ empirical coefficients.

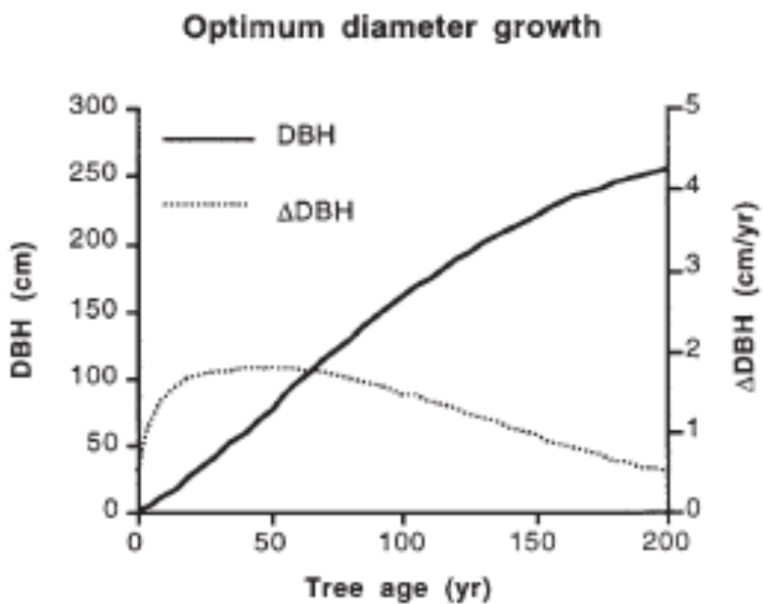


Figure 6.23: The JABOWA equation of maximum tree growth plotted for a tree with $H_{max} = 40$ m, $D_{max} = 285$ cm, and $G = 143$ cm/yr. (Buggman 2001)

The figure 6.24 illustrates the allometries and growth factor of two tree species in an IBM, subplots a and b represent the height-D allometry and the leaf area -D allometry for two species. Subplot c shows the cumulative leaf area index vs the fraction of full sunlight and subplot d indicates the effect of light availability on the growth factor. Exceptionally, the growth factor can be higher than one, for the shade tolerant species in full sunlight. This indicated that the maximum obtained growth can be higher than the modeled maximum under certain circumstances.

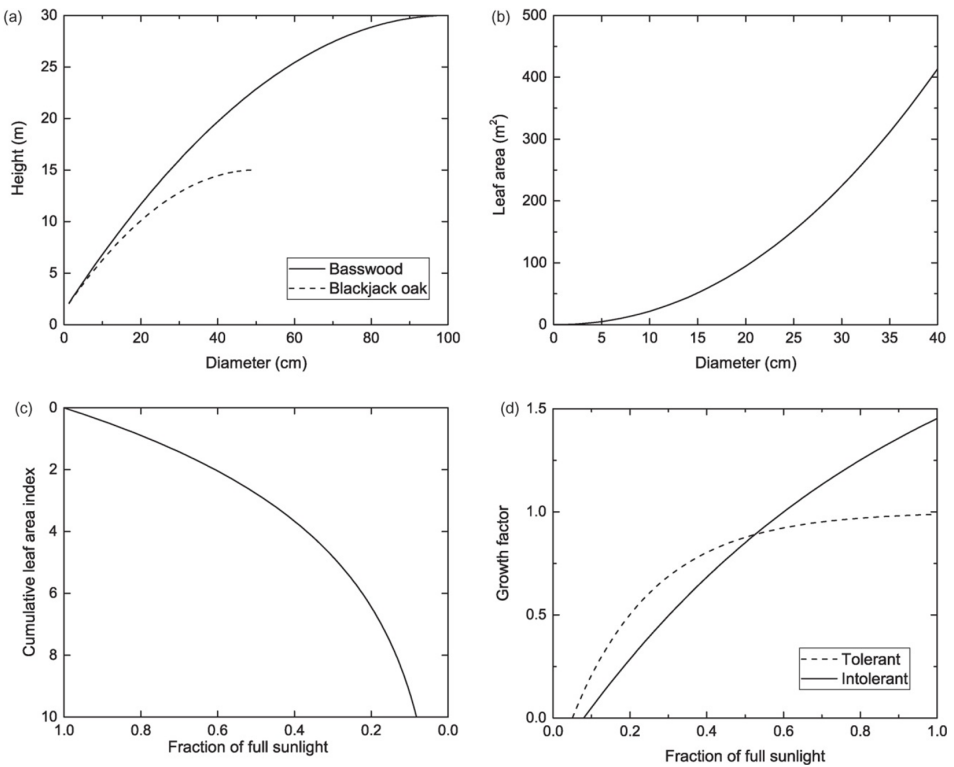


Figure 6.24: Tree height and light competition in a forest gap model. (a) Height in relation to stem diameter for two species of trees. (b) Leaf area in relation to stem diameter. (c) Light profile in relation to cumulative leaf area index. (d) Light growth factors for shade tolerant and intolerant species. Height is shown for basswood (*Tilia americana*) and blackjack oak (*Quercus marilandica*) with parameters from a model of forests in eastern North America (Pastor and Post 1985). Leaf area and light extinction are from FORET (Shugart 1984). (Figure from Bonan)

Figure 6.25 illustrates other dependencies of the growth factor on environmental conditions, for the dependency on growing days, drought and nitrogen availability. Some models also link the growth factor to the basal area of the total stand, where a high basal area lowers the growth factor, because of the high competition.

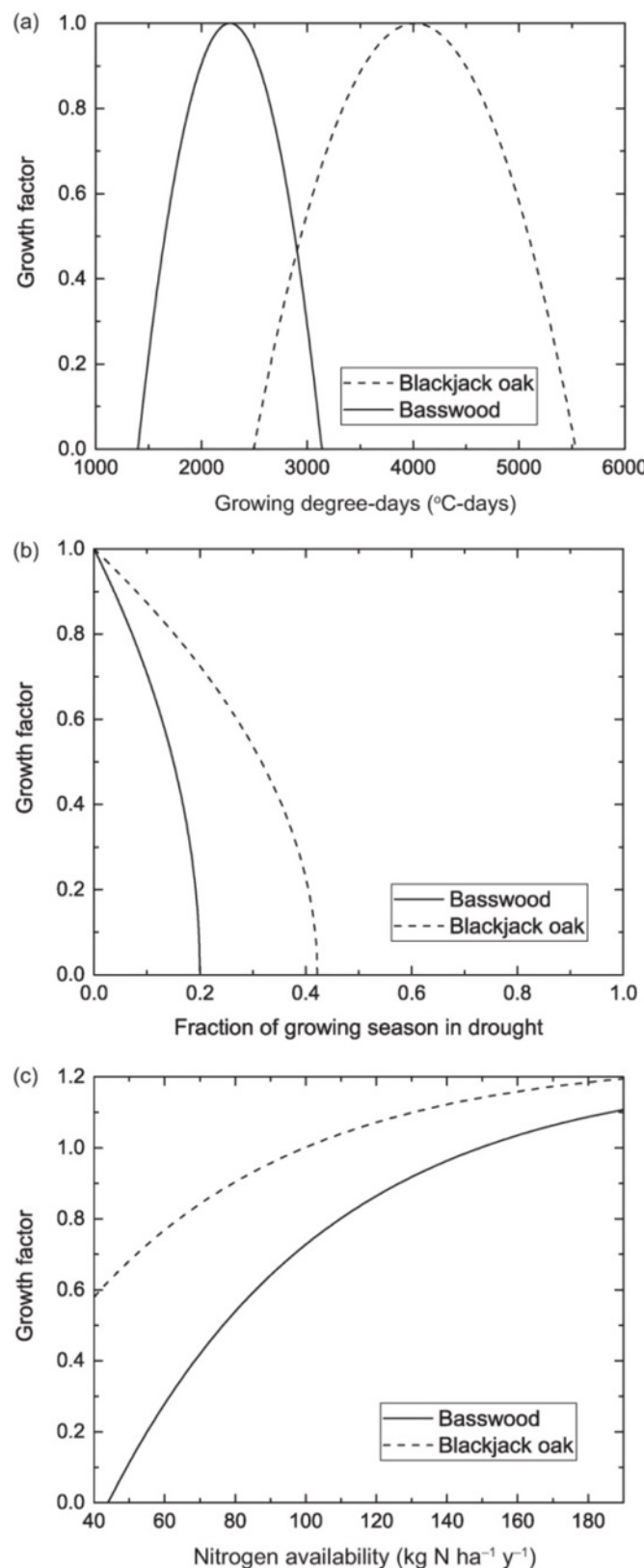


Figure 6.25: Growth factors for (a) temperature (growing degree-days), (b) soil moisture, and (c) soil nitrogen illustrated for basswood and blackjack oak (Pastor and Post 1985). Basswood grows at more northern locations than blackjack oak, on wetter soils, and is intolerant of low soil nitrogen. (Bonan)

Figure 6.26 shows the growth functions of the two species discussed above. Basswood is more a pioneer species as its peak annual growth falls early, whereas oak is more a climax tree, as its peak falls later and is more spread over time. The maximum growth shown on these curves is then corrected by the growth factor which is shown in the figures above.

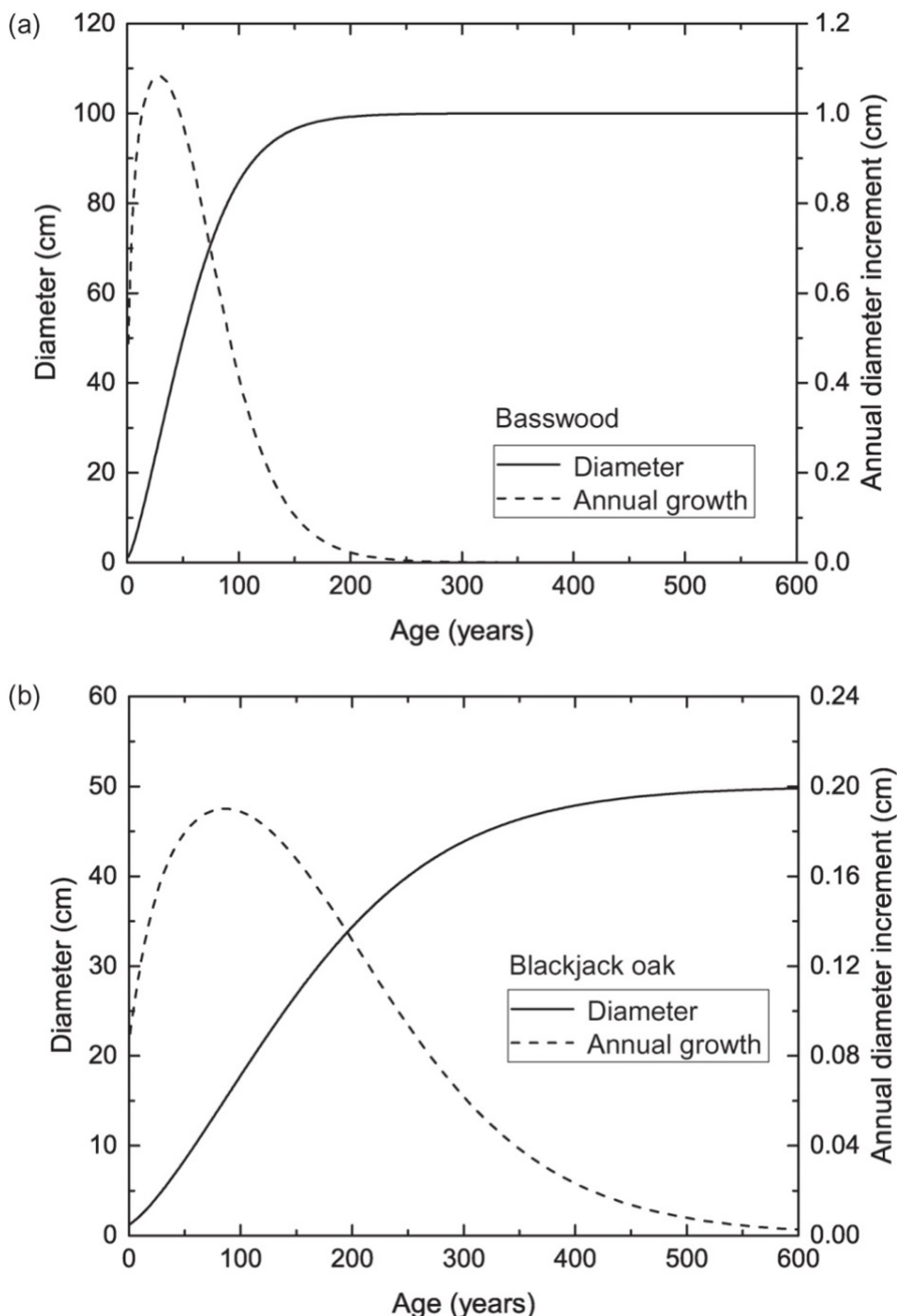


Figure 6.26: Stem diameter growth in relation to age as represented in gap models. Relationships are shown for basswood ($D_{max} = 100$ cm, $h_{max} = 30$ m, $G_0 = 188.7$ cm y $^{-1}$, maximum age 140 years) and blackjack oak ($D_{max} = 50$ cm, $h_{max} = 15$ m, $G_0 = 34.0$ cm y $^{-1}$, maximum age 400 years). Parameter values are from Pastor and Post (1985). (Bonan)

6.4 Competition for light in demographic models

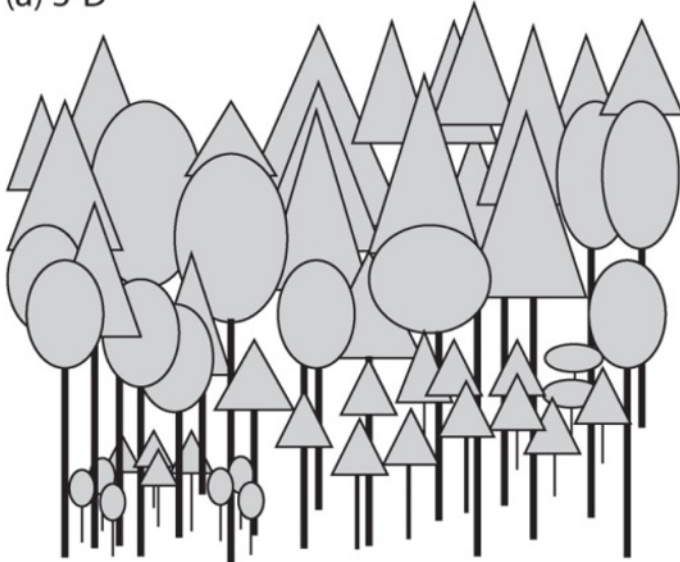
In this section we focus on how competition for light is implemented in demographic models. This is important because it largely determines the dynamics of the forests.

Cohort based models are usually not specially explicit. This implies that plants have no specific place in the patch, so it is impossible to know which individual has an influence on another, e.g. which individuals shades another individual. To be able to apply the exponential decay of light in the canopy, we need to have a vertical canopy profile. This needs to be build with the cohorts that grow in the patch and can be done in different ways (Fig 6.27), depending on the assumption we make on the shape of the crowns and the spatial (vertical) organization of these crowns within the patch. The easiest approach is the approach of “flat-topped crowns”. In this approach, each cohort has all its leaf area at its maximum height and the largest tree in the patch is shading all the other trees within the patch. A second approach is the perfect plasticity approximation (PPA). This approximation assumes that the available horizontal space in the patch is first filled by the largest trees, followed by the lower trees, until a layer of $\text{LAI} = 1$ is reached. The remaining trees are then considered as understory trees. In this approach, smaller trees that are still in the top layer are not shaded by the highest tree, which is more realistic than the first approximation. This approach assumes that crowns are not interfering, so crowns don't grow into each other (i.e. are perfectly plastic). It further results in a critical height that represents the height that is needed to be in the overstory, and thus to be fully sunlit (Fig 6.28).

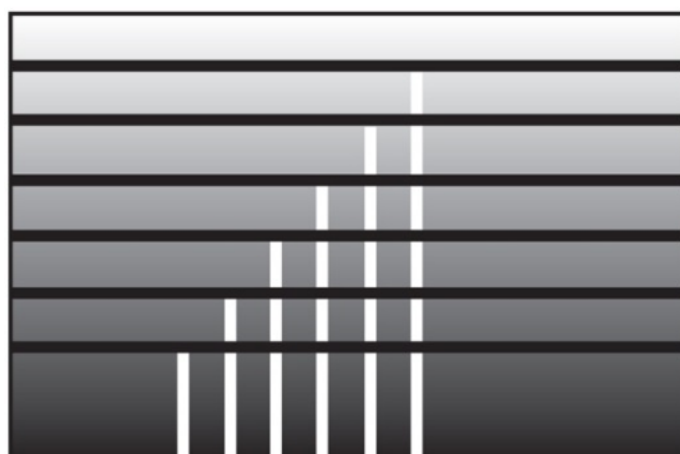
Among various demographic models, there are different approaches. Some models assume multiple layers within one cohort, so only the top layer can be sunlit. There are attempts to model in three dimensions, but this will not be discussed in this course.

Both methods have advantages and disadvantages: e.g. shading by neighboring trees is not accounted for in the PPA model, while it is in some way included in the flat crown approach.

(a) 3-D



(b) Thin, flat crowns



(c) PPA

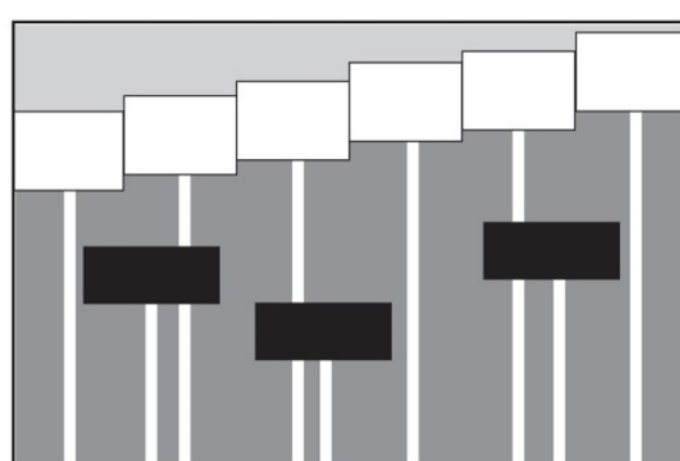


Figure 6.27: Representation of plant canopies in vegetation dynamics models.(a) Actual canopies have complex three-dimensional structure determined by the spatial location of trees and their crown geometry. (b) Gap models simplify the canopy so that the crown of an individual tree is a thin, flat layer of leaves at the top of the tree. Shown are six trees with different heights (white vertical lines). The leaf area of each tree (black horizontal

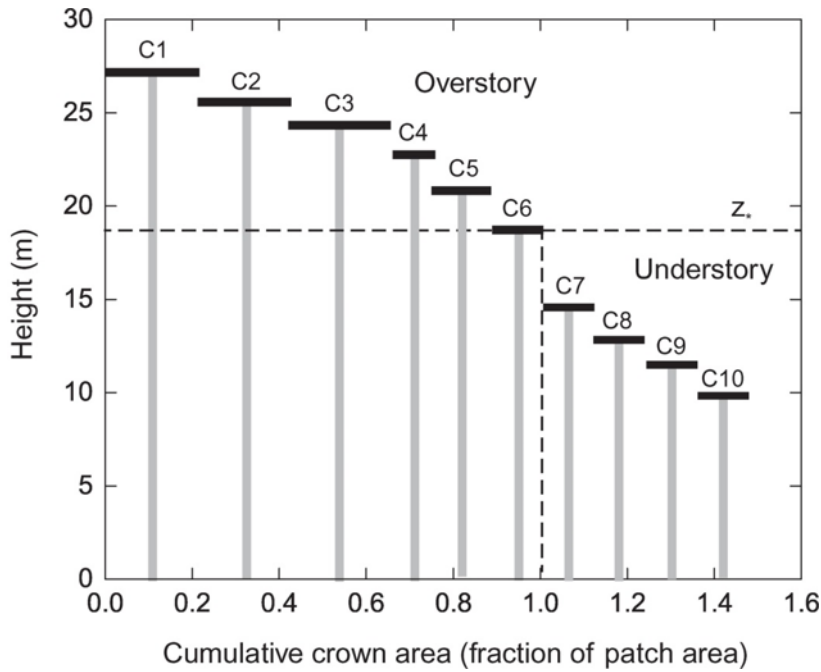


Figure 6.28: Canopy organization in the perfect plasticity approximation. Shown are 10 cohorts arranged from tallest to shortest. The cumulative crown area of the six tallest cohorts (C1–C6) sums to one, and these form the overstory. The remaining cohorts (C7–C10) form the understory. The height z^* separates the two canopy layers. (Bonan)

We further some critical issues of these approximations. If we consider an open canopy (no canopy closure yet), the flat top crown will simulate shading, while there is none. Also, the impact of a height advantage is magnified in the flat top crown approach, i.e. the highest tree has a huge advantage over all the other trees. This leads to monodominance, which makes it difficult to simulate co-existence of multiple trees.

In the PPA approximation (Fig 6.29), it is assumed that gaps are filled, which removes magnification of small height advantages, but it assumes that all trees in the top layer are fully sunlit, which is likely not the case in reality. Also, all understory trees have all the same light environment in this model, which is different from reality.



Figure 6.29: Crown shapes modelled by the Ideal Tree Distribution model (ITD) following the perfect plasticity approximation (Purves et al. 2007)

The simulated vegetation dynamics (growth, mortality, recruitment) can have an impact on the light regime within the patch and the light availability of the respective cohorts. Figure 6.30 shows how growth can lead to demotion (opposite of promotion) of certain cohorts. Subplot a: the growth of the largest cohorts leads to an increased LAI of these cohorts. Because of that, they become too large to fit as one lai layer in the patch, so a part of the smallest cohort will be demoted to the shaded canopy, creating a new cohort. For mortality, there are two options: in subplot b, mortality leads to the death of a certain fraction of the crown of each cohort, resulting in a more open space, and thus place for new cohorts to reach the top of the canopy. The new open space is filled starting with the highest cohort of the shaded cohorts, until the top layer is filled again. In subplot c, the mortality leads to new open space which is used to create new patches of newborn vegetation. Both approaches lead to a different forest dynamic.

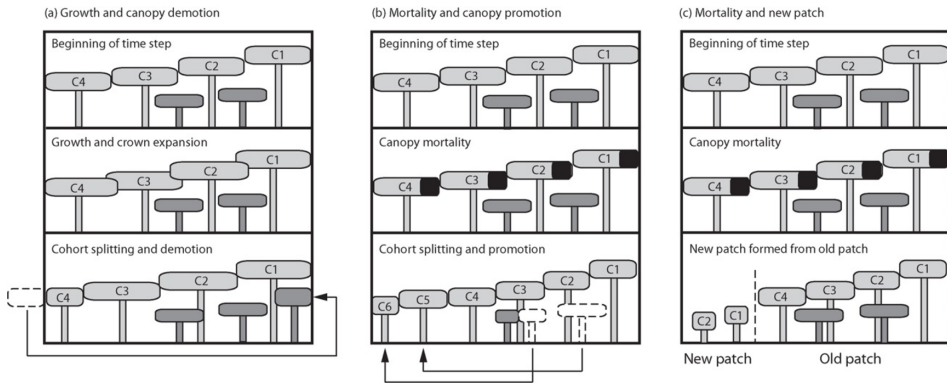


Figure 6.30: Depiction of cohort and patch dynamics. (a) Growth of cohorts leads to crown expansion, resulting in splitting of a cohort and demotion to the understory. Shown are four overstory cohorts (C1–C4). Part of the shortest cohort (C4) is demoted to the understory to form a new cohort. (b) Mortality leads to open canopy space that can be filled by promotion of understory cohorts to the overstory. In this example, the two understory cohorts form new cohorts (C5, C6) in the overstory. Patch area is unchanged. (c) The open canopy space upon mortality can also be used to create a new patch that is filled by new cohorts. The area of the old patch decreases, and a new patch is formed from the open canopy area.(Bonan)

6.5 Competition for water and nutrients in demographic models

The implementation of competition for water and nutrients depends on how detailed the soil is represented in the model. The soil representation varies between models, ranging from a one-bucket model (i.e. one soil water reservoir with inputs and outputs), to multiple soil layers with an explicit rooting depth or profile. In demographic models (i.e. models with multiple PFTs), plants can compete with each other. In these models, the rooting profile is often the key to determine competition for water and nutrients; e.g. a plant with superficial roots will be more vulnerable to drought than a plant with roots that reach the ground water table.

Models also differ in the scale at which they represent the competition for resources. Some models consider that all patches in the same gridcell have access to the same resource pool (fig 6.31 b), while other models track a resource pool for each patch separately (fig 6.31 a). In the former case, water uptake by a tree in for example patch 3, has a direct impact on the water availability for trees in patch 1.

The below ground competition in models is generally less well developed than the above ground competition for resources. This is mainly because there is less information and data available on variables that determine the below ground competition, such as root distribution, root biomass in different soil layers, ...

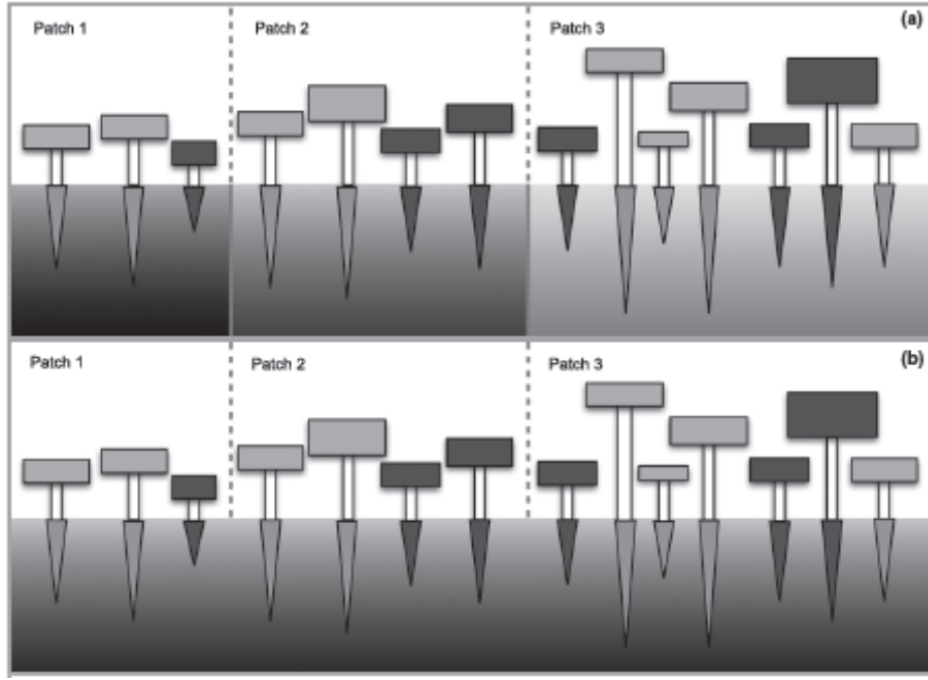


Figure 6.31: Illustration of resource partitioning in vegetation demographic models. (a, b) show two alternative depictions of resource partitioning in an age-since-disturbance resolving (ED-type) model. In (a) resources (water/nutrients) are resolved for each age-since-disturbance patch, meaning that different extraction levels can affect resource availability over the successional gradient, a situation made more likely by large spatial-scale disturbances. In (b) all patches share a common pool, a situation more relevant to smaller (individual) scale disturbances. (Fischer et al. 2018)

6.6 Seed dispersal and recruitment

In most models, recruitment and dispersal are stochastic processes, and the model implementations are much less process-based compared to for example photosynthesis. Most models assume that seeds of all PFTs that potentially grow in the patch are available everywhere in the patch, i.e. there is a constant available seedbank for all PFTs. By consequence, most models don't simulate seed arrival, germination and establishment, but only how many new young trees establish. However, some models are more spatially explicit, and only allow establishment of certain PFTs, only those PFTs that grow in the neighborhood of the establishment site (seed input of neighboring patches allows for gap-colonization by specific PFTs).

Establishment of new seedlings further depends on light availability and other climatic conditions, such as water availability or temperature. The initial dimensions of new seedlings/saplings are highly model dependent. Some models assume a new tree to be 0.5 m high from the start, without explicitly simulating the growth of that young tree, while other models assume a variation in the size of new young trees.

6.7 Mortality

Mortality is typically a stochastic process, which consists of three different components. First, there is a **background mortality**. This is a constant probability for a tree/plant to die each year throughout the tree life, which typically ensures that only a limited number (a few percent) of trees reach the maximum age (maximum age is a PFT dependent parameter in most models). In area-based models, this component is included by removing a certain fraction of the wood biomass each year, whereas in demographic models, a certain number of individuals dies each year.

The second component of mortality is the **stress related mortality**. Typical examples of this are drought stress or heat stress. Some models link these stresses to actual physiological processes simulated by the model, e.g. if actual drought stress is simulated on photosynthesis, the model also increases the mortality because of the drought (process based mortality). Other models, such as the JABOWA model (shown in figure 6.32), link mortality empirically to the diameter growth of trees (higher mortality rates for low growth rates). In this case, trees that only grow very little according to their prescribed growth curve, have a higher mortality. Figure 6.32 shows how mortality over the life cycle of a tree is included in the JABOWA model. The full line is the background mortality. On the left hand, the stress related mortality for young trees is shown. Young trees have a higher mortality because they have only a limited diameter growth, as they are mostly shaded and heavily competing in their early life stages. On the right hand of the graph, the increased stress related mortality for old trees is shown. Again, the mortality becomes higher as older trees show less diameter growth. The total probability of mortality over the lifetime of a tree is shown by the dark black line and is the result of the sum of all individual probabilities.

Third, there is **disturbance related mortality**. This mortality is related to individual events, such as wind or fire. The simplest models assume a constant annual mortality related to disturbance, while more complicated models link this mortality to, for example, wind speed or have an explicit fire module. Mortality is, just like recruitment and dispersal, not fully developed, because our knowledge on these processes is rather limited.

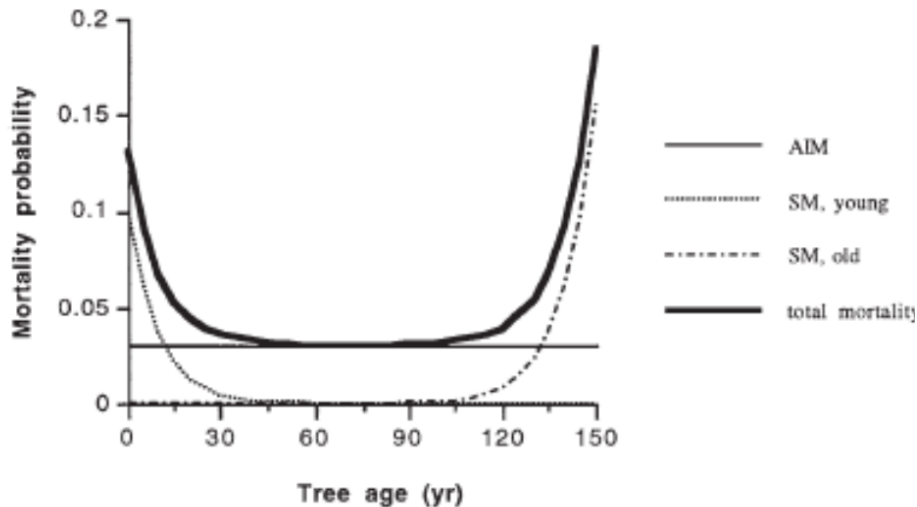


Figure 6.32: Changes of mortality patterns with tree age and their approximation in the JABOWA model. AIM – age-independent ‘background’ mortality; SM – stress-related mortality.(Buggman 2001)

6.8 Conclusion

Demographic models (individual based or cohort based) simulate forest dynamics as an outcome of the life history traits (such as maximum height, maximum age and climate tolerance), attributed to the species or the PFT. In these models, the different PFTs compete with each other, limited by their life history traits, resulting in a vegetation composition. When we provide other input values for the life history traits, the simulated vegetation community (PFT composition, size distribution) will also be different. For this reason, these models are also called ‘trait filtering models’: properties of the individuals/cohorts determine which species can become dominant during succession.

From that perspective, these models could be used to replace standard species distribution models, which need species abundance data, climate data and soil data to predict where a certain species can occur. In a well-working demographic model, only species that suit to a certain place and climate are able to grow. For example, in Belgium, no tropical trees would survive, but temperate tree species would, and will dominate the vegetation in the model after some time. However, more data on more traits should be accounted for to allow such model to predict species distribution reliably. In the meantime, demographic models are often run with prescribed potential species or PFTs that can grow in a certain region, which results in figures as Figure 6.33.

Figure 6.33 b shows the stem density at a certain point in time during the simulation. It shows a typical pattern, namely that of multiple small diameter trees, and only a few large diameter trees. Subplot c shows the biomass distribution over the diameter classes. Here we see that most of the biomass is concentrated in the trees with an average diameter, and less in trees with a small, or large diameter. The results of this model can be related to inventory data to validate the model output.

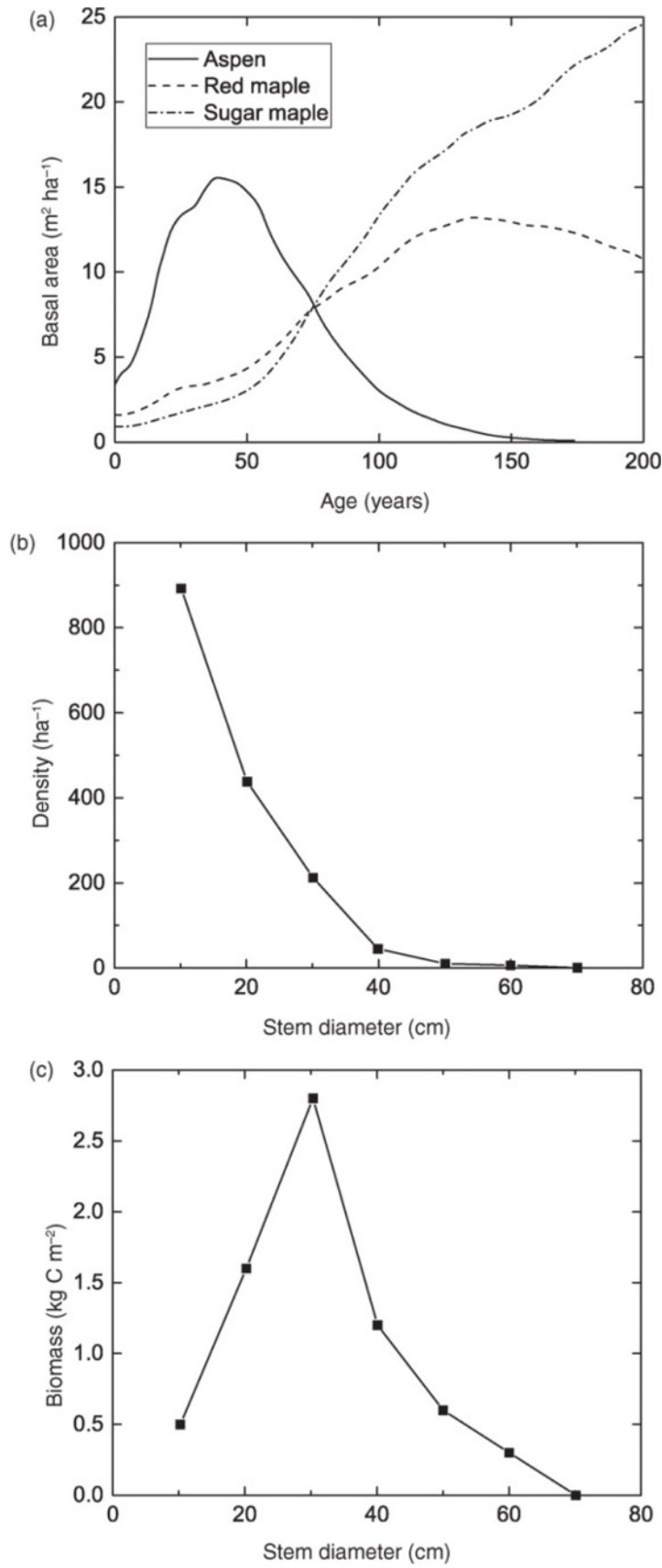


Figure 6.33: Forest dynamics simulated by LM3-PPA. Shown is (a) basal area of aspen (*Populus tremuloides*), red maple (*Acer rubrum*), and sugar maple (*Acer saccharum*) in relation to stand age. Also shown for year 80 are (b) stem diameter distribution and (c) biomass distribution. (Bonan))

Area-based models are the models that are now standard in global models, but cohort-based models will likely take over this task in the future. The table below gives a general overview of the main properties of area- based models, cohort-based models and gap models. Please note that not every model can fit exactly into one of these groups, some models combine properties of different groups.

Models are not only used to make simulations or predict what will happen in the future, but they can also be used as a diagnostic tool. Combing the model with available data (model-data fusion) leads to better estimates of parameters that are more difficult to derive from the original dataset that was used to feed the model. This allows people to extract more information from the data.

Area based models (DGVMs)	Cohort based models	Gap models
Applicable at large scale, and link with ESM	Still challenging to apply at large scale and to link with ESMs	Hard to apply at large scale, not linked to ESMs
Deterministic	Deterministic	Stochastic
Accounts for biophysics and leaf scale processes	Accounts for biophysics and leaf scale processes	Does not account for biophysics and leaf scale processes
Lower computational time	High computational time	High computational time
Biogeochemistry is core of the model	Demography and biogeochemistry are balanced	Demography is core of the model
Lower amount of parameters, easier to parameterize	Hard to parameterize all parameters	Empirical parametrization
Fine temporal resolution, coarse spatial resolution	Fine temporal and spatial resolution	Coarse temporal resolution, fine spatial resolution

Figure 6.34: Summary of the differences between area based, cohort based and individual based vegetation models.

6.9 Case study 6.1

Bohn, F. J., May, F., & Huth, A. (2018). Species composition and forest structure explain the temperature sensitivity patterns of productivity in temperate forests. Biogeosciences, 15(6), 1795-1813.

The FORMIND model is an individual-based model that was used in this study to simulate how the forest structure and composition affects the temperature sensitivity of woody productivity. The model showed that structure and species composition are both relevant for temperature sensitivity. The results were diverging for young and old forests. In young forests, low diversity and low heterogeneity resulted in a positive impact of the temperature on the NPP, whereas in old forest, the opposite is true. If you plant a new forest, the authors therefore advice to start with a closed, even aged pioneer canopy, with a climax species rich understory.

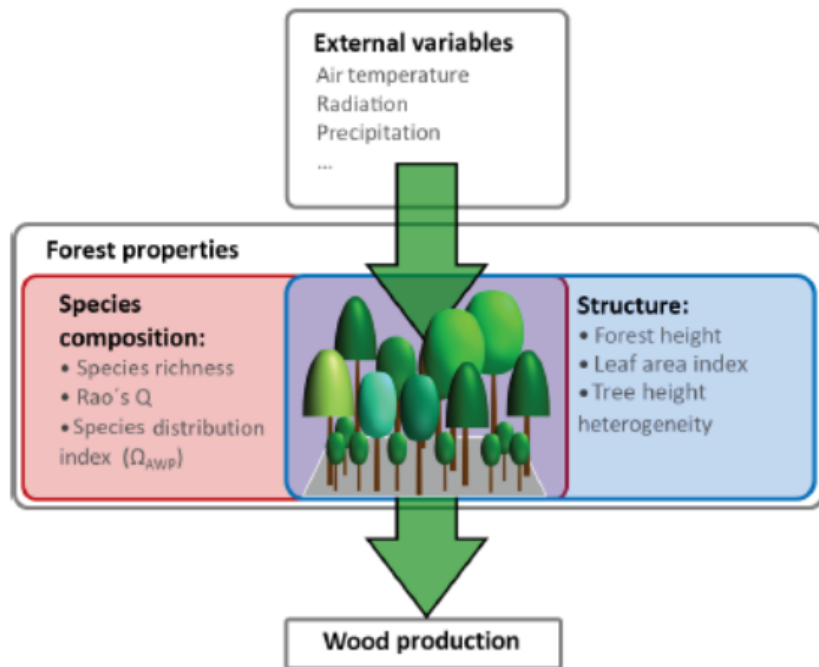


Figure 6.35: Overview of drivers influencing wood production. External variables in this study are temperature, radiation and precipitation. Forest properties are divided into two groups: species composition properties (e.g. Rao's Q as a measure of functional diversity and species distribution index OAWP) and forest structure properties (e.g. forest height, leaf area index and tree height heterogeneity). (Bohn et al. 2018)

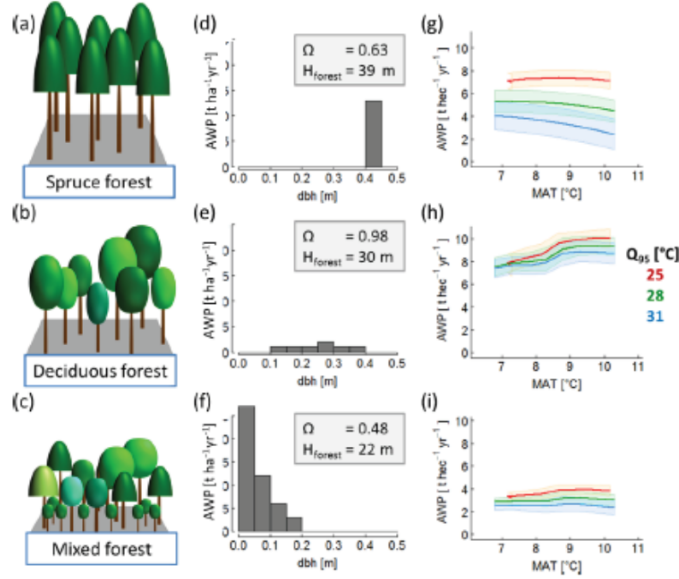


Figure 6.36: Overview of forest properties and resulting temperature sensitivity of AWP of three exemplary forests: (a) old even-aged spruce forest; (b) mature deciduous forest; (c) a quite young mixed species forest. The middle (panels d, e and f) shows the corresponding stem size distributions and provides information on the highest tree in the forest (H_{forest}) and species distribution index OAWP (which quantifies the suitability of a species distributed within the forest structure with regard to AWP). Each forest is treated with 320 climate time series; the last column (panels g, h and i) shows the AWP as a function of mean annual temperature (MAT). The colours indicate different inter-annual temperature amplitudes (Q_{95}) of the used time series. (The coloured bands show the standard deviation due to the variability of the five different time series that exist for each combination of mean annual temperature and intra-annual temperature amplitude.(Bohn et al. 2018).

6.10 Case study 6.2

Levine, N. M., Zhang, K., Longo, M., Baccini, A., Phillips, O. L., Lewis, S. L., ... & Moorcroft, P. R. (2016). Ecosystem heterogeneity determines the ecological resilience of the Amazon to climate change. *Proceedings of the National Academy of Sciences*, 113(3), 793-797.

This study used a demographic model (ED2) to find out whether or not there would still be a dieback of the Amazon forest if demographic processes are included in the model (compared to the dieback simulated by the area-based model in Fig 6.8). To test the effect of demography, they used the ED2 model, and a big leaf version of that model, which has no demographic processes. Figure 6.37 shows some of the results of the study. The left side of the figure shows the result of the model with demography, the right side shows the results of the big leaf model. Different colors indicate different dry season lengths. Subplot A and C show the AGB vs clay fraction. The demographic model shows a smooth relation, while the big leaf model simulated big jumps in the

driest patches. The same results were obtained when AGB was plotted vs plant water stress. In the demographic model, a smooth relationship appears, whereas the big leaf model suddenly drops to zero and predicts a dieback.

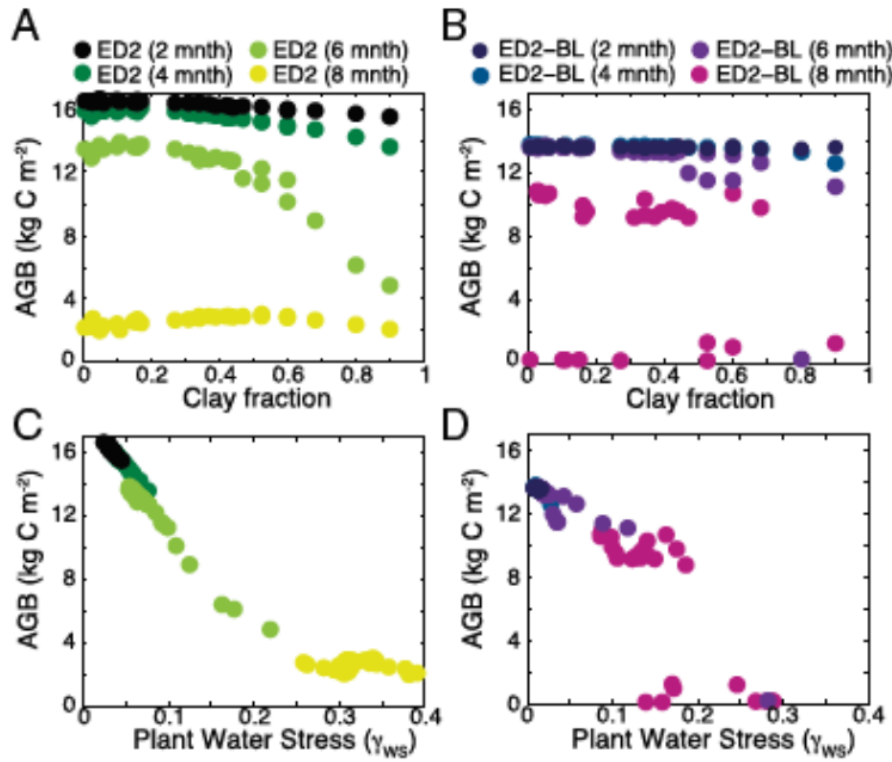


Figure 6.37: Impact of changes in soil clay fraction (A and B) and plant water stress (C and D) on AGB in the ED2 (A and C) and ED2-BL (B and D) model simulations. Four climatological conditions are shown, a 2-month dry season, a 4-month dry season, a 6-month dry season, and an 8-month dry season. (Levine et al. 2016)

The next Figure 6.38 shows the same pattern, in A, the green dots show a gradual decrease of AGB with increasing dry season length, while the purple dots (big leaf model) remain at the same level until a threshold is reached and the system goes to an AGB of zero. The black dots show what is observed via satellites, and correspond more to the green dots.

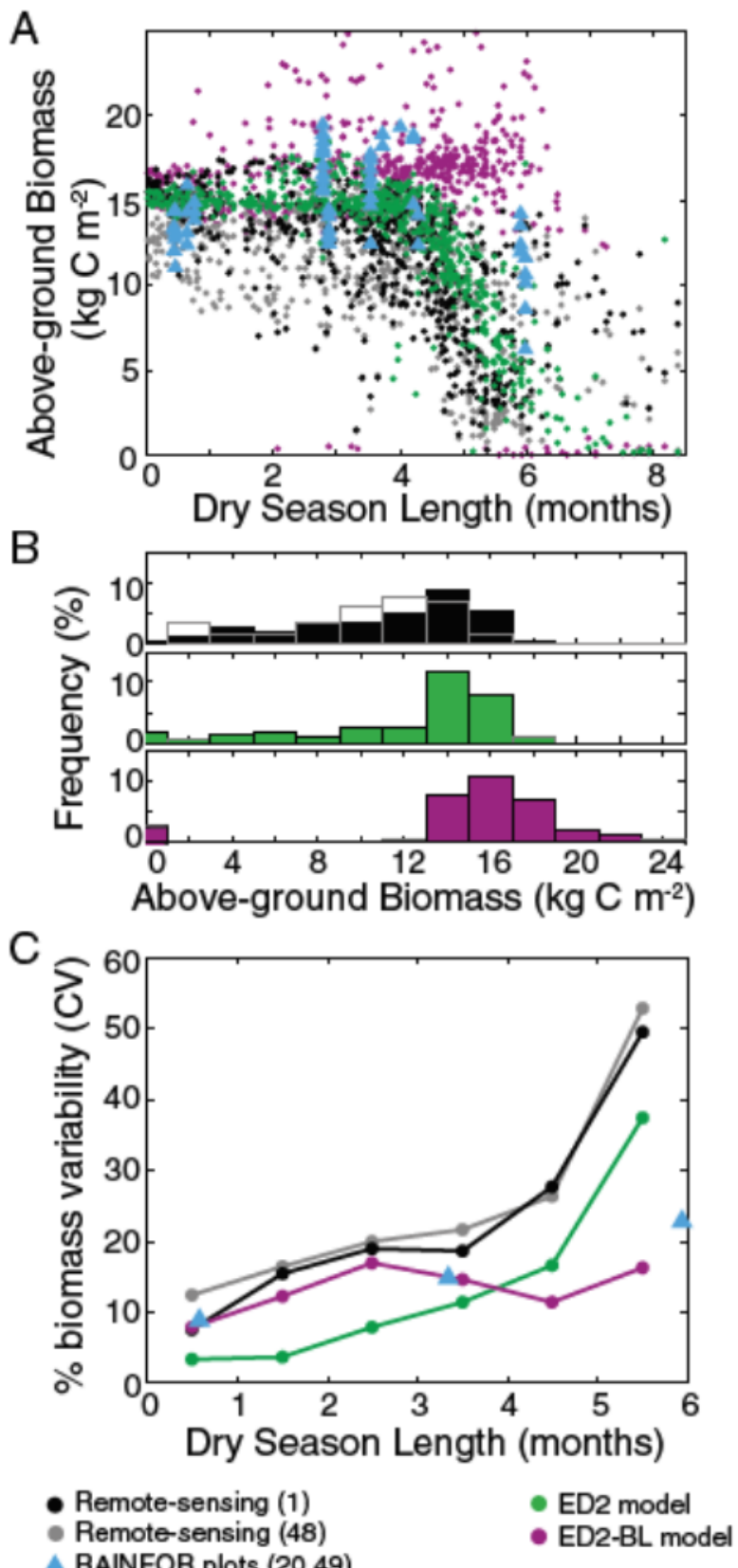


Figure 6.38: (A) Change in AGB with DSL (dry season length) for remote sensing-based estimates (black and gray circles), ground-based plot measurements (blue triangles), ED2 model output (green circles), and ED2-BL model output (purple circles). (B) Distribution of AGB in the observations and the two models. (C) Change in the percentage of biomass variability, with the coefficient of variation (CV) defined as $1 / \text{mean}$. Results are for undisturbed primary vegetation forests. (Levine et al. 2016)

Chapter 7

Representing functional biodiversity in vegetation models

7.1 Introduction

7.2 Functional diversity

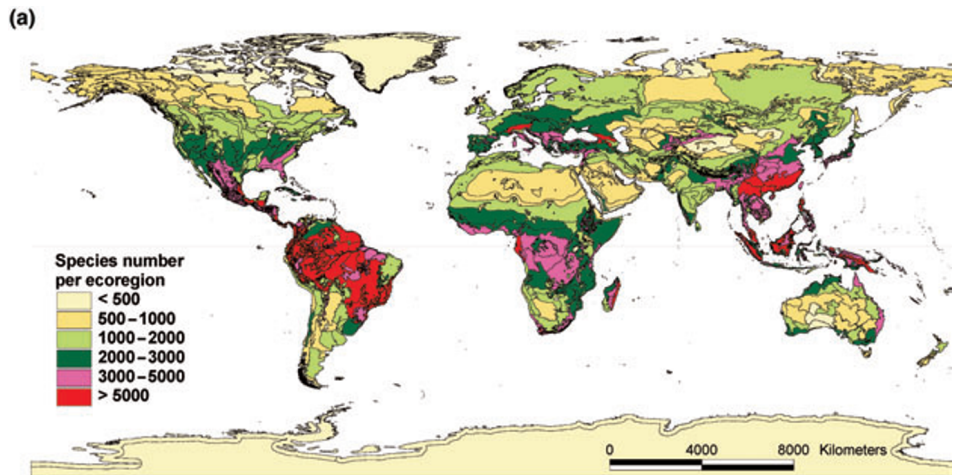


Figure 7.1: Estimated vascular plant species richness per ecoregion (Kier et al. 2005)

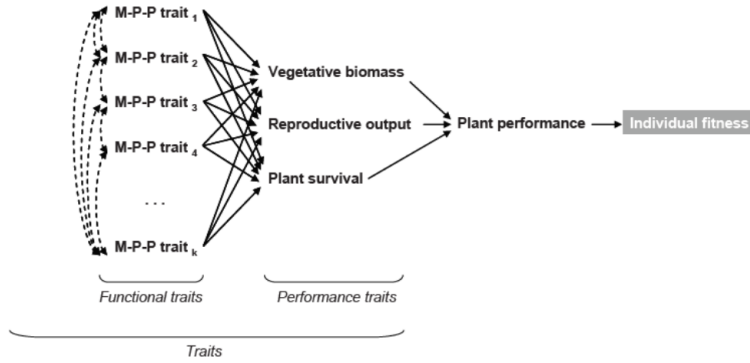


Figure 7.2: Arnold's (1983) framework revisited in a plant ecology perspective. Morphophysiological (M-P-P) traits (from 1 to k) modulate one or all three performance traits (vegetative biomass, reproductive output and plant survival) which determine plant performance and, in fine, its individual fitness. M-P-P traits may be inter-related (dashed double-arrows). For clarity, interrelations among performance traits and feedbacks between performance and M-P-P traits are not represented. (Viole et al. 2007)

Any morphological, physiological or phenological feature measurable at the individual level, from the cell to the whole-organism level, without reference to the environment or any other level of organization. It is functional if it affects fitness indirectly via its effects on growth, reproduction and survival.

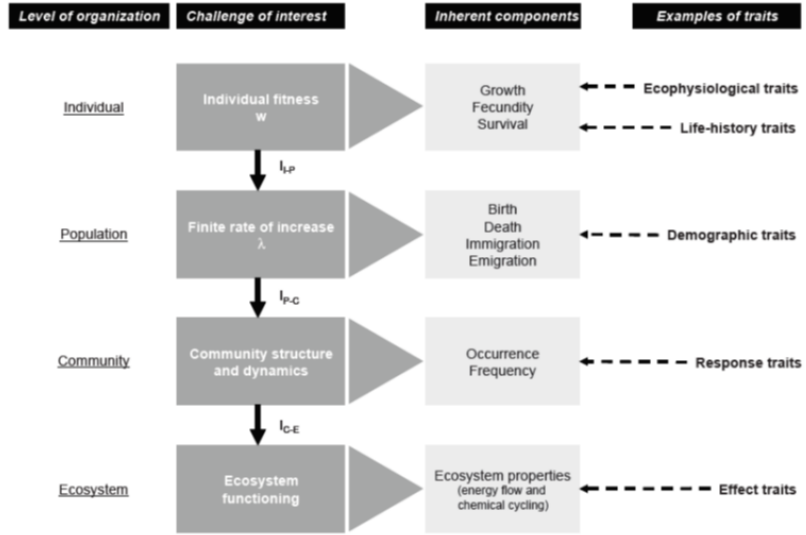


Figure 7.3: Pathways linking the challenge of interest of different organizational levels, through their related inherent components, to some examples of traits found in the literature. Without trait-based information, scaling-up to higher organizational levels needs complex integration information (I). Thus fitness components of an individual determine the components of the finite rate of increase (λ) of the population (I_{i-p}). Occurrence and frequency of species at the community level encompass components of λ through complex integration (e.g. biotic interactions) (I_{p-c}). Finally, scaling-up to ecosystem properties can be done by combining functional property of each species of the community (I_{c-e}). Using traits as proxies of a process at a particular organizational level can sometimes be done without such integration function. For example, at the ecosystem level, ecosystem productivity (one component of ecosystem functioning) shows a strong positive relationship with plant height (an effect trait) (Saugier et al. 2001; Viole et al. 2007)

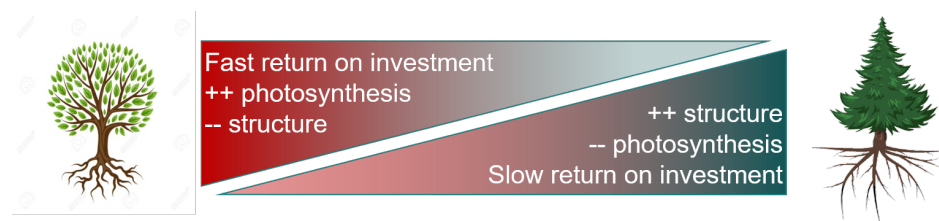


Figure 7.4: Illustration of the leaf economics spectrum.

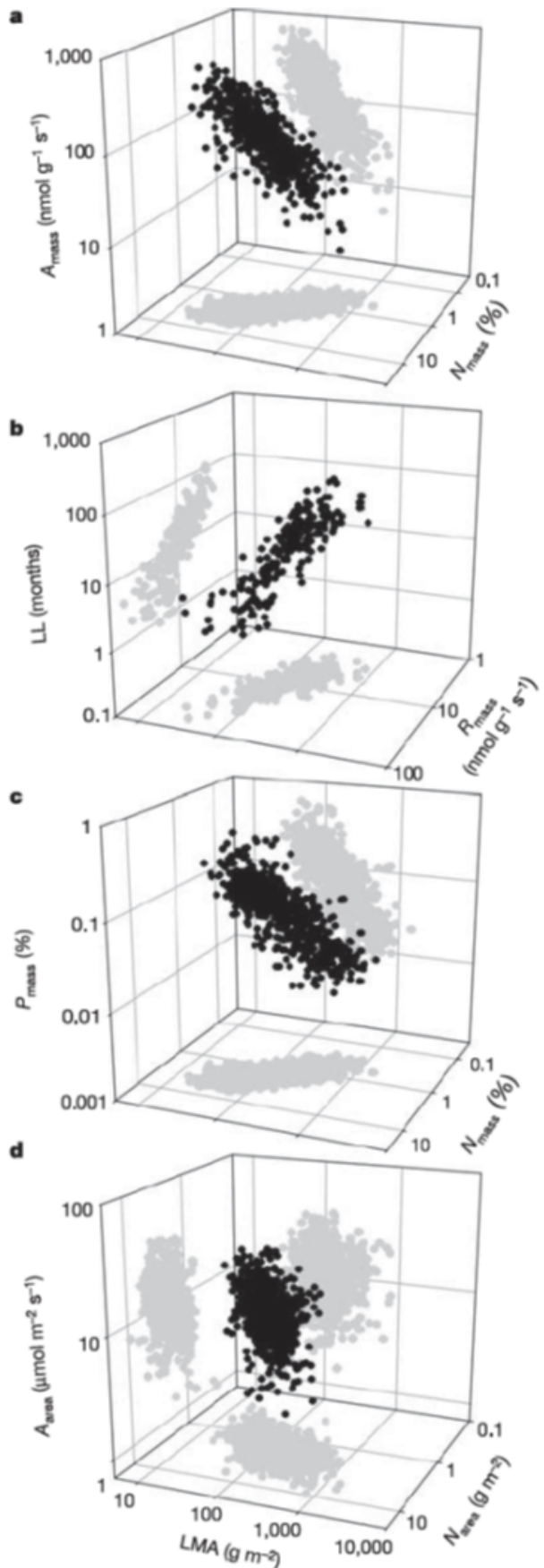


Figure 7.5: The leaf economic spectrum. Three-way trait relationships among six leaf traits with reference to LMA (leaf mass¹⁶⁷ per area), one of the key traits in the leaf economics spectrum. The direction of the data cloud in three-dimensional space can be obtained from the black points in each of the four panels, all of them pointing in roughly the same direction.

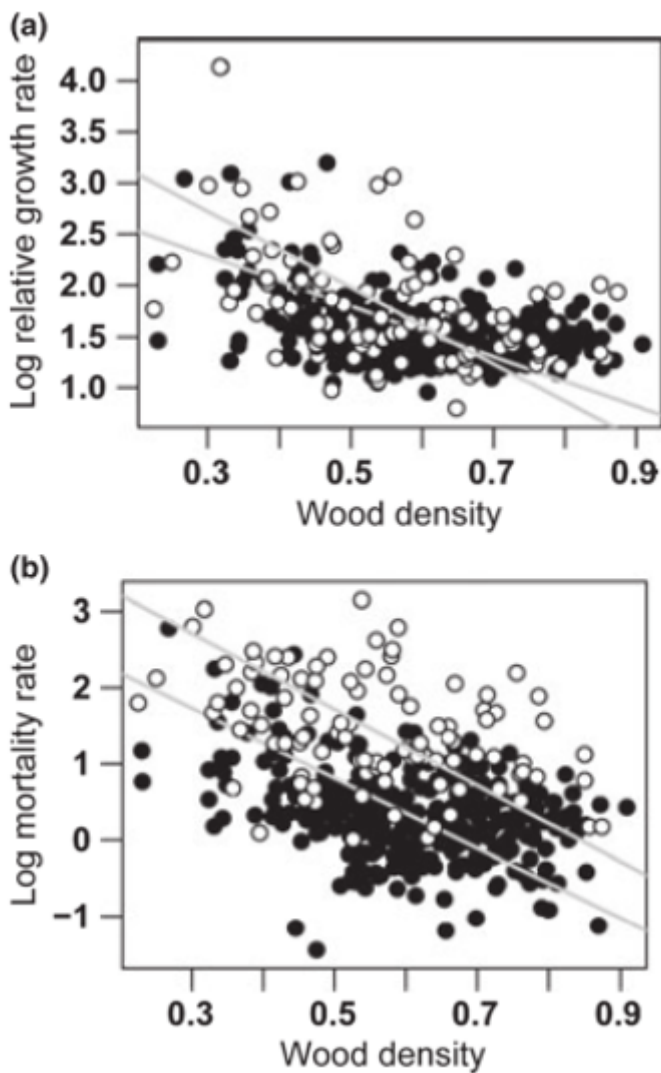


Figure 7.6: Illustration of the wood economics spectrum. Relationship between wood density and relative growth rate (log-transformed, a), and mortality rate (log-transformed, b), for two tropical forest sites (Barro Colorado Island, Panama, white circles, and Pasoh, Malaysia, black circles). All correlations were highly significant ($P < 0.001$), and the correlation coefficients ranged between $r^2 = 0.13$ and 0.19 . Demographic data were collected from saplings 1–5 cm in diameter. (Chave et al. 2009).

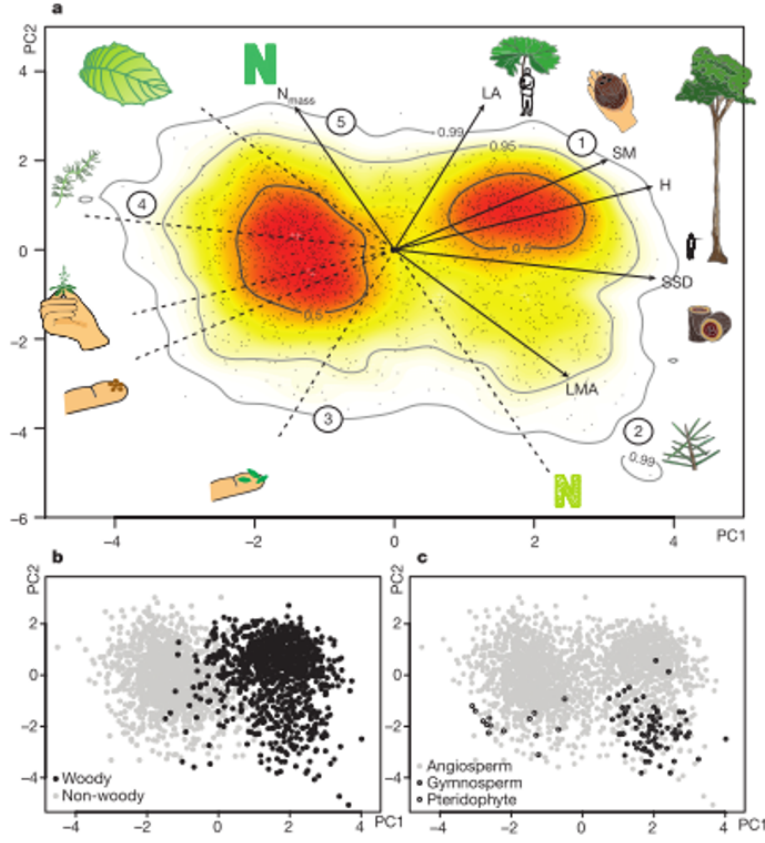


Figure 7.7: The global spectrum of plant form and function. a, Projection of global vascular plant species (dots) on the plane defined by principal component axes (PC) 1 and 2 (based on PCA of gloabl trait data). Solid arrows indicate direction and weighing of vectors representing the six traits considered; icons illustrate low and high extremes of each trait vector. Circled numbers indicate approximate position of extreme poles of whole-plant specialization, illustrated by typical species. The colour gradient indicates regions of highest (red) to lowest (white) occurrence probability of species in the trait space defined by PC1 and PC2, with contour lines indicating 0.5, 0.95 and 0.99 quantiles. Red regions falling within the limits of the 0.50 occurrence probability correspond to the functional hotspots. b, c, location of different growth-forms (b) and major taxa (c) in the global spectrum. (Diaz et al. 2015).

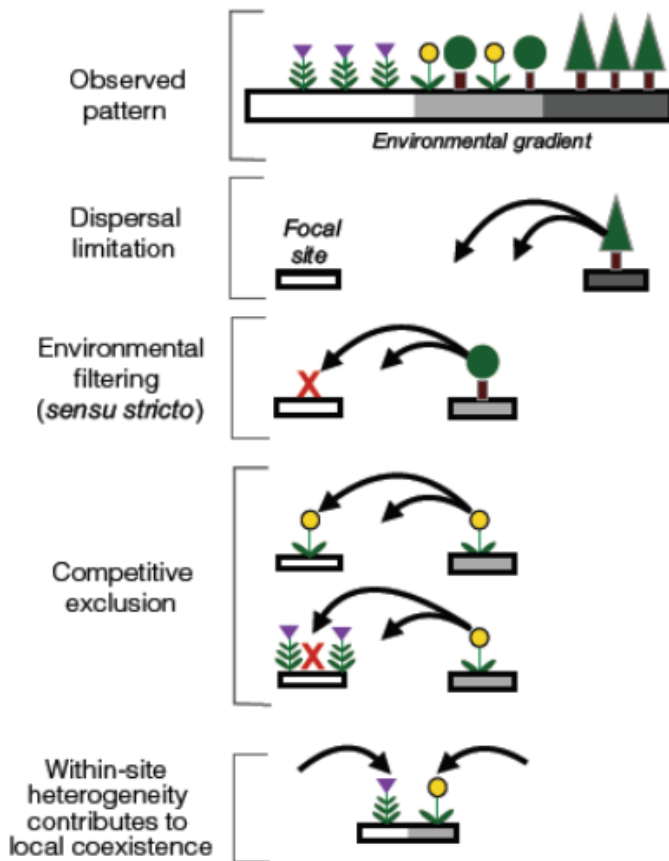


Figure 7.8: Environmental filtering in relation to other community assembly processes in the context of species abundance changes across an environmental gradient. Firstly, a species may be absent from a focal site on the gradient because of dispersal limitation. Next, environmental filtering (*sensu stricto*) occurs when a species arrives at a focal site but fails to establish or persist with neighbours removed. Competitive exclusion occurs when a species arrives and can persist in the absence of neighbours but not in their presence. Finally, at a different focal site, within-site abiotic heterogeneity (not typically defined as environmental filtering) can contribute to the ability of community members to persist locally. Note that in this hypothetical example, the observed pattern of species abundance shifts across the gradient emerges from the combined action of all four processes. (Kraft et al. 2015).

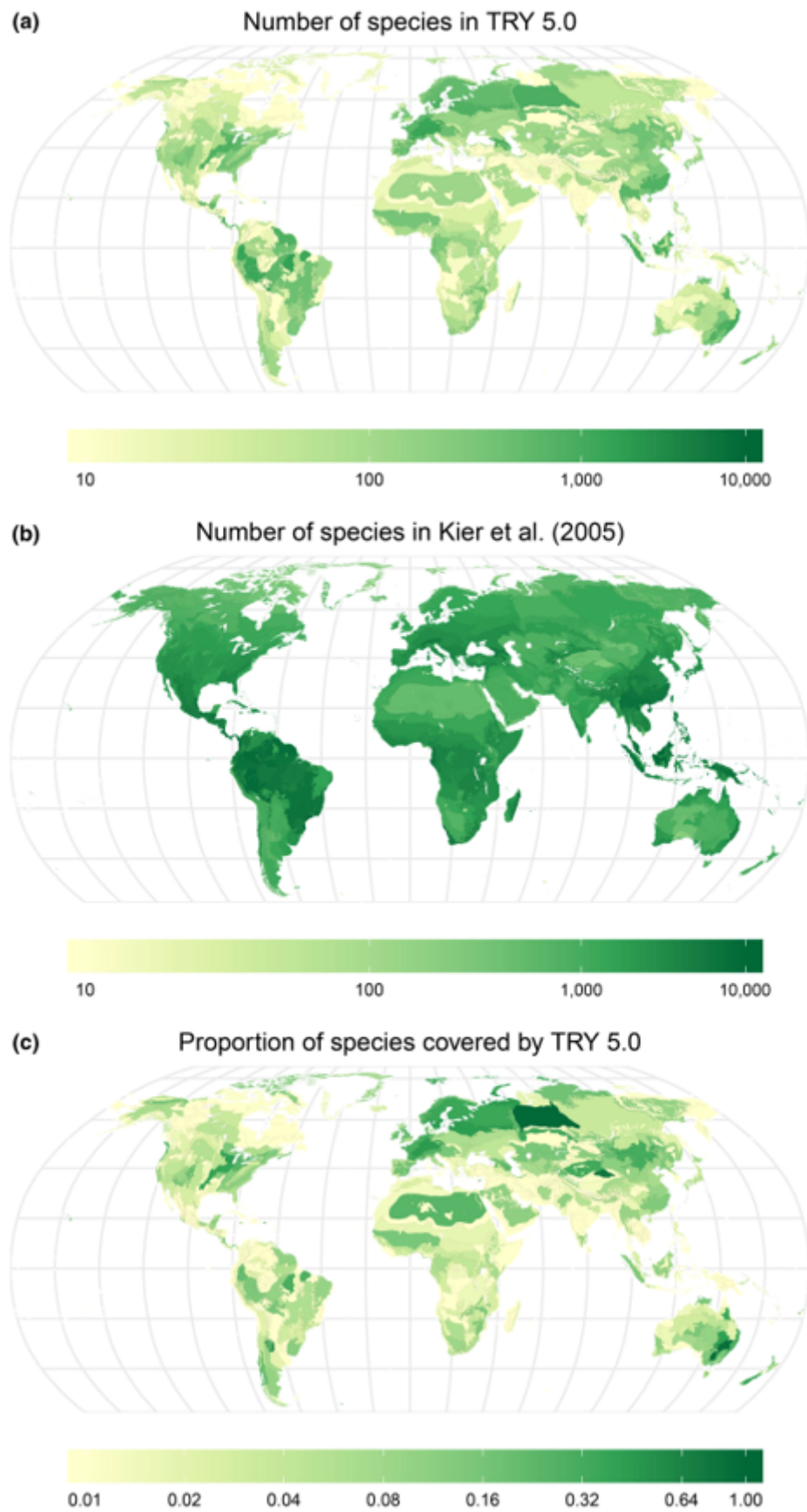


Figure 7.9: Geographic representativeness of the TRY database: (a) the number of species with at least one trait measurement in an ecoregion in TRY version 5; (b) number of species per ecoregion estimated by Kier et al. (2005); (c) fraction of species represented in TRY version 5 versus number of species per ecoregion estimated by Kier et al. (2005). (Kattge et al. 2020)

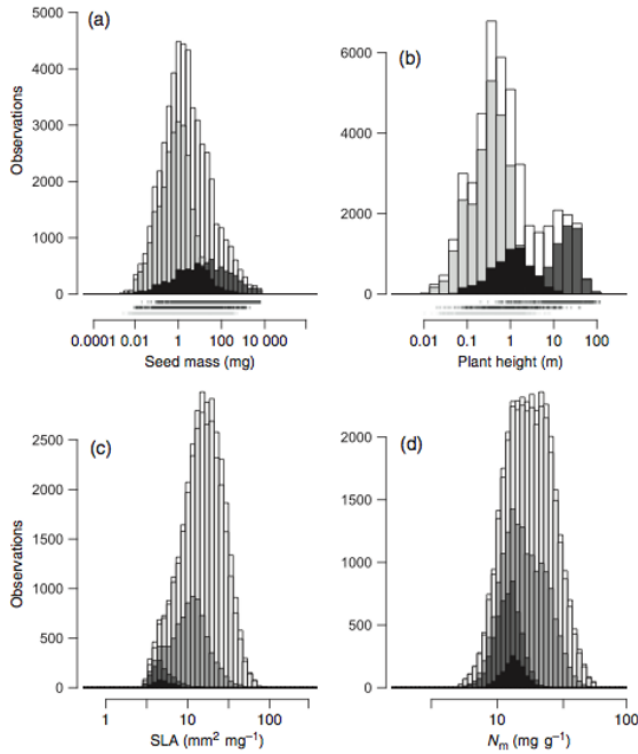


Figure 7.10: Examples of trait frequency distributions for four ecologically relevant traits in the first version of the TRY database. Upper panels: (a) seed mass and (b) plant height for all data and three major plant growth forms (white, all database entries; light grey, herbs/grasses; dark grey, trees; black, shrubs). Rug-plots provide data ranges hidden by overlapping histograms. Lower panels: (c) Specific leaf area (SLA) and (d) leaf nitrogen content per dry mass [Nm, white, all database entries excluding outliers (including experimental conditions); light grey, database entries from natural environment (excluding experimental conditions); medium grey, growth form trees; dark grey, PFT needle-leaved evergreen; black, *Pinus sylvestris*]. (Kattge et al. 2011)

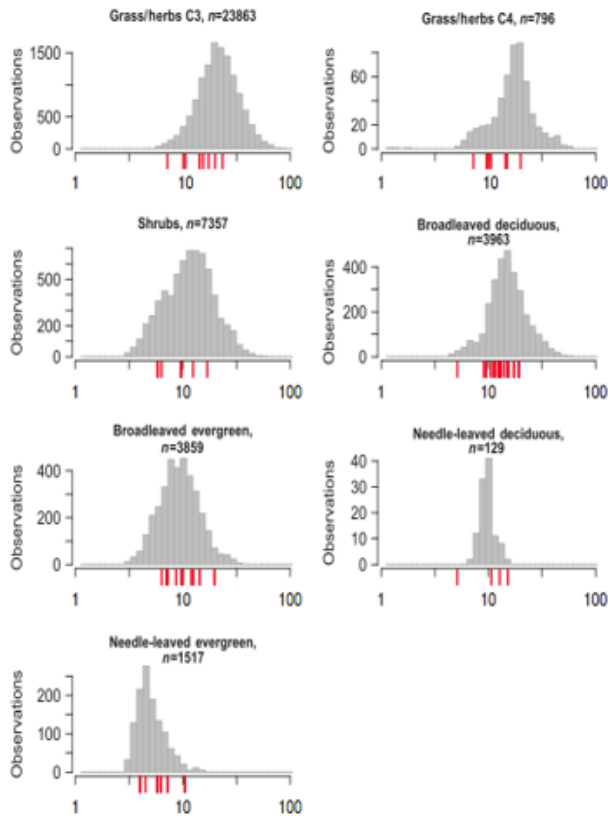


Figure 7.11: Frequency distributions of specific leaf area (SLA, $\text{mm}^2 \text{ mg}^{-1}$) values (grey histograms) compiled in the TRY database and parameter values for SLA (red dashes) published in the context of the following global vegetation models: Frankfurt Biosphere Model (Ludeke et al., 1994; Kohlmaier et al., 1997), SCM (Friend and Cox, 1995), HRBM (Kaduk and Heimann, 1996), IBIS (Foley et al., 1996; Kucharik et al., 2000), Hybrid (Friend et al., 1997), BIOME-BGC (White et al., 2000), ED (Moorcroft et al., 2001), LPJ-GUESS (Smith et al., 2001), LPJ-DGVM (Sitch et al., 2003), LSM (Bonan et al., 2003), SEIB-DGVM (Sato et al., 2007). n, number of SLA data in the TRY database version 1 per PFT.(Kattge et al. 2011)

7.3 Representing 400.000 plant species in a single model: the PFT approach

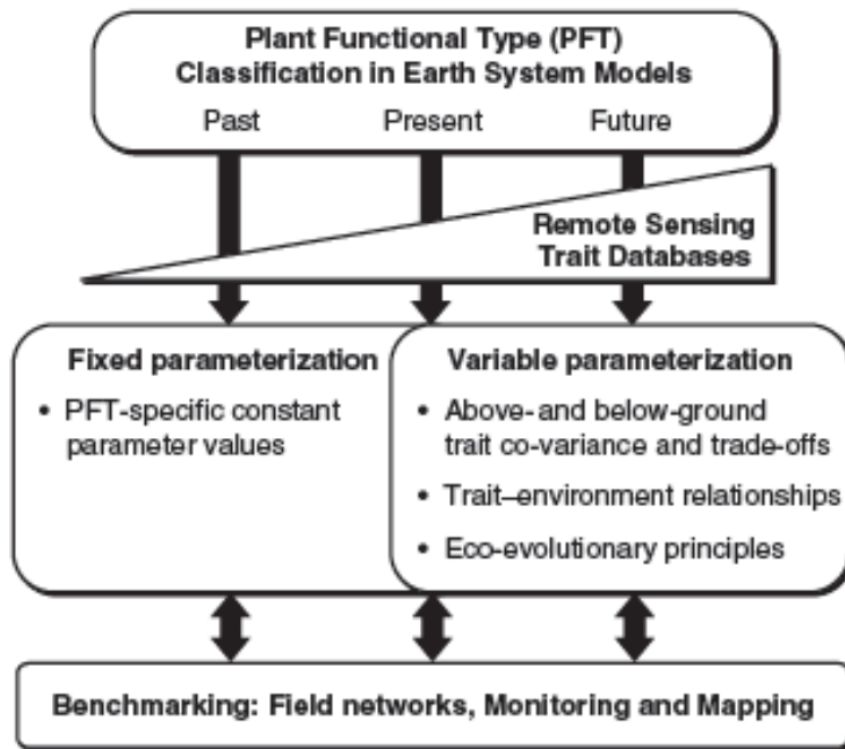


Figure 7.12: A conceptual diagram showing critical aspects of PFT classification, remote sensing, trait databases and methods of PFT parameterization that will be important as DGVMs develop into the future. (Wullschleger et al. 2014)

PFT	T _{c, min} (°C)	T _{c, max} (°C)	GDD _{min} (°C)	T _{w-c, min} (°C)
Tropical broad-leaved evergreen	15.5	-	-	-
Tropical broad-leaved raingreen	15.5	-	-	-
Temperate needle-leaved evergreen	-2.0	22.0	900	-
Temperate broad-leaved evergreen	3.0	18.8	1200	-
Temperate broad-leaved summergreen	-17.0	15.5	1200	-
Boreal needle-leaved evergreen	-32.5	-2.0	600	-
Boreal needle-leaved summergreen	-	-2.0	350	43
Boreal broad-leaved summergreen	-	-2.0	350	-
Temperate herbaceous (TeH)	-	15.5	-	-
Tropical herbaceous (TrH)	15.5	-	-	-

Figure 7.13: PFT bioclimatic limits in the LPJ model. T_{cmin}: minimum coldest temperature for survival; T_{cmax}: maximum coldest-month temperature for establishment; GDD_{min}: minimum degree-day sum (5°C base) for establishment; T_{w-cmin}: minimum warmest minus coldest month temperature range. (Sitch et al. 2003)

PFT	W/H*	z_1	z_2	g_{\min}	r_{fire}	a_{leaf}	f_{leaf}	f_{sapwood}	f_{root}	$T_{\text{mort,min}}$	S_{GDD}
Tropical broad-leaved evergreen (TrBE)	W	0.85	0.15	0.5	0.12	2.0	0.5	0.05	0.5	-	-
Tropical broad-leaved raingreen (TrBR)	W	0.70	0.30	0.5	0.50	0.5	1.0	0.05	1.0	-	-
Temperate needle-leaved evergreen (TeNE)	W	0.70	0.30	0.3	0.12	2.0	0.5	0.05	0.5	-	-
Temperate broad-leaved evergreen (TeBE)	W	0.70	0.30	0.5	0.50	1.0	1.0	0.05	1.0	-	-
Temperate broad-leaved summergreen (TeBS)	W	0.80	0.20	0.5	0.12	0.5	1.0	0.05	1.0	-	200
Boreal needle-leaved evergreen (BoNE)	W	0.90	0.10	0.3	0.12	2.0	0.5	0.05	0.5	23	-
Boreal needle-leaved summergreen (BoNS)	W	0.90	0.10	0.5	0.12	0.5	1.0	0.05	1.0	23	100
Boreal broad-leaved summergreen (BoBS)	W	0.90	0.10	0.3	0.12	0.5	1.0	0.05	1.0	23	200
Temperate herbaceous (TeH)	H	0.90	0.10	0.5	1.00	1.0	1.0	-	0.5	-	100
Tropical herbaceous (TrH)	H	0.90	0.10	0.5	1.00	1.0	1.0	-	0.5	-	100

*W=Woody; H=Herbaceous.

Figure 7.14: PFT parameter values in the original LPJ model. z_1 and z_2 are the fraction of fine roots in the upper and lower soil layers, respectively; g_{\min} is the minimum canopy conductance; r_{fire} is the fire resistance; a_{leaf} is the leaf longevity; f_{leaf} , f_{sapwood} , f_{root} are the leaf, sapwood and fine root turnover times, respectively; $T_{\text{mort,min}}$ is the temperature base in the heat damage mortality function and S_{GDD} is the growing degree day requirement to grow full leaf coverage? (Sitch et al. 2003)

Plant Functional Types	Species
Early successional hardwood	<i>Betula Papyrifera</i> , <i>Betula Populifolia</i> , <i>Betula Lenta</i> , <i>Prunus spp.</i>
Midsuccessional hardwood	<i>Quercus rubra</i> , <i>Quercus velutina</i> , <i>Acer rubrum</i> , <i>Fraxinus Americana</i> , <i>Sorbus microcarpa Pursh.</i>
Late successional hardwood	<i>Acer saccharum</i> , <i>Fagus spp.</i> , <i>Betula alleghaniensis</i>
Northern pine	<i>Pinus resinosa</i> , <i>Pinus strobus</i>
Late successional conifer	<i>Thuja occidentalis</i> , <i>Picea rubens</i> , <i>Picea glauca</i> , <i>Tsuga canadensis</i> , <i>Abies balsamea</i>

Figure 7.15: Summary of PFTs in the ED2 model for temperate forest. (Medvigy et al. 2009)

Property	Early Successional Hardwoods	Midsuccessional Hardwoods	Late Successional Hardwoods	Northern Pines	Late Successional Conifers	C ₃ Grasses and Forbs
Leaf habit	CD	CD	CD	E	E	DD
SLA (m ² (kg C) ⁻¹)	40 (30)	30 (24)	60	6	10	22
Density independent mortality rate (a ⁻¹)	0.006	0.004	0.004	0.003	0.001	0.07
Global dispersal (fraction)	1	0.33	0.07	0.77	0.001	1
V_{m0} (μmol m ⁻² s ⁻¹)	18.3 (20.1)	15.6 (17.2)	6.3 (6.9)	15.6 (11.4)	6.3 (4.6)	18.3
I_1 (kg C)	0.0047 (0.013)	0.024 (0.048)	0.017	0.024	0.045	0.08
I_2	2.25 (1.75)	1.86 (1.46)	1.73	1.9	1.68	1.0
h_1 (m)	22.68	25.2	23.4	27.1	22.8	0.48
h_2 (cm ⁻¹)	-0.065	-0.05	-0.054	-0.039	-0.044	-0.75
s_1 (kg C)	0.026	0.16	0.23	0.15	0.16	1 × 10 ⁻⁵
s_2	2.96	2.46	2.25	2.24	2.15	1

*The initial and optimized model used the same values except for the parameters SLA, V_{m0} , I_1 and I_2 ; for these, optimized model values are in parentheses. The leaf habits include CD, cold deciduous; DD, drought deciduous; E, evergreen.

Figure 7.16: Eco-Physiological, Life-History, and Allometric Parameters for the Plant Functional Types in the ED2 model for temperate forest. (Medvigy et al. 2009)

7.4 Limitations of the PFT concept

7.5 Alternative approaches to account for trait variability

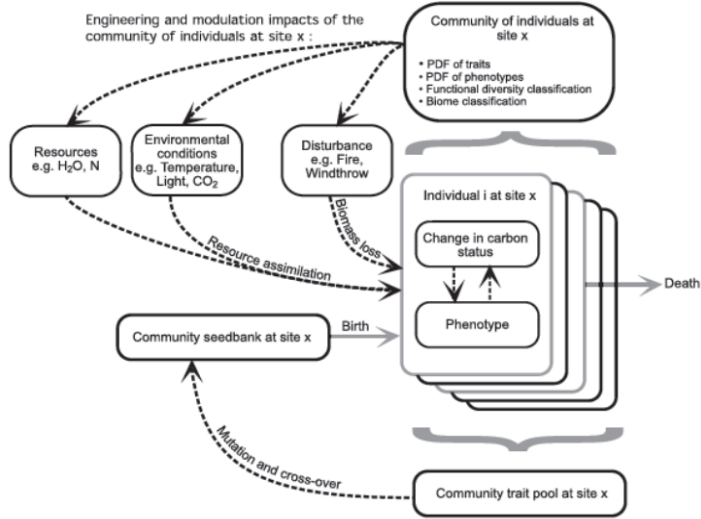


Figure 7.17: Conceptual modelling framework for a next-generation dynamic global vegetation model (DGVM). Individuals are characterized by their traits that influence their carbon (C) status and phenotype. All individuals at a site form the community, which influences resources, environmental conditions and disturbances via engineering and modulating impacts. These conditions interact to influence growth of the individuals. Individuals, through reproduction, can add their traits to the community trait pool. Crossover and mutation of the community trait pool yield the community seed bank. PDF, probability density function. (Sheiter et al. 2013)

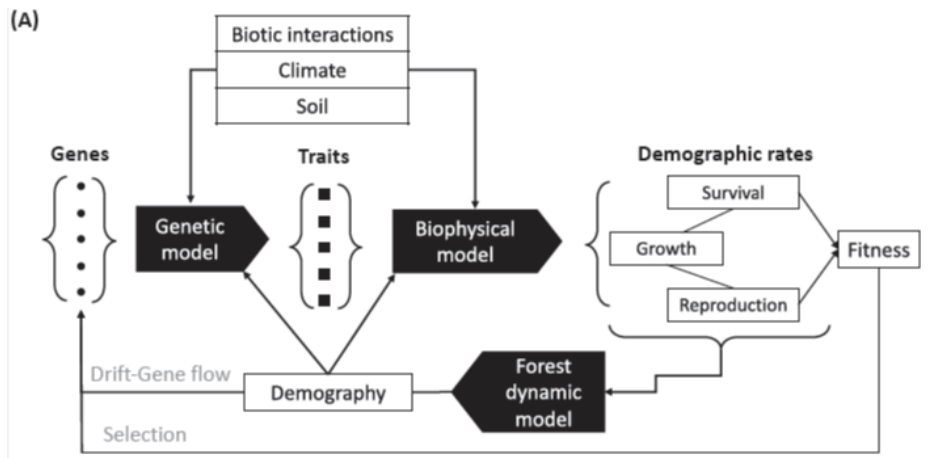


Figure 7.18: Physio–demo–genetic (PDG) models integrate physiological, demographic, and evolutionary processes. They have been developed to better understand the interplay among plasticity and genetic adaptation and the effects of both processes on tree population dynamics under global change. The advantage of PDG models is their ability to account for the variability in functional traits due to both standing genetic variation and evolutionary change in response to changing local environmental conditions. This figure shows the conceptual framework of PDGmodels. PDGmodels couple: (i) a biophysical module to simulate carbon and water fluxes at the tree level using climate observations; (ii) a forest dynamics module to calculate demographic rates for adult trees (growth, mortality, and reproduction) based on carbohydrate reserves, and to simulate ecological processes across the life cycle; and, (iii) a quantitative genetics module relating genotype to the phenotype of one or more functional traits. (Berzaghi et al. 2019)

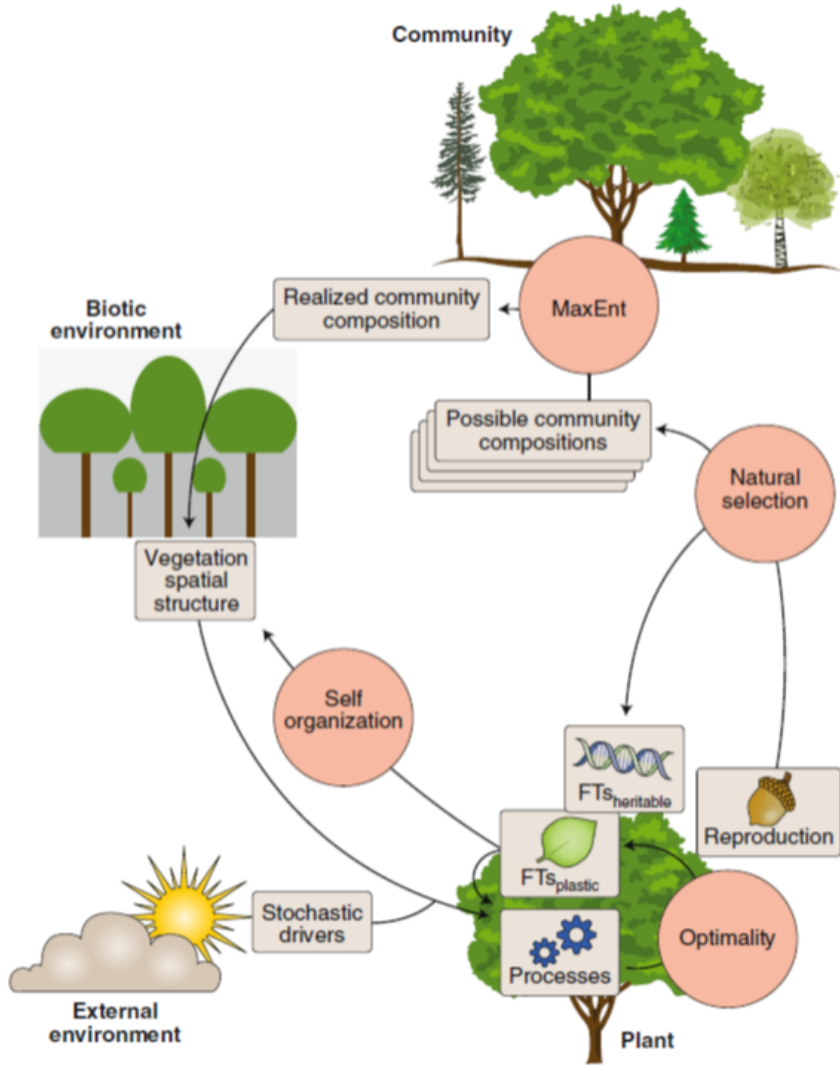


Figure 7.19: Framework for the use of organizing principles in vegetation modelling. The application of organizing principles (circles) helps predict (arrows) vegetation properties (boxes). Natural selection drives the evolution of species (or plant types) and their heritable functional traits, modelled as emergent evolutionary stable strategies. Natural selection is also the reason that phenotypic plasticity in response to environmental variation is predictable through fitness-proxy maximization (optimality). At the community level, collective self-organization among many plants results in predictable patterns of spatial structure at the stand level (for example, due to plasticity of stem angles in the perfect plasticity approximation). Self-organization influences the biotic environment, which, together with the abiotic (external) environment, feeds back on plant reproduction and survival—that is, the natural selection of community composition. Many different community compositions may be possible, and the most likely can be predicted by MaxEnt. The external environment includes abiotic factors and all other external drivers, including disturbance regimes. (Franklin et al. 2020)

7.6 Case study 7.1

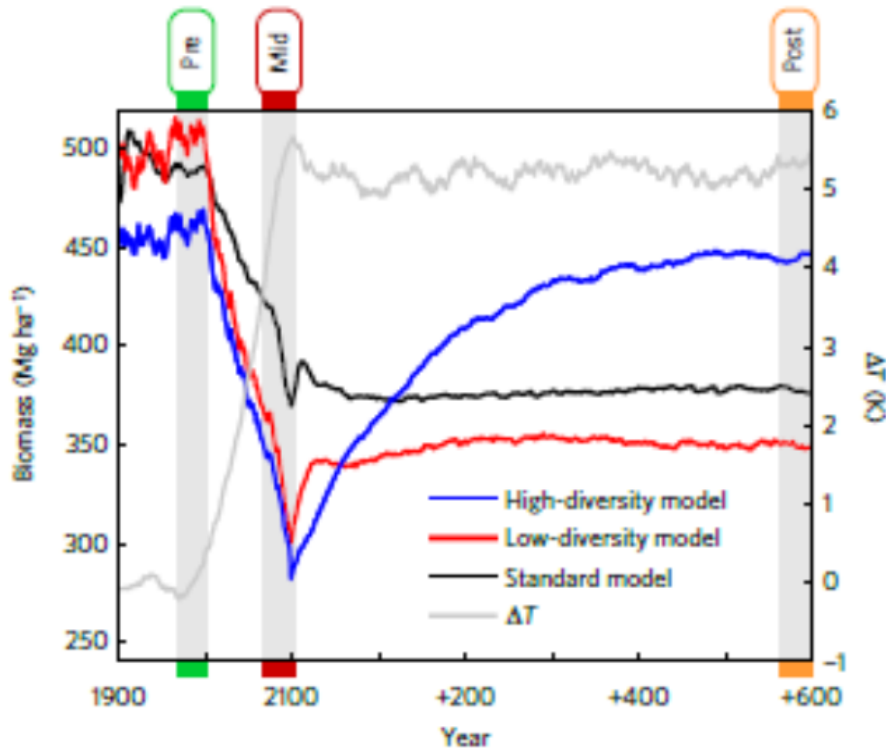


Figure 7.20: Simulated rainforest biomass under climate change and different plant trait diversity. Annual biomass over 800 simulation years for 400 ha of Ecuadorian rainforest (longitude: 77.75 W; latitude: 1.25 S) from three different versions of the vegetation model LPJmL under a severe climate change scenario (RCP 8.5 HadGEM2). ΔT : annual temperature difference to the mean temperature of pre-impact time (1971–2000) in K. (Sakschewski et al. 2016)

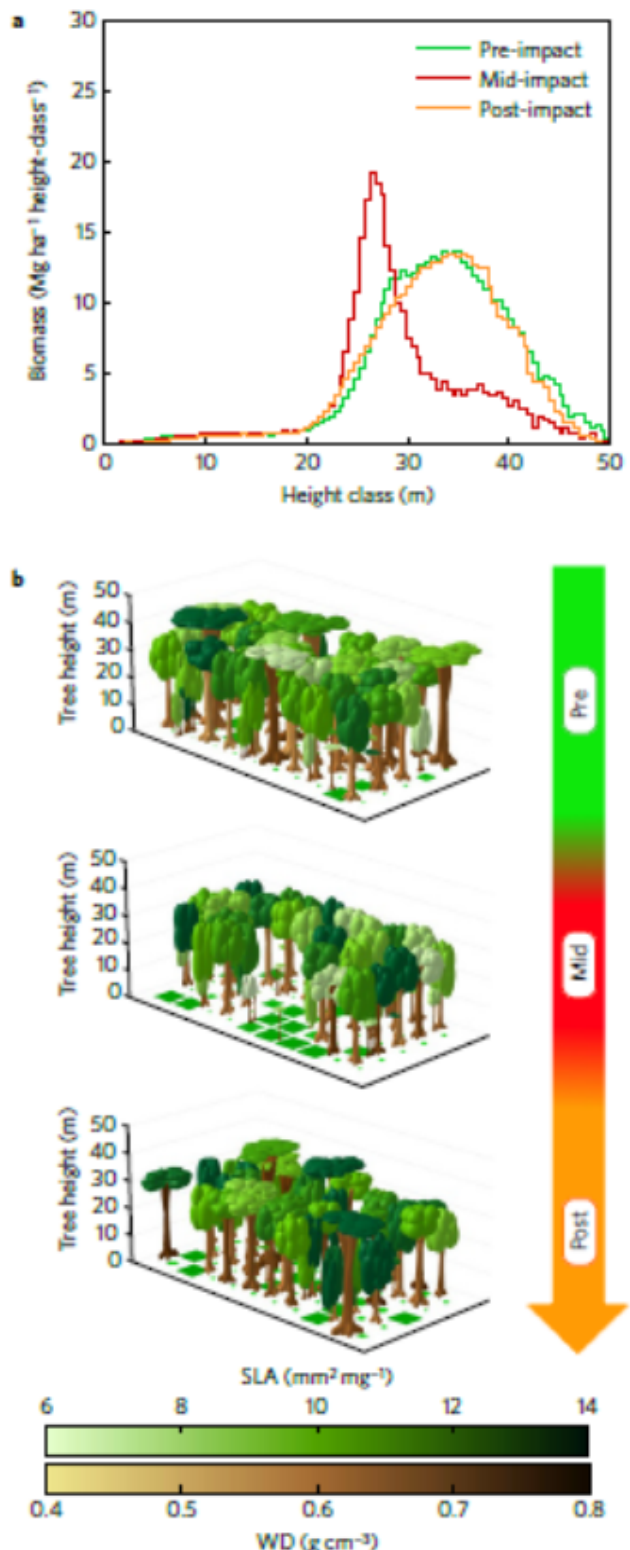


Figure 7.21: Forest height structure recovers with biomass. a, Mean biomass contribution of tree height classes for pre-, mid- and post-impact time. b, Visualization of model output showing 0.5 ha of the 400 ha of Ecuadorian rainforest in a selected year during pre-, mid-, and post-impact time, respectively (top to bottom). Different crown (stem) colours denote different SLA (WD) values of individual trees. Crown size, stem diameter and tree height are scaled by model output. Green squares indicate tree gaps covered by herbaceous plants. (Sakschewski et al. 2016)

7.7 Case study 7.2

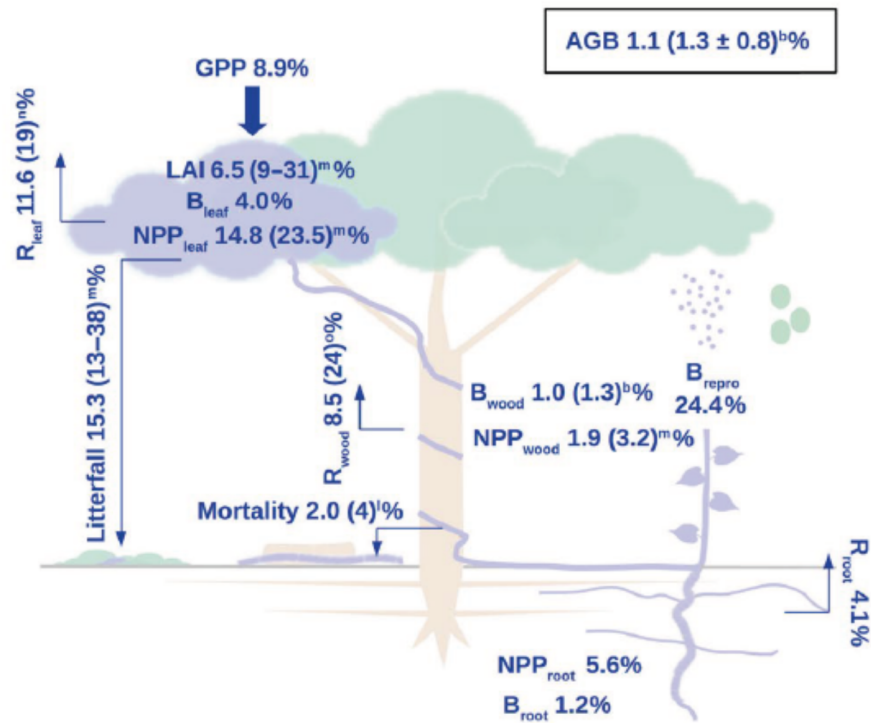


Figure 7.22: Simulated liana contributions to forest carbon pools and fluxes for the Paracou site in French Guiana, with observed liana contributions in parentheses. B, biomass; GPP, gross primary productivity; NEE, net ecosystem exchange (negative values mean carbon uptake); NPP, net primary productivity; R, respiration. (di Porcia et al. 2019)

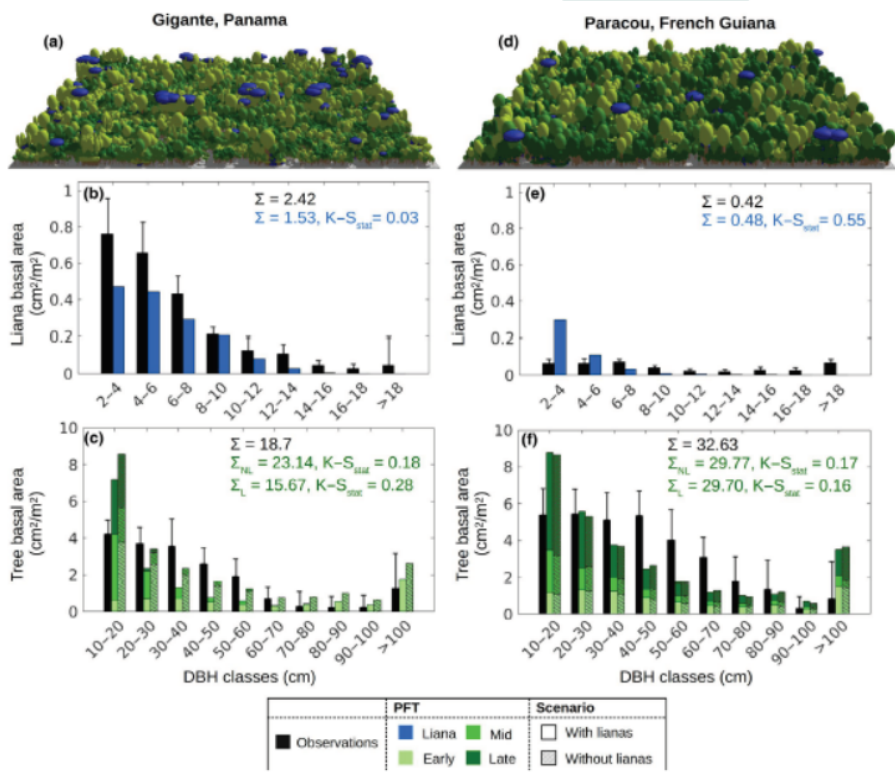


Figure 7.23: Forest demographic composition for two simulated sites: young forest in Gigante, Panama (a–b–c), and old growth forest in Paracou, French Guiana (d–e–f). Panels (a) and (d) show a representative area of modeled forest of 1 ha. To visualize the forest composition, the forest is decomposed into patches according to their simulated relative area, and the three cohort densities and sizes are preserved (as well as the liana tree tracking). Panels (b–c) and (e–f) compare the basal area distributions of liana and tree PFTs, respectively, as observed locally (black) or simulated according by ED2 (shades of blue and green). Tree basal area values (panels c and f) are compared for the simulations with (solid bars) or without (hatched bars) lianas. Σ represents the total basal area according to the model (blue or green) and field observations (black). Error bars represent the standard deviation of the different plot measurements (smaller error bars correspond to more homogeneous plots). The $K-S_{\text{stat}}$ is the test statistic of the two-sample Kolmogorov–Smirnov test between the observed and simulated size distributions (with a sampling size of 250 for each distribution). Liana basal area in Gigante was the only case in which the observed and simulated distribution did not significantly differ. (di Porcia et al. 2019)

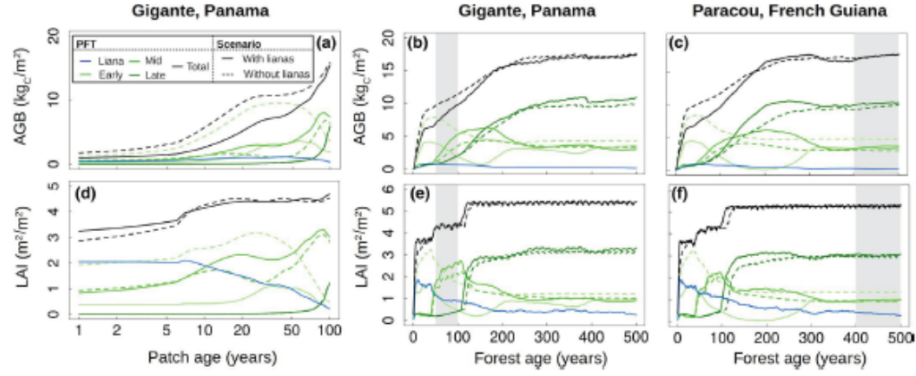


Figure 7.24: Comparison of simulations of forest succession with (solid lines) and without (dashed lines) lianas. The upper graphs (a–c–e) show the aboveground biomass (AGB), while the bottom graphs (b–d–f) represent LAI as a function of time for one patch (a–d) and for the forest aggregate (b–c–e–f). The gray zones represent the period during which the model outputs were averaged for all other plots (corresponding to the approximate stand age of the forest sites). The increases in LAI are caused by the crossing of the reproductive thresholds for the different plant functional types (PFTs). (di Porcia et al. 2019)

Paracou, French Guiana

R_{total}	-0.5%	-4.2%
R_{auto}	-0.1%	-2.3%
R_{hetero}	-1.0%	-6.2%

Gigante, Panama

NPP_{total}	-0.4%	-2.6%
NPP_{AG}	+1.5%	+3.3%
NPP_{BG}	-4.7%	-15.5%

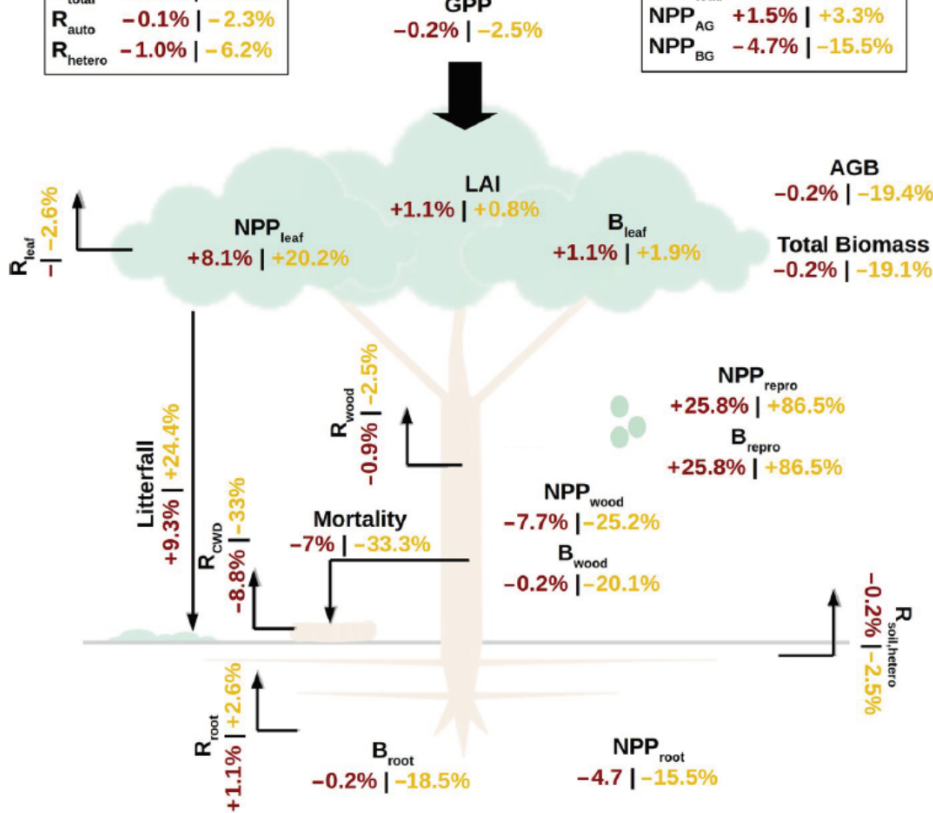


Figure 7.25: Relative changes in carbon pools and fluxes for Paracou, French Guiana (brown), and Gigante, Panama (yellow), upon inclusion of the liana plant functional type in the simulations (by comparing a simulation with and without the liana PFT). B, biomass; GPP, gross primary productivity; NPP, net primary productivity; R, respiration. (di Porcia et al. 2019)

Part III

Upscaling and applications

Chapter 8

Spatial heterogeneity, landscape scale and disturbance

8.1 Introduction: landscape scale

In this chapter we discuss how vegetation models can deal with spatial heterogeneity at the landscape scale and how disturbance can be accounted for. These elements are key when applying vegetation models to **large spatial and temporal scales**. We first define a few important landscape ecology terms that are relevant to have in mind when applying vegetation models at the landscape scale.

Landscape ecology studies the spatial patterns and the impact of ecological processes on spatial patterns and vice-versa. Landscape ecologists try to understand the causes and consequences of **spatial heterogeneity** across spatial scales. For such processes, it is important to consider the **role of humans** changing/disturbing the landscape patterns (deforestation, land conversion). Spatial heterogeneity in the landscape depends on the abiotic factors (e.g. soil, topography, climate, etc...) and biotic heterogeneity (land cover, land use, natural disturbances), and anthropogenic disturbances. In many ecosystems (natural) disturbance helps to maintain the heterogeneity of the landscape and habitats. The **scale and resolution** are very important aspects of landscape ecology and landscape scale modelling (Fig. 8.1). Heterogeneity is present at every scale. Scale and resolution need to be carefully defined based on the research questions, the objective and the available data.

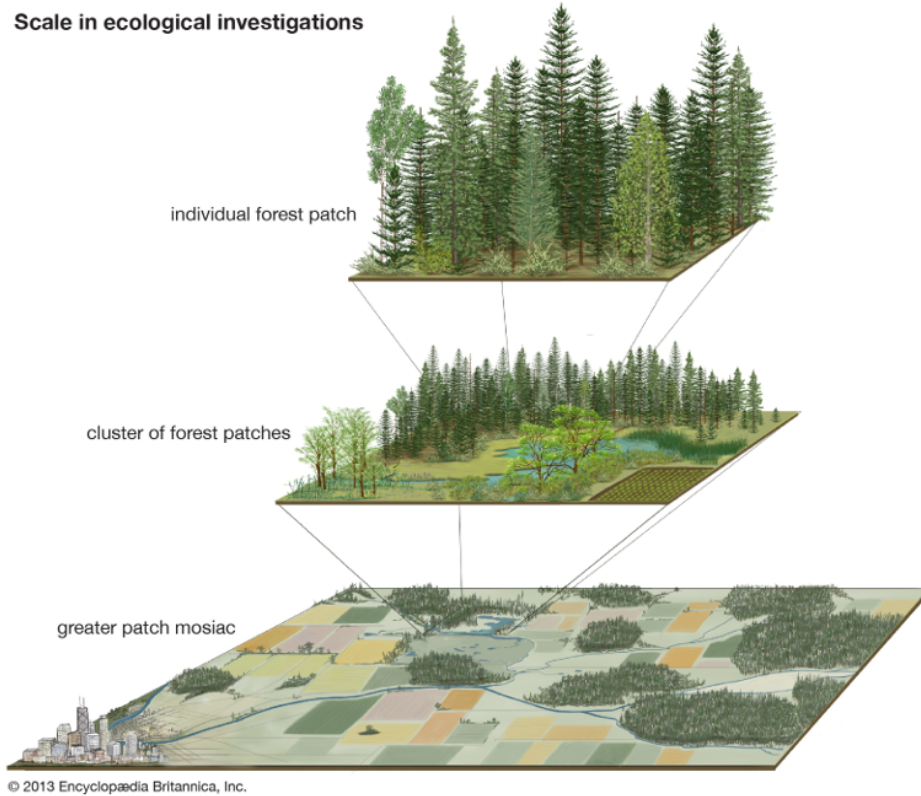


Figure 8.1: Illustration of the importance of scale in landscape ecology.

In vegetation models, we typically divide the landscape in homogeneous patches. Models can then be used to analyze the **patch dynamics** (Fig. 8.2). In other words, we need to study the changes of landscape in terms of interacting patches, models are used to analyze:

- Spatial patterns, e.g. to study the distribution of PFTs or biomass over the patches in the landscape.
- Changes within and between patches.
- Interaction between patches (however, neglected by many vegetation models); there are many processes of interaction (e.g. via fires, seed dispersal, ...)
- Metapopulations (populations of a species or PFT spread over multiple patches) and the related processes of migration, extinction or colonization of species.
- Fragmentation, edge effects, and connectivity (these aspects are important and depend on our objective of research). If we model the carbon stock is important to consider these aspects (fragmentation). For conservation studies these elements are key (see course ‘natuurbehoud’).

Most (global) vegetation models consider patch dynamics in a very aggregated way and are not spatially explicit. However, a few specific models focus on landscape dynamics explicitly. For example the PICUS model. This model is spatially explicit and it is very useful for landscape scale applications but is more difficult to apply on very large scale because it needs detailed spatial input data on soil and land cover.

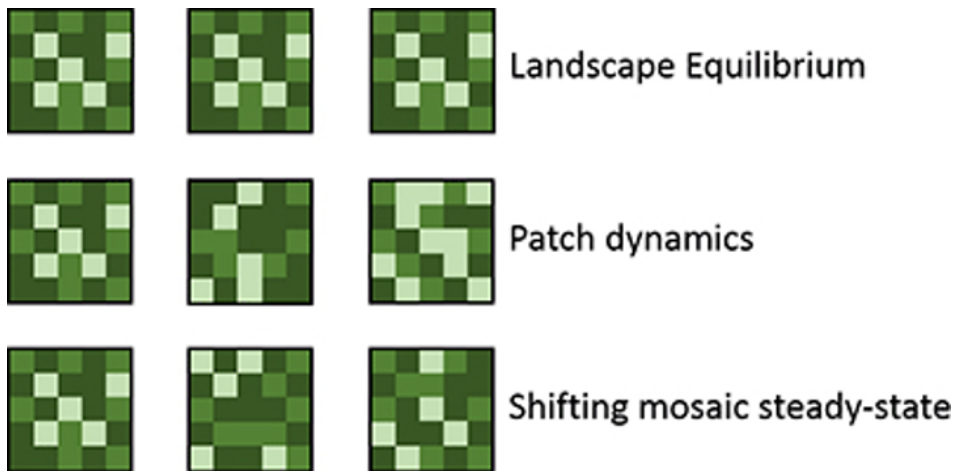


Figure 8.2: Illustration of 3 situations in landscape dynamics represented by patches on 3 time steps: a landscape in equilibrium, a landscape with patch dynamics, an averaged landscape in steady-state but with dynamics in individual patches.

8.2 Land use change

Land use change is a very important factor for vegetation modelling at large spatial scales. In most vegetation models land use change is accounted for, by using land use maps as input. The model user has the choice to simulate a static landscape based on a single land use/cover map or to have dynamic maps as model input (e.g. a land use/cover map that is updated every simulation year). Specific models exist to simulate historical or future land use change scenarios.

There are two general categories of land-use change. They need to be accounted for in a different way in vegetation models. The first category is **extensification**, which is the expansion of land area used by people. Within this category there are two sub-categories: (1) **Land-use conversion**, which is the change in dominant plant functional type (PFT) (e.g. forest is converted into grassland); (2) land-use modification, which is a significant change in human impact without change in PFT (e.g. introducing cattle grazing in a savanna). The second land use change category is **intensification**, which is the increase of inputs (subsidies) per unit area (e.g. intensifying the grazing of the savanna).

Large scale vegetation models are particularly suited to study the impact of land use change on various ecosystem and land surface processes. For example, in the study of Akkermans et al. 2014 (see lecture slides) a deforestation scenario for the Congo Basin was analyzed for its impact on biophysical fluxes and biogeochemistry. In this study a land surface model (CLM) was coupled to a regional climate model (COSMO), allowing to study the feedback of deforestation in the Congo Basin on the regional climate. A second example is the study of Guimberteau et al. (2017) where 3 vegetation models were used to evaluate various land use change scenarios in the Amazon basin. The 3 vegetation models had a river routing component to evaluate the impact of land use change on hydrology and river discharge. It illustrates that deforestation scenarios reduced the evapotranspiration in multiple regions in the Amazon resulting

in a significant change in the Amazon river discharge rate and seasonality (especially the impact on the discharge peaks can result in important flooding). This example illustrates the power of vegetation models to use for land and river management.

8.3 Disturbance

Natural or anthropogenic disturbance can have very large impact on ecosystem functioning and should be accounted for when applying vegetation models at large spatial scales. Disturbances can be gradual (e.g. climate change) but are very often event-based and have a stochastic nature. There are different types of disturbances: wind, fire, management, drought, herbivory, ... and each of them has different characteristics and processes through which they impact ecosystem functioning. When modelling disturbance impacts it is important to consider the properties of the disturbance :

- Intensity (e.g. how intense is the forest fire, how intense is the thinning)
- Severity (e.g. how much biomass was affected)
- Frequency (e.g. how many fires per year in a region)
- Size (e.g. fraction of the landscape impacted by an insect outbreak)
- Timing (e.g. fire in the wet or dry season will have a very different impact)

These properties are of course interrelated, for example the disturbance severity (% of organic material removed) depends on the type of disturbance (Fig 8.3). For example, herbivory has in many cases a low impact while that agricultural clearing always has a larger impact.

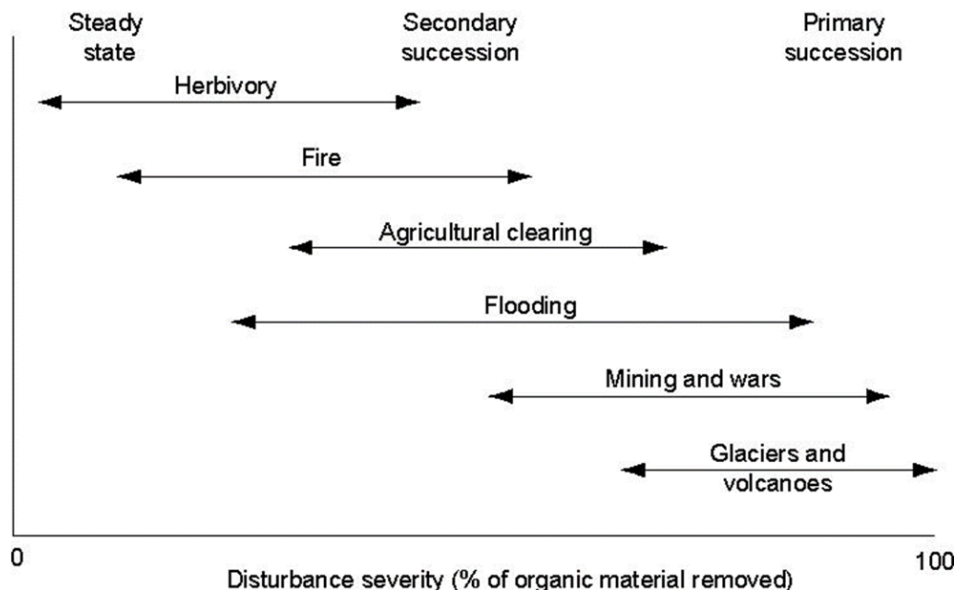


Figure 8.3: Spectrum of disturbance severity associated with major types of disturbance, ranging from normal steady-state functioning of ecosystems to primary succession. (Chapin 2012)

Vegetation models are often used to study the effect of disturbance. We know that the properties of the system and the disturbance will determine the influence the disturbance will have. In many current studies the ‘resilience’ of ecosystems is highlighted. It is however important to define multiple aspects of the influence of disturbance. In the first place there is the **resistance** of an ecosystem, which is its tendency not to change (example some forests are resistant to moderate fires). The **response** of the ecosystem is the magnitude of the change due to a perturbation. The **resilience** is defined as the rate of return of the ecosystem to its original state. While the **recovery** is the extent of return to the original state (Fig. 8.4). In the sections below, we will highlight 3 types of disturbance and how they are implemented in vegetation models: fire, herbivory and forest management.

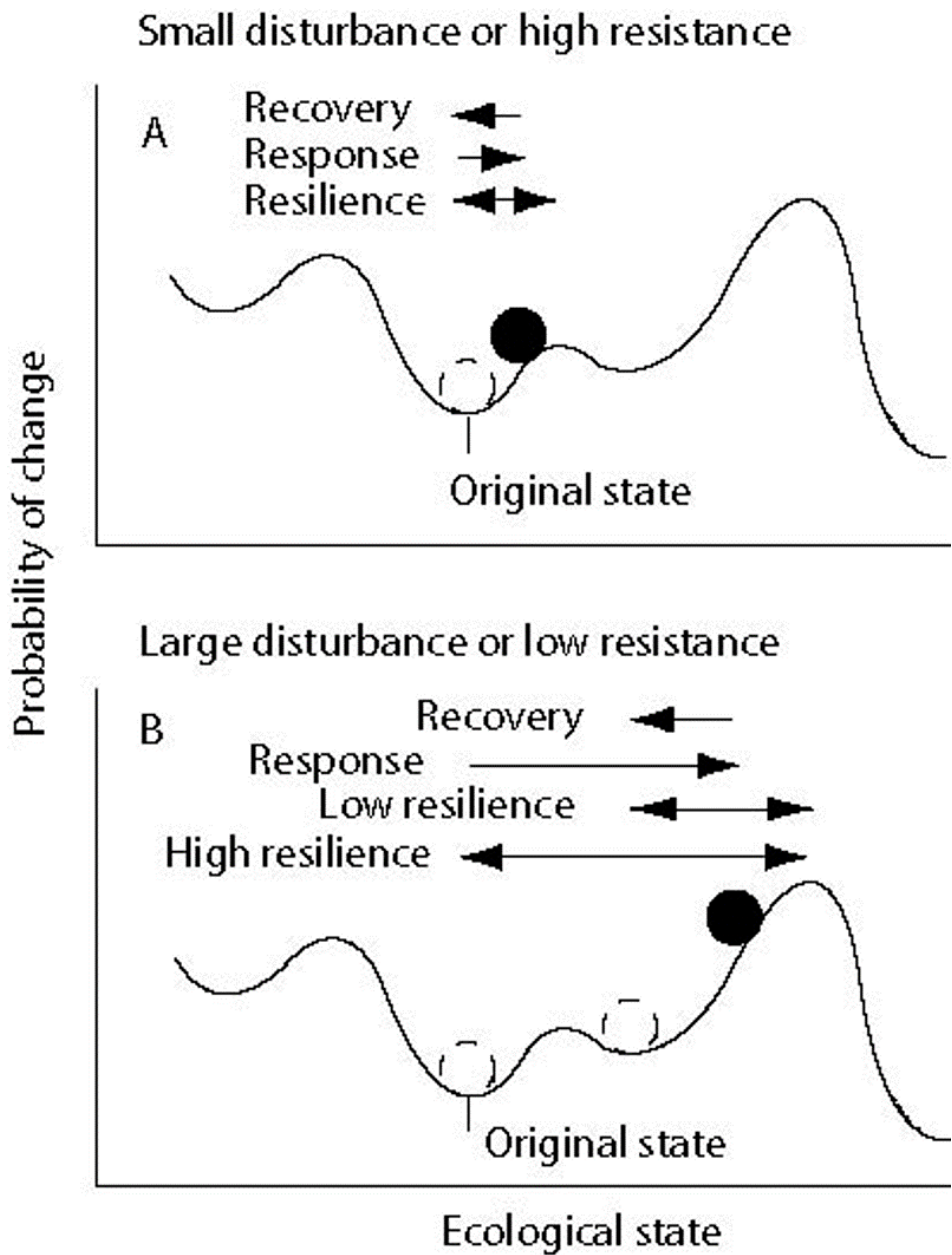


Figure 8.4: Properties of a system that influence its probability of changing state. The solid ball represents the state of the system after a perturbation. The open ball shows the most likely future states of the system. A, A system shows a small response to a perturbation if the perturbation is small or the system is resistant to change.B, After a perturbation, a system can assume many possible states; if it is highly resilient, it may return quickly to its original state; if it is less resilient, or if the perturbation is large, the system may move to a new state.(Chapin 2002)

8.3.1 Fire

Modeling of wildfires is a very specific branch of ecological modelling. It is beyond the scope of this course to go into the technical details. Therefore, we will highlight the key elements needed for fire modeling based on an example of the LPJ model. LPJ was one

of the first vegetation models that included the impact of fire in a large scale vegetation model (Thonicke et al. 2001). The model assumed litter moisture as the main driver of the day-to-day vegetation fire probability (if the litter is dry, the fire probability is high). To estimate the burnt fractional area per year, they used an empirical relation with the length of the fire season. And finally, the model included a PFT parameter for fire resistance (e.g. high resistance for tropical evergreen trees and low resistance for grass PFT). This initial model was able to simulate quite well large-scale global patterns of fire occurrence and intervals.

In the decade that followed, multiple fully-developed fire models emerged. The LPJ-spitfire model is one of them (Thonicke et al. 2010). Such models account for many processes and interactions between vegetation and climate, as illustrated by Fig. 8.5, and can simulate detailed spatial patterns (Fig. 8.6). A process-based fire model accounts for a multitude of inputs that influence wildfires: climate, soil, PFT composition, vegetation structure and fuel (dead organic matter). The fire model itself typically consists of 3 parts:

- A module simulating the **ignition** (probability) or fire occurrence
- A module simulating the **fire spread**
- A model simulating the **fire effects/impact** on the vegetation

Each of those modules depends on multiple input factors (Fig. 8.5). the outputs of such a fire model are the carbon emission by the biomass burning, other trace gas emission, the fire impact on the PFT composition, carbon pools and stand structure. Other fire models have a very similar overall structure (e.g. Fig. 8.7) but differ in the details of the equations, parameter values and inputs accounted for. The burnt area is often simulated as an elliptical area starting from the point of ignition into the direction of the wind (Fig. 8.8). Fire models typically rely on empirical relationships relating fire occurrence to various driving variables (Fig. 8.9).

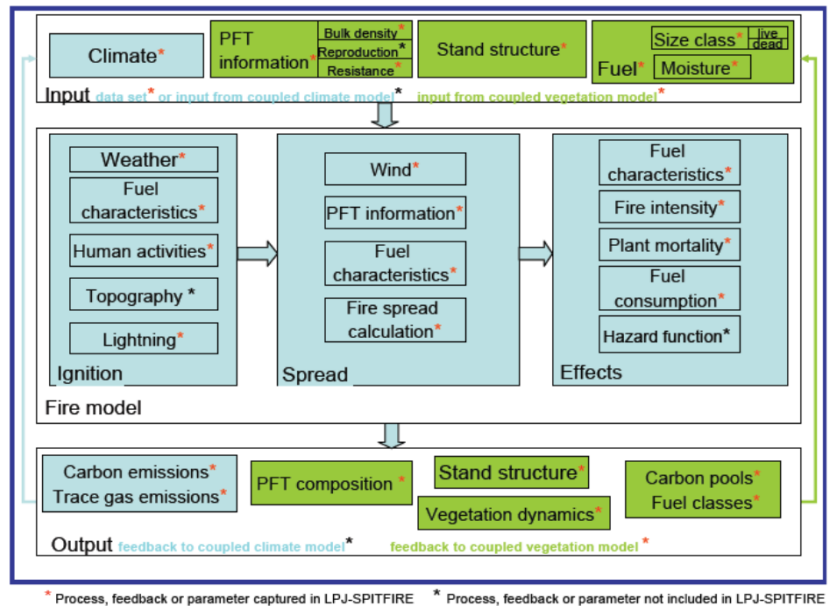


Figure 8.5: Scheme describing model features a process-based fire model for dynamic vegetation models or climate-vegetation models should consider. (Thonicke et al., 2010).

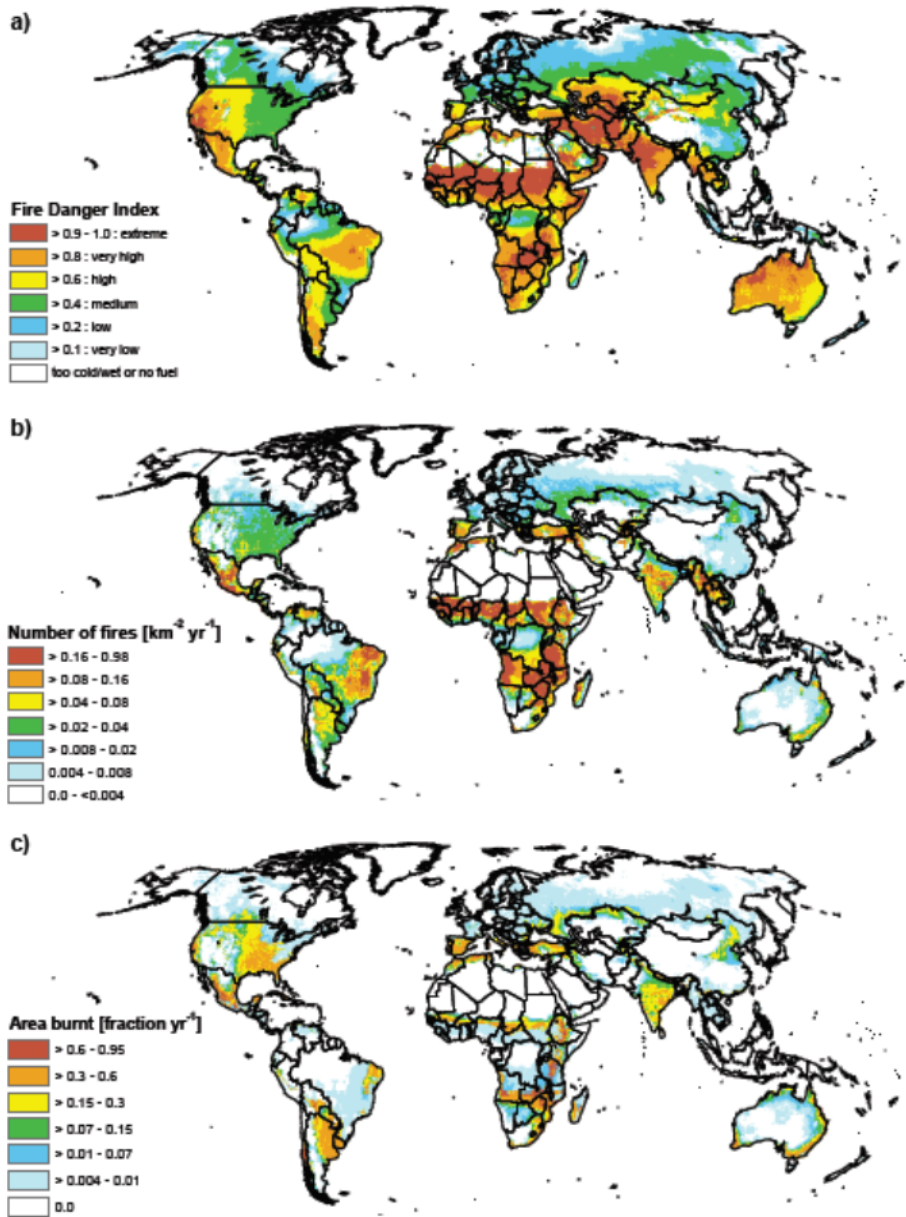


Figure 8.6: Simulation results of the SPITFIRE model: (a) fire danger index, (b) number of fires, (c) fractional area burnt (all as annual averages for 1982–1999). (Thonicke et al. 2010).

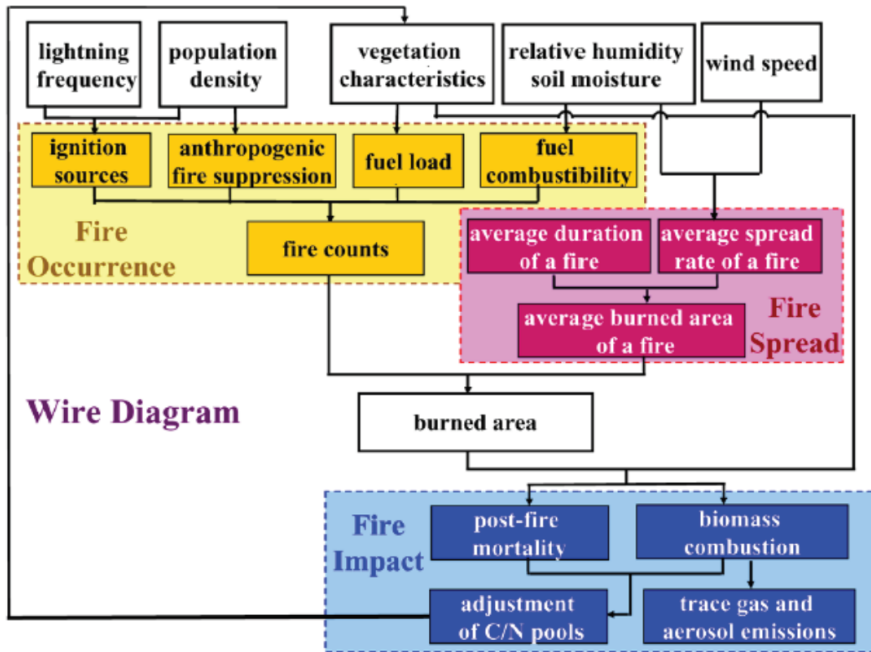


Figure 8.7: Structure of the fire parameterization developed for CLM by Li et al. 2012. Text boxes in yellow, red, and blue colors represent three parts in the fire module: fire occurrence, fire spread, and fire impact.

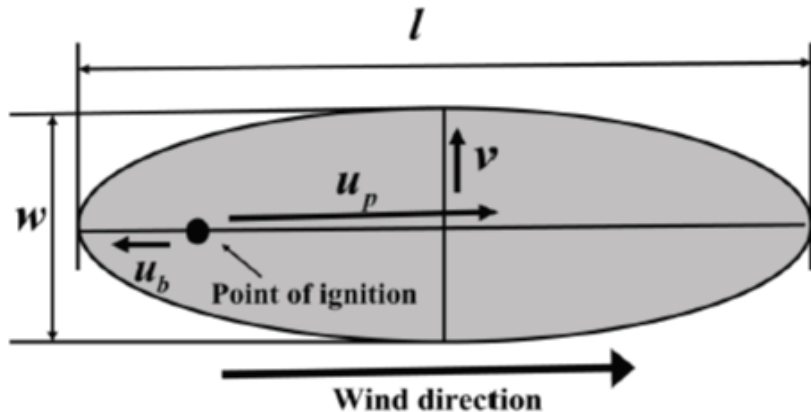


Figure 8.8: Conceptual elliptical fire shape that is used to estimate the burned area with the wind direction along the major axis and the point of ignition at one of the foci in the CLM model. (Li et al. 2012)

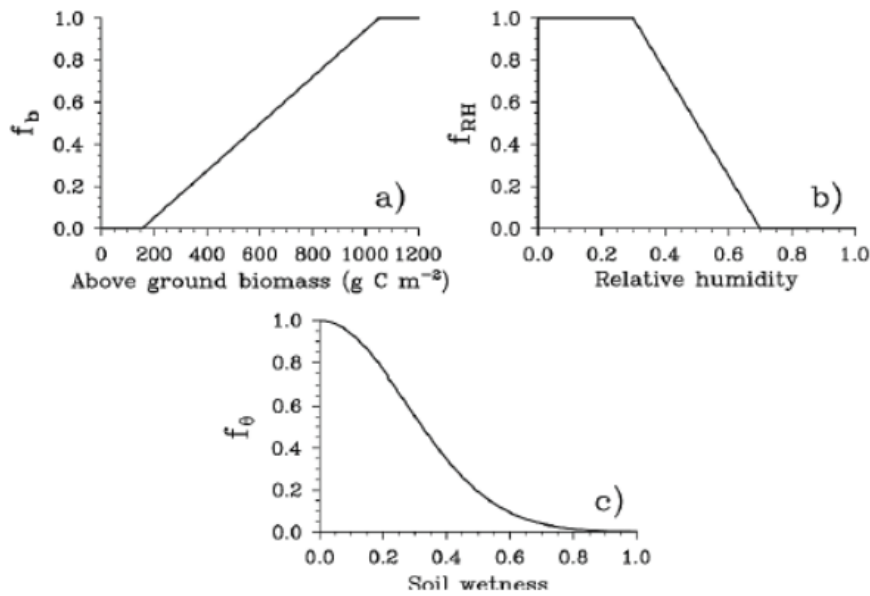


Figure 8.9: Dependence of fire occurrence on (a) fuel availability f_b , (b) relative humidity f_{RH} , and (c) soil wetness $f(\theta)$ in the CLM model. (Li et al. 2012)

8.3.2 Herbivory (Case study 8.1)

Kurz, W. A., Dymond, C. C., Stinson, G., Rampley, G. J., Neilson, E. T., Carroll, A. L., ... & Safranyik, L. (2008). Mountain pine beetle and forest carbon feedback to climate change. *Nature*, 452(7190), 987-990.

We illustrate the modelling of herbivory by a study on the impact of an enormous outbreak of the Mountain pine beetle, in British Columbia (CA) in 2006 (Fig. 8.10). The study evaluated the impact of the outbreak on tree mortality and the carbon cycle. These impacts were estimated using the CBM-CFS3 model, which is an empirical data driven forest model. The results (Fig. 8.11 and 8.12) indicate a very large long-term impact of the carbon stock of 279 MegaTons of carbon, turning the affected area into a large source of carbon. The study concluded that climate change contributed to the extent of the outbreak.

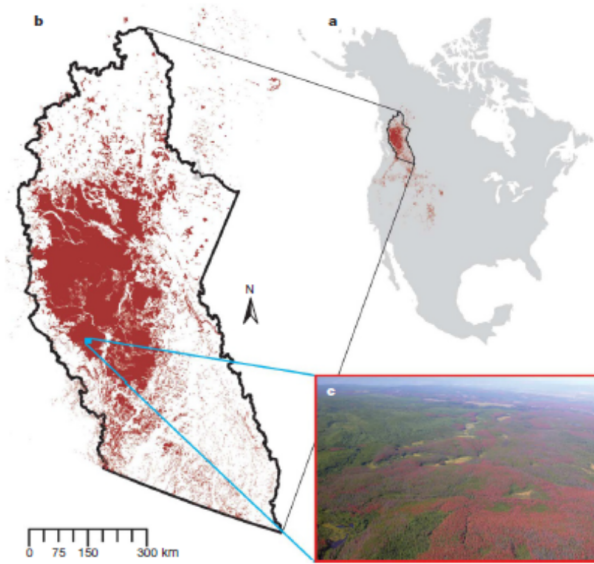


Figure 8.10: Geographic extent of mountain pine beetle outbreak in North America. a, Extent (dark red) of mountain pine beetle. b, The study area includes 98% of the 2006 outbreak area. c, A photograph taken in 2006 showing an example of recent mortality: pine trees turn red in the first year after beetle kill, and grey in subsequent years. (Kurz et al. 2008) Photo credit: Joan Westfall, Entopath Management Ltd.

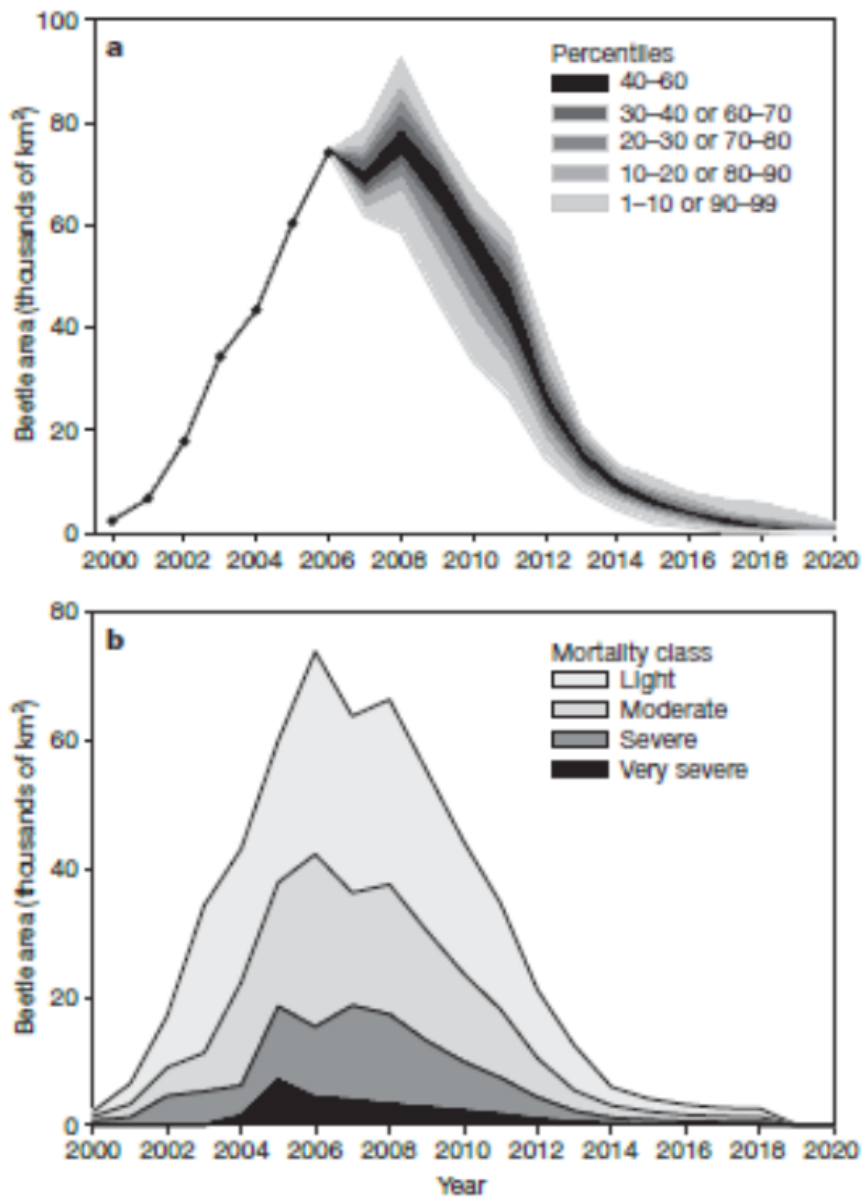


Figure 8.11: Area infested with the mountain pine beetle during the simulation period. Statistics are used from 2000 to 2006 and projections are used from 2007 to 2020. a, Percentiles describing the parameter space resulting from 100 Monte Carlo projections of the beetle-infested area. Our projections of decreasing area after 2009 are largely based on the decline in available live host (pine) area. b, Area statistics for the single Monte Carlo simulation used for scenario analysis broken down by host mortality class. (Kurz et al. 2008)

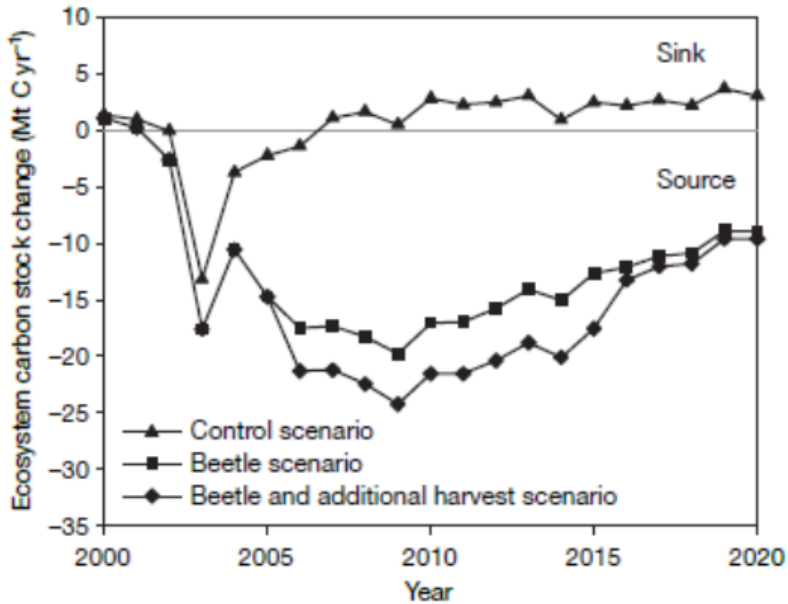


Figure 8.12: Total ecosystem carbon stock change for three scenarios. The control simulation was run with no beetle outbreak, and with base harvest and fires. The beetle simulation added insect impacts to the control scenario. The additional harvest simulation added the management response of increased harvest levels from 2006 to 2016 to the beetle simulation. Negative ecosystem carbon stock change values represent fluxes from the forest to the atmosphere (net source of carbon). The source in 2003 was, in part, the result of the large area burned (2,440km² in the study area) that was included in all three scenarios.(Kurz et al. 2008)

8.3.3 Forest management

Demographic models that track individual trees or the number of trees in cohorts allow to study the impact of forest management. Management practices like thinning can be simulated by removing individuals in specific size classes, clear cuts can be simulated by changing the PFT in specific patches with a predefined rotation period, and species conversion can be simulated by introducing additional PFTs (species) in patches. These models allow then to simulate the impact of such management practices on various model variables (productivity, hydrology, etc...). The LPJ-guess model is one of these models where this is now possible (Fig. 8.13, 8.14, 8.15).

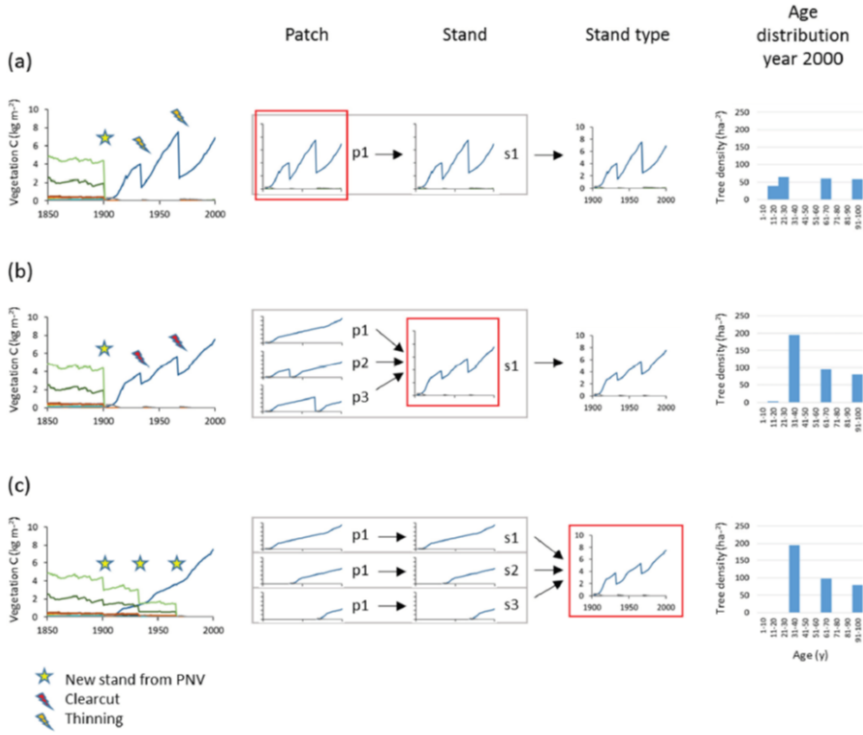


Figure 8.13: Forest management in LPJguess (Lindeskog et al. 2021). Examples of age structure setup at three different structural levels, patch, stand and stand type. Beech monocultures are created from clearcut of potential natural vegetation. The target in year 2000 was three cohorts of 100, 67 and 33 years. (a) Within-patch. One secondary stand with 1 patch created in 1901. Thinnings in 1933 and 1967. Age structure depends on timing of increased light 150 and subsequent reestablishment of seedlings. (b) Among-patch. One secondary stand with 3 patches created in 1901. Clearcut in patches 2 and 3 in 1933 and 1967 (evenly spread age distribution). (c) Among-stand. Three secondary stands with 1 patch created in 1901, 1933 and 1967. Age structure from area fraction input.

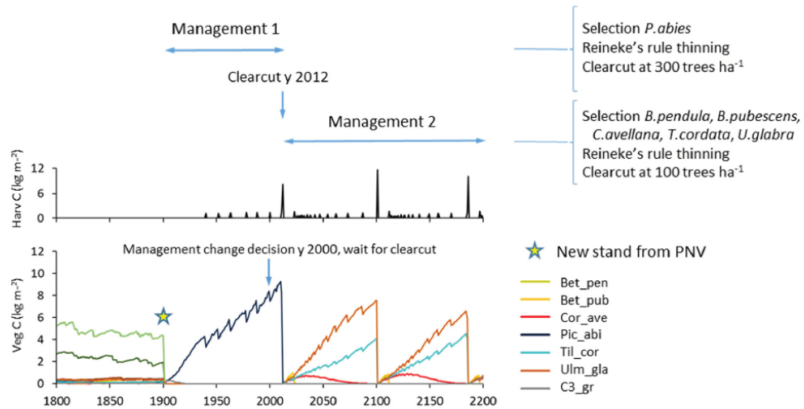


Figure 8.14: Example of forest management change in LPJ-GUESS (Lindeskog et al. 2021). Spruce monoculture changed to mixed broadleaved, both with automated thinning and clearcut. Management change is activated after first management has completed by a clearcut event.

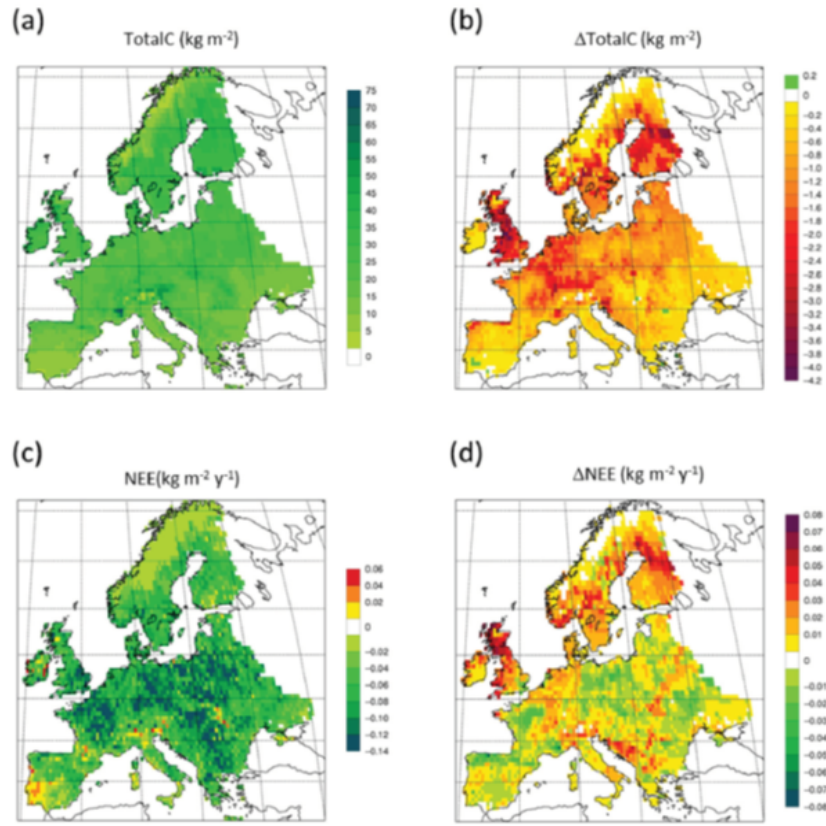


Figure 8.15: Simulated European forests with LPJguess including forest management (Lindeskog et al. 2021): (a) total carbon pool 2010 in a simulation with thinning, (b) total carbon pool 2010 difference between simulations with and without wood harvest in regrowth forest, (c) Mean 2001-2010 NEE (net ecosystem exchange) in a simulation with thinning, (d) Mean 2001-2010 NEE difference between simulations with and without thinning.

8.3.4 Case study 8.2

Naudts, K., Chen, Y., McGrath, M. J., Ryder, J., Valade, A., Otto, J., & Luyssaert, S. (2016). Europe's forest management did not mitigate climate warming. *Science*, 351(6273), 597-600.

In this case study, we zoom in on a study by Naudts et al. (2016) that evaluated the impact of the historical European forest management since 1750 on climate change. They used the ORCHIDEE-CAN model coupled to an atmosphere model to evaluate the effects of European forest management on climate via biogeochemical and biophysical effects and feedbacks. Since 1750 forest management changed a lot in Europe, with coniferous PFTs becoming more important and high stands replacing unmanaged or coppice forest (Fig 8.16). The model simulations showed that 2.5 centuries of forests management in Europe have not cooled the climate. They show that wood extraction caused a loss 3.1 Pg C and that species conversion caused a temperature increase of

0.12 Kelvin (Fig. 8.17), through albedo and energy balance effects.

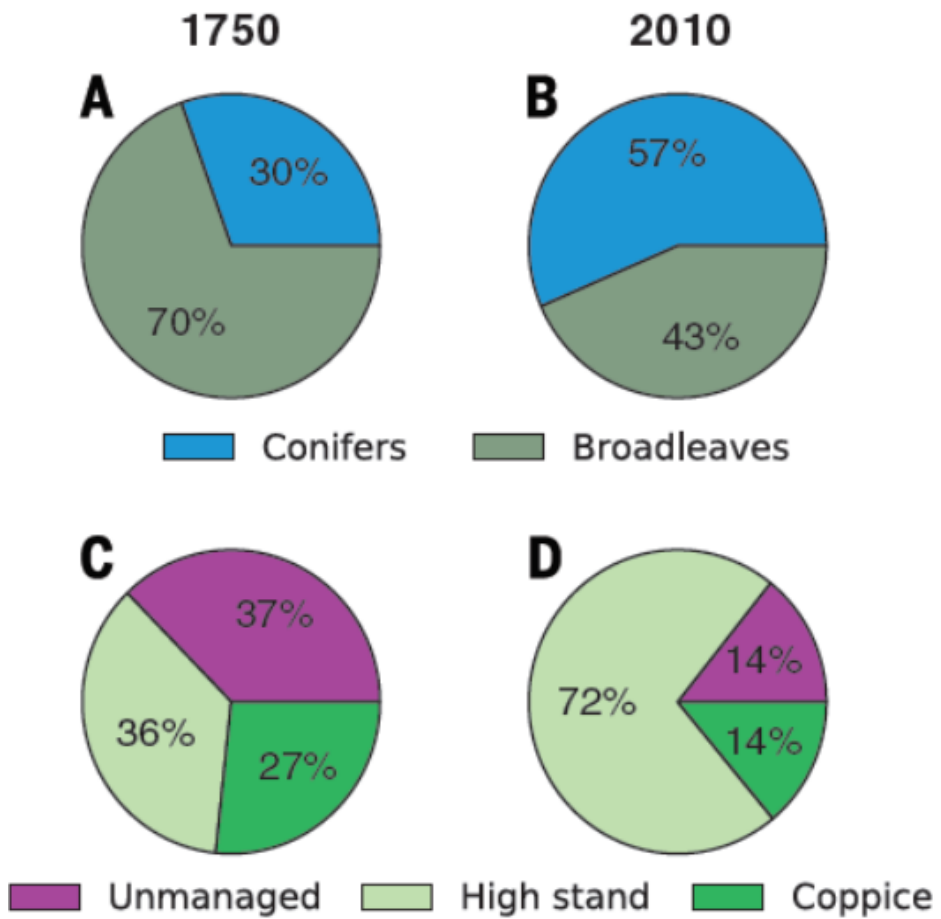


Figure 8.16: Main changes in European forest management between 1750 and 2010. (A) Relative distribution (percent) of tree growth forms in 1750 and (B) 2010. Total forest area in 1750 was 1,929,000 km² and increased to 2,126,000 km² by 2010. (C) Relative distribution (percent) of wood extraction strategies in 1750 and (D) 2010. (Naudts et al. 2016)

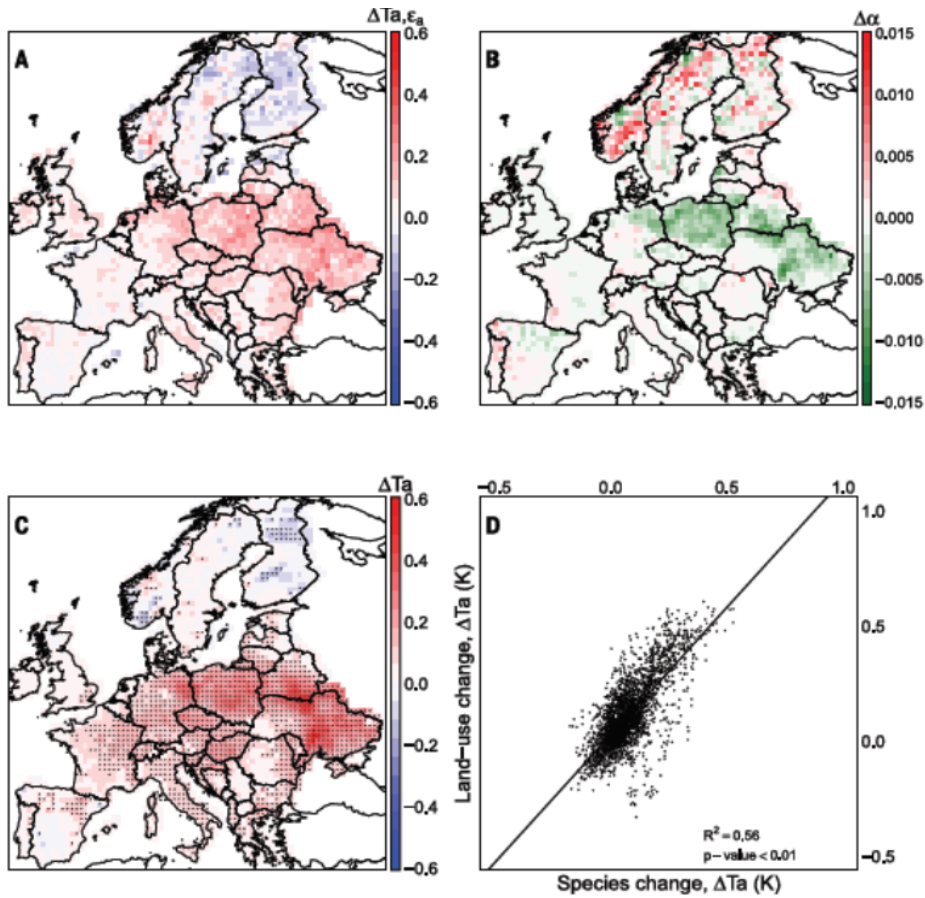


Figure 8.17: Effects of species conversion in Europe since 1750 as simulated by the ORCHIDEE-CAN model coupled to the LMDZ atmospheric model (Naudts et al. 2016). Temperature changes are for boundary layer temperature during summer (kelvin). (A) Temperature change due to changes in emissivity ($\Delta T_{a,ea}$) caused by species conversion, (B) changes in albedo ($\Delta \alpha$) due to species conversion, (C) total temperature change (ΔT_a) due to species conversion, and (D) correlation between species-induced and land use-induced temperature change. In (C), black dots denote significant temperature changes at the 0.05 significance level, as determined by a modified paired one-sample t test.

Chapter 9

Upscaling from the leaf to the globe

9.1 The problem of upscaling

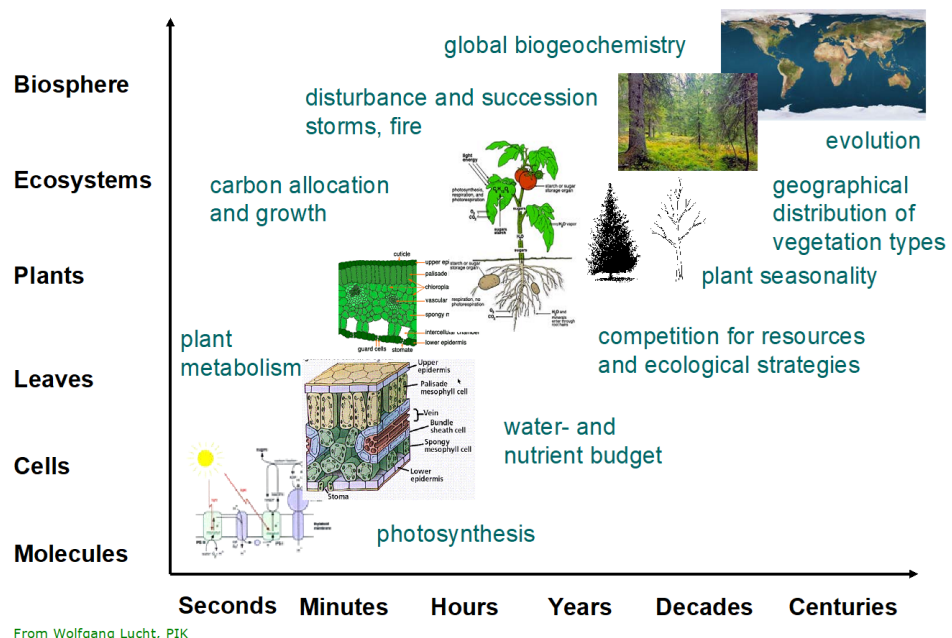


Figure 9.1: Illustration of the correlation between the spatial and temporal scales at which various vegetation processes dominate. (Wolfgang Lucht, PIK)

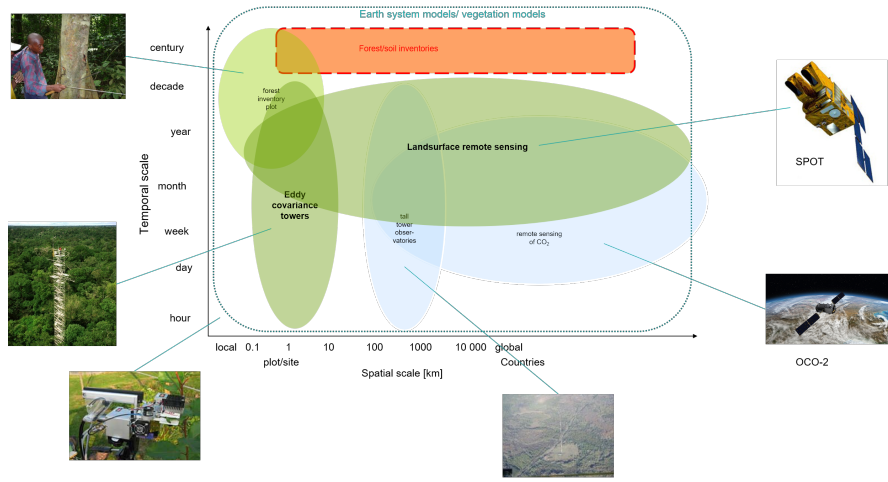


Figure 9.2: Illustration from the course Inventory of Forest and Nature showing the temporal and spatial scale of different carbon cycle monitoring methods and the integrative power of vegetation models.

9.2 Vegetation models as part of earth system models

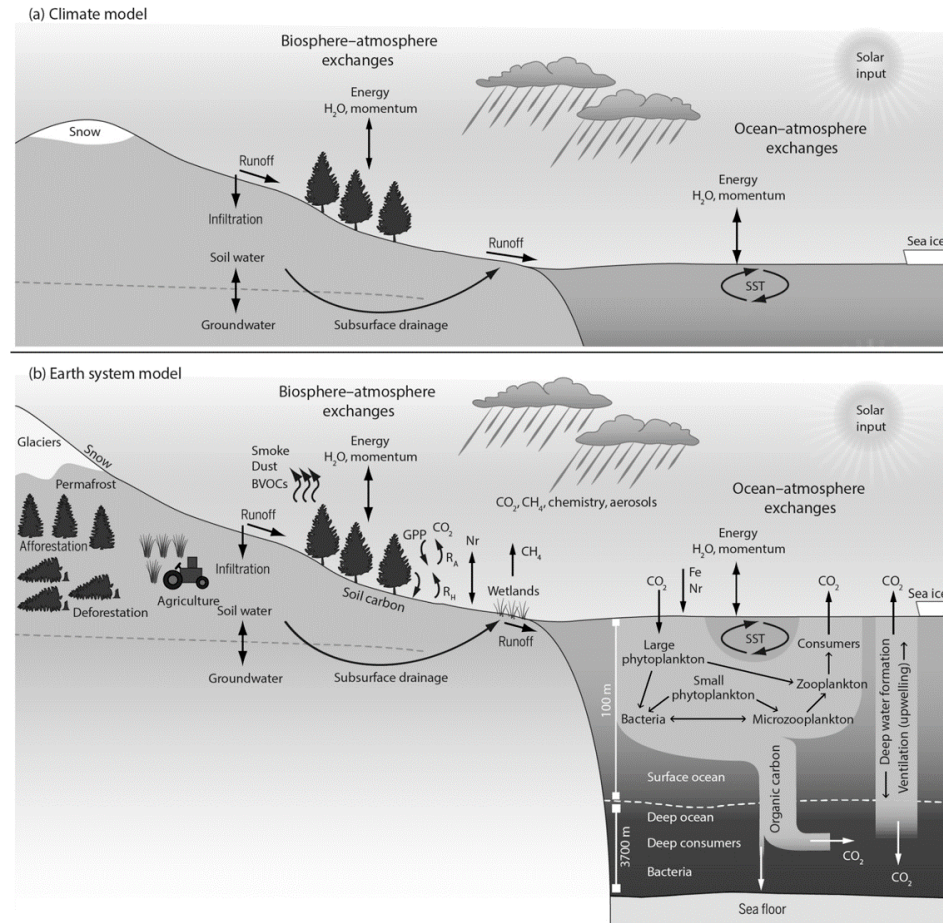


Figure 9.3: Scientific scope of (a) climate models and (b) Earth system models. Climate models simulate biogeophysical fluxes of energy, water, and momentum on land and also the hydrologic cycle. Terrestrial and marine biogeochemical cycles are new processes in Earth system models. The terrestrial carbon cycle includes carbon uptake through gross primary production (GPP) and carbon loss from autotrophic respiration, heterotrophic respiration, and wildfire. Many models also include the nitrogen cycle. Anthropogenic land use and land-cover change are additional processes. The fluxes of CO_2 , CH_4 , aerosols, biogenic volatile organic compounds (BVOCs), and wildfire chemical emissions are passed to the atmosphere to simulate atmospheric chemistry and composition. Nitrogen is carried in freshwater runoff to the ocean.(Bonan)

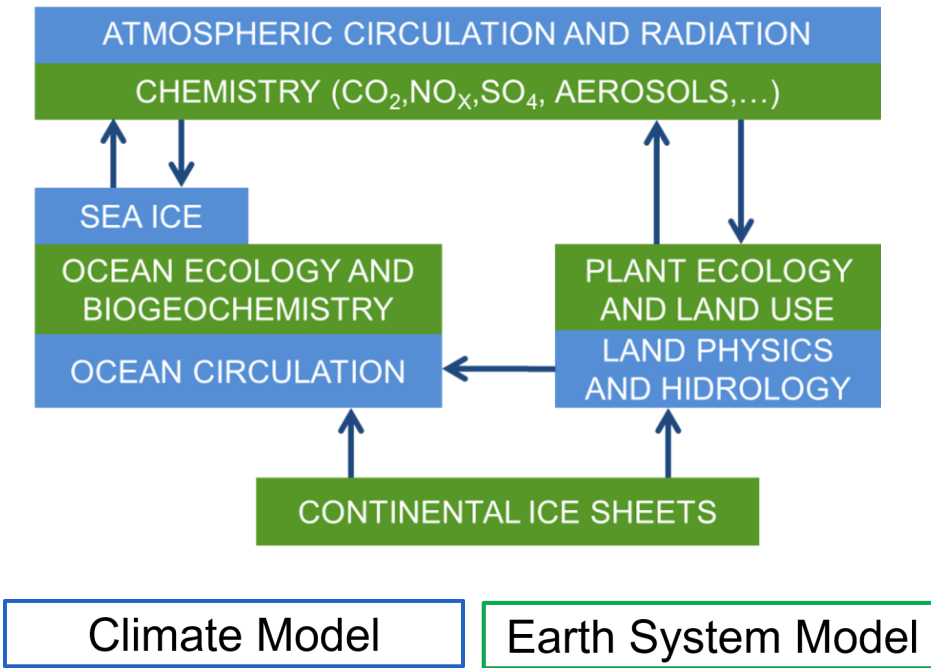


Figure 9.4: Illustration of the difference between climate models and earth system models. Climate models include the blue processes, earth system models include both the blue and green processes.

Climate models

For decades scientists have been using mathematical models to help us learn more about the Earth's climate. Known as climate models, they are driven by the fundamental physics of the atmosphere and oceans, and the cycling of chemicals between living things and their environment. Over time they have increased in complexity, as separate components have merged to form coupled systems.

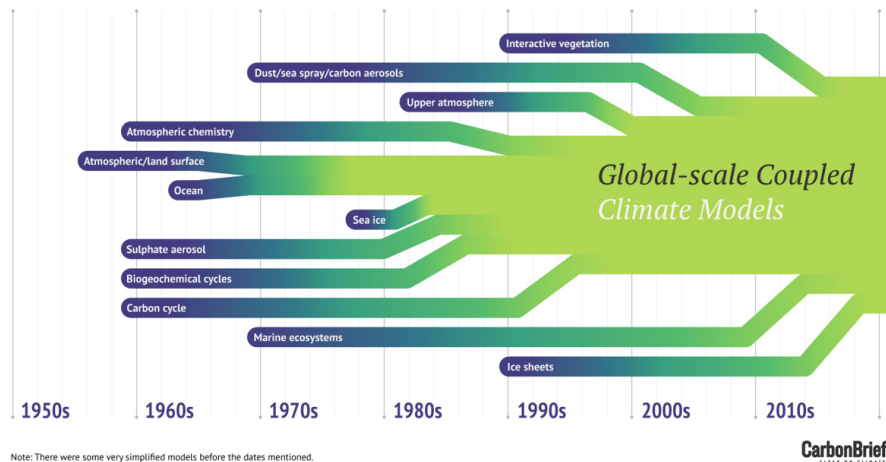


Figure 9.5: Illustration of the evolution of climate models into earth system models, with more and more processes and components added through time over the past decades.

9.3 MOdelling work flow

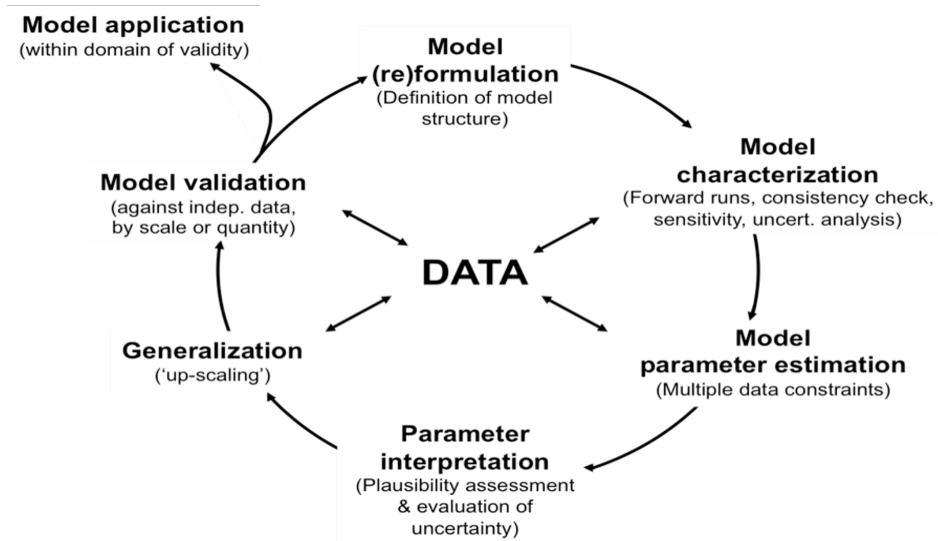


Figure 9.6: Model data fusion in every step of the model development cycle. (Williams et al. 2009)

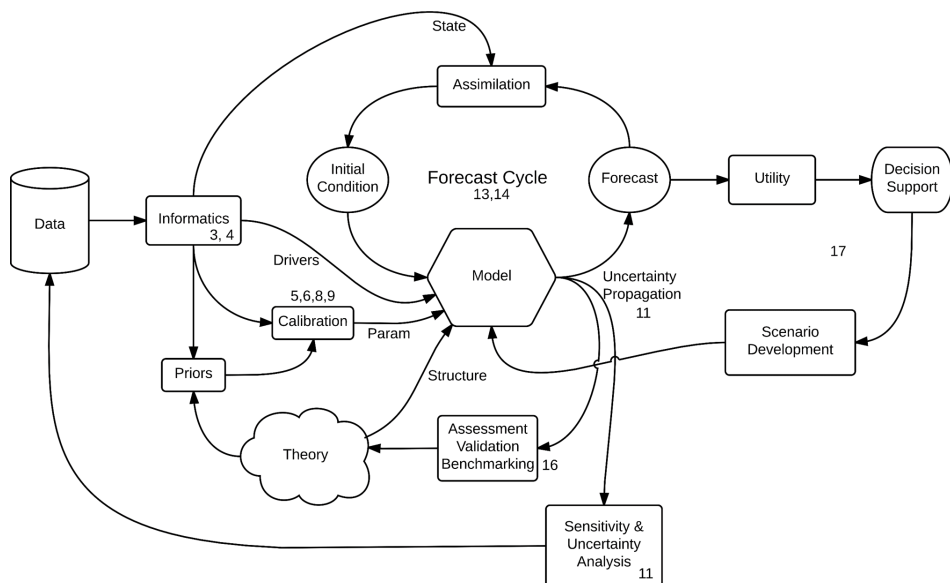


Figure 9.7: Methodological workflow of model data fusion. (Dietze: Ecological Forecasting)

9.4 Case study 9.1

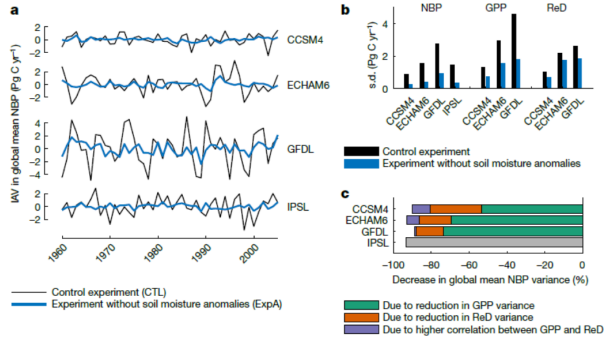


Figure 9.8: Carbon fluxes in CTL and experiment A. a, IAV (inter annual variability) in global mean NBP as simulated by four ESMs (CCSM4, ECHAM6, GFDL and IPSL) in coupled model experiments with (CTL) and without (experiment A; ExpA) anomalies in soil moisture. Positive NBP indicates carbon uptake. b, Standard deviations of global mean NBP, GPP and respiration and disturbance (ReD) in the two experiments. c, Drivers of change in global mean NBP variance. Global mean NBP variance decreases in the experiment with prescribed seasonal soil moisture mainly because GPP variance is reduced. GPP and ReD fluxes are not available for the IPSL model. (Humphrey et al. 2021)

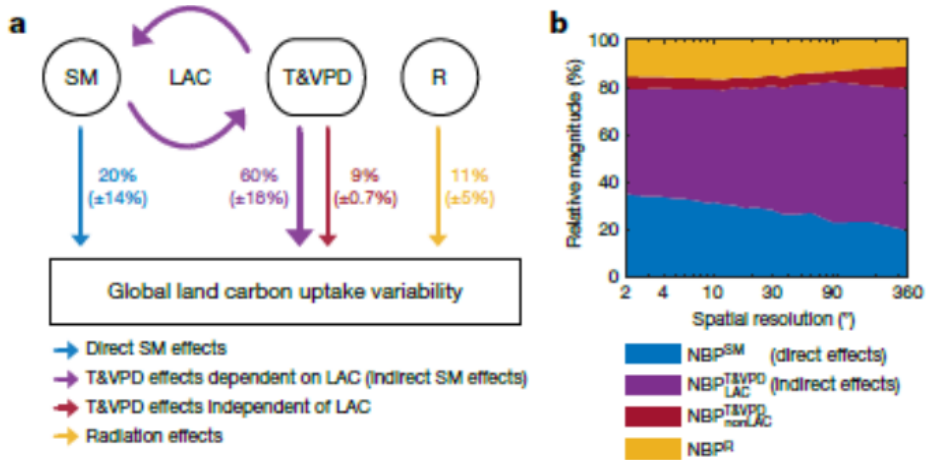


Figure 9.9: Drivers of NBP IAV. a, b, Contribution of meteorological drivers to NBP IAV: direct soil moisture effects (NBPSM), indirect LAC-dependent (land atmosphere coupling) temperature and VPD effects (NBPLAC T&VPD), non-LAC-dependent temperature and VPD effects (NBPNonLAC T&VPD) and radiation (NBPR) globally (a; mean of the four models ± 1) and from local to global scales (b). (Humphrey et al. 2021)

9.5 Case study 9.2

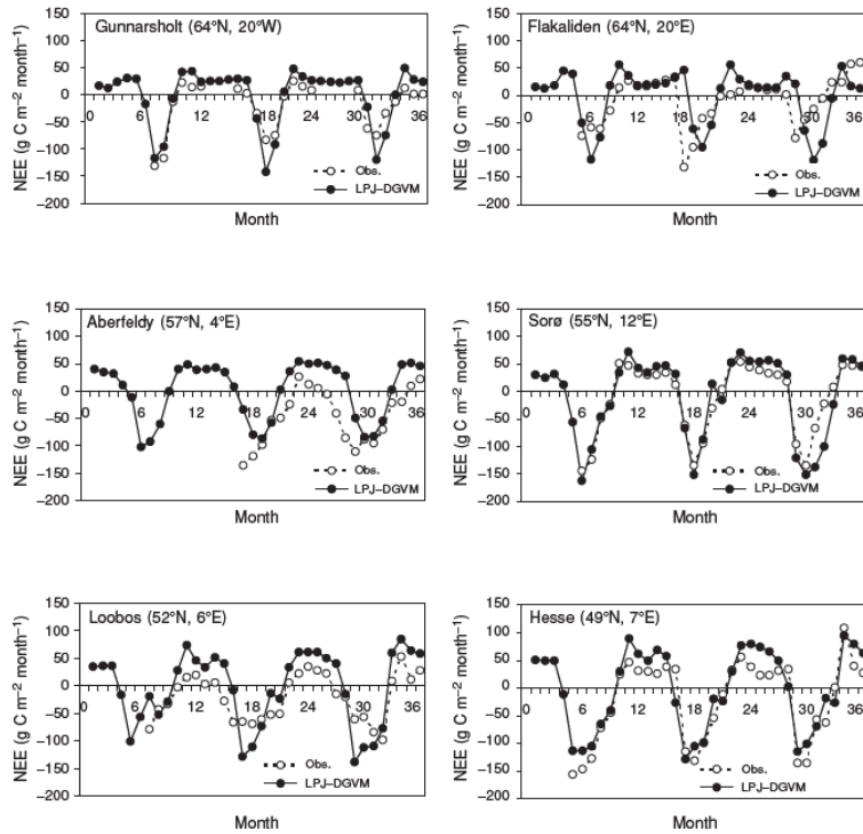


Figure 9.10: Validation of LPJ model at the site level. Comparison between simulated and observed Net Ecosystem Exchange at 6 fluxtower sites in Europe. (Sitch et al. 2003)

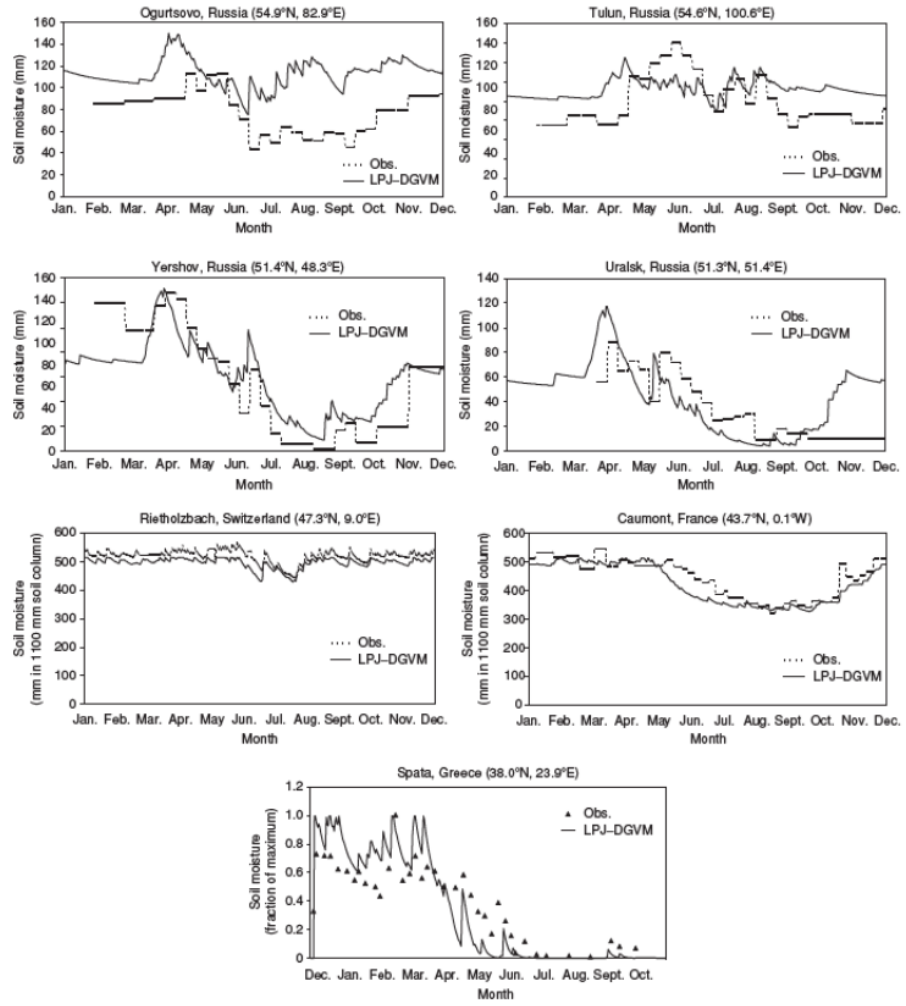


Figure 9.11: Validation of the LPJ model at the site level. Observed vs. simulated soil moisture at seven sites.(Sitch et al. 2003)

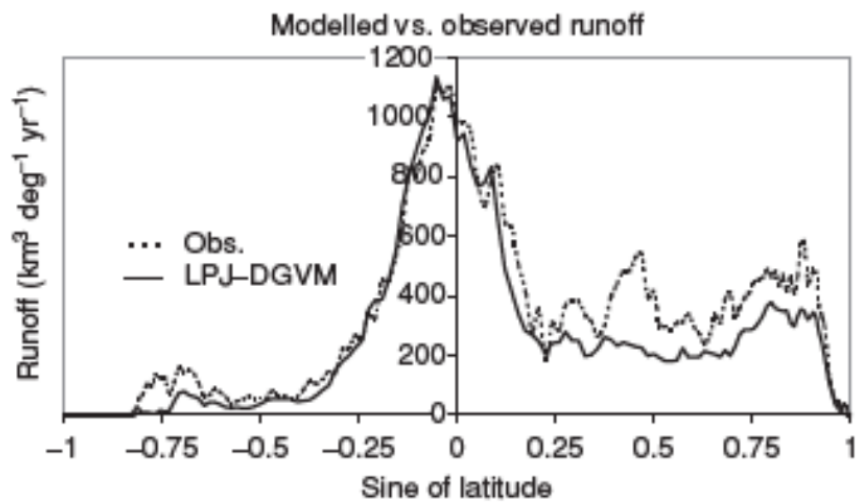


Figure 9.12: Validation of LPJ at the global scale, comparison with observed annual runoff per latitude. (Sitch et al. 2003)

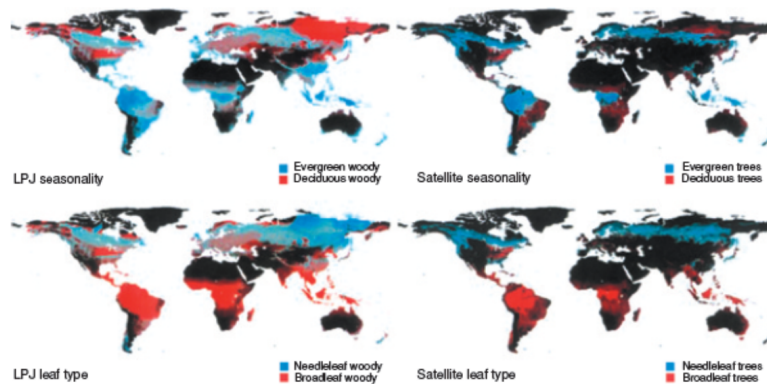


Figure 9.13: Global comparison of LPJ simulated distributions of woody vegetation with satellite based maps. (Sitch et al. 2003)

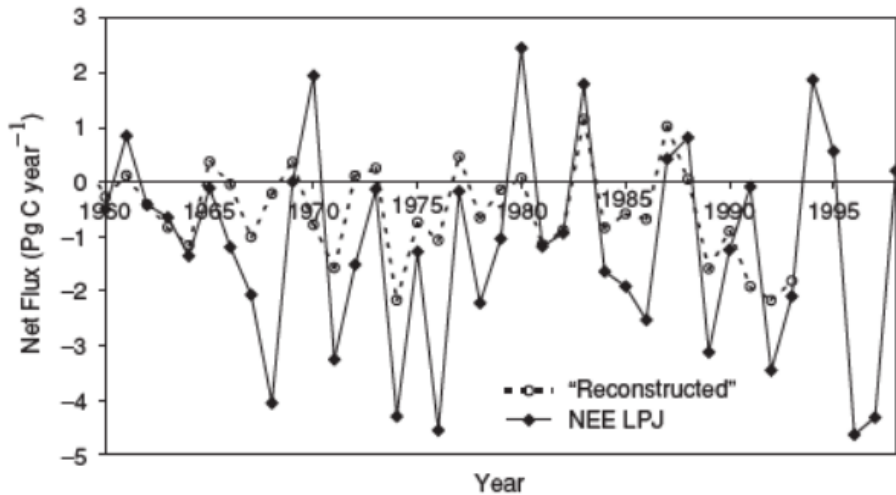


Figure 9.14: LPJ simulated vs. reconstructed interannual variation in net ecosystem exchange for the globe. (Sitch et al. 2003)

Chapter 10

Model simulations, projections and scenario analysis

10.1 Simulation setup

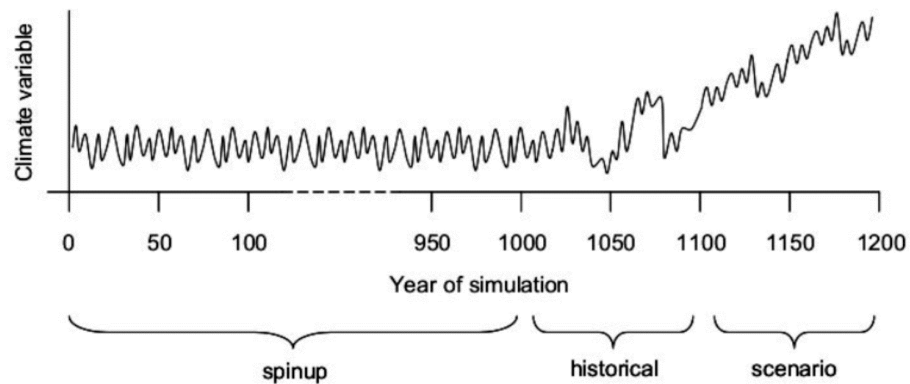


Figure 10.1: Sequention of the different parts of a simulation setup: the model spinup, the historical run, and the scenario run.

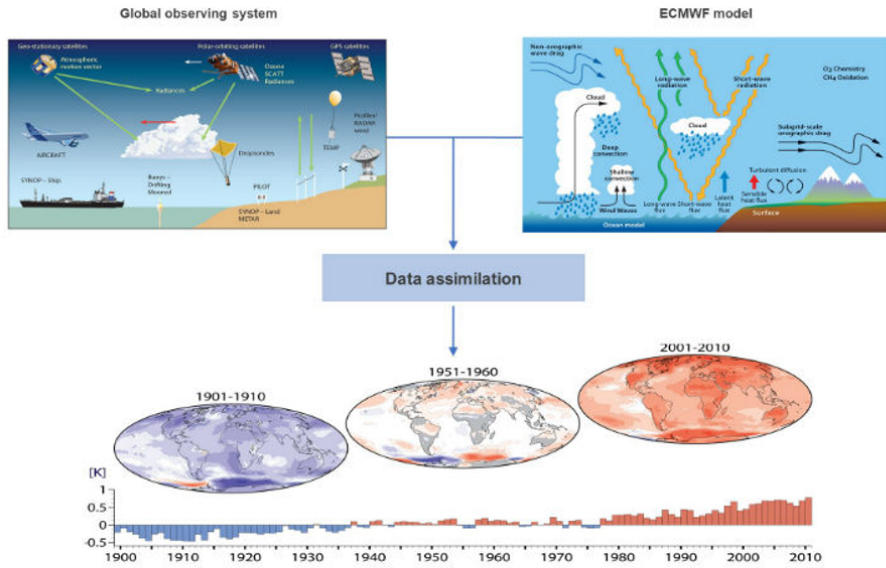


Figure 10.2: The principle of the construction of a historical global climate reanalysis dataset. Global observations are combined with a climate model to obtain a complete gridded consistent global dataset. (ECMWF)

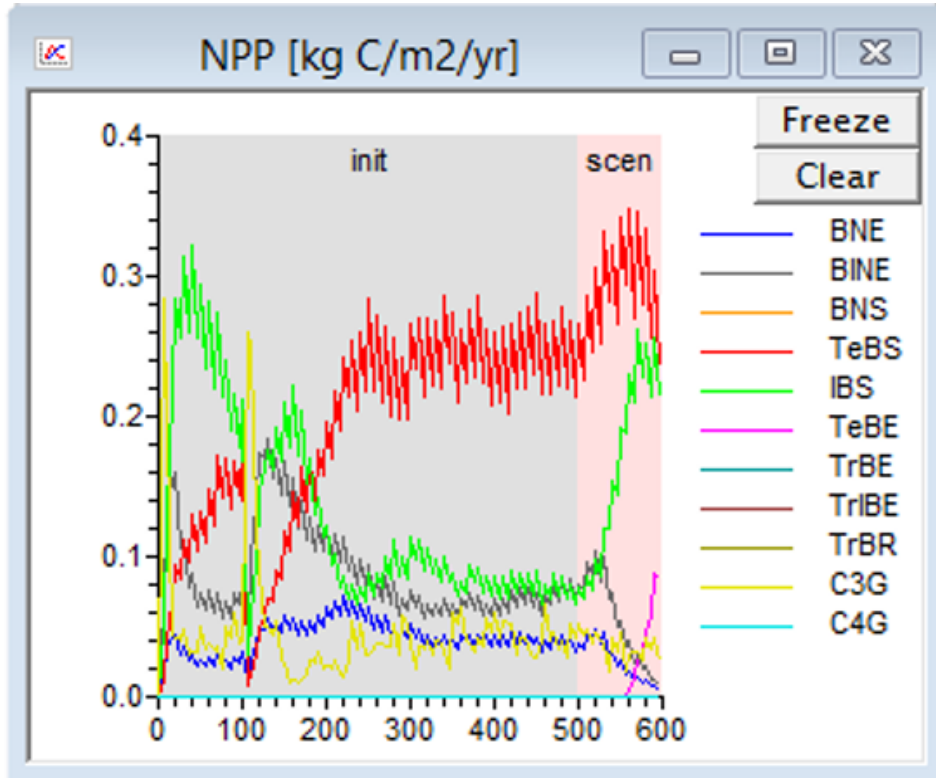


Figure 10.3: Example of a model spinup for the LPJguess educational model. PFTs are initialized during the spinup, before a scenario run is performed.

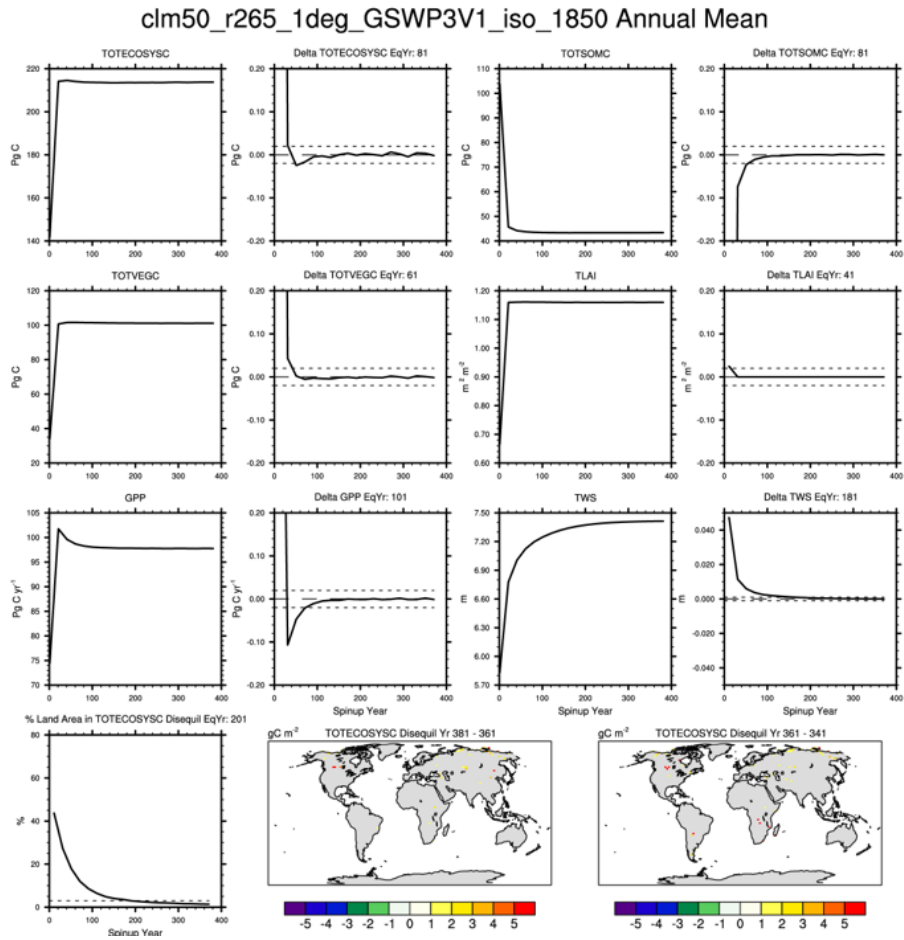


Figure 10.4: Pre industrial (pre 1850) spinup run for the CLM 5.0 model, showing various model state variables reaching equilibrium.

10.2 Model experiments

10.3 Paleo studies

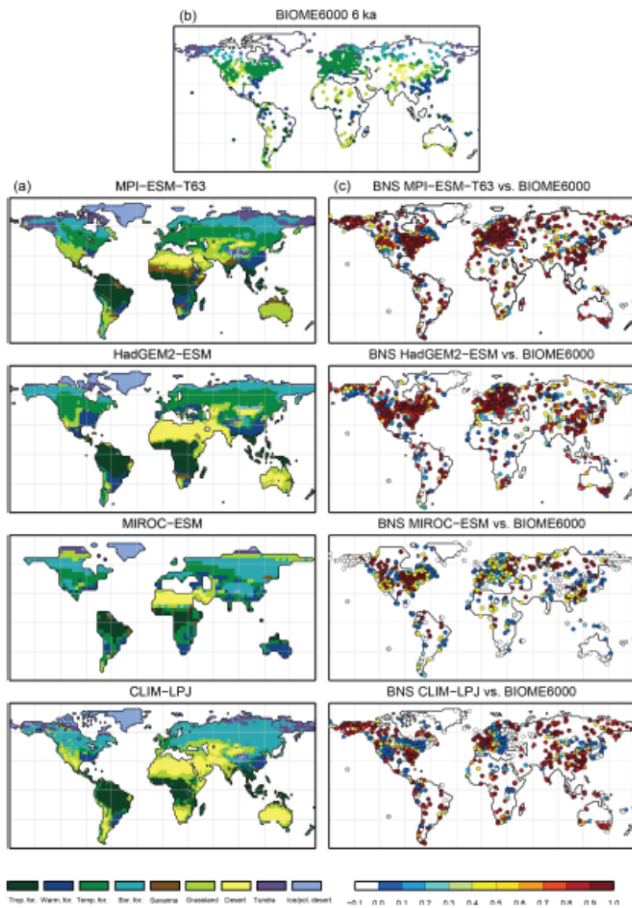


Figure 10.5: a) Simulated mid-Holocene biome distribution in different models (ESMs) based on the PFT method, b) pollen-based biome reconstructions of the mid-Holocene biome distribution (BIOME6000 database) and c) the best neighbour score (BNS) for all individual sites showing the agreement of the reconstructed biomes and the biome distribution in the neighbourhood of the sites, ranging from 0 (no grid cell in the surrounding area shows the same biome as reconstructed) to 1 (the grid cell locating the site and the record at the site indicate the same biome). (Dallmeyer et al. 2019)

10.4 Climate scenarios

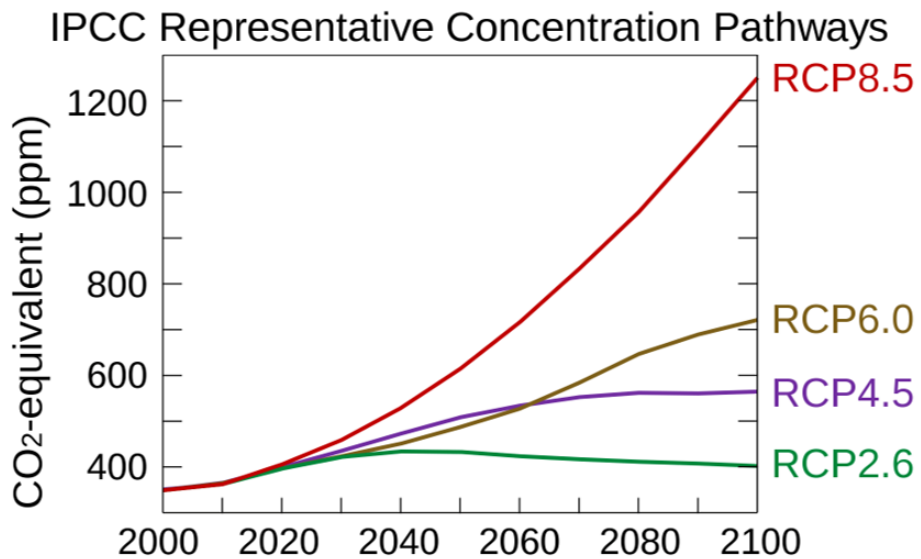


Figure 10.6: Atmospheric CO₂ concentration for the 21st century according to the IPCC Representative Concentration Pathways. (IPCC)

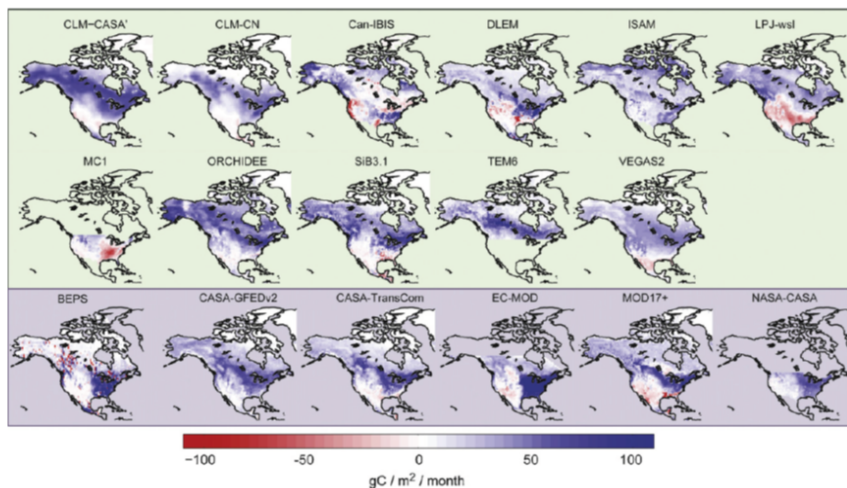


Figure 10.7: Long-term mean summer (June, July, August) net ecosystem productivity by model (2000–2005), as simulated by the models participating to the Model Intercomparison Project of the North American Carbon Program (NACP-MIP). A positive sign indicates net terrestrial carbon uptake from the atmosphere, while a negative sign signifies net carbon release to the atmosphere. Prognostic models are shown above with a green background; diagnostic models are below with a purple background. (Huntzinger et al. 2012)

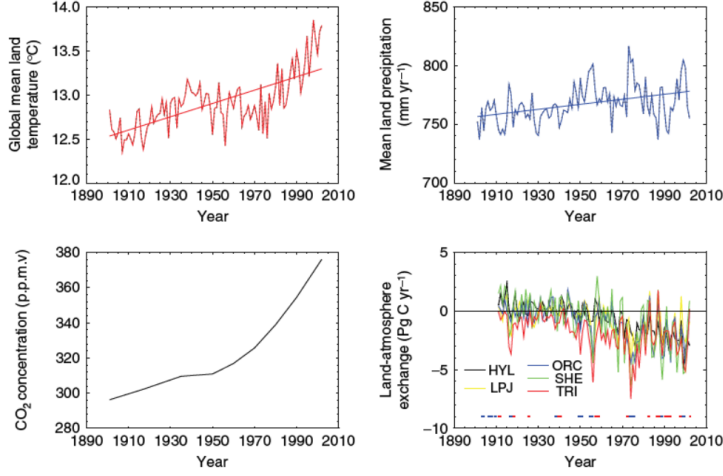


Figure 10.8: Model Ensemble of 5 DGVMs, run for multiple climate SRES climate scenarios as simulated by the HAdGCM global climate model. Global mean land climatology (temperature, $^{\circ}\text{C}$, red; precipitation, mm/yr , blue), atmospheric CO_2 content (black) and simulated land–atmosphere exchange over the 20th century by HyLand (HYL, black), Lund–Potsdam–Jena (LPJ, yellow), ORCHIDEE (ORC, blue), Sheffield (SHE, green), and TRIFFID (TRI, red). Red and blue dashes represent periods of strong El Nino (red) and La Nina (blue), respectively. Linear regressions are also plotted through the temperature and precipitation data. (Sitch et al. 2008)

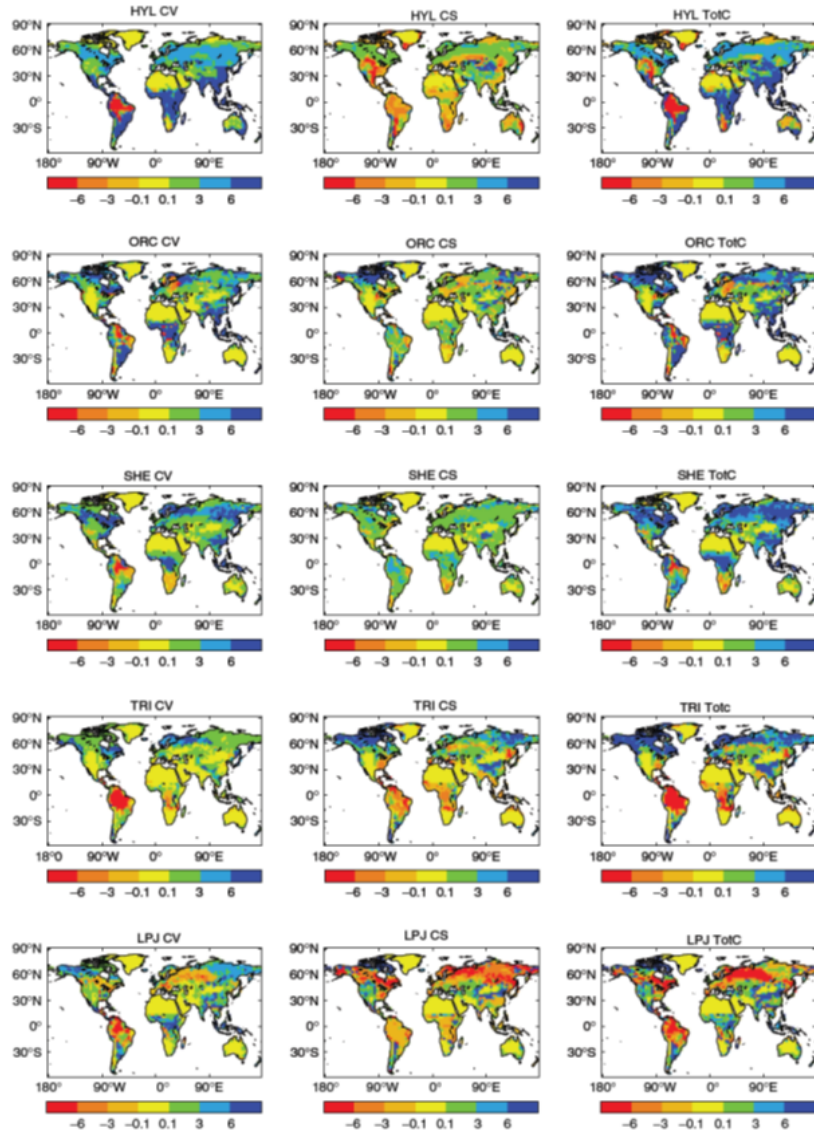


Figure 10.9: Model Ensemble of 5 DGVMs, here compared for 1 SRES climate scenario as simulated by the HAdGCM global climate model. Change in land carbon storage (TotC) and component vegetation (CV) and soils (CS) carbon stocks between 1860 and 2099 from the coupled climate-carbon cycle simulation under Special Report Emission Scenarios (SRES) emission scenario A1F1 (units are Pg C) for HyLand (HYL), Lund-Potsdam-Jena (LPJ), ORCHIDEE (ORC), Sheffield (SHE) and TROLL (TRI). (Sitch et al. 2008)

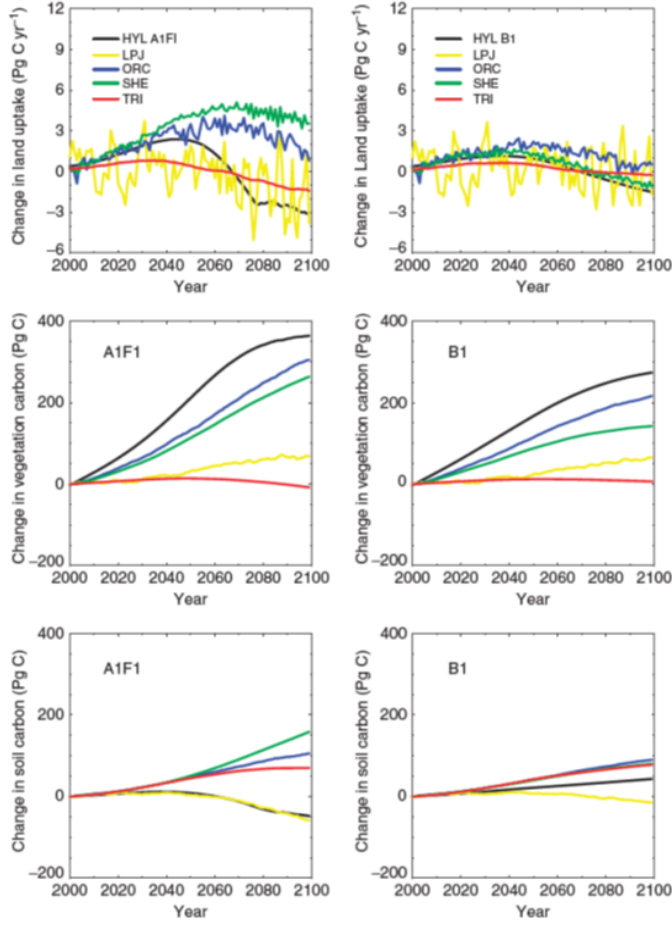
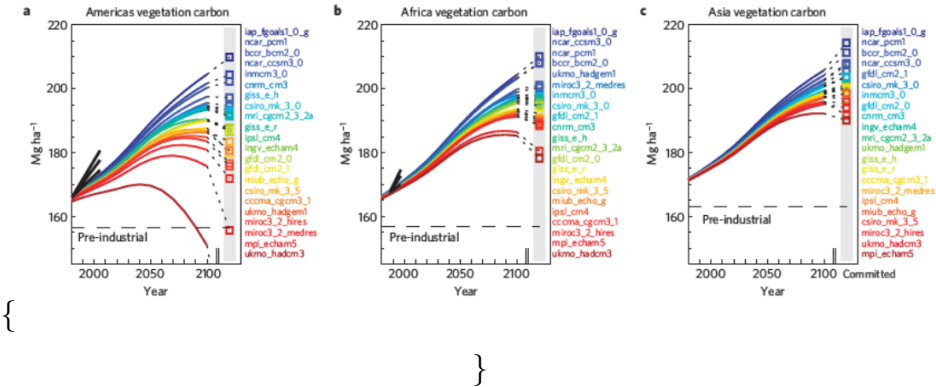


Figure 10.10: Model Ensemble of 5 DGVMs, here the response of the 5 models is compared for 2 SRES climate scenarios as simulated by the HAdGCM global climate model. Change in land carbon uptake, PgCyr-1, (top panels) relative to the present day (mean 1980–1999) for five Dynamic Global Vegetation Models (DGVMs) from coupled climate-carbon cycle simulations with two Special Report Emission Scenarios (SRES) emission scenarios, A1FI (solid lines), B1 (dashed lines), bracketing the range in emissions. Change in global vegetation (middle panels) and soil carbon (top panels), Pg C, between 2100 and 2000 under scenarios A1FI (solid lines) and B1 (dashed lines) for HyLand (HYL, black), Lund–Potsdam–Jena (LPJ, yellow), ORCHIDEE (ORC, blue), Sheffield (SHE, green), and TRIFFID (TRI, red). Note: only LPJ is run with interannual variations in climate. (Sitch et al. 2008)

\begin{figure}



\caption{Tropical forest biomass predictions for the Americas (a), Africa (b) and Asia (c) by the MOSES–TRIFFID model forced by 22 climate models. Climate models emulated are colour-coded, from dark blue to dark red for decreasing year 2100 values of Cv. Grey regions and squares are committed Cv values with climate constant at year 2100 values, and small dashes link back to the same model in transient predictions. Committed equilibrium values are year-independent, hence the x-axis break (small vertical bars). Normalized estimates of Cv from inventory data (2.5%, mean and 97.5% confidence levels) are the short black curves for Americas and Africa. Horizontal lines (large dashes) are estimated pre-industrial values, year 1860 (Huntingford et al. 2013)} \end{figure}

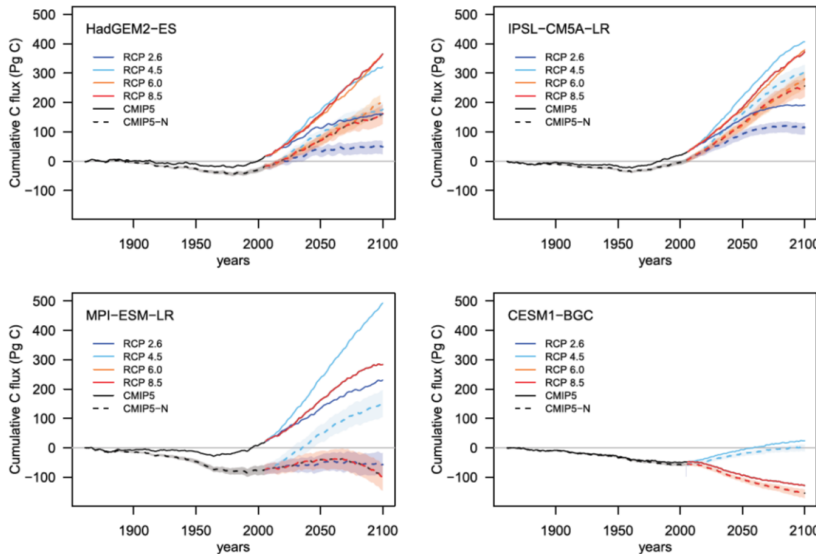


Figure 10.11: Comparing ESMs for multiple RCPs. Cumulative C sequestration from a few CMIP5 models and plausible range of C sequestration considering N constraints (CMIP5-N) for the HadGEM2-ES, IPSL-CM5A-LR, MPIESM-LR, and CESM1(BGC) models.(Zaehle et al. 2015)

10.5 Land use scenarios

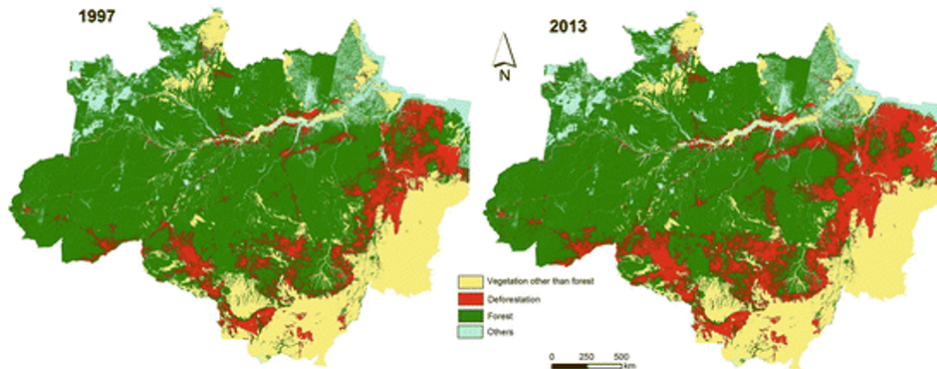


Figure 10.12: Historical land use scenario for the Amazon (INPE)

10.6 Management scenarios

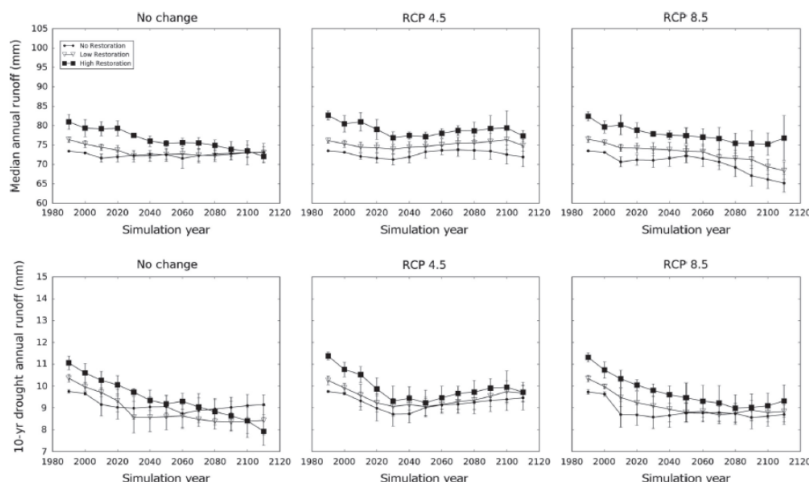


Figure 10.13: Simulating the impact of restoration on hydrology. Predicted total runoff from a study area of semi arid forests in SW-USA by the LANDIS II model, normalized by area, from 1990 to 2110 under future vegetation distributions and restoration rates. Precipitation inputs are not adjusted to account for the effects of climate change. The top row of panels shows runoff for a median (50th percentile) annual precipitation and the bottom row of panels shows runoff for a 10-yr drought (10th percentile) annual precipitation scenario. Values are means and SD across model runs. (Donnell et al. 2018)

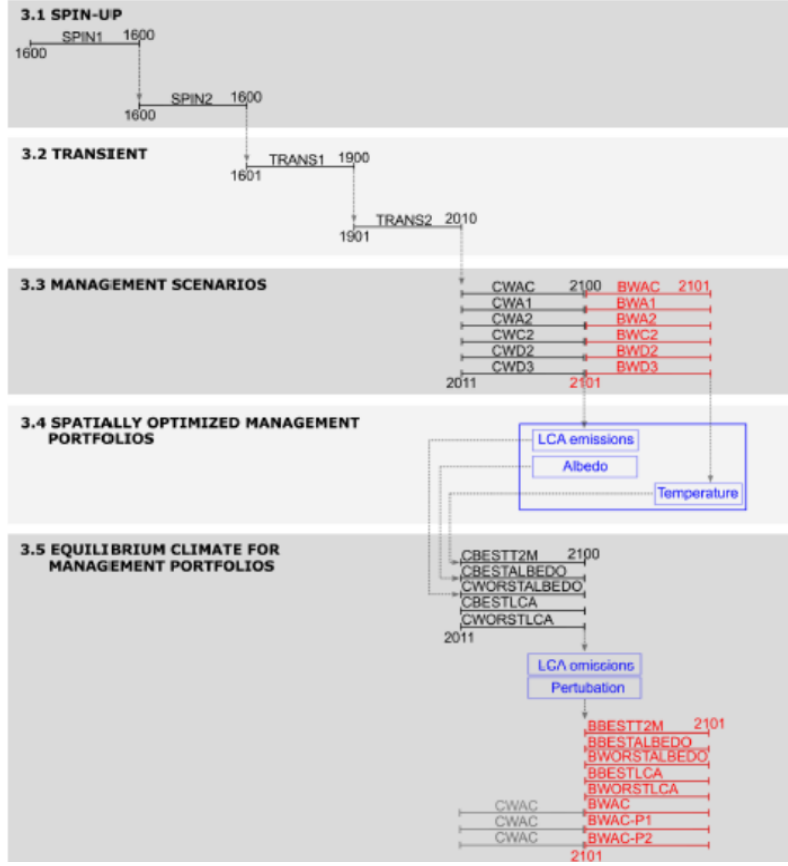


Figure 10.14: Setup of simulation experiments in a study on European forest management scenarios. The experiments are described in publication of Lyussaert et al. 2018. Simulations with the ORCHIDEE-CAN vegetation model are shown in black and simulations with LMDzORCAN (couple climate model) are shown in red. Blue boxes denote intermediate calculations using the simulation results. The simulations shown in this figure correspond to runs with reduced air temperature (BBESTT2M), maximized surface albedo (BESTALBEDO), minimized surface albedo (BWORSTALBEDO), maximized carbon sink (BBESTLCA), minimized carbon sink (BWORSTLCA) and business as usual (BWAC). BWAC, BWAC-P1 and BWAC-P2 were used to calculate the minimal model noise. (Lyussaert et al. 2018)

Part IV

Appendix

Contributing to this document

First steps

First, visit the course webpage on https://github.com/femeunier/VegMod_course, and fork it to your own github account. Open a RStudio session and (if it is your first time with git) introduce yourself:

```
git config --global user.name "FULLNAME"  
git config --global user.email you@yourdomain.example.com
```

Note that you can do every single step below using the terminal and the git tabs in RStudio. Clone the newly forked folder to your local machine:

```
git clone https://github.com/femeunier/VegMod_course.git
```

or using SSH (to set up it first, see for instance <https://help.github.com/en/github/authenticating-to-github/connecting-to-github-with-ssh>)

```
git clone git@github.com:femeunier/VegMod_course.git
```

Define upstream

```
cd VegMod_course  
git remote add upstream git@github.com:femeunier/VegMod_course.git
```

New pull request

Get the latest code from the main repository

```
git pull upstream master
```

Create a new branch (here new_branch is the new branch's name)

```
git checkout -b new_branch
```

Do some coding, add files and commit them

```
git add filepath  
git commit -m "Message"
```

Push your changes to your github (when a feature is working, a set of bugs are fixed, or you need to share progress with others).

```
git push origin new_branch
```

Before submitting code back to the main repository, make sure that book compiles (buikd book). Open the PR online by visiting your github repository. To ease those previous steps you can take advantage of the git GUI in RStudio. To do so, create a new project from an existing directory.

Supporting material

Crash course, basic programming (R), theory about model evaluation etc.

Part V

Practicals

Practical A

PC-room, supervised exercise

Simple model on diurnal variation in solar angle, radiation extinction and photosynthesis in vegetation types with different canopy structure and LAI:
grassland, broadleaved forest, coniferous forest

Scale: aggregated stand level (big leaf model)

Methodological focus: model formulation: translating a few equations into code

Methodological focus: compiling code, running model, reading input-output

Practical B

Group work, report, PC room

Modelling diurnal cycle of carbon and water fluxes for flux tower sites (Savanna's Sahel)

Scale: aggregated stand level

Methodological focus: model-data comparison (goodness-of-fit), simple parameter optimisation

Practical C

PC-room, supervised exercise

Modelling the size structure of a temperate forest (stand diameter distribution)

Scale: forest stand

Methodological focus: initial conditions

Practical D

Group work, report, PC room

Modelling carbon stocks (above and belowground) and fluxes

Scale: ecosystem

Methodological focus: Spinup and sensitivity analysis (testing which climate variables have strongest impact on stocks)

Practical E

PC-room, supervised exercise

Simulating forest succession, meta-analysis of trait dataset to prescribe vegetation
functional composition (using PEcAn-framework)

Scale: landscape

Methodological focus: parameter meta-analysis (PFT construction), data assimilation

Practical F

PC-room, group work, microteaching

Climate/land use/management scenario analysis

Scale: site/globe? (Pecan framework) each group chooses a question and a model

Methodological focus: sensitivity and uncertainty analysis